The Interaction of the Madden-Julian Oscillation and the Quasi-Biennial Oscillation in Observations and a Hierarchy of Models

Zane Karas Martin

Submitted in partial fulfillment of the
requirements for the degree of
Doctor of Philosophy
under the Executive Committee
of the Graduate School of Arts and Sciences

COLUMBIA UNIVERSITY

2020

ABSTRACT

The Interaction of the Madden-Julian Oscillation and the Quasi-Biennial Oscillation in Observations and a Hierarchy of Models

Zane Karas Martin

The Madden-Julian oscillation (MJO) and the quasi-biennial oscillation (QBO) are two key modes of variability in the tropical atmosphere. The MJO, characterized by propagating, planetary-scale signals in convection and winds, is the main source of subseasonal variability and predictability in the tropics. The QBO is a ∼28-month cycle in which the tropical stratospheric zonal winds alternate between easterly and westerly regimes. Via thermal wind balance these winds induce temperature anomalies, and both wind and temperature signals reach the tropopause.

Recent observational results show a remarkably strong link between the MJO and the QBO during boreal winter: the MJO is stronger and more predictable when QBO winds in the lower stratosphere are easterly than when winds are westerly. Despite its important implications for MJO theory and prediction, the physical processes driving the MJO-QBO interaction are not well-understood.

In this thesis, we use a hierarchy of models – including a cloud-resolving model, a forecast model, and a global climate model – to examine whether models can reproduce the MJO-QBO link, and better understand the possible mechanisms driving the connection. Based in part on our modeling findings, we further explore observed QBO temperature signals thought to be important for the MJO-QBO link.

After providing necessary background and context in the first two chapters, the third chapter looks at the MJO-QBO link in a small-domain, cloud-resolving model. The model successfully simulates convection associated with two MJO events that occurred during the DYNAMO field campaign. To examine the effect of QBO, we add various QBO temperature and wind anomalies into the model. We find that QBO temperature anomalies alone, without

wind anomalies, qualitatively affect the model MJO similarly to the observed MJO-QBO connection. QBO wind anomalies have no clear effect on the modeled MJO. We note however that the MJO response is quite sensitive to the vertical structure of the QBO temperature anomalies, and for realistic temperature signals the model response is very small.

In the fourth chapter, we look at the MJO-QBO link in a state-of-the-art global forecast model with a good representation of the MJO. We conduct 84 hind-cast experiments initialized on dates across winters from 1989-2017. For each of these dates, we artificially impose an easterly and a westerly QBO in the stratospheric initial conditions, and examine the resulting changes to the simulated MJO under different stratospheric states. We find that the effect of the QBO on the model MJO is of the same sign as observations, but is much smaller. A large sample size is required to capture any QBO signal, and tropospheric initial conditions seem more important than the stratosphere in determining the behavior of the simulated MJO. Despite the weak signal, we find that simulations with stronger QBO temperature anomalies have a stronger MJO response.

In the fifth chapter, we conduct experiments in recent versions of a NASA general circulation model. We find that a version with a high vertical resolution generates a reasonable QBO and MJO, but has no MJO-QBO link. However, this model has weaker-than-observed QBO temperature anomalies, which may explain the lack of an MJO impact. To explore this potential bias, we impose the QBO by nudging the model stratospheric winds towards reanalysis, leading to more realistic simulation of QBO temperature anomalies. Despite this, the model still fails to show a strong MJO-QBO link across several ensemble experiments and sensitivity tests. We conclude with discussion of possible reasons why the model fails to capture the MJO-QBO connection.

The sixth chapter examines QBO temperature signals in a range of observational and reanalysis datasets. In particular, we are motivated by two elements of the MJO-QBO relationship which are especially puzzling: the seasonality (i.e. that the MJO-QBO link is only significant in boreal winter) and long-term trend (i.e. that the MJO-QBO link seems

to have only emerged since the 1980s). By examining QBO temperature signals around the tropopause, we highlight changes to the strength and structure of QBO temperature anomalies both in boreal winter and in recent decades. Whether these changes are linked to the MJO-QBO relationship, and what more generally might explain them, is not presently clear.

Overall, we demonstrate that capturing the MJO-QBO relationship in a variety of models is a difficult task. The majority of evidence indicates that QBO-induced temperature anomalies are a plausible pathway through which the QBO might modulate the MJO, but the theoretical description of precisely how these temperature anomalies may impact convection is lacking and likely more nuanced than the literature to date suggests. Most models show only a weak modulation of the MJO associated with changes in upper-tropospheric temperatures, and even when those temperature signals are artificially enhanced, comprehensive GCMs still fail to show a significant MJO-QBO connection. Our observational study indicates that temperature anomalies associated with the QBO show striking modulations on various timescales of relevance to the MJO-QBO link, but do not conclusively demonstrate a clear connection to the MJO. This difficulty simulating a strong MJO-QBO connection suggests that models may lack a key process in driving the MJO and coupling the tropical stratosphere and troposphere. It is further possible that the observed link may be in some regards different than is currently theorized – for example statistically not robust, due to non-stratospheric processes, or driven by some mechanism that has not been suitably explored.

Contents

List of Figures

Page

List of Tables

Page

ACKNOWLEDGMENTS

This thesis was only possible thanks to the tireless wisdom of my advisors, Adam Sobel and Shuguang Wang. From essentially our first meeting, Shuguang's kindness, patience, technical know-how, and sterling edits saved me from innumerable headaches and helped shape me into the scientist I am today. Adam taught me many, many things: about the role an academic can play in the world, about how to write and think and speak about the tropics, about parts of the world I never dreamed I would visit, and most of all about how to conduct myself as a scientist, and sometimes as a person. Working with Adam and Shuguang has inspired me more than I can say.

Thanks to Michael Tippett, Arlene Fiore, and Clara Orbe, for somehow finding the time in their schedules to serve on my committee, and for their assistance and input at many stages in my graduate career. And thanks to Lorenzo Polvani for his guidance and mentorship, and for helping convince me that atmospheric science and Columbia University were the right next steps.

I am grateful, in particular, to three educators who helped guide me during formative years early in my scientific education. Lisa Baldwin and Kathy Erickson saw me off from Monument Mountain Regional High School with a good grasp of the ideal gas law and a solid foundation in calculus, which served me well through college and graduate school. But more than that, both instilled in me a curiosity about the natural world, a love of mathematics and science, and the confidence and courage to think that I could contribute to those fields. Professor Frank Morgan fostered my love of math and science during my time at Williams College with his unbridled enthusiasm, and has always been a source of sage advice, especially during difficult times.

Many friends at Columbia and elsewhere provided inspiration and support, both professionally and personally, including Bernard Lipat, Alex Watson, Mark England, Anirban Sinha, Jessie Oehrlein, Ivan Mitevski, Mel Abler, and Alex Saperstein.

Special thanks to Daeus Jorento, Ethan Walker, and Dr. Buddy Ferris, for always making me laugh and for keeping me myself, and to Dr. Melanie Bieli – I could not have asked for a better companion on the long and winding road of graduate school; thank you for showing me the way.

Thanks to my family, near and far, for the certitude and steadfastness of your love. Mom, Dad, Quinn, and Regan – I love you, and assuredly could not have done it without you. Special thanks to Marian Holmes, for always at least taking a stab at reading my papers, if only to compliment my "charming graphs."

Most of all, thanks to my wife Sara who, through countless hours of editing drafts and listening to practice talks, has almost certainly become an authority on the MJO-QBO link herself. Sara: during my graduate career you gave me five years of love, support, guidance, and joy, and in return took only my last name. You have all my love, all my days.

Chapter 1

Tropical Meteorology in the 1960s and 1970s: A Prelude

The tropical region of Earth's atmosphere consists of the wide, hot, humid band running around the equator of the planet. Marked by omnipresent heat and moisture, large swaths of ocean, and lessened effects of Earth's rotation, the tropics represent a largely distinct regime from the populated mid-latitudes or the frigid poles. "Tropical meteorology" is the distinct sub-field within the broader discipline of atmospheric science that considers itself with the unique characteristics and mysteries of this portion of our planet.

The field of tropical meteorology can trace its origins to the second World War,[1] when nations fighting throughout the Pacific Ocean had to contend with distinct and unfamiliar tropical weather patterns. Spurred by both the war effort's need for forecasts and a scientific dearth of understanding, research facilities specializing on the tropics were established in the 1940s, as pioneers of atmospheric science and tropical meteorology such as Carl-Gustaf Rossby and Herbert Riehl convinced universities and governments to allocate resources towards this emerging discipline.

[1] Much of the historical background in this section, unless otherwise noted, is from Sobel (2014) and Hand (2015).

As the war effort came to a close, the scientific presence in the tropics remained and expanded into the 1950s: observational sites were maintained throughout the tiny islands dotting the tropical Pacific. Breakthroughs in observing systems using radio allowed scientists to measure vertical profiles of temperature, wind, and humidity in the atmosphere, and these "radiosonde" measurements began to be taken routinely throughout the tropics.

By the 1960s and 1970s these tropical radiosonde sites had been collecting measurements for at least a decade. Atmospheric scientists now had enough data to not only study the weather of the tropics, but to begin to think about its climate. The bitter national rivalries that flourished during the two World Wars had also dulled, and as radiosonde networks extended globally, data from around the world became increasingly available (Maruyama (1997)). Increased computational power, theoretical breakthroughs, and new analysis techniques offered new windows through which scientists could look at their data. It was a time ripe for discovery.

* * *

The stratosphere is the gateway to the upper reaches of Earth's atmosphere. Sitting high above the troposphere, the stratosphere is by many metrics more quiescent than the ever-convecting troposphere below it. In the tropics the stratosphere is especially high, typically beginning at around 18 km above sea-level when the temperature profile hairpins and begins to increase with height.

Atmospheric scientists' early knowledge of the wind patterns in the stratosphere were born out of a series of violent events in the troposphere below. In 1883, the massive volcano Krakatoa, near Sumatra, erupted, sending particulate spewing up into the stratosphere where it was picked up and advected by the winds. Tracked by eye at sites around the world, scientists at the time noted that these particles moved rapidly westward around the globe, leading to the discovery of winds that were known as the "Krakatoa easterlies". This was largely believed to be the dominant flow pattern in the stratosphere for much of the next century (Hamilton (1998); Baldwin et al. (2001)).

The behavior of upper-level winds gained renewed importance to the U.S. military during the 1940s and 1950s, as nuclear tests began to be carried out across the Pacific. These blasts launched radioactive fallout into the stratosphere, occasionally with disastrous consequences: one incident in particular, the 1954 Castle Bravo disaster, lead to widespread fallout over populated areas when unpredicted upper-level flows spread radioactive materials to ships and nearby islands (Maruyama (1997)). As such, measurements of the stratospheric winds became common around times of nuclear detonations, and an unintended positive consequence of these tests was the relatively high quality meteorological datasets they produced.

By the late 1950s and early 1960s scientists had long records of these stratospheric winds and began to examine them with renewed energy. What they found surprised them. Rather than observing the steady Krakatoa easterlies, two scientists in 1961 – R.A. Ebdon at the UK Met Office and R.J. Reed at the University of Washington – used several years of radiosonde measurements to show that the stratospheric wind around the entire tropics oscillated between easterly and westerly states with a period of around two years (Ebdon and Veryard (1961); Reed et al. (1961)). The aptly-titled quasi-biennial oscillation (QBO) had been discovered.

The QBO would profoundly challenge the imagination of atmospheric scientists in the coming decade, but remarkably its discovery coincided with new theory and the ability to perform numerical modeling experiments which were perfectly suited to understanding it. Within around ten years, the basic principles that drive the QBO as we understand it today were reasonably settled. Still, at the time of its discovery the QBO demonstrated there were insights and mysteries embedded in the tropical radiosonde records that other scientists were eager to examine.

* * *

Among those scientists looking for hidden signals in tropical data records were two tropical meteorologists at the National Center for Atmospheric Research in Boulder, Colorado – Roland Madden and Paul Julian. Not only did Madden and Julian have long tropical

datasets, they were armed with state-of-the-art computational capacities, with dozens of kilobytes of memory at their disposal. They also possessed the know-how to bring novel statistical methods to bear: Julian had just completed his Ph.D. at Penn State, which included study of spectral methods of data analysis, and the recently developed fast Fourier transform allowed these spectral techniques to be carried out efficiently.

In 1971, Madden and Julian applied these methods to the long radiosonde records from Canton Island, one of the same sites used by Reed in his 1961 analysis. Unlike Reed, Madden and Julian were examining the tropospheric winds and sea-level pressure rather than stratospheric signals, though like Reed what they found suprised them. They identified a theoretically inexplicable spectral peak around 40-50 days. Their statistical testing indicated that the signal was significant despite the fact that "no prior evidence or reason existed for expecting such a spectral feature" (Madden and Julian (1971)).

Madden and Julian quickly recognized the importance of their finding, and published a second breakthrough paper a year later that expanded upon their newly discovered, intraseasonal oscillation (Madden and Julian (1972)). They showed that this 40-50 day oscillation did not oscillate throughout the tropics all at once, nor was it a unique feature limited near Canton Island. Rather, what they had uncovered was a large-scale, coherent structure that linked circulation, convection, and surface pressure over vast regions of the tropics, and that propagated slowly to the east. At the time, no theory had predicted it, or seemed suited to fully explain what it might be.

At the close of their seminal pair of papers, Madden and Julian conclude: "it is hoped that these current investigations will establish what role the 40-50 day tropical oscillation plays in the general circulation of the atmosphere" (Madden and Julian (1972)). Nearly 50 year later, many papers on what we now call the Madden-Julian oscillation (MJO) could very well end the same way. Unlike the QBO, whose discovery seemed perfectly situated at the confluence of the theoretical and modeling groundwork which underpin it, the MJO has eluded the best efforts of several generations of tropical meteorologists to explain key

features like its size, time scale, and propagation. While in recent years the community seems to be coalescing around a handful of promising theories, consensus has yet to emerge. Today, a complete MJO theory vies with only a handful of other questions as perhaps the most scientifically sought-after prize in tropical meteorology.

The MJO and the QBO were born out of largely the same era and in some sense discovered out of the same datasets. They represent dominant modes of variability in the atmosphere, are profound theoretical curiosities, and encouraged a new wave of interest into the study of the tropics. They have, until recently, proven difficult to capture in comprehensive models of the Earth's climate, and their impacts on the Earth system have been found to be more far-reaching than their original discoverers likely ever would have anticipated.

They are also different in many regards. One is theoretically well-understood, while the other has remained stubbornly difficult to define. They occupy largely distinct regions of the atmosphere, in which different dynamical and thermodynamical regimes are at play. They occur on very different timescales – one subseasonal, the other interannual – and occupy somewhat different spatial scales: the QBO extends fairly symmetrically around the globe, whereas many elements of the MJO signal are confined to the Indian Ocean and West Pacific.

And yet, somehow, they appear to be linked.

* * *

This thesis explores the unexpected connection between the MJO and the QBO. Chapter 2 describes the necessary scientific background in more detail: we introduce the main features of the QBO and MJO in observations and review theoretical and modeling work on both phenomena. We then discuss coupling between the stratosphere and troposphere, and describe prior work on how the QBO might impact the troposphere in general, and deep convection in the tropics specifically. We then turn to the recently discovered MJO-QBO relationship in detail.

The following three chapters explore the MJO-QBO link in a variety of numerical models,

each with their own strengths and weaknesses. The goal in using models is primarily to help us better understand the physical mechanism through which the MJO and the QBO might interact, and to catalogue the degree to which the strong observed MJO-QBO connection is simulated (or not) in different models.

Chapter 3 examines the impact of QBO wind and temperature anomalies on MJO convection in a small-domain, idealized, cloud-resolving model.

Chapter 4 examines the MJO-QBO link in a forecast model with an exceptional representation of the MJO, focusing on the role of the stratosphere (as opposed to the tropospheric initial state) on the simulated MJO.

Chapter 5 looks at whether a free-running global climate model can represent the MJO-QBO connection, and on whether "nudging" the stratosphere to remove biases in the QBO can improve the model's ability to capture an MJO-QBO relationship.

Chapter 6, the final scientific chapter, pivots to an observational perspective and looks more at QBO-related temperature anomalies through the lens of the MJO-QBO connection. In particular it focuses on temperature anomalies in the upper troposphere and lower stratosphere, and on how those temperature anomalies differ on annual and inter-annual timescales.

Chapter 7 concludes the thesis with a synthesis of its key findings and some final remarks.

Chapter 2

Variability and Interactions in the Tropical Troposphere and Stratosphere

In this chapter we provide background necessary to the following discussion of the relationship between the Madden-Julian oscillation (MJO) and the stratospheric quasi-biennial oscillation (QBO), which is the main topic of this thesis.

The two sections introduce the quasi-biennial oscillation (Sect. 2.1) and the Madden-Julian oscillation (Sect. 2.2). In brief, the QBO is a reversal in the stratospheric zonal winds between easterly (QBOE) and westerly regimes (QBOW), with a period of approximately 28 months (Reed et al. (1961); Ebdon and Veryard (1961); Baldwin et al. (2001)). Through thermal wind balance, the QBO also induces temperature anomalies, and these QBO wind and temperature signals propagate downward through the stratosphere to around the tropopause. The Madden-Julian oscillation (Madden and Julian (1971); Madden and Julian (1972); Zhang (2005)) is the main mode of intraseasonal (∼30-60 day) variability in the tropical troposphere. The MJO is a planetary-scale system of circulation and convection anomalies that canonically forms over the Indian ocean and propagates east into the central

Pacific. A consensus theory for the MJO has not emerged despite almost 50 years of research, making it one of the most enduring and alluring mysteries in tropical meteorology.

Section 2.3 reviews stratosphere-troposphere interactions. We review some general ways in which the stratosphere and troposphere are connected, before discussing three routes through which the QBO can influence the troposphere – polar, subtropical, and tropical pathways. A significant connection between the QBO and the poles has been known for some time (Holton and Tan (1980); Holton and Tan (1982); Baldwin and Dunkerton (2001)), but the QBO's impact on deep convection in the tropics is not especially strong, and the mechanism is unclear (Collimore et al. (2003), Liess and Geller (2012), Nie and Sobel (2015)). Other QBO connections in the tropics, for example to the El Niño-Southern Oscillation (ENSO) or tropical cyclones, are inconsistent over the observed record (Garfinkel and Hartmann (2007); Camargo and Sobel (2010)) and present thinking is that they are also not especially significant.

However, as discussed in Section 2.4 a very strong link between the MJO and the QBO was recently (re)discovered, prompting a new wave of interest in stratosphere-troposphere interactions and the ability of the QBO to influence the tropics (see Kuma (1990), but more recently Yoo and Son (2016); Son et al. (2017); Marshall et al. (2017)). The boreal winter MJO tends to be much stronger and more active when QBO winds in the lower stratosphere are easterly versus westerly. In addition to being stronger, the MJO is more predictable (Marshall et al. (2017); Lim et al. (2019); Wang et al. (2019b)) and displays stronger teleconnections (Son et al. (2017); Toms et al. (2020)) when the QBO is easterly. The mechanism behind this MJO-QBO interaction is not clear, though several hypotheses have been put forth and will be explored more in Chapters 3-7. Additionally, models struggle to show a strong MJO-QBO link, as will be demonstrated and discussed at length in this thesis.

Section 2.5 concludes this introduction.

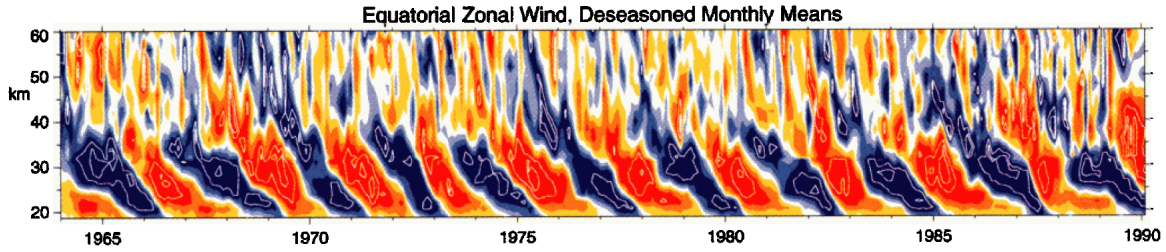

Figure 2.1: Adapted from Baldwin et al. (2001), their plate 1. This time-height plot shows descending easterly (blue) and westerly (red) zonal-mean zonal winds; the hallmark feature of the QBO. Data are monthly-mean values from 1964-1990 with the seasonal cycle removed, using combined radio- and rocketsonde sites around the tropics. The contour interval is 6 m/s with ±3 m/s unshaded.

2.1 The Quasi-Biennial Oscillation

The quasi-biennial oscillation (QBO) is perhaps the most striking mode of variability in the equatorial stratosphere. Discovered in the early 1960s (Reed et al. (1961); Ebdon and Veryard (1961)), the main feature of the QBO is a complete reversal in the direction of the tropical stratosphere's zonal wind with an average period of just longer than two years, which lends the oscillation its name.

This section presents an overview of the main observed features of the QBO and explains the basic QBO theory, credited primarily to Lindzen and Holton (Lindzen and Holton (1968); Holton and Lindzen (1972)). We then briefly address the representation of the QBO in models. Discussion of how the QBO impacts (or does not impact) the troposphere is deferred to Section 2.3.

2.1.1 Basic Features

The characteristic signature of the QBO is the descending, oscillating pattern of the zonal wind in the tropical stratosphere between easterly (QBOE) and westerly (QBOW) phases, shown in Figure 2.1. These zonal winds reverse their direction with a period around (but not exactly) two years; the average period of the oscillation is $\sim$ 28 months (Baldwin et al. (2001)), though it has been as short as 21 months (1972-1974) and as long as 35 months

(1983-1986) (Andrews et al. (1987)). The magnitude of the oscillation in zonal wind is on the order of 10-20 m/s, with winds in the mid-stratosphere of around -20 m/s in QBOE and around 15 m/s in QBOW (Gray (2013)). The signals directly associated with the QBO (i.e. those driven by the wave-mean flow interaction described in Section 2.1.2, as opposed to any QBO teleconnections) are largely zonally symmetric, and are confined to the tropics: the QBO is symmetric in magnitude about the equator and decays with a half-width of around 12° in latitude.

As the winds reverse, they also descend through the stratosphere from around 40 km to 20 km with a rate of around 1 km/month, evident in Figure 2.1. The westerly phase of the QBO often descends faster (attributed to the meridional circulation discussed in Section 2.1.1.1), while the easterly phase has greater amplitude and generally lasts longer (Gray (2013); Baldwin et al. (2001)).

While the period of the oscillation is not an integer multiple of the annual cycle, the QBO shows some tendency to phase lock to the annual cycle, such that the majority of transitions between phases (at ∼50 hPa) happen between April and July (Dunkerton and Delisi (1985); Dunkerton (1990); Rajendran et al. (2016)). This spring transition preference will be discussed additionally in Chapter 6.

2.1.1.1 QBO Temperature Anomalies and Meridional Circulation

In addition to the zonal wind signal, the QBO displays temperature anomalies down to the tropopause that are consistent with thermal wind balance, as well as a secondary meridional circulation. In regions of westerly zonal wind shear, the QBO has a warm anomaly centered at the equator, and during easterly shear there is an associated cold anomaly. These temperature anomalies in the lower stratosphere/upper troposphere tend to be on the order of 1-2K; Figure 2.2 shows latitude-height plots of the QBOE minus QBOW wind and temperature (QBO defined at 50 hPa). Evident there are cold anomalies on the equator slightly below the region of easterly winds, with warm anomalies above in the westerly regime and another

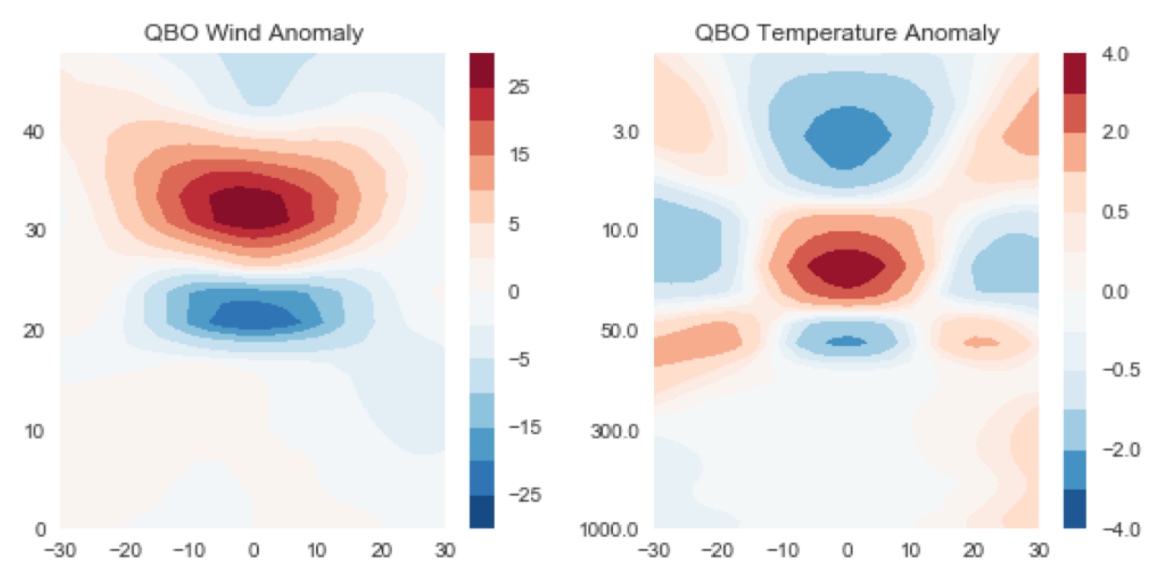

Figure 2.2: QBOE minus QBOW zonal-mean zonal wind and temperature anomalies from ERA Interim reanalysis data (Dee et al. (2011)) from 1979-2018. The data are monthly means, and the QBO is defined using the zonal-mean, 10°N to 10°S averaged, 50 hPa zonal wind. QBOE and QBOW months are defined when these 50 hPa winds are less than or greater than 0.5 standard deviations.

cold anomaly in the upper stratosphere.

In order to maintain these warm or cold anomalies against radiative damping, the atmosphere must be warmed or cooled adiabatically by vertical motion. Thus, a warm anomaly is maintained through adiabatic descent at the equator, while a cold anomaly is maintained by adiabatic ascent. During QBOW sinking on the equator sets up rising motion off the equator, with meridional wind closing the circular cells. This sets up a QBO meridional circulation, as shown in a schematic form in Figure 2.3. Note that for a easterly shear regime, the rising at the equator acts against the descending winds, one proposed reason why the easterly QBO phase may descend slower than the westerly phase (Plumb and Bell (1982); Gray (2013)).

This secondary QBO circulation also acts to creates temperature anomalies outside of the tropics, where the rising or sinking associated with the return flow leads to temperature changes. These off-equatorial temperature anomalies can be seen at around 20°N/S in Figure 2.2. Further, the meridional circulation has implications for the width of the QBO, its

influence on chemical tracers, and its interaction with other atmospheric phenomena like the polar vortex (Baldwin et al. (2001)).

While the QBO meridional circulation can be understood via a thermal wind balance, the theory behind what sets the zonal wind pattern in the first place is not straightforward. The QBO winds display several puzzling aspects: any successful theory of the QBO needs to address why a reversal in the zonal wind takes place, what sets the quasi-biennial period, and what makes the regimes descend through the stratosphere.

2.1.2 Basic Theory

The theory of the QBO was first successfully described by Lindzen and Holton (1968) and later refined by Holton and Lindzen (1972).

Consider an atmosphere in which there is a mean zonal flow $u_0(z,t)$ and waves forced at the lower boundary (e.g. the tropopause). Imagine we have a pair of vertically propagating gravity waves that are identical in amplitude, but which have opposite phase velocities, $\pm c$ (set up shown schematically in Fig. 2.4).

Critical to the understanding of the theory of the QBO are two theorems credited to Eliassen and Palm on the interaction between the mean flow of a fluid and waves propagating through it (our discussion here loosely follows Lindzen (1990)). Stated informally for the purposes of discussion, these two theorems are:

1. If the zonal momentum carried in an upward propagating wave moving at zonal phase speed c is deposited into the mean flow, it will bring the mean flow towards the phase speed of the wave.

2. In inviscid, un-damped flow, upward propagating waves will not deposit momentum into the mean flow except at *critical levels*: where the mean flow equals the phase speed of the wave (i.e. $u_0 = c$).

In the presence of linear damping, waves deposit some momentum into the mean flow

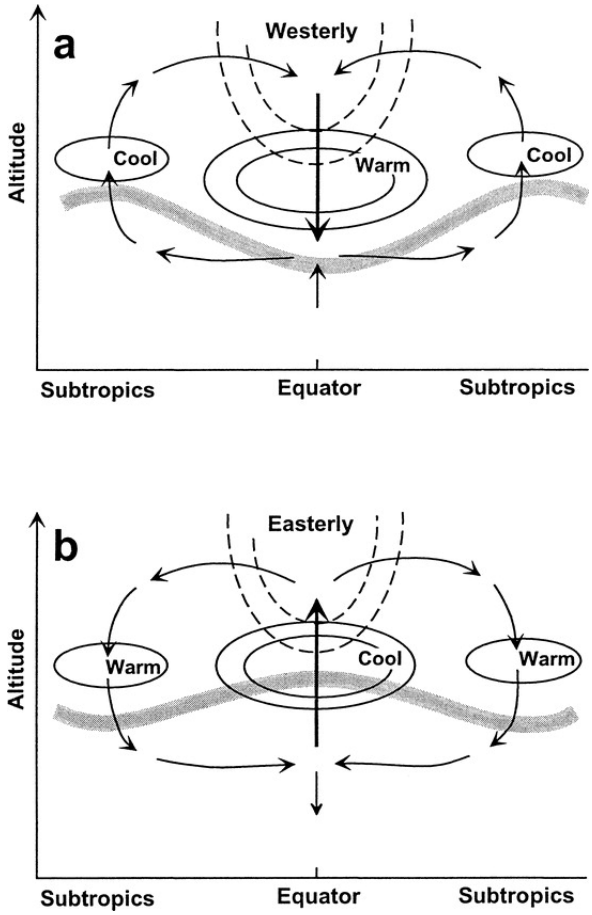

Figure 2.3: Adapted from Collimore et al. (2003), Figure 1. The panels shows schematically the induced meridional circulation set up by the QBO when lower stratospheric winds are westerly (a; top) and easterly (b; bottom). Dashed contours represent zonal wind, solid represent temperature, and the thick grey line represents the tropopause.

even where $u_0 \neq c$, but at a rate inversely proportional to $|(u_0 - c)|$. That is, waves deposit more momentum the closer the mean flow is to their phase speed. The majority of wave's momentum when damping is included is still deposited at or near critical levels where $u_0 \approx c$.

Returning to our two waves with phase speed $\pm c$, by the first Eliassen-Palm (EP) theorem these two waves will carry westerly and easterly momentum, respectively, relative to the mean flow. Say we have some small perturbation such that the mean flow is westerly at low levels, as in Figure 2.4a. Since the waves are linearly damped, both the easterly and westerly wave will deposit that momentum as they propagate upward. Since $u_0 > 0$, the mean flow at low levels absorbs more momentum from the westerly wave than from the easterly wave (by the second EP theorem). This leads to westerly acceleration of the mean flow at lower levels (double arrow pointing right in Figure 2.4a).

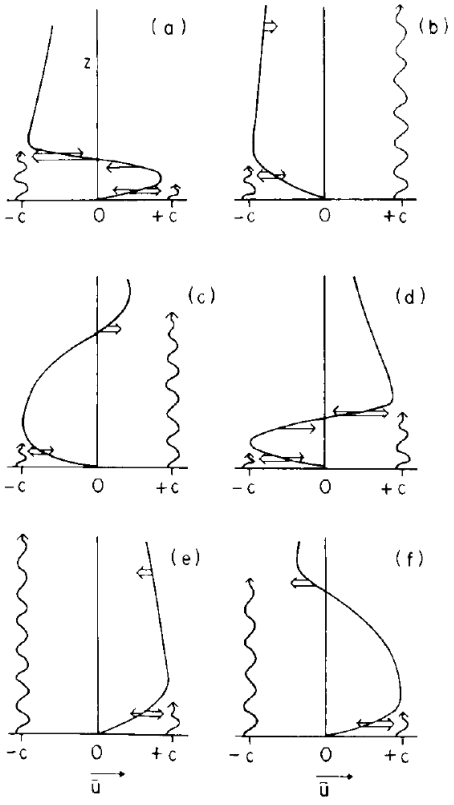

Figure 2.4: Adapted from Andrews et al. (1987), their Figure 8.7. The panels show how the mean flow (solid line on the y-axis, $u_0(z,t)$) evolves through idealized stages of the QBO. The wavy, vertical lines at ±c represent momentum carried by vertically propagating waves with zonal phase speeds of ±c. Double arrows indicate forcing of the mean flow by the waves, and single arrows indicate viscous forces.

This deposition of westerly momentum at low levels damps the amplitude of the westerly wave higher up, "shielding" the upper level flow from westerly momentum. At upper levels therefore, the westerly wave carries less momentum than the easterly wave, which stays relatively undamped. In addition, at upper levels viscous diffusion keeps the mean flow near zero. Thus, the stronger momentum source at these levels is from the easterly

wave, and the mean flow experiences easterly acceleration.

As time goes on, this situation will continue, with the westerly flow growing at low levels and easterly flow being established aloft. Plumb (1977) showed that the maximum acceleration of the flow occurs just underneath the maximum in u_0, which leads to the descent of the easterly regime. This eventually traps the westerly regime in a narrower and narrower layer, where viscous forces finally break up this westerly layer and establish a regime of easterlies throughout (Fig. 2.4b). The cycle will then repeat, leading to the establishment and descent of a westerly regime (Fig. 2.4c,d,e) and eventually the return of the original configuration (Fig. 2.4f,a).

This describes the basics of the now widely-accepted QBO mechanism. From this perspective, the zonal phase speed of the waves, c, determines the amplitude of the oscillation, as it controls how strongly the mean flow is accelerated. The amplitude of the waves and the amount of viscous diffusion control the period of the oscillation, through setting the speed of descent and the level at which the lower shear layer is destroyed.

2.1.2.1 Refinements to the Theory of the QBO

While the basic theory of the QBO is largely settled, in the approximately four decades since it was originally developed several refinements have emerged. Chapter 6 concerns itself with one aspect of the QBO which this theory does not seem well-suited to address, and here we present a review of other issues noted in the literature.

First, the 1-D description of the QBO does not include the effects of rotation, which may be important in several regards. Chief among them is that rotation is responsible for the existence of for a number of equatorially-trapped waves, including Kelvin, Rossby, and Rossby-gravity waves (see Section 2.2.2). These waves have more complex meridional and vertical structures than gravity waves and do not propagate at the same speed or with the same amplitude, but do appear important in driving the QBO. Holton and Lindzen (1972) demonstrated that a QBO-like result may be derived by considering forcing by eastward

propagating Kelvin waves and westward propagating Rossby-gravity waves and not gravity waves. However, Takahashi and Boville (1992) showed in a more comprehensive model that larger-than-observed Kelvin and Rossby wave momentum fluxes were needed to adequately simulate the QBO. Dunkerton (1997) re-established that gravity waves were key momentum sources in addition to the Kelvin and Rossby-gravity waves, and it is now recognized that waves which force the QBO fall into two main categories (see Gray (2013) and Baldwin et al. (2001)):

1. Waves with slower vertical group velocity, which deposit momentum via damping (these include Kelvin and Rossby-gravity waves).

2. Waves with faster vertical group velocity, which deposit momentum directly into critical levels (these include a spectrum of gravity and inertia-gravity waves).

The simple description we have presented above also fails to describe why the QBO is confined to the equator. One hypothesis contends that outside the tropics, there is not sufficient wave forcing (both due to changes in gravity wave properties and fewer large-scale equatorially trapped waves; Lindzen (1990); Baldwin et al. (2001)). Perhaps more likely, Haynes (1998) noted that at higher latitudes forcing provided by vertically propagating waves does not primarily accelerate the mean flow, but is instead canceled out by the Coriolis term and a mean meridional circulation, which may stop a QBO from forming.

It was also noted after the Holton-Lindzen theory had gained wide acceptance that the upwelling associated with the Brewer-Dobson circulation acts against the downward propagating QBO signal (Gray and Pyle (1989); Gray (2013)). The Brewer-Dobson circulation (Dobson et al. (1929); Brewer (1949); Dobson (1956); Andrews and Mcintyre (1976); Boyd (1976); Butchart (2014)) is a large-scale, global mass circulation that extends through the stratosphere, and includes a slow upwelling of air in the tropical lower stratosphere. As a result, the original momentum transport used by Holton and Lindzen was found to be insufficient to drive the QBO in a more realistic model; the QBO could only be captured

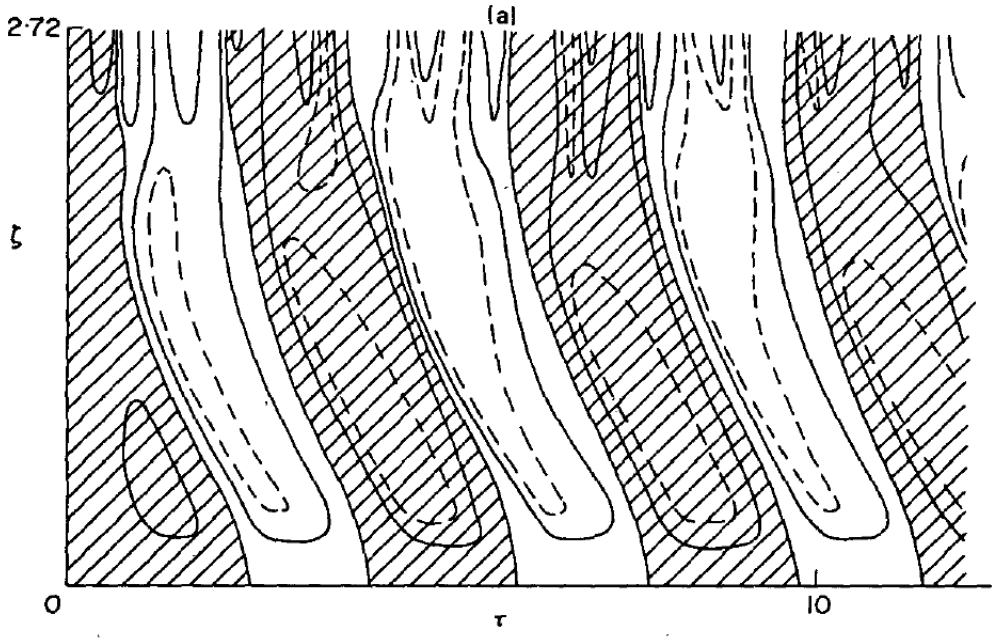

Figure 2.5: Adapted from Plumb (1977) Figure 8, showing mean zonal velocity on a time-height plot (units are non-dimensionalized and idealized). Contours are the results from a simple model of the QBO which solves a single PDE for the zonal-mean zonal wind, described more in Plumb (1977). Westerlies are shaded, and solid lines are intervals of 0.5 with dashed contours at ± 0.75.

in such models if the momentum flux was increased to three times the previously accepted value. The source of this additional momentum, and in general a precise momentum budget for the QBO, is still imprecisely accounted for.

2.1.3 Modeling of the QBO

A simple numerical model of the QBO that captured the main features and incorporated the theory described above was first presented in Holton and Lindzen (1972). Several subsequent 1-D models in the following years refined the theory to more realistic cases. In general, these models solved a single PDE for the zonal-mean zonal wind given forcing by upwelling waves with oppositely signed phase speeds as described in the preceding section. Plumb (1977) presented a particularly robust modeling study using a 1-D model in a range of contexts, from a single wave in a Boussinesq atmosphere up to a more realistic Holton-Lindzen set up

in a "real" atmosphere forced by Rossby-gravity and Kelvin waves. This model captured the main features of the observed QBO rather accurately, as shown in Figure 2.5, although the period is closer to three years rather than the 28 months (not evident in Figure 2.5 due to non-dimensionalization). Another study that helped confirm the basic QBO theory was work by Plumb and McEwan (1978) showing in lab experiments that momentum driving from waves in stratified flow could lead to periodic, descending reversals in the mean flow.[1] In addition to helping decisively settle the main features of the QBO theory, these "Plumb-McEwan" experiments comprise one of the best examples of physical laboratory experiments confirming theoretical results in geophysical fluid dynamics.

Until recently the QBO was considered difficult to simulate in comprehensive global climate models (GCMs). The first widely-accepted simulation that attained a reasonably realistic QBO in a GCM was by Takahashi (1996) who increased the vertical resolution in the stratosphere from the more standard $\sim$2 km to 500 m, and also increased the horizontal diffusion by an order of magnitude. Other realistic QBO simulations followed, and many demonstrated that a high resolution stratosphere drastically improved the representation of the QBO (Baldwin et al. (2001)).

Giorgetta et al. (2006) conducted a systematic test of the QBO in a model with a particularly accurate representation of the QBO and found that a stratospheric vertical resolution of less at least 1 km was necessary to simulate the "resolved waves" like upwelling Kelvin and Rossby-gravity modes. A gravity wave parameterization was also needed to supply additional momentum forcing from small-scale, non-resolved waves. These two ingredients – high vertical resolution and a carefully tuned and state-of-the-art gravity wave scheme – seem to be the crux of a GCM's ability to capture QBO signals.

Despite advances around that time, the CMIP5 models generally struggled to simulate the QBO. Charlton-Perez et al. (2013) found QBO signals in only 3 of the 27 CMIP5 models

[1]For a video recreating the results of this experiment see http://dennou-k.gaia.h.kyoto-u.ac.jp/library/gfd_exp/movies/avi32/vbo02.mp4

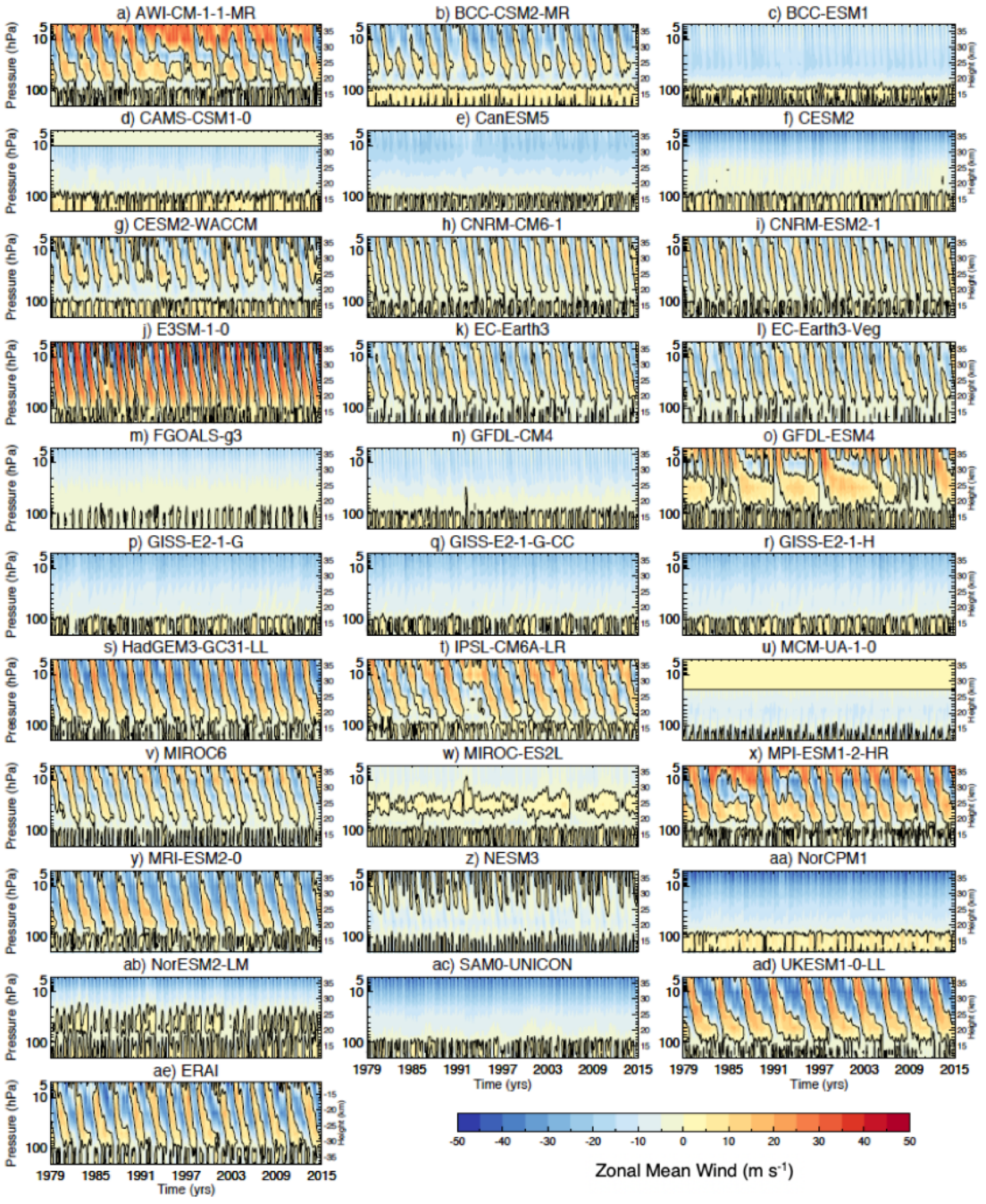

Figure 2.6: Adapted from Richter et al. (2020), zonal-mean zonal wind averaged between 5°S and 5°N as function of time and pressure for CMIP6 models and ERAI renalysis in m/s. Model names and additional details specified in Richter et al. (2020).

they considered. Richter et al. (2020) found that no CMIP3 models and only 5 CMIP5 models had oscillating stratospheric winds of approximately the correct form. Progress has been better in recent CMIP6-class models (Schenzinger et al. (2017)): Richter et al. (2020) find that 15 CMIP6 models (of those submitted to date) capture the QBO reasonably well, a tripling over CMIP5. Figure 2.6 shows the QBO winds averaged equatorially for observations (bottom left panel ae.) as well as for many of the CMIP6 models. There it is evident that even among state-of-the-art models there is a good deal of diversity in QBO behavior. Some models have a reasonable QBO (e.g. panels s, v, y,...), some are marginal (e.g. panels b, j, t, ad,...), some are very odd (e.g. panels a, o, w,...), and some are all together absent (e.g. panels c,d,e,f,...).

As discussed in Richter et al. (2020), this range is likely due to a number of factors. Some models still have too low a resolution in the stratosphere, and most models have imperfect gravity wave parameterizations which, for example, don't differentiate between the natures of gravity waves in the tropics versus the extratropics, or don't agree on how much gravity wave momentum flux should be generated by tropical convection. Additionally, since the stratosphere is often tuned last in models, the priorities of individual modeling centers may play a role in the spread, though Richter et al. (2020) point out that even those models that explicitly tuned their gravity waves to improve the QBO (as part of the "QBOi" project; Butchart et al. (2018); Bushell et al. (2019)) show deficiencies in QBO amplitude. Thus, tuning alone can not account for all the differences.

Today, while the general behavior of the QBO – its amplitude, period, and subtler features like the east/west amplitude asymmetry – can be simulated by models with appropriate tuning and computational resources (Schenzinger et al. (2017)), a continued deficiency in QBO simulation is the representation at lower levels, especially below 20-30 hPa (Richter et al. (2020)). This deficiency may be especially important in the present context, and is addressed more in Section 2.4.

2.2 The Madden-Julian Oscillation

The Madden-Julian oscillation (MJO), which owes its name to its two discoverers (Madden and Julian (1971), Madden and Julian (1972)), is a prominent mode of variability in the tropical troposphere, arguably second only to El Niño in terms of its global impacts. The MJO consists of a large, eastward propagating signal in which wind and convection are coupled together over the Indian Ocean and West Pacific. Unlike the QBO, the basic theory underpinning the MJO is still unsettled, though in recent years the field has coalesced around several promising advances.

Here we present some basic observed features of the MJO. We then discuss very briefly the theory governing similar propagating modes of variability in the tropics in which circulation and convection are coupled. We address a promising, but not yet consensus theory of the MJO known as the "moisture mode" hypothesis, as well as other MJO theories, before concluding with a section on efforts to model the MJO.

2.2.1 Basic Features

The main features of the MJO were recognized early in its discovery by Madden and Julian (1972). The schematic shown in Figure 2.7, from Madden and Julian (1972), illustrates many of the key features of the MJO as it moves through a typical life cycle of the oscillation.

The MJO consists broadly of a region of enhanced convection known as its "active phase" and a region of decreased convection called the "suppressed phase". Typically only one suppressed and active phase exist at the same time (Zhang (2005)). Coupled to the convection are circulation anomalies: with regions of enhanced and suppressed convection associated with, respectively, low-level convergence and divergence of zonal wind. The MJO wind pattern at upper levels reverses sign relative to the lower levels.

Other key features of the MJO, some of which can be seen in Figure 2.7, include:

1. **Intraseasonal Timescale:** The MJO tends to oscillate with a timescale of approxi-

mately 30-60 days, though within that time band it shows a good degree of variability. This timescale is uniquely situated between weather timescales of 1-10 days and climate timescales on the order of years, in what is called an intraseasonal or subseasonal window.

2. **Planetary Spatial Scale:** The MJO occupies very large spatial scales. Circulation fields show coherent patterns on the order of tens of thousand of kilometers, whereas the convective signature is more limited, but can still be up to 1000 km in active regions. In this regard, the MJO should not be thought of as a single, self-contained system like a tropical cyclone or squall line, but instead is a systematic change in the mean behavior of convection and winds (among other variables) over large regions, with smaller scale structures embedded in the overall large-scale envelope.

3. **Eastward Propagation:** The MJO is not a standing oscillation like the up-and-down motion of a trampoline, but instead a moving signal which propagates in space. MJO events, whose active phases canonically (but not always) form in the Indian Ocean, propagate eastward at approximately 5 m/s into the West Pacific. There, as the sea-surface temperature decreases to the east, the convective signal dies out, though MJO winds (especially at upper levels) can continue to propagate at faster phase speeds.

These four key elements: (1) the coupling of circulation and convection; (2) the planetary spatial scale, (3) the intraseasonal timescale, and (4) the 5 m/s eastward propagation, form the core signatures of the MJO signal, though they are all inter-connected. Aside from these features, the MJO has many confounding aspects and richer temporal and spatial structure. The MJO influences a host of other variables including moisture, radiation, and the ocean, in ways which (for clarity and brevity) we will only briefly touch on throughout this and subsequent sections.

The MJO wind structure does not solely consist of zonal wind anomalies. The schematic diagram in Figure 2.8, from Zhang (2005), shows the upper and lower tropospheric winds in

an idealized sense relative to the MJO active phase. Note that the overall pattern shows the same reversal with height as the simpler zonal wind schematic in Figure 2.7 – this is a general feature of MJO wind signals. Also evident are off-equatorial structures in the meridional winds, in particular a pair of low-level cyclonic gyres (often called "Rossby wave gyres") to the west of the main convective signals. To the east the gyres are less well-defined both in the schematic and in observed MJO events, though at upper levels can still be pronounced. Instead, the wind to the east of the MJO active phase tends to be primarily easterly at low-levels (sometimes called the "Kelvin-wave response.")[2]

The MJO wind pattern, and its behavior more generally, also display pronounced seasonal differences. Figure 2.9, from Wheeler and Hendon (2004), shows MJO-associated low level winds and outgoing longwave radiation (OLR), a proxy for deep convection in the tropics (lower OLR values correspond to colder cloud top temperatures, or deeper convection). These plots are formed by compositing many years of daily data onto into eight "phases" that define various stages in a typical MJO lifecycle (see Wheeler and Hendon (2004)). In that regard, the panels (read top to bottom in each column) can be thought of as representing time, and are indicative of the mean behavior of the MJO over many individual events.

The left-hand panels are composites of the MJO formed in December through February (DJF), whereas the right panels are May and June events. Evident in both panels is the eastward propagation of MJO signals, but also more nuanced seasonal structure. MJO activity in the tropics tends to follow the sun, such that in DJF MJO activity tends to be just south of the equator. Additionally, more coherent eastward propagation can be seen. The MJO activity in May-June is north of equator, and also has less well-defined eastward propagation, a hint of northward propagation, and a northeast-to-southwest tilt in the convection. This northward propagating and tilted convection seems distinct from the canonical MJO, and do not appear due to aliasing from other signals such as the monsoon. It

[2]Though, memorably for the author, also called "Johnny" once at a summer school lecture given by Dr. Michela Biasutti, for reasons that made sense at the time.

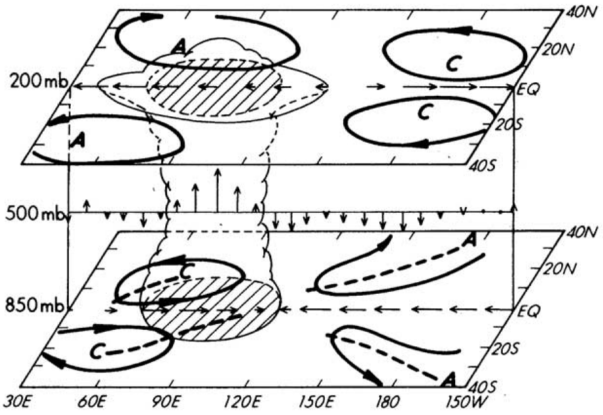

Figure 2.8: From Zhang (2005) Figure 5, a schematic depiction of the MJO wind signals in the troposphere. Clouds indicate the MJO active phase and arrows show wind anomalies at 850 and 200 hPa, as well as vertical velocity at 500 hPa. "A" and "C" correspond to anticyclonic and cyclonic motion, and dashed lines mark pressure troughs and ridges.

is often considered its own feature called the boreal summer intraseasonal oscillation (BSISO; Wang and Rui (1990), Lawrence and Webster (2002)). As a final note on the seasonality of the MJO, in addition to being shifted somewhat to the south in boreal winter the MJO overall is strongest in December-February (Madden (1986); Zhang (2005)). This will be important when discussing the MJO-QBO relationship in Section 2.4.

While the signals discussed thus far are all tropical in nature, the MJO exerts an influence on weather and climate around the world. These wider influences and teleconnections are part of why the MJO has remained a topic of interest for as long as it has, and why MJO predictability is an integral component of skillful subseasonal forecasts. In brief, the MJO has a significant impact on many features of the climate, including but not limited to global rainfall variability (Zhang (2005)), the genesis of tropical cyclones (Maloney and Hartmann (2000); Maloney and Hartmann (2001)), land-falling atmospheric rivers (Guan et al. (2012)), monsoons (Jones and Carvalho (2002), Lavender and Matthews (2009)), and extreme temperature and rain events in the US (Higgins et al. (2000), Riddle et al. (2013), Zhou et al. (2012)). Aside from these well-accepted effects, other MJO impacts are topics of

frequent study, including its purported effects on tornadoes and hailstorms in the mid-west (Tippett (2018)) or whether it influences stratospheric sudden warmings (Garfinkel et al. (2012)). This sampling of MJO impacts, far from being entirely comprehensive, is intended to indicate the degree to which the MJO modulates other features of the climate system, and to underscore its global importance.

Having covered some of the major observed features of the MJO and its impacts, we are now in a position to consider theories of the MJO. To do that, and to help motivate much of what follows, we find it useful to briefly discuss other modes of variability in the tropics which are, at first glance, similar to the MJO: a class of phenomena typically called convectively-coupled tropical waves.

2.2.2 Convectively-Coupled Tropical Waves

Convectively-coupled waves in the tropics organize convection across a wide range of temporal and spatial scales. Different types of these waves propagate eastward and westward with a variety of characteristic wind patterns. For a comprehensive review of these waves, including their history and a much more detailed taxonomy than we will discuss here, see Kiladis et al. (2009).

Matsuno (1966) showed that a variety of tropical waves existed as theoretical solutions to the shallow-water equations on a β-plane, linearized about a state of rest. These equations govern the behavior of an idealized system akin to the atmosphere of Earth's tropics: they describe the motion of fluid of constant density on a Cartesian plane, under gravity and in which Coriolis force is present and varies linearly with latitude about an equator on which it is zero.

Matsuno's wave solutions each have their own characteristic flow patterns, propagation speeds, and time scales. Among these waves are the aforementioned Kelvin and equatorial Rossby waves, which serve as sources of momentum that impact the QBO, though vertical

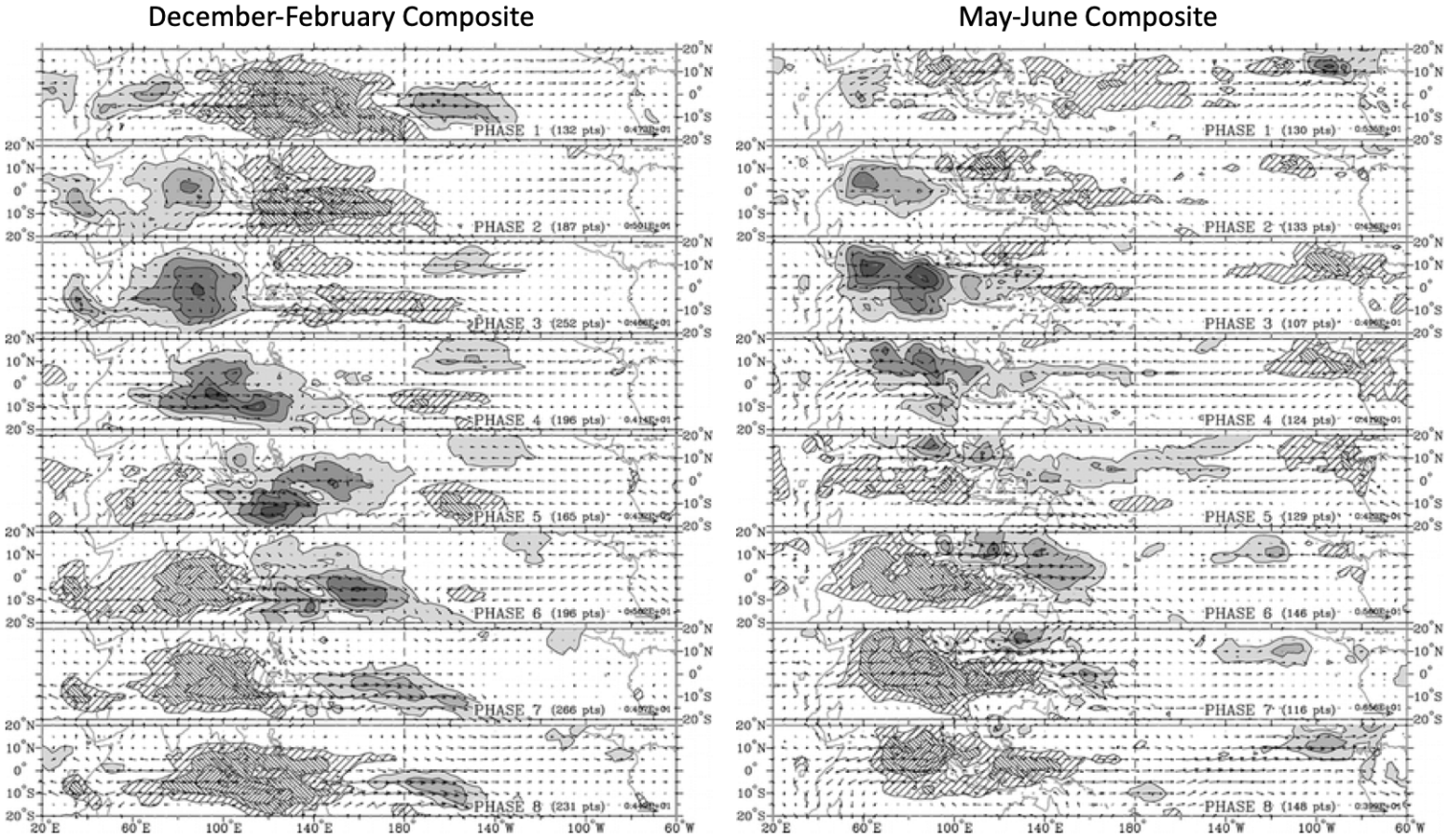

Figure 2.9: Adapted from Wheeler and Hendon (2004) Figures 8 and 9. Panels show composites of the MJO OLR and 850 hPa wind anomalies, as processed for intraseasonal timescales via a method described in Wheeler and Hendon (2004). Each panel corresponds to a phase in the MJO life cycle, defined using the real-time MJO index (RMM; see Wheeler and Hendon (2004) and discussion in Chapters 4, 5, and C.1). Left panels are for December - February data, and right are May-June. Shading levels denote OLR anomalies less than 7.5, 15, 22.5, and 30 W/m^2, respectively, and hatching levels denote OLR anomalies greater than 7.5, 15, and 22.5 W/m^2, respectively. Black arrows indicate wind anomalies that are statistically significant at the 99% level, and the number of days within each phase category is given in each panel.

propagation discussed there was not considered in Matsuno's work.[3] Kelvin waves are similar to the MJO in that they propagate to the east, but they are faster than the MJO, with a phase speed closer to 15 m/s (compared to the 5 m/s of the MJO), and smaller. Rossby waves, in contrast, have a planetary spatial scale similar to the MJO and also move slowly, but propagate west. Both Kelvin and Rossby waves have structures that distinguish them from the MJO, though, as discussed in the preceding section, the MJO wind signal contains characteristics of both of these wave types (e.g. the Rossby gyres and the Kelvin-wave response.) Other types of waves also exist, including mixed Rossby-gravity waves, and eastward and westward propagating intertio-gravity waves.

In a classic paper, Wheeler and Kiladis (1999) combined Matsuno's theory with observational evidence to identify these waves in the tropical troposphere. From a long record of observed OLR over the entire tropics, Wheeler and Kiladis (1999) took a temporal and spatial (in longitude) Fourier transform, and then removed a low-frequency red noise background signal. This allowed them to examine the spatial and temporal variabilty of tropical convection. The resulting plot, now called a Wheeler-Kiladis diagram (see Figure 2.10), shows the spectral power of OLR as a function of wavenumber (i.e. spatial scale) and frequency (i.e. timescale). In Figure 2.10, from their paper, darker regions are areas with more power; the left panel shows anti-symmetric OLR signals about the equator and the right panel is the symmetric component.

Overlain on top of the observed power spectrum in Figure 2.10 are theoretical dispersion curves based on the Matsuno solutions, modified slightly to account for the impact that convection has on these waves. Kelvin waves and Rossby waves ("$n = 1$ ER"), for example, can be seen in the right panel: Rossby waves with low zonal wave numbers from 1-10 moving west (the negative values on the x-axis) and the Kelvin wave at a range of eastward

[3]In fact, Matsuno's theoretical discovery of these waves and subsequent evidence of their existence in observations (Yanai and Maruyama (1966), Maruyama and Yanai (1967)) helped with the development of the theory of the QBO.

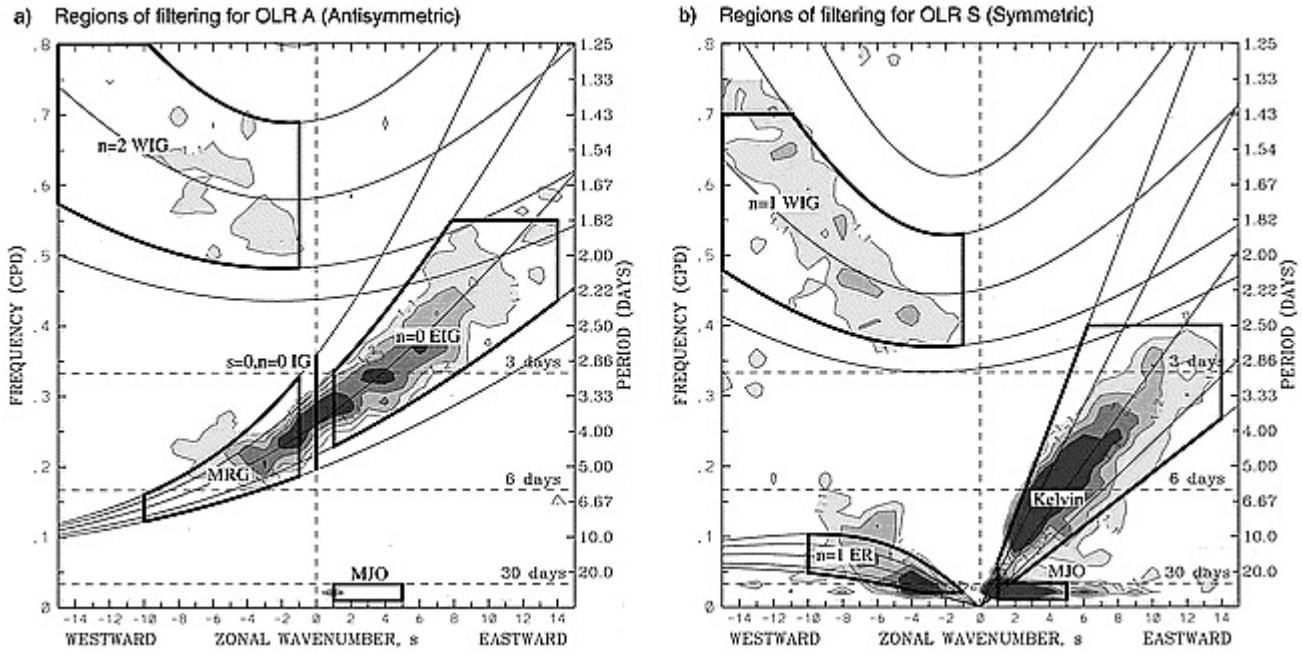

Figure 2.10: From Wheeler and Kiladis (1999) Figure 6, a space-time power spectrum of outgoing longwave radiation in the tropics, with a background red-noise signal removed. The left and right panels are, respectively, the symmetric and antisymmetric components of the data. Contour interval is 0.1, including only those contours between 1.1 (at which point the signals are significant at the 95% level), and 1.4. Thin lines are the theoretical dispersion curves of various tropical wave types, with assumed equivalent depths, h, of 8, 12, 25, 50, and 90 m as discussed in Wheeler and Kiladis (1999). Darker black boxes indicate regions used in Wheeler and Kiladis (1999) to define various types of tropical waves: Kelvin waves, equatorial Rossby waves ($n = 1$ ER), mixed-Rossby gravity waves (MRG) and eastward and westward propagating inertio-gravity waves (E/WIG). Also shown is the MJO band.

propagating wave numbers with a relatively linear relationship between their frequency and wavenumber.

Other wave types, such as the asymmetric mixed Rossby-gravity waves and inertio-gravity waves, can also be seen – remarkably, every type of wave predicted by Matsuno's theory (with appropriate assumptions) appears in the data. One mode stands out as the exception: the MJO, with its intraseasonal period and slow eastward motion, has no theoretical counterpart in Matsuno's theory. Its closest cousin in many regards is the Kelvin wave, but a balance of evidence today suggests rather conclusively that the MJO is not a Kelvin wave for at least portions of its life cycle (e.g. Wheeler and Kiladis (1999); Sobel and Kim (2012)).[4]

Then, what is it? This question remains unanswered; what drives the MJO, sets its scale, makes it move, and explains some of the features set forth above are still unknown. The next section provides an overview of prominent MJO theories, including especially the increasingly popular "moisture mode" hypothesis.

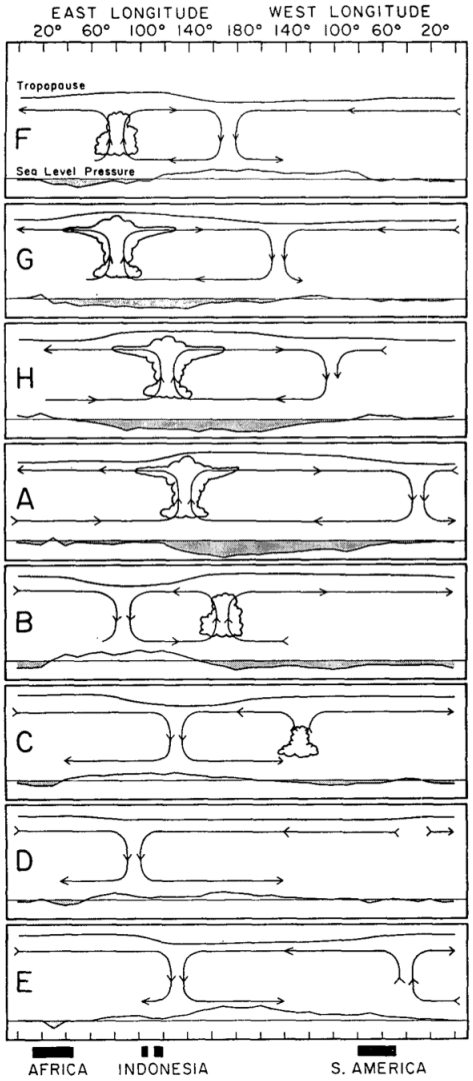

Figure 2.7: From Madden and Julian (1972) Figure 16, a schematic depiction of the height-longitude MJO signals in pressure (x-axis at bottom of each panel), wind (arrows), and convection (clouds) as it moves through its life cycle.

[4]Over the central and eastern Pacific, as the MJO decouples from convection, it more closely results a Kelvin wave.

2.2.3 MJO Theories

2.2.3.1 The Moisture-Mode Theory

In this section we first present a theory of the MJO developed beginning in the late 1990s and early 2000s known as the "moisture mode" theory (Neelin and Yu (1994); Sobel et al. (2001); Fuchs and Raymond (2002); Andersen and Kuang (2012); Sobel and Maloney (2012); Sobel and Maloney (2013); Adames and Kim (2016)). This theory argues to first order that the MJO would not exist in a dry atmosphere. Instead, humidity plays a key role in driving the oscillation, determining its scale, and explaining its propagation characteristics. The MJO can be understood as a mode in which water vapor in the atmosphere interacts with the dynamics and convection. Stated another way, if the MJO is construed as the solution to some system of equations (in the same way that Kelvin or Rossby waves are solutions to the shallow water equations on a β-plane), the moisture mode theory states that those equations must include a prognostic expression for moisture.

In this view, the key variables through which the MJO can be understood are column integrated moisture, or column *moist static energy*: the energy an air parcel has that is conserved under adiabatic ascent and descent, including condensation of water vapor (but neglecting kinetic energy, which is assumed to dissipate into heat and is small except perhaps in the boundary layer; Ma et al. (2015)). The MJO consists of planetary scale regions of anomalously high or low moist static energy which move in time to the east. The processes which lead to the amplification and the propagation of this "moisture wave" can then be understood through the sources, sinks, and tendencies of moist static energy anomalies on intraseasonal timescales.

The moisture mode framework and use of moist static energy budgets as a vehicle to study the MJO are now well-established as tools of great utility in observations (Benedict and Randall (2007), Sobel et al. (2014), Hannah and Maloney (2014)), GCM simulations (Benedict and Randall (2009), Pritchard and Bretherton (2014), Kim et al. (2015)), as well

as simplified modeling frameworks including several mentioned in Subsection 2.2.4 (Sobel and Maloney (2012); Sobel and Maloney (2013); Adames and Kim (2016)). Out of this body of work, current thinking on key aspects of the MJO through the lens of the moisture mode theory can be explained as follows:

1. **MJO Amplification:** The MJO in this theory is amplified through the interaction of clouds and moisture with long-wave radiation; in particular through cloud-radiative feedbacks (Raymond (2001)).

2. **MJO Propagation:** The propagation of the MJO is driven by the horizontal advection of moisture, in particular at low levels. Recent work has shown that meridional advection of the climatological moisture by MJO-associated circulation is likely of special importance (Adames and Kim (2016), Jiang et al. (2018), Kim et al. (2018)).

Of additional importance to moisture mode theories are the role that surface winds play in driving the flux of heat and especially of moisture into the column. The role of such feedbacks between surface winds and latent heat flux, often called wind-induced surface heat exchange (WISHE; Emanuel (1987)), is not entirely settled. Initial theories attempting to explain the MJO entirely through a WISHE framework have generally not been supported by observational studies (see a review in Kim and Maloney (2016)), but this does not rule out WISHE as an important factor in other MJO theories, including the moisture mode theory.

The relevance of the moisture-mode theory to the MJO-QBO relationship will be discussed at several points in this thesis. An appeal of this theory is that it presents a unifying framework that draws together seemingly disparate ideas like cloud-radiative interaction and surface wind-latent heat feedbacks into a coherent system.

2.2.3.2 Other MJO Theories

Many, many alternate theories for the MJO exist. Over the past 40 years, dozens of ideas have been disproven, discarded, or fallen out of favor. Other have endured modeling and observational tests, but have not yet been recognized by the wider community as wholly correct. We touch on some here, but are not entirely comprehensive. Note that much of the theoretical interest in the MJO-QBO relationship is the hope that it may help elucidate, support, or refute particular MJO theories, as any coherent theory of the MJO should be able to explain why the QBO exerts such a large influence on it.

A popular early theory, in particular because of the MJO's eastward movement, contended that the MJO was essentially a Kelvin wave which was somehow modulated, enhanced, and slowed by coupling to deep convection (Lau and Peng (1987); Emanuel (1987), Wang (1988)), though this seems largely to have been disproven in its most straightforward form.

Theories along these lines have highlighted the role of friction in the planetary boundary layer, which can cause moisture convergence, as a key driver of the MJO. This boundary layer convergence then acts to couple Kelvin and Rossby waves (Wang and Rui (1990); Wang (2005); Kang et al. (2013)), leading to what some call a moist coupled Kelvin-Rossby wave theory of the MJO. Related versions of this theory that combine the dynamical and boundary-layer perspective to a moisture framework have also been developed (e.g. Wang et al. (2016a)), in which convective heating, moisture, and boundary layer dynamics all play a role. However, modeling experiments seem to suggest that boundary layer frictional convergence may not be of central important driving the MJO (e.g. Kim et al. (2011a)).

A second school of thought stems from the observation that the MJO is fundamentally a phenomenon that spans many scales. While the main MJO signal is a planetary-scale eastward moving regime, within that the MJO contains smaller mesoscale clusters of convection, clusters of clusters, and synoptic scale motions that propagate both eastward and westward on a variety of short timescales. A category of MJO theories invokes these multi-

scale interactions in various ways: in most of these models, small-scale synoptic waves move moisture, heat, and/or momentum to the larger planetary scales associated with the MJO. The simplest of these models is the so-called "MJO skeleton" (Majda and Biello (2004)) with refinements to that model involving the introduction of stochastic synoptic convection (Majda and Stechmann (2009)). Several other MJO-synoptic wave interaction models have been developed (Wang and Liu (2011); Khouider and Majda (2006); Khouider and Majda (2007)), as have models in which gravity wave feedbacks and interference are key (Yang and Ingersoll (2014)).

A wide range of other theories exist, and have proposed a role for ocean-atmosphere interactions (Liu and Wang (2013)), forcing from the extra-tropics (i.e. driven by baroclinic instability, as opposed to say tropical heating or other phenomena which are confined to the tropics; Liebmann and Hartmann (1984), Straus and Lindzen (2000)), forcing from within the tropics (Yasunari (1979)) or even marine plankton as plausible causes (Gildor et al. (2003)). Still, even in the last 10-15 years, the number of MJO theories under active consideration seems to be decreasing as a few schools of thought, including especially the moisture mode theory, have gained traction. More work needs to be done to formalize and convincingly demonstrate the utility of these theories, and to continue to reconcile them. In this regard, modeling studies – from the simple to the complex – will be key in guiding and examining theoretical hypotheses. The general performance of the MJO in models is the final topic of this section.

2.2.4 A Brief Modeling Overview

2.2.4.1 Simple Models

Simple models of the MJO are closely linked and in some sense inseparable from MJO theory, as most theoretical studies are inevitably accompanied by minimal models that make them explicit. Usually these take the form of either a system of equations that can be

solved analytically, or a handful of PDEs (often linear or quasi-linear) that can be solved numerically. For example, several simple moisture mode models exist which encode and demonstrate the key features of that hypothesis (Sobel and Maloney (2012), Sobel and Maloney (2013), Adames and Kim (2016)). Such simple models will remain the backbone of MJO theory, and similar to the 1-D models of the QBO by Holton and Lindzen (1972) and Plumb (1977), they will be key for explaining what fundamentally the MJO is.

One simple model that deserves special mention however, despite not being a model of the MJO per se, is the so-called Gill model. The Gill model, named after its developer A.E. Gill, was set forth in a classic 1980 paper (Gill (1980); see also earlier work by Webster (1972)). Gill there considers the question of how the circulation of the tropics responds to a diabatic heating – for example due to persistent latent heat release from convection. In that sense, because the MJO is a mode in which convection and circulation are coupled, the connection of the MJO to Gill's work is straight-forward.

Gill's model was a linear model that solved the linearized shallow water equations on a β-plane of the same type as Matsuno (1966). Gill was able to show that (assuming an imposed heating anomaly of a particular vertical and horizontal structure, as well as making assumptions about heat and momentum damping) that this model could be solved analytically for a circulation pattern that would develop in steady state, provided the heating anomaly were fixed in space and time.

The solution Gill found is shown in Figure 2.11; here the heating (not shown) has been applied symmetrically about the equator with a center at $(0, 0)$; the arrows denote the circulation at lower levels (the upper level winds by construction have the opposite sign) and the contours are the pressure.

The response is notably similar to the MJO schematic in Figure 2.8, as well as to certain phases in Figure 2.9 (though there off-equatorial heating is more accurate; Gill (1980) also demonstrated solutions to heating patterns of that type in his work). In particular, the Gill wind pattern shows the same Rossby wave response to the west and Kelvin wave response

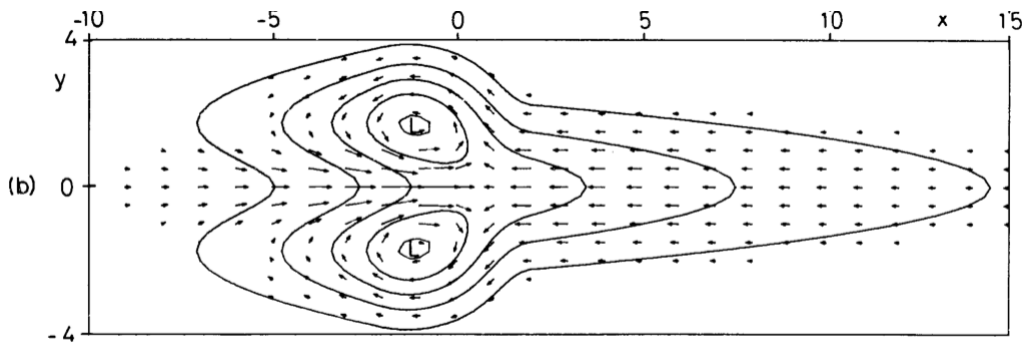

Figure 2.11: Adapted from Gill (1980) Figure 1, the circulation response to induced diabatic heating in an idealized shallow-water configuration, as a function of (nondimensionalized) latitude and longitude. Here symmetric heating is applied about the equator centered at $(0, 0)$ and occupying in the region $|x| < 2$ as described more in Gill (1980). Contours show negative perturbation pressure (interval: 0.3) with circulation shown in arrows representative of the low-level flow.

to the east as the MJO – many simple models (e.g. Sobel and Maloney (2012); Sobel and Maloney (2013), Adames and Kim (2016)) consider the MJO circulation to be essentially Gill-like in some regard. Still, Gill's model characterises the *response* of the wind to an imposed heating: it does not explain how that heating arises, what sets its scale, or contain any insights into its propagation. For that, additional complexity is needed.

2.2.4.2 Comprehensive Models

The representation of the MJO in more complex models is, like representation of the QBO, a difficult task. In this section we focus on comprehensive global models, but the MJO is studied in many intermediate types of models (for example the model presented in Chapter 3) which are also highly intricate and complex, but not fully comprehensive global models like this in Chapters 4 or 5.

The lack of a cohesive MJO theory has made modeling advancements of the MJO somewhat haphazard, as it is difficult to know which features of the model cause deficient representation, or why a particular change improves the MJO. Two MJO features in particular that models have struggled to represent are its strength (it tends to be too weak in models;

Zhang (2005)) and its propagation (it tends not to propagate, especially around the Maritime Continent (Inness and Slingo (2003)), or to propagate too fast; Ahn et al. (2017)).

Complicating matters, features that improve the MJO in comprehensive models, such as changes to the convection scheme, often deteriorate the mean state of the climate. This "MJO-mean state tradeoff" (Kim et al. (2011b)) underscores the lack of a strong theoretical underpinning for the MJO and mean climate of the tropics, and often forces modeling centers to make difficult decisions about what to prioritize, typically, though understandably, to the detriment of simulation of the MJO.

Despite these issues, progress has been made improving the MJO in models. Slingo et al. (1996) showed in the first Atmospheric Model Intercomparison project (AMIP I; Gates (1992)) that all GCMs that showed some form of an MJO were too weak and too fast. Models also failed to capture any MJO seasonality (Slingo et al. (1996)). The CMIP3 models showed some improvement, in particular with regards to the eastward propagation of large-scale convective anomalies that formed in the Indian ocean (Sperber and Annamalai (2008)), but those models struggled to extend the propagation into the West Pacific. CMIP5 models were improved over CMIP3 (Hung et al. (2013)) but still showed large amplitude and propagation biases relative to observations (Ahn et al. (2017)). Early results indicate that CMIP6 models are better still than their CMIP5 counterparts, in particular with regards to MJO propagation (Ahn et al. (2020)).

Key improvements in models' represention the MJO are due to changes in aspects of the convective parameterization. As a general rule, models tend to display deep convection that triggers too frequently in the tropics. Changes to the convection scheme that inhibit this too-frequent triggering tend to improve the MJO (Kim et al. (2012); Benedict et al. (2013); Kim and Maloney (2016)). Atmosphere-ocean coupling in models also generally improves representation of the MJO (Waliser et al. (1999b); Klingaman and Woolnough (2014)), but frustratingly not always (Hendon (2000); Liess et al. (2004)). Other sensitivities have also been explored with somewhat equivocal results on what, if anything, leads to systematic MJO

improvements, including the horizontal and vertical resolution, the treatment of boundary layer closure, and cloud radiative interactions. Results still seem model dependent, marginal, or unconstrained by a clear theory, and no "silver bullet" has been found that guarantees that a model will faithfully simulate the MJO (see a review by Lau et al. (2012)).

One area in which significant progress modeling the MJO has been made is in forecast models. In the context of the MJO, these are global models very similar to free-running GCMs, but initialized from observations and usually run at higher resolution for shorter periods. Such models are optimized to predict weather on the timescale ranging from weeks to around a year. Because the MJO is one of the greatest sources of intraseasonal variability and predictability in the climate system, on the subseasonal timescale many forecast model developers have invested time and resources into making skillful MJO predictions.

Up to the early 2000s, the most skillful forecast models of the MJO tended to be so-called "empirical" or "statistical" models, distinct from dynamical models in that they do not integrate fluid dynamical equations, but instead rely on statistical methods such as linear regression to predict features of the MJO. Early empirical MJO models (von Storch and Xu (1990), Waliser et al. (1999a)) tended to show skill out to approximately 2 weeks predicting MJO related velocity potential or OLR. A number of empirical MJO forecast models proliferated in the early 2000s; reviews and comparisons by Kang and Kim (2010) and Waliser (2005) describe many such models and generally showed that the MJO was predictable in some sense out to at most 3 weeks.

By the early 2010s, the landscape began to change as dynamical models were run at higher resolution, included air-sea coupling and better data assimilation, and as modelers began to focus their attention more on MJO prediction. These dynamical models began to catch up to, and then surpass, their empirical counterparts (see a review in Kim et al. (2018)). Figure 2.12, from Kim et al. (2018), shows the improvement in the European Centre for Medium-Range Weather Forecasting (ECMWF) forecast model as a function of time: the y-axis shows the number of days over which the MJO has skill with various curves denoting

various thresholds of how skill is defined (see. Kim et al. (2018) or Chapter 4 for more discussion of how MJO skill is measured). Evident here is a steady rise in skill on the order of approximately 1 day of lead time per year, such that over the last 15 years MJO skill in this model has improved by approximately 2 weeks. Today, cutting-edge dynamical models, including the model discussed in Chapter 4, have MJO skill greater than 30 days, though biases to amplitude and propagation through the Maritime Continent still persist, even in skillful models (Kim et al. (2018)).

Simulation and prediction of the MJO in recent decades have also benefited from more multi-model efforts in MJO prediction, in which many forecast models are compared and combined to make an ensemble-mean, multi-model mean forecast. These include the recent S2S project (Vitart et al. (2017)) and others (like the Subseasonal Experiment (SubX; Pegion et al. (2019)) and the North-American MultiModel Ensemble (NMME; Kirtman et al. (2014))). In these multi-model, dynamical, state-of-the-art forecasts, MJO predictability has been found to be as high as 6-7 weeks (Kim et al. (2018)). It remains to be seen whether, with the rise of machine-learning techniques and related non-linear methods, empirical prediction may be able to once again overtake dynamical MJO prediction (for an example involving ENSO prediction, see Ham et al. (2019)).

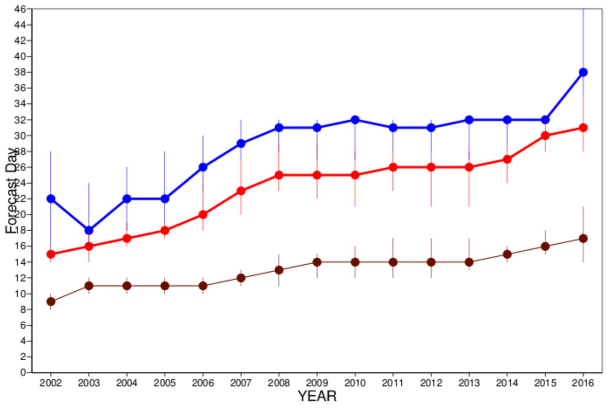

Figure 2.12: From Kim et al. (2018) Figure 3, the evolution of the MJO skill scores since 2002 in ECMWF hindcasts (measured using the RMM bivariate correlations; see Kim et al. (2018) or Eqn. 4.4 and Chapter 4 for more discussion). The MJO skill scores have been computed on the ensemble mean of the ECMWF hindcasts produced during a complete year. The blue, red, and brown lines indicate the day when the MJO bivariate correlation reaches 0.5, 0.6, and 0.8, respectively.

The MJO has stimulated decades of study and thousands of papers, because of its global teleconnections, the lack of a unified theory, and its central role in subseasonal variability

and prediction. Recent decades in particular have shown exciting and promising advances in MJO theory and modeling, but much work remains to be done. Continued advancements stand to have long-lasting scientific and societal benefits. In particular, any process that strongly affects the MJO may offer insights into more fundamental theories of the oscillation. In seeking processes central to modulating the MJO, scientists over the years considered many other modes of variability, from ENSO (Hendon et al. (1999)) to climate change (Maloney et al. (2019)), without finding strong connections. It wasn't until very recently, when scientists turned their eyes higher than many thought should matter, that a connection to the MJO emerged in the stratosphere.

To understand the nature of that connection, we turn now to the history of stratosphere-troposphere interaction, especially in the tropics, and then discuss the relationship between the MJO and the QBO.

2.3 Tropical Stratosphere-Troposphere Interactions

The general field of stratosphere-troposphere interactions is broad and full treatment would be book-length, such that our review here will be by necessity partial and cursory. The ways in which the troposphere and stratosphere interact with one another occur through many pathways and mechanisms across a range of timescales. Interactions can be top-down, bottom-up, or two-way, and can occur through dynamic, thermodynamic, and chemical interactions and processes. They can be local (e.g., the tropical stratosphere affecting the tropical troposphere), or remote (like an upward impact from the tropical troposphere to the polar stratosphere). It comes as little surprise, given the rich dynamical and convective variability in the troposphere and it's much larger mass than the stratosphere, that tropospheric processes might exert an upward influence on the stratosphere. In contrast, the downward impact of the middle atmosphere on tropospheric weather and climate is more difficult to detect and understand.

In the first subsection, we discuss some (but by no means all) ways in which the stratosphere and troposphere are or might be coupled. Some of these include QBO effects, but others are unrelated to the QBO. Much is uncertain, as this field is relatively young and more modeling work, data, and observational analysis is needed.

In the second subsection, we look specifically at the literature surrounding the QBO impacts on the tropical troposphere, which brings us nicely to the paradigm shift in this area which has spurred renewed interest in stratosphere-troposphere interactions: the MJO-QBO relationship.

2.3.1 General Pathways of Influence

That the troposphere impacts the stratosphere has been widely accepted in atmospheric science for some time, especially in the field of tropical meteorology where the explanation of the QBO was centered on the theory of tropospheric tropical waves and their upward propagation. Aside from the QBO, the broader dynamical theory of how vertically propagating waves from the troposphere move through and break in the stratosphere is a well-accepted and studied subfield of stratosphere-troposphere interactions. This dynamical coupling of the troposphere and stratosphere is also not limited to the QBO or the tropics. For example, upward wave propagation of planetary scale Rossby waves into the stratosphere is key in influencing the stratospheric polar vortex (Matsuno (1971); Waugh et al. (2017)). In particular, this wave interaction is important in driving sudden-stratospheric warmings (SSWs): winter-time events characterized by a breakdown in the vortex and accompanied by swift changes in the temperature of the polar stratosphere (Charlton and Polvani (2007)). Some evidence even indicates that waves associated with the MJO could impact SSWs (Garfinkel et al. (2012), Kang and Tziperman (2018)).

The troposphere is also understood to be important in setting the water budget of the stratosphere. The stratosphere is incredibly dry, and early studies struggled to explain this lack of water vapor until Brewer (1949) claimed that the only explanation for the dryness

of the stratosphere is that most stratospheric air enters through the tropical tropopause. This region of the atmosphere is incredibly cold, and thus acts to "freeze dry" ascending air by condensing out most of the water (though the details of this dehydration are still incompletely understood; Holton and Gettelman (2001), Jensen et al. (2013)). This work and other tracer measurements (Dobson et al. (1929), Dobson (1956)) led to the discovery of the planetary meridional overturning mass circulation that extends from the troposphere up into the stratosphere, known as the Brewer-Dobson circulation (Butchart (2014)). It further laid the groundwork for another area in the field of stratosphere-troposphere interactions, which is the transport and exchange of chemical substances and air between these two layer of the atmosphere (Holton et al. (1995)).

In these theories, the stratosphere is largely a passive player, or the beneficiary of the dynamical or chemical richness coming up out of the troposphere. That the stratosphere might exert a downward impact was less well-studied, though as recent results demonstrate (Sect. 2.4) it is a field which is still quite relevant. One major caveat to this often-stated paradigm, and a way in which the stratosphere largely entered the public awareness, was the role that stratospheric ozone plays in Earth's climate, and the depletion of stratospheric ozone that led to the ozone hole (Solomon (1999)). In particular, the importance of the stratospheric polar vortex on ozone depletion led to a flourishing of research on the stratosphere in the 1980s and 1990s, and demonstrated that the stratosphere indeed had a key role to play in Earth's climate system with major implications for human society and health. Global treaties and regulation of chlorofluorocarbons under the Montreal Protocol have limited and, by most metrics, begun to reverse stratospheric ozone depletion in recent decades (Newchurch et al. (2003); Chipperfield et al. (2017)), but this topic serves as an early example of the importance that stratospheric processes can have on the troposphere.

In addition to the importance of chemical species in stratosphere, another important work that showed that the stratosphere could have an impact on the troposphere was that of Baldwin and Dunkerton (2001). Their study showed that the stratospheric polar vortex

could exert a significant influence on the tropospheric jets and the surface climate.

Figure 2.13, from Baldwin and Dunkerton (2001), shows a time-height view of the Northern Annular Mode index (the lead EOF pattern at each pressure level formed after 90-day low-pass filtering) composited over many strong and weak stratospheric vortex events during November-April. Note that, while the main signals at lag 0 are, by construction, in the stratosphere, at later lead times signals propagate down into the troposphere. These "dripping paint" diagrams are among the first and still most striking examples of how the stratosphere can influence lower levels, as the downward impacts evident in Figure 2.13 can cause extreme weather as far down as the surface despite having their origins in the stratosphere. Impacts of the polar stratosphere on tropospheric climate are now broadly accepted as robust features of the climate system (Baldwin and Dunkerton (2001); Polvani and Kushner (2002); Shepherd (2002); Simpson et al. (2009); Waugh et al. (2017)).

This body of work shows strong evidence of stratosphere-troposphere coupling in the extratropics driven by polar stratospheric processes. But can the tropical stratosphere, and the QBO in particular, exert an influence on the troposphere? This is the question we address in the next subsection.

2.3.2 QBO Impacts on the Tropical Troposphere

There are several ways the QBO could impact the troposphere. These pathways falls into three categories:

1. **A polar route:** The QBO is known to impact the planetary waves that modulate the stratospheric polar vortex, and both these waves and the vortex have impacts on the surface climate (per Section 2.3.1). Thus, the QBO may impact the troposphere through an impact on the polar vortex.

2. **A mid-latitude route:** It has been hypothesized that the QBO can modulate the strength and position of the mid-latitude jets, especially over the Pacific. Changes

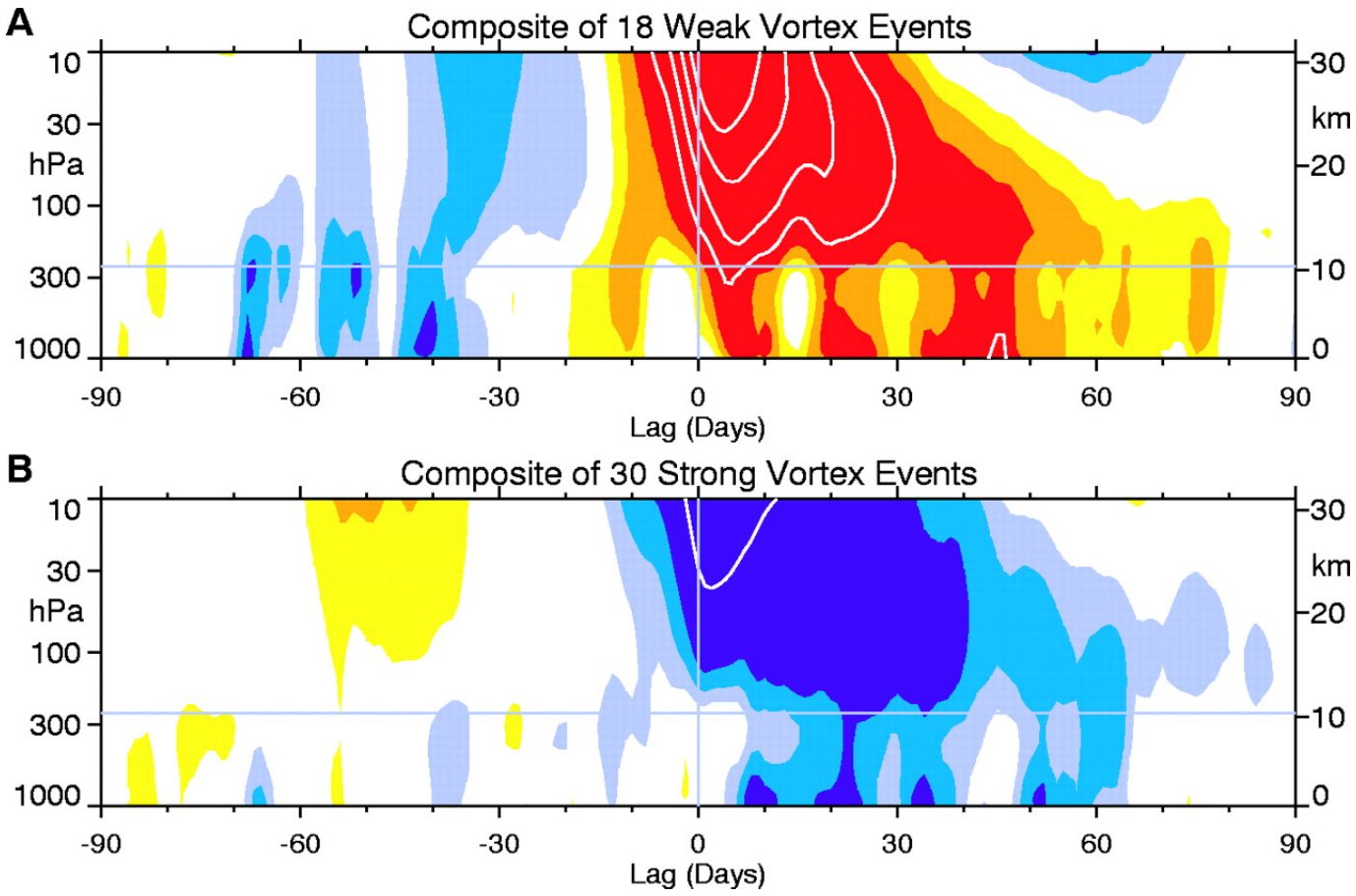

Figure 2.13: From Baldwin and Dunkerton (2001) Figure 2, showing composites of time-height development of the northern annular mode for (A; top) weak stratospheric polar vortex events and (B; bottom) strong vortex events. The events are determined by the dates on which the 10-hPa annular mode values cross -3.0 and $+1.5$, respectively (see Baldwin and Dunkerton (2001) or the text for a more discussion of annular modes.) The indices are non-dimensional; the contour interval for the color shading is 0.25, and 0.5 for the white contours. Values between -0.25 and 0.25 are unshaded. The thin horizontal lines indicate the approximate boundary between the troposphere and the stratosphere.

to jets may affect any number of elements of the climate system, ranging from tropical teleconnections to atmospheric rivers, and therefore constitute a second pathway through which the QBO might affect the troposphere.

3. **A tropical route:** The largest stratospheric QBO signals exist in the tropics, including temperature and wind signals which extend down to near the tropopause. It is therefore possible that these or related anomalies could directly affect the tropical troposphere.

The general features of these three pathways are nicely summarized by Gray et al. (2018), and are laid out in schematic form in Figure 2.14. There the various colored arrows represent the different routes of influence as sketched out above, along with important features of each pathway.

Of course, distinctions between these three pathways are somewhat artificial, and the inter-connectedness of the climate system means that these pathways are far from independent (QBO changes in the tropical tropopause could, for example, changes teleconnections at the poles or in the subtropics). Still, it is a useful framing for reviewing the literature on this topic, and takes into account pathways which to first order seem relatively distinct from one another.

2.3.2.1 QBO-Polar Impacts

The most well-known and studied way in which the QBO affects the surface is via a polar route. In a pair of papers, Holton and Tan (Holton and Tan (1980); Holton and Tan (1982)) showed that the QBO winds act to modulate the large-scale planetary waves which propagate through the stratosphere. When QBO winds are westerly, planetary waves (and in particular Rossby waves) can move equatorward, and tend to have a limited impact on the polar vortex. During QBOW, the polar vortex remains relatively strong and undisturbed. In contrast, when QBO winds are easterly these Rossby waves cannot propagate through the equatorial stratosphere, and propagation tends to increase in the poleward direction. The

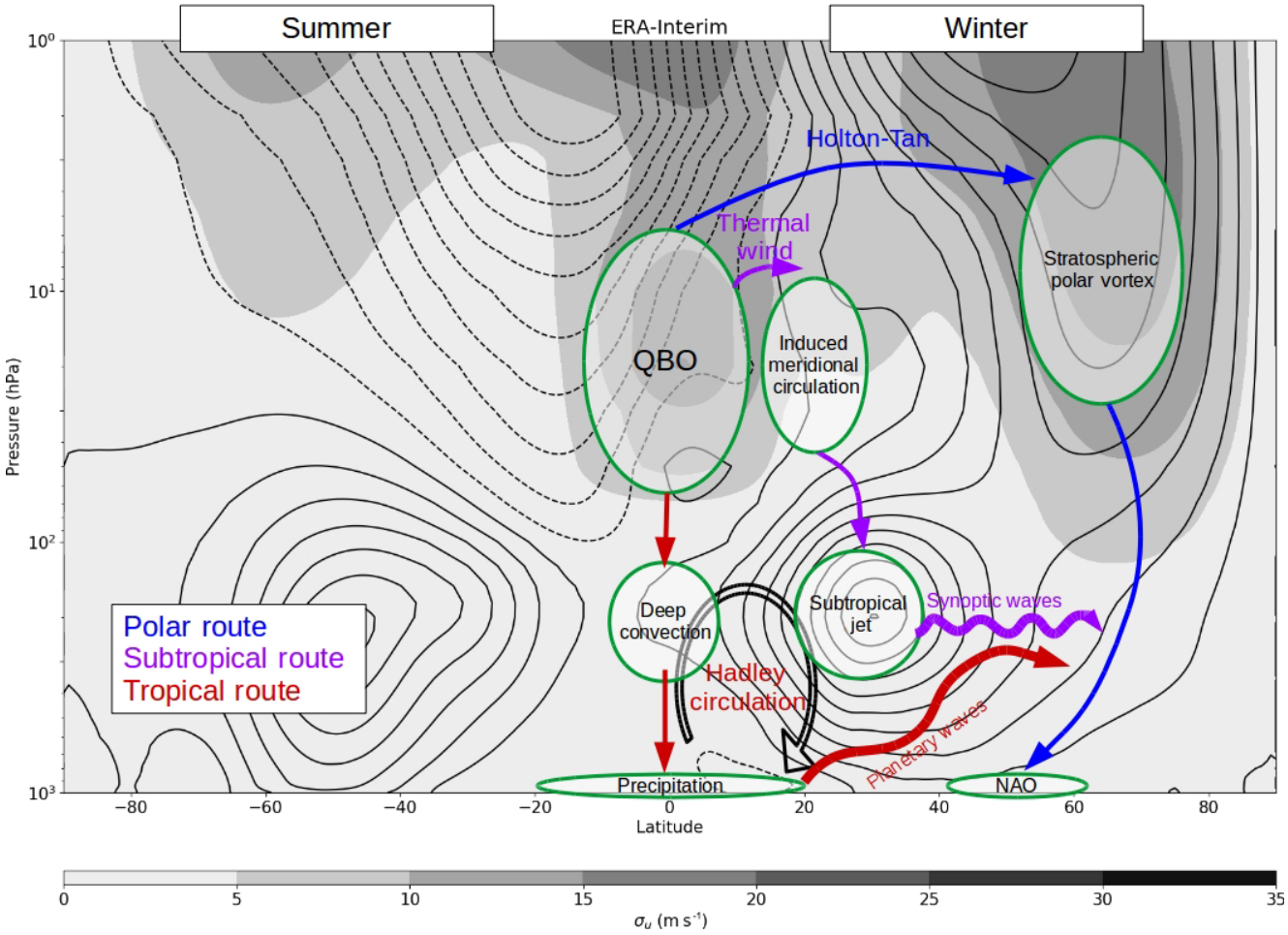

Figure 2.14: From Gray et al. (2018) Figure 1, a schematic summarizing the three primary routes (tropical, subtropical, polar) through which the QBO might influence the troposphere. Contours show the DJF averaged, zonally averaged zonal winds for 1979–2016 from ERA-Interim (interval is 5 m/s; solid and dashed contours denote westerlies and easterlies respectively). Grey-scale shows the standard deviation of the zonal winds in m/s.

waves can then influence the vortex, such that in QBOE the polar vortex is weaker and more frequently disrupted. This process, which operates primarily in boreal winter, is now known as the Holton-Tan relationship.

The Holton-Tan relationship has been found to be more complex than the description above suggests. One straightforward issue is that the QBO winds descend and vary with height, such that at any given point there are both easterly and westerly regions of the equatorial stratosphere. Further, the Holton-Tan effect is sensitive to the precise definition of the polar vortex, seems to show robust modulation by the 11-year solar cycle (Labitzke and Loon (1988)), and displays a seasonality that simple theory does not entirely explain (e.g. Lu et al. (2014)). Still, the Holton-Tan relationship, combined with the findings of Baldwin and Dunkerton (2001) suggest the possibility of a QBO impact on surface climate via the poles. The QBO changes the vortex, making SSWs and disruptions more or less likely, and that influence gets communicated, albeit via a somewhat indirect pathway, to the ground via the changes to the Northern Annular Mode (Boer and Hamilton (2008); Gray et al. (2018)).

2.3.2.2 QBO-Subtropical Impacts

Less work has been done on QBO impacts on the subtropics. However, several recent results have demonstrated the ability of the QBO to modulate extratropical features of the climate in the troposphere. In particular, it has been shown in several studies that the QBO winds, while having peaks in the tropical stratosphere, display a "horse-shoe" like pattern in which anomalies can extend down into the subtropical troposphere and influence the subtropical jets. (Haigh et al. (2005); Simpson et al. (2009); Garfinkel and Hartmann (2011a); Gray et al. (2018)).

During the easterly phase of the QBO relative to the westerly, the subtropical jet tends to be weaker, and does not extend as far to the east especially across the Pacific. Early work by Haigh et al. (2005), who were considering lower-stratospheric heating associated

with the 11-year solar cycle and volcanoes, found that heating in the lower stratosphere in observations and a simplified GCM impacted the position and strength of the subtropical jet. Simpson et al. (2009) also found that imposition of a stratospheric heating tended to shift the subtropical jets poleward, and argued that eddy fluxes and feedbacks with the mean flow were important. Garfinkel and Hartmann (2011a) carried out a study in both reanalysis and model simulations showing that during easterly QBO periods relative to westerly ones, the subtropical jet tended to be weaker, especially in late winter and late fall. They found that this response was strongest around the jet-exit region in the Pacific. Gray et al. (2018) further found evidence of a QBO modulation of the jet, especially in winter and over the North Pacific, and while they couldn't identify a mechanism, they did show that it was unlikely that these impacts stemmed from polar regions.

QBO-driven changes to the subtropical jet could have a host of important tropospheric effects, including modulation of the storm tracks (Ho et al. (2009)) and of tropical teleconnection patterns (Feng and Lin (2019)). Yet, while this work is suggestive, no entirely satisfactory mechanism has been proposed. Dynamical arguments have involved changes in the Brewer-Dobson circulation induced by the QBO, effects of the QBO meridional circulation (Gray et al. (2018)), or eddy fluxes (Simpson et al. (2009); Garfinkel and Hartmann (2011a)) but uncertainty remains. Further confounding attempts to study this impact, these apparent subtropical impacts might be linked to direct QBO changes in the tropics (Gray et al. (2018)).

2.3.2.3 Direct QBO Impacts in the Tropics

The direct impact of the QBO in the tropics has the most bearing on the MJO-QBO relationship discussed in the next section. Prevailing thinking, at least into the early 2000s, was that QBO anomalies did not penetrate far enough down into the troposphere to impact convection directly (e.g. Baldwin et al. (2001)). Further, around that time there was only limited evidence of a strong connection between the QBO and most tropical phenomena.

Perhaps the earliest work showing an apparent impact of the QBO on the tropical troposphere examined whether the QBO affects tropical cyclones (TCs). The QBO impact on TCs was first pointed out by Gray in two 1984 papers (Gray (1984a); Gray (1984b)) in which they found that during westerly QBO periods Atlantic hurricane activity was stronger compared to QBOE periods. This spawned a series of papers that examined the QBO impact on tropical cyclones during the next fifteen years (see a brief review of this literature in Camargo and Sobel (2010)), and the QBO was even used as a predictor in seasonal Atlantic hurricane forecasts developed at Colorado State University through the late 2000s (Klotzbach (2007a), Klotzbach (2007b)).

The mechanism of this modulation was unclear despite its apparent statistical significance, and a substantial advancement on this QBO-TC connection was not forthcoming until Camargo and Sobel (2010) showed, somewhat puzzlingly, that the observed relationship discovered by Gray in the 1980s was no longer significant in a longer record into the 2000s. Figure 2.15, from Camargo and Sobel (2010), shows the correlation between the QBO and various metrics of tropical cyclone activity for a running 30-year period, with filled bars showing significance. Evident across all metrics considered is a decreasing correlation between the QBO and TCs, which ceases to be significant around the mid-nineties.

Camargo and Sobel (2010) examined ENSO, decadal variability, solar cycle impacts, and volcanic activity, but were unable to conclusively show why the QBO-TC relationship vanished. They did note, however, that fully disentangling QBO and ENSO signals is somewhat difficult.

The QBO-ENSO relationship, like the QBO-TC link, has been a topic of research for some time. Studies have considered both the downward impact of the QBO on ENSO, and the possibility that ENSO could modulate the QBO through changing the strength, location, or character of upwelling waves. As we shall see, this research has been inconclusive, and there does not appear to be a strong physical relationship between these two phenomena.

Early QBO-ENSO studies were hampered by relatively short data records (given the

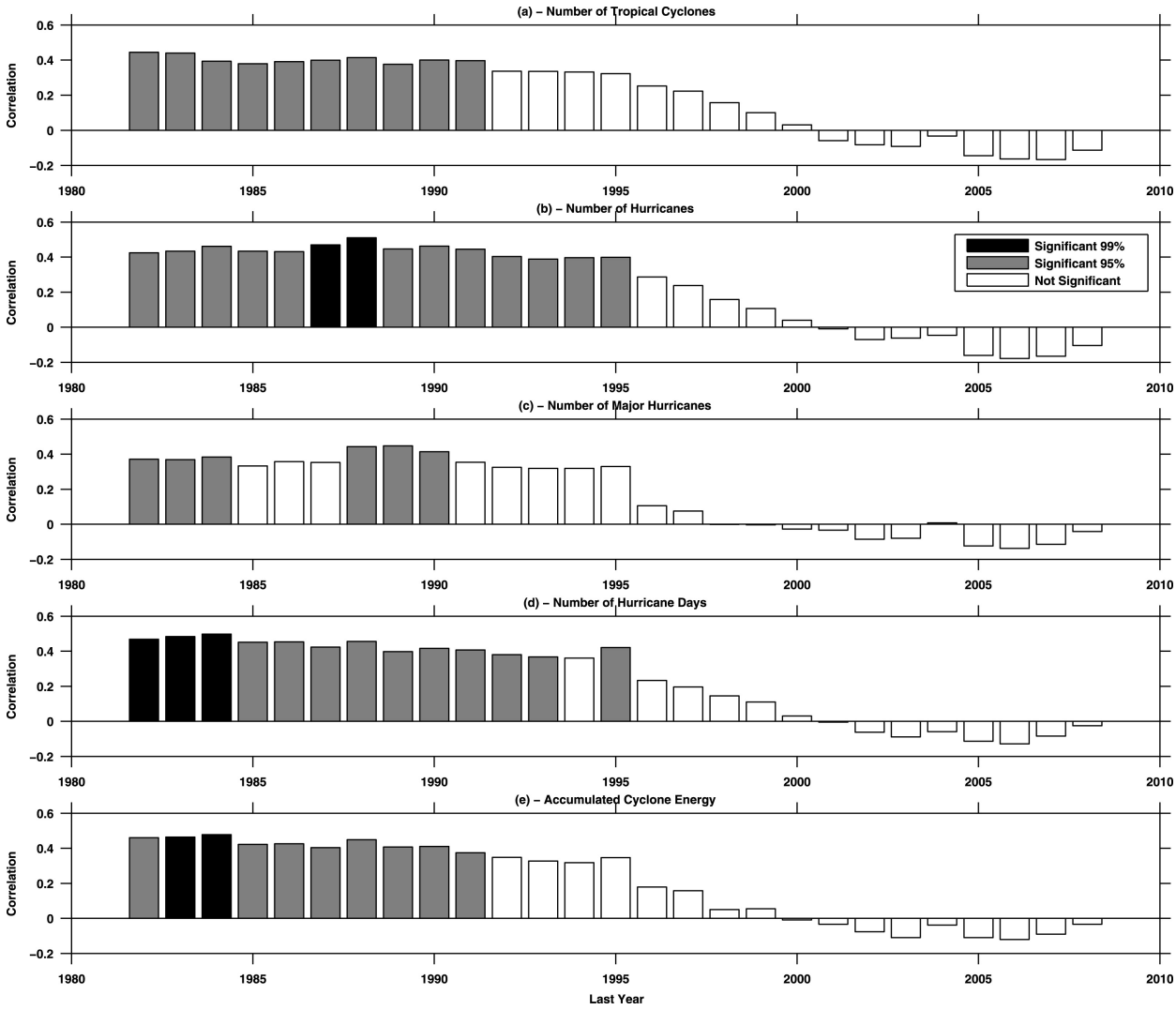

Figure 2.15: From Camargo and Sobel (2010) Figure 3, showing running 30-year correlations of a 30 hPa QBO index with (a) number of tropical cyclones, (b) number of hurricanes, (c) number of major hurricanes, (d) number of hurricane days, and (e) accumulated cyclone energy. The first correlation (first bar) is calculated for the period 1953–82, the subsequent one is calculated for the next 30-yr period (1954–83), and so on until in the last bar the last 30 yr are considered (1979–2008). The x-axis shows the last year that was included in the calculation. The statistical significance is calculated by bootstrap; for more information about the TC data see Camargo and Sobel (2010).

interannual nature of these phenomena) that made the statistics difficult and led to mainly weak conclusions. (Wallace and Chang (1982); Quiroz (1983); van Loon and Labitzke (1987); Barnston et al. (1991)). Gray et al. (Gray et al. (1992a); Gray et al. (1992b)) described a mechanism by which the QBO could impact the timing of ENSO events through wind shear (see below), but their mechanistic argument was not comprehensive nor strongly supported by data. More recently, Garfinkel and Hartmann (2007) showed no QBO-ENSO correlation in a long reanalysis record from 1957 to 2007. However, through dividing the record in half they demonstrated that the QBO and ENSO were negatively correlated during the early period and positively correlated over the later period, a result reminiscent of Camargo and Sobel (2010). Christiansen et al. (2016) reexamined the problem and found, consistently with Garfinkel and Hartmann (2007), that over the whole of the observed records there was not a strong link between the QBO and El Niño.

In terms of an upward effect of ENSO on the QBO, the results are also inconclusive. Taguchi (2010) found that the QBO has a larger amplitude and longer period during La Niña episodes, a result which was confirmed using additional data by Yuan et al. (2014). However, Geller et al. (2016) demonstrated, again channeling Garfinkel and Hartmann (2007) and Camargo and Sobel (2010), that these signals change on longer timescales and seemed evident only since the 1990s. Christiansen et al. (2016) also considered the upward impact, and they contended based on reviewing other results and their own updated analysis that no strong, linear relationship existed.

The current consensus seems to be clear that the QBO does not exert a strong downward influence on ENSO and ENSO does not have a first order impact on the QBO (Domeisen et al. (2019)). This of course does not preclude non-linear links or the possibility that in some cases the stratosphere and ENSO interact. The possibility that very large ENSO events could impact the stratosphere has been suggested (Christiansen et al. (2016)), and further recent scholarship has theorized that an unexpected disruption of the QBO in 2016 (Osprey

et al. (2016))[5] could be linked to the strong 2015/6 El Niño (Barton and McCormack (2017)).

Even without a strong or significant relationship between the QBO and ENSO, there may still be overlap between QBO and ENSO signals due to chance. Over much of the observed period, QBOW winters tend to correspond to La Niña periods (Garfinkel and Hartmann (2011b)). While possibly coincidental, this requires that studies of the QBO (especially in boreal winter) remove possible ENSO influences or possible contamination from any results whenever possible.

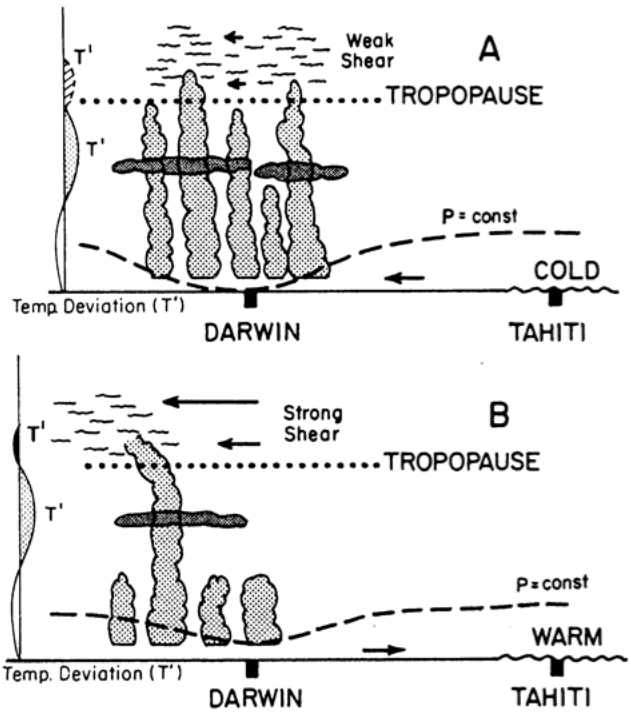

Figure 2.16: From Gray et al. (1992b), showing a conceptual illustration of how QBO wind shear might lead to a displacement of the tops of deep off-equator convective storms penetrating the lower stratosphere. The lower panel is QBOE, and the upper is QBOW. The difference in lower stratospheric temperature anomalies for the two modes is indicated as T' (left side of the panels) and the anomalous pressure values at Darwin and Tahiti are also indicated. As noted in Gray et al. (1992b): "a conceptual qualitative representation rather than precise difference values is intended."

Aside from the QBO-TC and QBO-ENSO connections, additional studies have considered the QBO's impact on tropical deep convection more generally. Naturally, there is some overlap between the literature on QBO-ENSO and QBO-convection links, as El Niño modulates convection over large swaths of the tropics. Perhaps the earliest in-depth study of the capacity of the QBO to have a direct impact on the tropical mean state was carried out by Yasunari (1989), who found QBO signals in the wind at 200 and 700 hPa at several tropical radiosonde

[5]The lower stratospheric westerly flow was interrupted by formation of an easterly jet around February 2016.

sites, especially those in the Maritime Continent and West Pacific. They hypothesized that their findings could indicate a QBO on impact convection, though did not speculate with regards any mechanism.

The first description of a detailed mechanism for a QBO impact on deep convection was put forth by Gray et al. (Gray et al. (1992a); Gray et al. (1992b)) in a pair of papers speculating that the QBO could change the distribution of deep convection. They pointed to both QBO temperature anomalies and vertical wind shear as ways in which the QBO could alter convection. In particular they described in detail (though without convincing data to support their hypothesis) how, in theory, altering the vertical structure of the wind and/or shearing off overshooting clouds might impact convection. A schematic from their work on this mechanism is shown in Fig. 2.16.

The topic was further studied by John Knaff in 1993, whose Master's thesis at Colorado State University centered on the QBO modulation of deep convection (Knaff (1993)). Knaff contended that the QBO could modulate deep convection over the warm pool region, and found QBO signals in precipitation, OLR, and cloud brightness over the warm pool during December-February, with enhanced precipitation on the equator during QBOE. Knaff found weaker signals in other seasons. He attributed these QBO modulations to changes in potential vorticity, though like Gray et al. (1992a) and Gray et al. (1992b) the mechanistic arguments were mainly speculative. Collimore et al. (1998) also found a modest and statistically marginal relationship between the QBO and tropical OLR data, but stressed the difficulty of separating upward and downward impacts and of establishing the causality of any QBO-deep convection link.

One of the first modeling studies of the QBO impact on convection was conducted the following year, when Giorgetta et al. (1999) examined whether the QBO might explain quasi-biennial patterns seen in the monsoon (for a review see Claud and Terray (2007)). Using a GCM, Giorgetta et al. (1999) imposed perpetual easterly and westerly QBO states as well as a realistic QBO, and found that the imposed QBO states led to differences in the model

boreal summer monsoon. They found that, in QBOW versus QBOE, the model showed less precipitation over the West Pacific, but more over India. To explain their findings, Giorgetta et al. (1999) emphasized the possible role of QBO temperature anomalies, as opposed to previous literature that had focused more on shear or potential vorticity. Giorgetta et al. (1999) showed that in fact the QBO could change static stability around the tropopause, which they noted might destabilize the atmosphere to very deep convection and increased high cloud cover, emphasizing the potential importance of cloud-radiative effects.

In a synthesizing paper in 2003 on the QBO impact on deep convection, Collimore et al. (2003) analyzed 23 years of OLR data. They found in general that convection was weaker in QBOW and stronger in QBOE during boreal winter, in particular over regions they dubbed "convectively chronic": regions like the warm pool where convection frequently reaches deep into the upper troposphere. Figure 2.17, from their paper, shows the observed QBO change in deep convection as a function of season. While there is a good deal of noise, there are weak signals over the warm pool region and South America. Stronger conclusions than this were hard to make because it was difficult for them to remove the effects of ENSO due to the short record, and they found the opposite relationship in boreal summer, a result they were unable to explain.

Collimore et al. (2003) spelled out clearly the three leading mechanisms through which the QBO might modulate deep convection:

1. changes to tropopause temperatures

2. changes to tropopause wind shear

3. changes to upper tropospheric vorticity variation

A systematic study of signals in their data associated with these three mechanisms led Collimore et al. (2003) to conclude that tropopause height or temperature changes were the most likely cause of any QBO effect. Shear effects seemed less strongly linked to changes, and vorticity anomalies were found not to play an important role. Still, it is worth reiterating

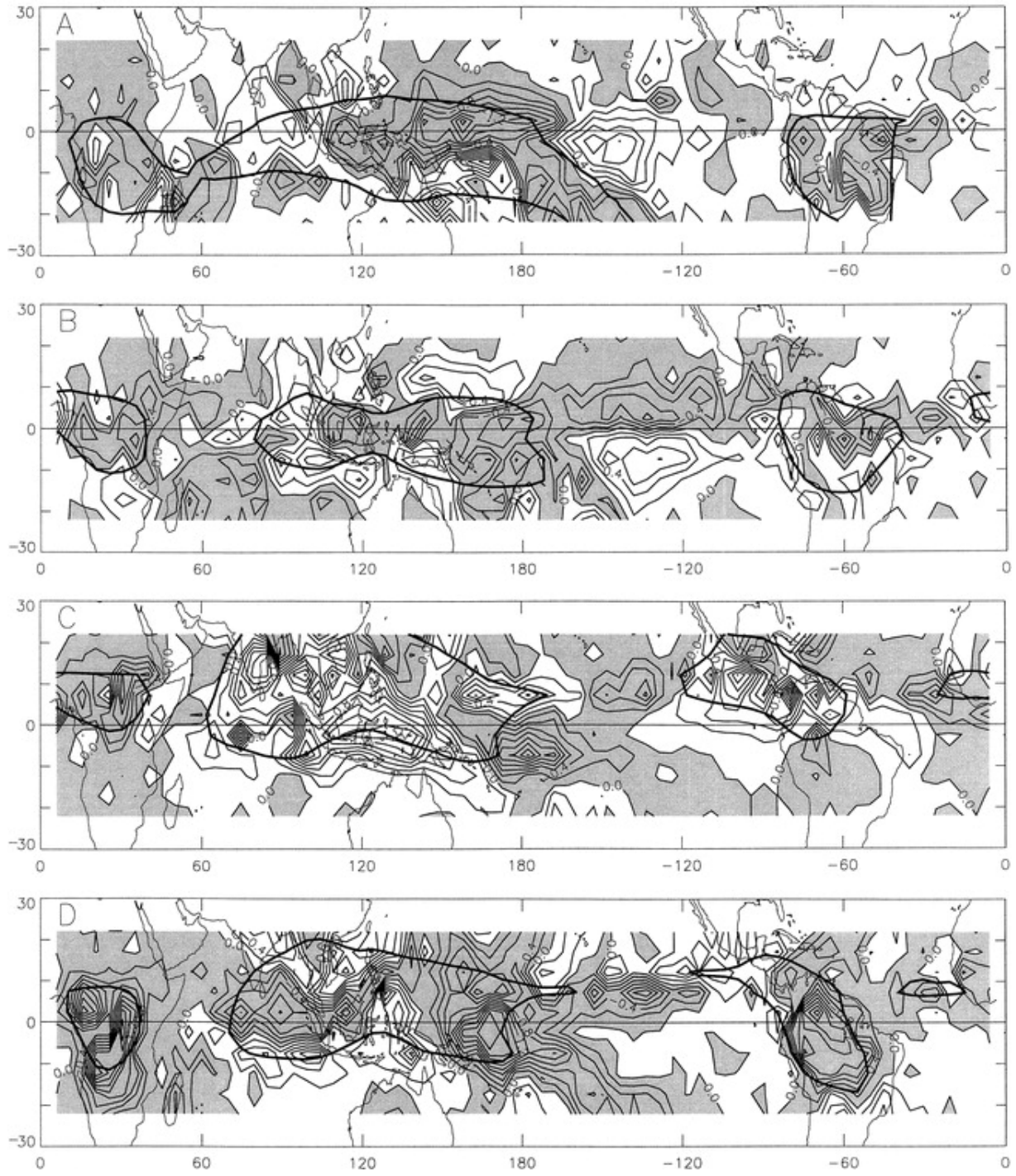

Figure 2.17: From Collimore et al. (2003) Figure 5, panels show the QBOW minus QBOE change in highly reflective clouds, used as a proxy for convection as defined in Collimore et al. (2003). Negative values (shaded) indicate decreased convection in QBOW relative to QBOE (no contour values are given in Collimore et al. (2003) for this figure). The panels show the mean change in (a) December-February, (b) March-May, (c) June-August, and (d) September-November. Dark lines envelop regions typically occupied by deep convection (defined here as regions where the seasonal mean value of OLR is less than 240 W/m^2).

that the differences observed by Collimore et al. (2003) were limited and statistically difficult to disentangle from ENSO.

A similar conclusion regarding the possibly important role that QBO temperature anomalies may play in modulating convection was noted by Claud and Terray (2007) in their study of the QBO impact of the monsoon, and by Huang et al. (2012) in work on the QBO impact on sea-surface temperatures. In a modeling study, Garfinkel and Hartmann (2011b) also invoked similar temperature mechanisms to explain a QBO impact they observed in a series of GCM experiments: while there were apparent QBO signals in model OLR, no QBO impact was evident in other variables linked to convection, such as convective mass flux, convective heating, or convective precipitation.

Recognizing that a good deal of ambiguity on this question remained, Liess and Geller (2012) looked at the QBO impact on deep convection with the benefit of, among other things, ten more years of data to work with than studies in the early 2000s had. In particular, Liess and Geller (2012) sought to remove aliasing of other signals onto the QBO more convincingly than prior work. They showed QBO-induced increases in cloud cover and precipitation over the west Pacific and decreases over the east Pacific in QBOE versus QBOW. They attributed this to a QBO modulation of the Walker circulation, and also showed some evidence for a QBO modulation of the Hadley cell, but, as with other work, they could not identify a mechanism and concluded that any link was modest in magnitude.

Finally, Nie and Sobel (2015) considered this question in a novel and idealized model framework, focusing in particular on the role of QBO temperature anomalies in the upper troposphere/lower stratosphere. Through imposing temperature anomalies associated with the QBO in their model (see Ch. 3 for more discussion) they found, consistent with others, that the QBO impact was not entirely straightforward, but that QBO-like temperature anomalies could in theory alter convection. Whether precipitation in their model increased or decreased in QBOE relative to QBOW depended on subtle changes to both the large-scale vertical velocity and cloud feedbacks, leading to modulation of convection by the QBO under

different sea-surface temperature states (though interestingly, changes were a non-monotonic function of SST).

This represents the state of the science up to around 2015 (the year I started my graduate work.). In general, the direct effect of the QBO on the tropics, and more broadly on the troposphere, was not an area of major attention because results tended to be speculative, relatively small in magnitude, hindered by contamination from other signals, and lacking in a clear mechanism. In particular, while some evidence suggested that the QBO could modulate deep convection in the tropics, the signals were small compared to other modes of variability in deep convection such as ENSO or the seasonal cycle. No QBO impact could clearly be seen on any particular tropospheric phenomena (including the monsoon, Walker circulation, or ENSO) and no coherent mechanism existed which theoretically indicated there should be a strong connection.

This changed with the discovery of a strong relationship between the QBO and the MJO – much stronger than the QBO impact on any other mode of variability in the tropics or perhaps anywhere in the troposphere. The MJO-QBO link has reignited interest in stratosphere-troposphere interactions in the tropics, and has received a wave of attention from the MJO community because suddenly the MJO was found to be strongly affected by a process and region of the atmosphere which, *a priori*, few MJO theorists predicted should matter.

2.4 The MJO-QBO Relationship

In this section, we describe the observed strong link between the MJO and the QBO which motivates this thesis. Credit for the current interest in the MJO-QBO connection should be given primarily to three papers published in 2016 and 2017. The first to introduce the MJO-QBO relationship in the modern era was Yoo and Son (2016), who laid out much of what we still understand about the MJO-QBO link. In a follow up paper, Son et al. (2017)

added additional detail and fleshed out key results and hypotheses, whereas Marshall et al. (2017) identified an important modeling aspect of the MJO-QBO link.

Before delving into the results, it is worth pointing out that the MJO-QBO connection was suggested as early as the 1990s, though little subsequent work was done on this topic. The first mention of an MJO-QBO link in the literature should be credited to Kuma (1990), who found that the intensity of upper-tropospheric winds associated with the MJO was well-correlated with the QBO. Figure 2.18, from their work, shows the power spectrum of an MJO index (described in Kuma (1990)) possessing both a clear annual peak and a significant signal at ∼2-3 years (consistent with the 28-month QBO).

Kuma's results seem to have garnered little attention at the time. Kuma's work was recognized in both of Grey et al.'s 1992 papers on the QBO-ENSO connection – "QBO easterlies should tend to promote a stronger 30-60 day oscillation with enhanced eastward propagation of deep convection" – and by Knaff (1993) in his conclusion ("these findings agree with Kuma (1990) who shows the intra-seasonal oscillation seems to operate more efficiently during the QBO east phase..."). But otherwise Kuma's paper was cited only five other times[6] until the modern return of the MJO-QBO link, and there only in passing and without any subsequent comment or additional findings.

Recognizing that the history of the MJO-QBO link begins before Yoo and Son (2016), we now move into the main results of the modern scholarship on this topic, including the key observed aspects of the MJO-QBO link, some proposed mechanisms, and some brief commentary on modeling efforts.

2.4.1 Observed Evidence and Features

Stated very broadly, when QBO winds in the lower stratosphere are easterly, the boreal winter MJO tends to be more active, more predictable, display different propagation characteristics,

[6]per Google Scholar

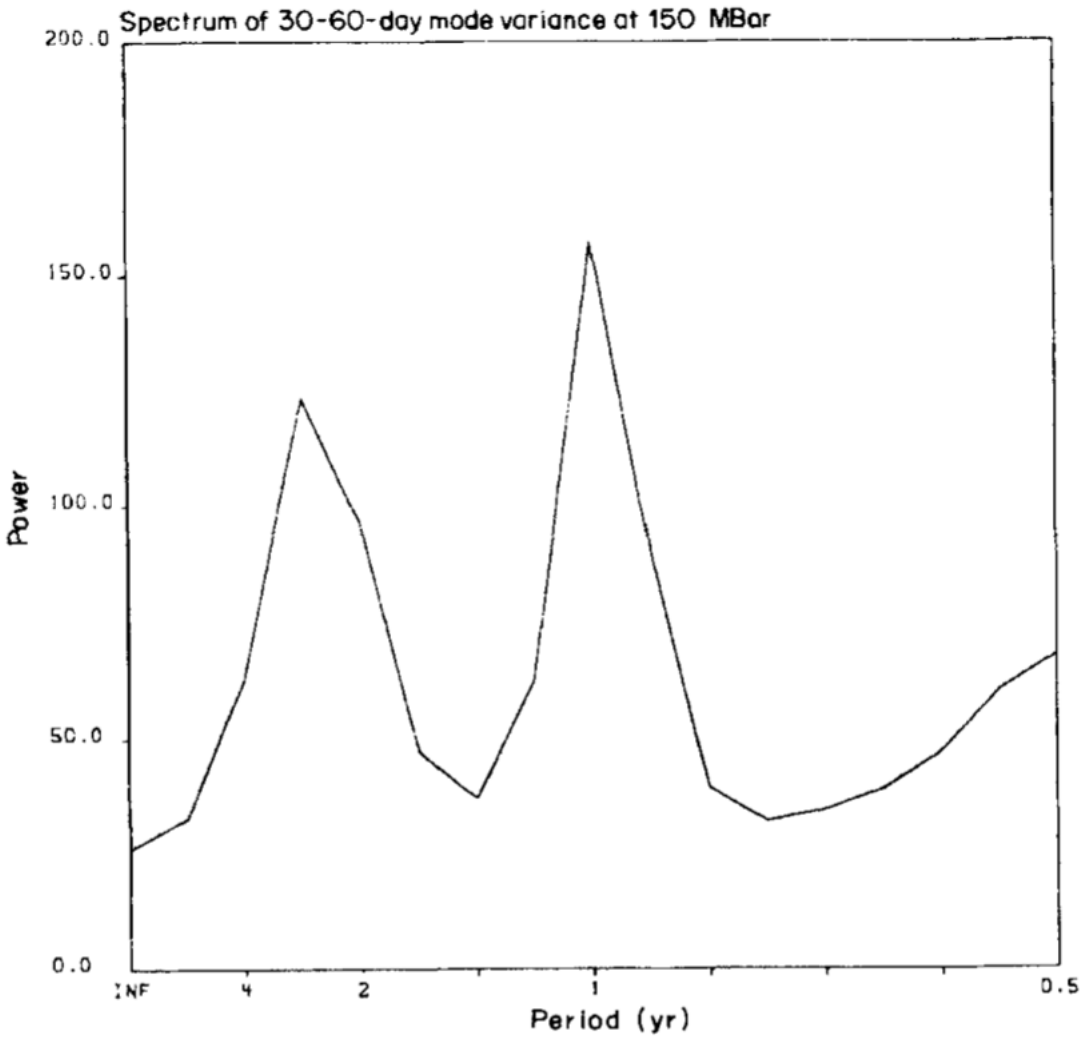

Figure 2.18: From Kuma (1990) Figure 5, the power spectrum of an MJO index, formed via bandpass filtering radiosonde data following a method described in Kuma (1990). The peaks occur on approximately annual and on 2-3 year (e.g. quasi-biennial) frequencies.

and demonstrate stronger teleconnections, with the opposite MJO modulations when the QBO is westerly.

The change in the activity of the MJO can be seen in several ways. Yoo and Son (2016) showed, as seen in Figure 2.19, that the MJO was more active and stronger during QBO easterly phases. The left panels show the standard deviation of DJF OLR that has been filtered to retain MJO timescales. The top panel shows a broad maximum over the Indian Ocean through the West Pacific, where the canonical MJO signature in convection is strongest. Taking the difference from the winter climatology in QBOW periods (panel b) and QBOE periods (panel c), one sees an increase in MJO activity during the easterly phase and a decrease in the westerly phase. The right panel, which shows the amplitude of the MJO as measured by a standard MJO index, indicates that across all of its eight phases the MJO is stronger when the QBO is easterly than when it is westerly. Son et al. (2017) and Nishimoto and Yoden (2017) show the same strong connection using other metrics and variables, including precipitation, which demonstrates that the change to the MJO signals in OLR are not just due to colder cloud top temperatures, but actually to the strength of convection. They also found that the MJO tends to propagate more slowly during the easterly phase of the QBO. Zhang and Zhang (2018) argued that the MJO-QBO link is not due to stronger MJO events, but more days on which the MJO is active, as well as longer-lasting MJO events that tend to propagate further east. In general, the literature seems unsettled regarding which of these characterizations is precisely correct, but the overall relationship between the QBO on the MJO viewed from both perspectives is strong and significant.

Additional research which is provocative but not entirely conclusive shows that the MJO may be particularly affected among tropical modes by the QBO in the region of the Maritime Continent (Zhang and Zhang (2018), Densmore et al. (2019); Chap. 4) and that strong MJO events may be modulated more than weak MJO events (Hood (2017)). Work has also shown that the precipitation response of the MJO to the QBO is subtler than early findings showed, through studies attempting to distinguish MJO precipitation changes in different

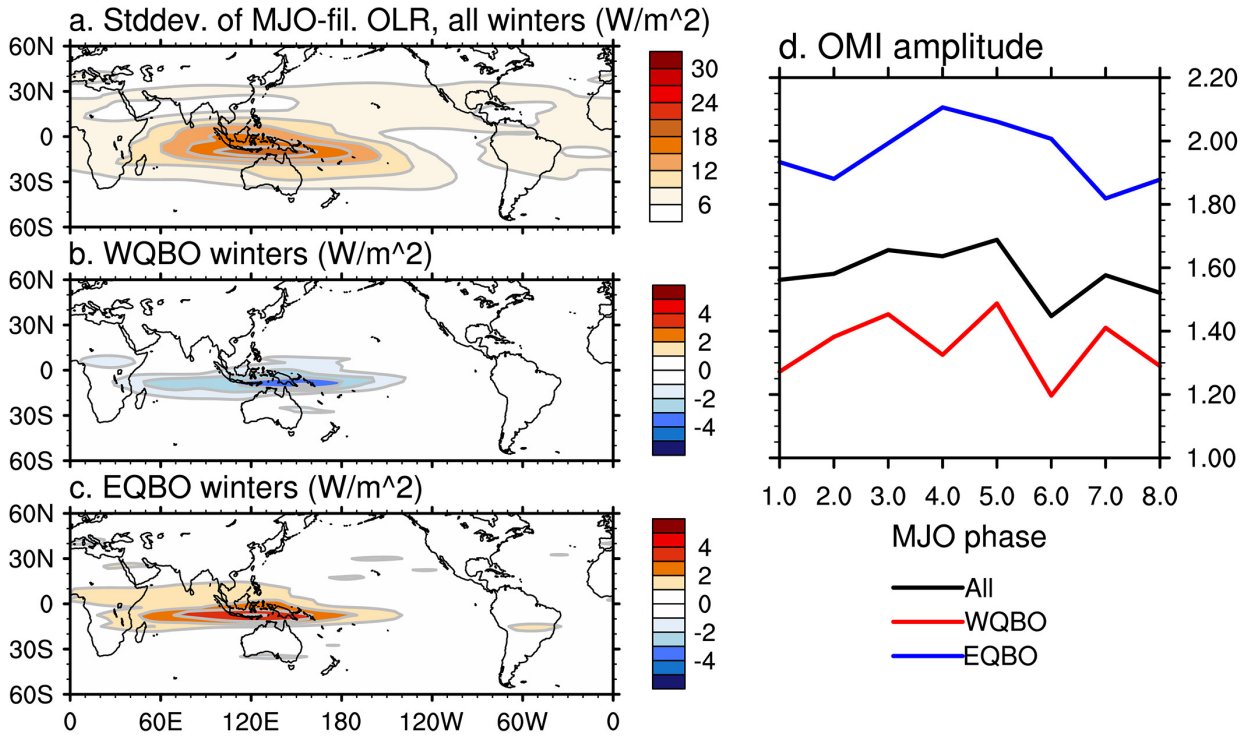

Figure 2.19: From Yoo and Son (2016) Figure 3, showing (a) the standard deviation of wintertime MJO-filtered OLR for all winters, where the MJO filtering retrieves eastward propagating wave numbers 1–5 and periods 20–100 days. (b, c) As in panel (a) but for the anomalies for the WQBO (EQBO) winters, respectively. (d) OLR MJO index (OMI; Kiladis et al. (2014)) amplitude composites (a measure of MJO strength) taken for eight MJO phases of all (black), WQBO (red), and EQBO (blue) winters.

QBO phases from QBO changes to climatological precipitation (Zhang and Zhang (2018); Chap. 3; Ji Nie and Adam Sobel, personal communication). In any event, the overall modulation of the MJO by the QBO is remarkably strong: the QBO phase appears to control almost 50% of the overall MJO strength on interannual timescales (Son et al. (2017), Zhang and Zhang (2018)). While the precise details of the modulation remain unsettled, the signal is clear and passes stringent statistical tests in a wide array of metrics, using different datasets and analysis techniques.

Importantly, the MJO-QBO link seems to only hold in boreal winter; conducting similar analyses across other seasons shows no strong, significant connection. This can be seen in Figure 2.20 which shows the MJO-QBO link as a function of season and the height at which

Table 1. Correlations Between Seasonally Averaged OMI Amplitude and Various QBO Indices[a]

	DJF	DJF-	NDJFM	MAM	JJA	SON
U70	**−0.56***	**−0.64**	**−0.49**	**−0.27**	0.10	0.13
U50	**−0.59***	**−0.61***	**−0.49**	−0.09	−0.09	0.10
U30	−0.17	−0.08	−0.12	0.19	**−0.23**	−0.03
U20	**0.33**	**0.53**	**0.27**	**0.22**	−0.17	−0.18
U10	**0.64***	**0.72***	**0.53**	0.20	−0.01	−0.18

Figure 2.20: From Yoo and Son (2016) Table 1. The zonal-mean zonal wind QBO indices at 70 (U70), 50 (U50), 30 (U30), 20 (U20), and 10 hPa (U10) as defined in Yoo and Son (2016). The correlations are computed for each season: December to February (DJF), March to May (MAM), June to August (JJA), and September to November (SON), along with an extended winter months from November to March (NDJFM). To remove the impact of the ENSO, correlations are also calculated for DJF excluding the ENSO years (denoted as DJF-). The values that exceed the 95 percent a priori (a posteriori) confidence level are marked in bold (by an asterisk).

the QBO is defined. The change in MJO-QBO correlation with the QBO height is due to the downward propagation of QBO signals. Otherwise, only boreal winter and extended winter shows a strong link which passes significance tests. MJO-QBO studies of the link in other seasons subsequently support this finding and tend to show relatively marginal results outside of DJF. One noted a decadally shifting change in the nature of the MJO-QBO link in boreal summer (Wang et al. (2019b)), but more research has not been conducted on this topic.

It does not appear that the strong MJO-QBO link is related to ENSO. The lack of a strong QBO-ENSO signal discussed in Section 2.3.2.3 supports this, and Son et al. (2017) examined this in detail in their study. Figure 2.21, from Son et al. (2017), plots DJF mean convection

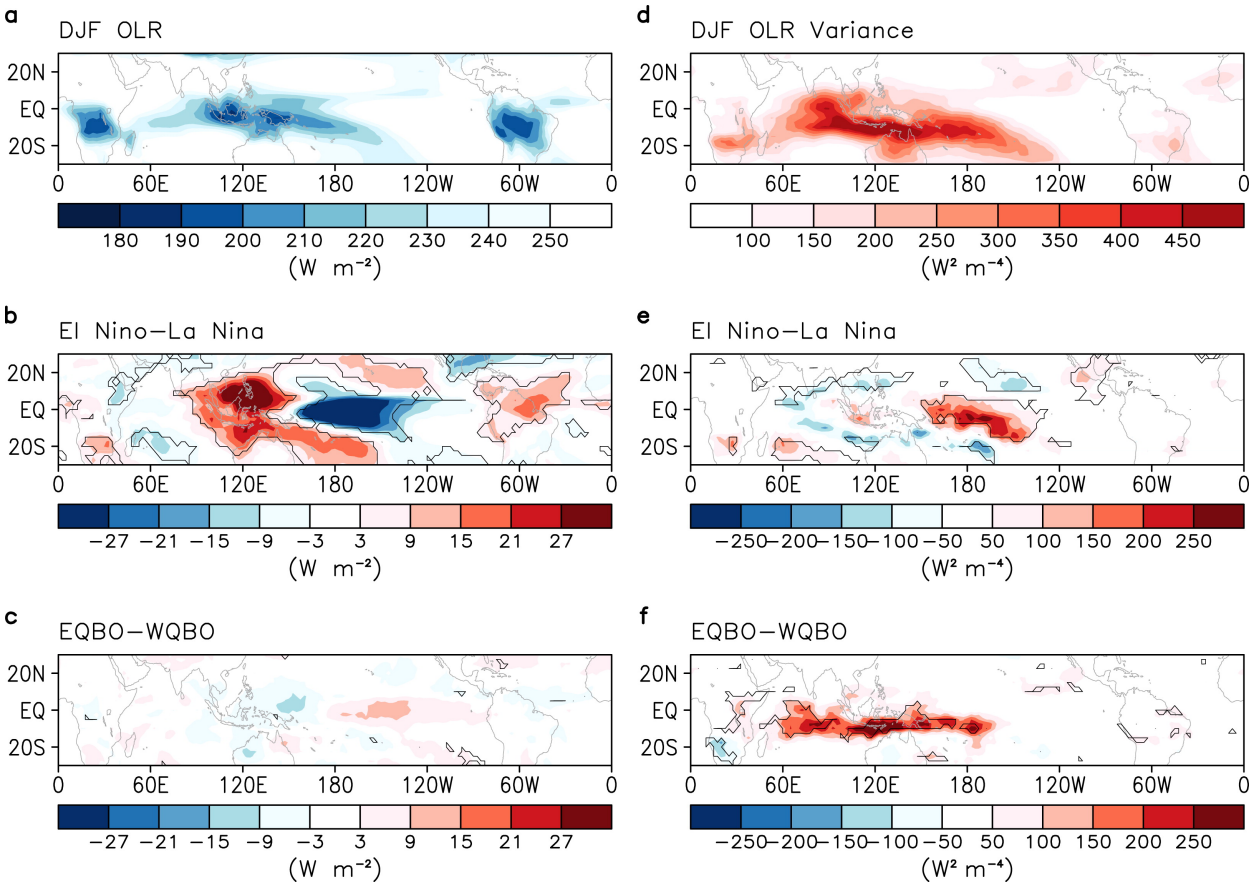

Figure 2.21: From Son et al. (2017) Figure 1. Left panels show either DJF-mean OLR (top) or changes to DJF-mean OLR, and right panels show bandpass-filtered (20–100 days) OLR variance or changes to that field. Individual panels are: (a),(d) long-term climatology, (b),(e) interannual difference between El Niño and La Niña winters, and (c),(f) difference between EQBO and WQBO winters. In (b),(c),(e),(f), statistically significant values at the 95% confidence level are contoured.

(left) and "MJO convection"; here defined using the standard deviation of bandpass filtered OLR, retaining only MJO frequencies similar to in Figure 2.19. Rows show the "all DJF" behavior, the El Niño minus La Niña changes, and the QBOE minus QBOW changes. This figure concisely demonstrates several findings we have already discussed.

First, note the QBO has a limited effect on mean-state convection (panel c) compared to its very strong impact on the MJO (panel f). By comparison, while ENSO modulates mean convection to a large degree (panel b), its impact on the MJO is limited (panel e) – the increase in MJO variance seen around the central Pacific is due to the fact that the warmer sea-surface temperatures in that region are more able to support MJO convection during El Niño periods than in La Niña periods. It is of course possible that a more subtle ENSO impact could play a role, but given that ENSO and the QBO are only weakly correlated, at present any ENSO impact appears not to be of central importance. Removing ENSO signals, a common practice in nearly all MJO-QBO studies, has not to date been shown to have a large impact on results.

Implicit in much of the discussion of the MJO-QBO link to this point, and indeed in much of the literature, is that the influence is generally downward: that is, the QBO affects the MJO. This has been supported by examination of the lead-lag relationship between the MJO and QBO, which shows that QBO changes tend to lead MJO changes, suggestive of a downward causal effect (Son et al. (2017), Marshall et al. (2017)). More work on this causality has not been carried out, though modeling studies (discussed below) are one avenue by which this question may be more definitely answered.

The most promising theory of the upward impact of the MJO on the QBO would likely contend that the MJO modulates overall wave activity in the tropics, including Kelvin and Rossby waves but also smaller scale gravity waves, that are known to force the QBO. But no strong evidence in the literature has shown this to be the case. It would also leave unresolved what controls the interannual amplitude of the MJO itself and why the MJO amplitude should independently vary approximately quasi-biennially. Throughout much of

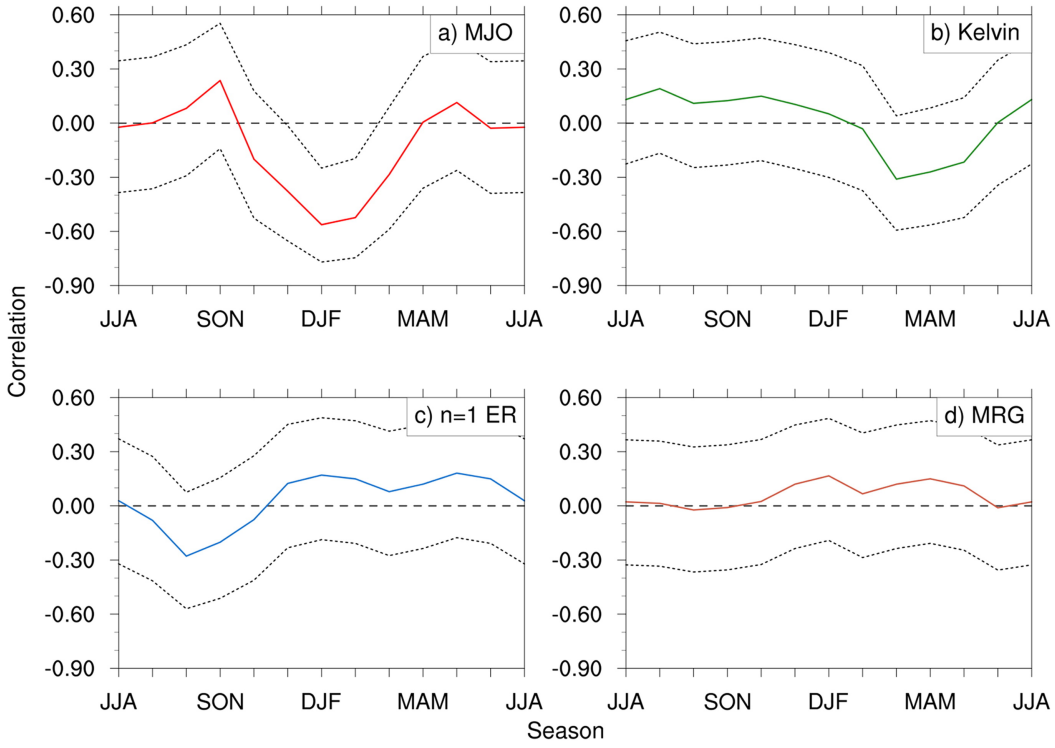

Figure 2.22: From Abhik et al. (2019) Figure 3, the correlation of the QBO and activity of (a) the MJO, (b) Kelvin waves, (c) $n = 1$ Rossby waves, and (d) mixed Rossby-gravity waves. The activity of the MJO and tropical waves is defined as the 3-month-mean OLR variance, filtered in wavenumber-frequency space in a manner similar to Wheeler and Kiladis (1999) (as described in Abhik et al. (2019)). After filtering and temporally averaging, the variance is averaged over 15°S-15°N, 0°-360° from 1979-2015. Dotted curves are 95% confidence intervals for the correlation.

this thesis therefore, a downward impact will be assumed.

Two more features of the MJO-QBO relationship should be noted. The first is that the MJO seems uniquely affected by the QBO, and not by other tropical wave types. The fact that the QBO has little effect on the mean state is one manifestation of this finding (Son et al. (2017). More to the point, Abhik et al. (2019) carried out an investigation which examined the relationship between the QBO and other modes of tropical variability, including Kelvin waves, equatorial Rossby waves, and mixed Rossby-gravity waves. Looking across wave types and seasons, they found that only the MJO showed significant differences in different QBO phases. Other waves showed no significant modulation by the QBO, though Kelvin wave

activity in spring was noted to be marginally modulated. Figure 2.22 shows the correlation between the QBO and various coupled waves (with indices defined in Abhik et al. (2019)) as a function of season. The colored lines represent the correlation, with dashed lines indicating the 95% significance level, from which one can see that only the boreal winter MJO shows a significant correlation at any time of year.

A second odd feature, reminiscent of the findings of Garfinkel and Hartmann (2007) and Camargo and Sobel (2010), was Klotzbach et al.'s (2019) finding that the MJO-QBO relationship seems only to have emerged in recent decades. Figure 2.23 shows the correlation between the MJO and QBO from a running 30-year mean over much of the 20th century – both the MJO and QBO have been reconstructed prior to the observed period, and the shading represents the uncertainty stemming from that reconstruction (as described more in Klotzbach et al. (2019)). After the 1980s, a clear emergence of a significant anti-correlation (consistent with a stronger MJO when the QBO winds are easterly) emerges in the data. While MJO and QBO reconstruction contains high uncertainty, similar findings have been obtained using reanalysis data extending back to the 1950s (George Kiladis, personal communication) supporting this result. This emergence of the signal, coupled with the unique ability of the QBO to affect the MJO, and the fact that the relationship is only significant in boreal winter, are three confounding parts of the MJO-QBO link that any successful theory must explain.

2.4.2 Consequences of the MJO-QBO Link

Having established the basic observed elements of the MJO-QBO relationship, we now briefly discuss some of the impacts of the MJO-QBO link. The two major features discussed are the influences the QBO has on MJO predictability and on MJO teleconnections. These impacts make the MJO-QBO link more than a theoretical curiosity, and indicate that the relationship has important effects on other aspects of the Earth system and on human society.

The recognition that the QBO seemed to have a large influence on predictability of the

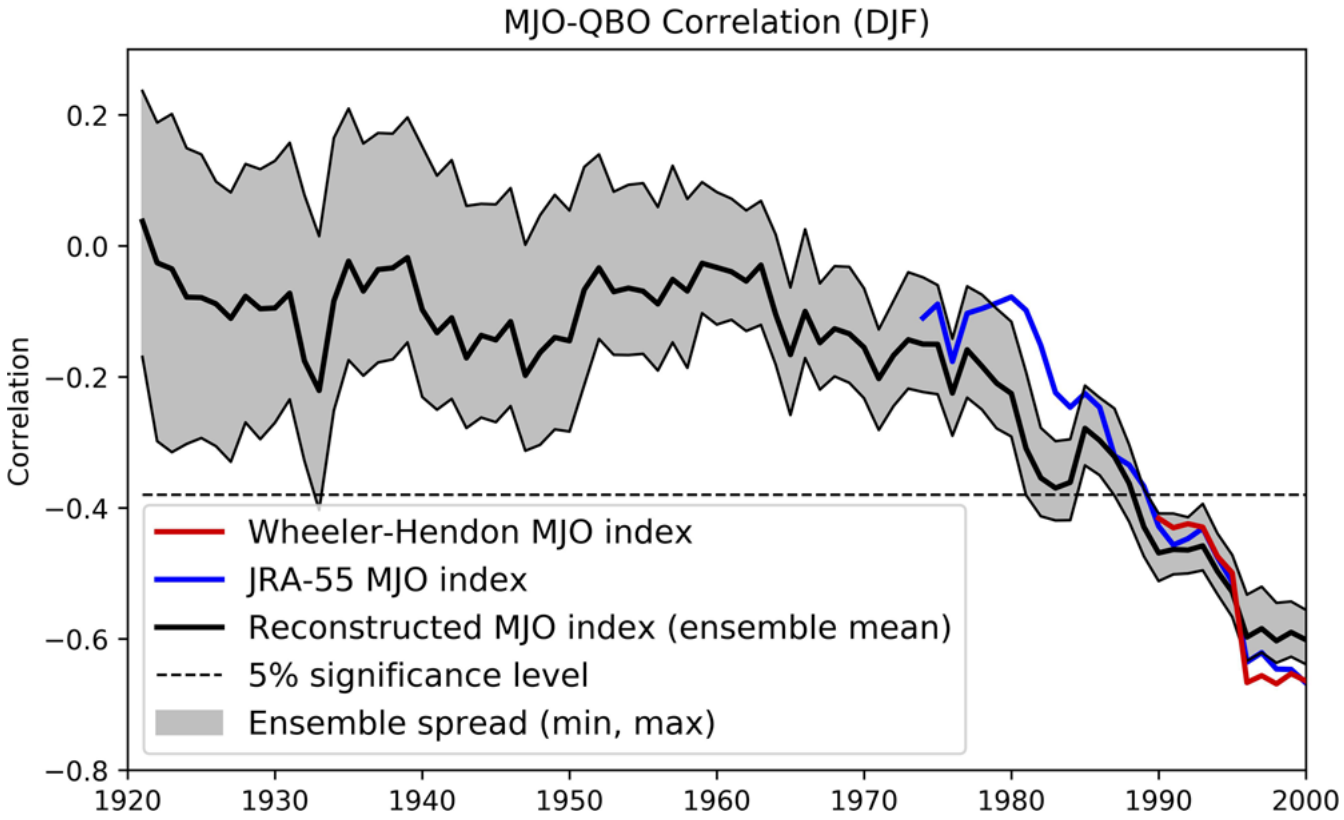

Figure 2.23: From Klotzbach et al. (2019) Figure 2, a 30-year running correlation between DJF-averaged MJO amplitude and the QBO. Correlation values are shown using the Wheeler-Hendon MJO index (Wheeler and Hendon (2004); red line), the JRA-55 MJO index (blue line) and the long-term reconstructed MJO (OT) index (thick black solid line) with the ordinate on the x-axis given by the central year of the 30-year running window (for more description of the MJO indices referenced see Klotzbach et al. (2019)). Maximum and minimum 30-year running correlations for the reconstructed index are also displayed (thin black solid lines), calculated from 56 members of the long-term MJO index ensemble. The dashed line represents the 5% statistical significance level.

MJO was noted alongside the discovery of the MJO-QBO relationship by Marshall et al. (2017). Using a coupled forecast model, Marshall et al. (2017) showed that during the easterly phase of the QBO, prediction skill of the MJO was improved by approximately one week relatively to QBOW (here the ability of the model to capture the MJO was calculated using the anomaly correlation coefficient, with skill defined as when the coefficient was greater than .5). While it is generally accepted that stronger MJO events tend to be more predictable (Kim et al. (2018)), Marshall et al. (2017) showed that the MJO during QBOE was more predictable even when controlling for MJO amplitude. Two more comprehensive studies – Lim et al. (2019) and Wang et al. (2019b) – looked at the changes in predictability across all the forecast models used in the S2S project (Vitart et al. (2017)). Using slightly different MJO indices and methodologies, both studies confirmed that the effect noted in Marshall et al. (2017) was not a model specific phenomena, but that essentially all major operational forecast models showed stronger MJO prediction in QBOE.

Figure 2.24 shows, across various S2S models, that MJO prediction skill (as defined using the bivariate correlation coefficient, see Chapter 4 or Wang et al. (2019b)) is increased by 5-10 days in QBOE relative to QBOW. Wang et al. (2019b) also confirmed, similar to Marshall et al. (2017), that the increased MJO skill was not merely a function of MJO amplitude in the initial conditions. They attributed the increase in MJO skill to some combination of initial state of the MJO and the increase in the consistency of observed MJO propagation through the Maritime Continent, which affected the observations the models were verified against. However, they were unable to state more quantitatively which is these two features was more important. Wang et al. (2019b) also found that the actual impact of the stratosphere in the model seemed minimal, a fact we will return to in Chapter 4.

Whatever their cause, these changes to MJO predictability are important for improving subseasonal forecasts. They further create additional confidence that the MJO-QBO link is a real phenomenon, and show systematic changes to the MJO during different QBO phases which are not necessarily linked to MJO amplitude. Finally, they suggest that forecast

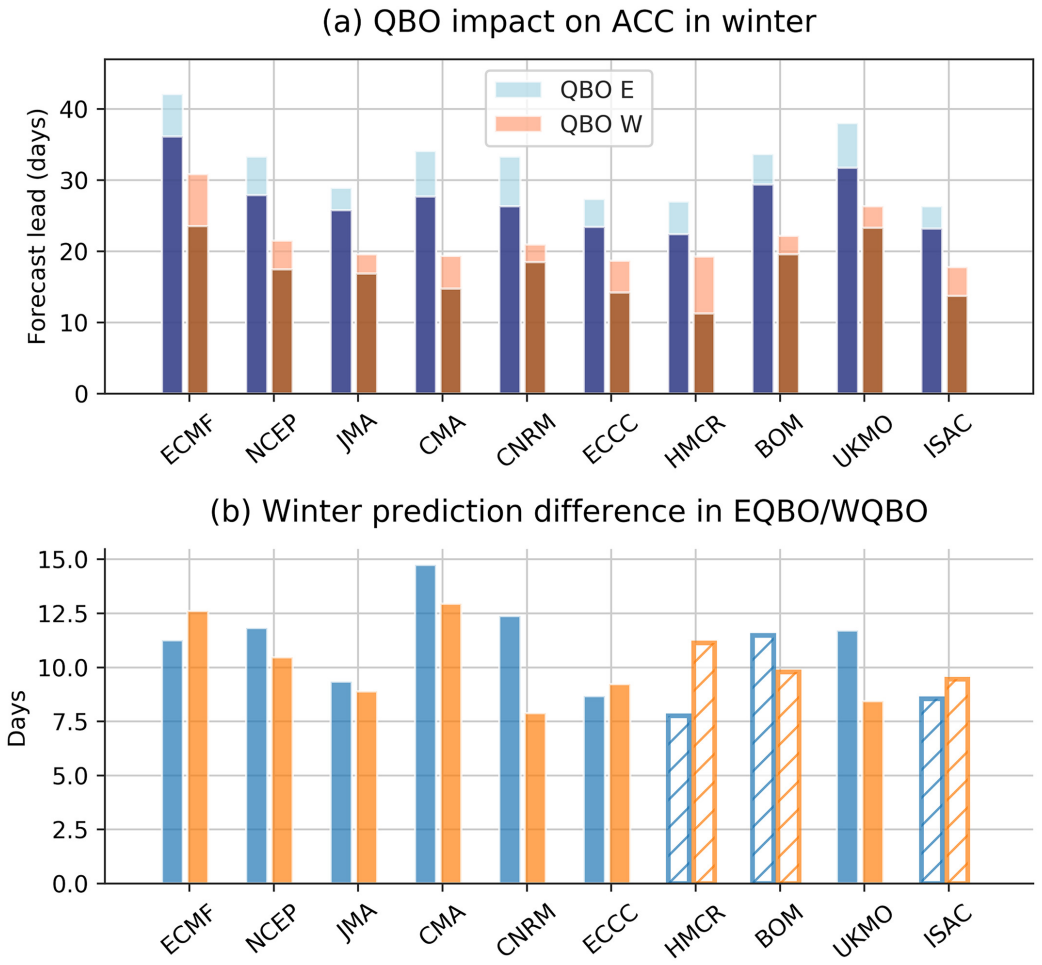

Figure 2.24: From Wang et al. (2019b) Figure 2. (a) Impact of the QBO on MJO prediction skill (using the OLR MJO index; OMI Kiladis et al. (2014)) in winter using the criteria that the bivariate correlation coefficient (see Wang et al. (2019b)) exceeds 0.5 (light) and 0.6 (dark) in boreal winter. (b) Difference in skill between QBOW and QBOE in boreal winters from 1999–2010. Blue and yellow are threshold values of skill of 0.5 and 0.6, respectively. Filled bars are models with a higher model top (<5 hPa) and hatched bars with lower model top ($\geq$ 5 hPa).

models may be able to capture an MJO-QBO link, as discussed more in the modeling section below and examined in detail in Chapter 4. However, recent scholarship shows that some caution should be taken in over-interpreting these results. Using the SubX database of forecast models (Pegion et al. (2019)) rather than the S2S database, Kim et al. (2019) showed that the QBO change to MJO prediction skill in the models, and while consistent quantitively with changes observed in Marshall et al. (2017), Lim et al. (2019), and Wang et al. (2019b), are not statistically significant, especially at lead times of more than two weeks. Indeed, even in previous studies the significance of QBO impact on MJO predictability was low at long lead times. More scholarship in the future will likely continue to examine how robust the impact on MJO predictability is, but an undeniable impact exists at present which has been leveraged to predict not only the MJO, but also the strength of its teleconnections.

The impact of the QBO on MJO teleconnections was noted in Son et al. (2017) who showed a stronger Rossby wave train was excited across the Pacific in QBOE relative to QBOW (see also Hood et al. (2020)). Son et al. (2017) also observed stronger MJO impact around South Asia in QBOE (see also Kim et al. (2020b)). A host of more recent studies have confirmed that the QBO leads to stronger MJO teleconnections globally in QBOE versus QBOW (Toms et al. (2020)), and affects the MJO impact on the location and strength of the North Pacific storm track (Wang et al. (2018)), East Asian precipitation (Kim et al. (2020b)), landfalling atmospheric river activity on the U.S. West Coast (Mundhenk et al. (2018)), and the connection of the MJO to the North Atlantic oscillation (Feng and Lin (2019)) and the Artic oscillation (Song and Wu (2020)). In addition to the changes to the strength of teleconnections, several studies have begun to show that MJO teleconnections are more predictable if both the MJO and QBO are considered (Mundhenk et al. (2018), Mayer and Barnes (2019)).

These studies have pointed to a variety of potential mechanisms explaining how the QBO modulates MJO teleconnections that have not been carefully disentangled. Factors contributing to these stronger teleconnections that have been discussed are changes in the

strength of the MJO (Son et al. (2017), and others), changes in the regularity of its propagation (Kim et al. (2020b)), changes in the nature of the diurnal cycle over the Maritime Continent (Sun et al. (2019)), and QBO-related changes to the subtropical jet (which may be unrelated to the MJO; Toms et al. (2020), Hood et al. (2020)). These effects are separable in principle in a modeling sense, and work is underway to investigate the relative contributions of changes to the MJO strength and behavior versus QBO changes to the subtropical jet or background state (Eric Maloney, personal communication).

2.4.3 Proposed Mechanisms

The work in the preceding two subsections demonstrates a strong link between the MJO and the QBO. Yet no study clearly establishes a physical mechanism connecting the two phenomena. Several such mechanisms have been proposed, however, including a QBO temperature stratification effect, cloud-radiative feedbacks, a QBO wind shear effect, or QBO changes to vertical wave propagation. Particular mechanisms and the relation to our modeling work are discussed in the individual chapters of this thesis, but we lay out some broad points here. As will be seen however, the difficulty in modeling the MJO-QBO relationship has made careful mechanistic studies hard to carry out.

Of the proposed mechanisms, the QBO temperature stratification effect has been the most well-studied and will be considered in much more detail throughout this thesis. It asserts that QBO temperature anomalies, which modify the thermal stratification in the TTL, destabilize the atmosphere during QBOE and promote more vigorous deep convection (and vice versa during QBOW). This is consistent with the previous works examining the QBO's effect on tropical mean convection (not necessarily associated with the MJO) which identified QBO temperature anomalies as a pathway to modulate convection (Gray et al. (1992a); Gray et al. (1992b); Giorgetta et al. (1999); Collimore et al. (2003); Garfinkel and Hartmann (2011b); Liess and Geller (2012); Nie and Sobel (2015)). However, the details of this temperature effect are not clear. The temperature anomalies associated with the QBO

are small around the tropopause, and in general it is not clear whether convection associated with the MJO frequently reaches deep enough into the tropopause region to be strongly affected by QBO temperature anomalies.

It is also not entirely clear why these temperature anomalies would affect the MJO exclusively. Abhik et al. (2019) note that perhaps the MJO is especially influenced because of its vertical structure and strong, deep convective component. Kelvin waves have a shallower and more tilted vertical structure, whereas Rossby and mixed-Rossby gravity waves have weaker divergence along the equator, which may explain the lack of a strong QBO effect on those waves (Abhik et al. (2019). The seasonality could be related to the fact that, in general, the tropopause is coldest during boreal winter (see also Chapter 6) and/or because the MJO is strong then, allowing it to access the QBO temperature signal. Klotzbach et al. (2019) argued that temperature changes associated with anthropogenic climate change, which lead to a warming of the troposphere and cooling of the stratosphere, could perhaps explain the emergence of the MJO-QBO link in recent decades.

In addition to the QBO's direct temperature stratification effect, cloud-radiative feedbacks may be a driver of the MJO-QBO link. During QBOE, cold TTL temperatures are conducive to the formation of high-altitude cirrus clouds, whereas warm TTL temperatures are less conducive (e.g. Son et al. (2017)). Such cirrus clouds may feed back on existing QBO temperature anomalies by cooling locally at high altitudes while warming the atmosphere below (Hartmann et al. (2001); Yang et al. (2010); Hong et al. (2016)). This may reduce the column-integrated radiative cooling, which in turn can increase large-scale ascent and precipitation (i.e. Nie and Sobel (2015)). As cloud-radiative feedbacks are potentially important for the maintenance of the MJO in general (e.g. Bony and Emanuel (2005)), especially per the moisture mode theory (Raymond (2001); Sobel and Maloney (2012); Sobel and Maloney (2013); Crueger and Stevens (2015)), this mechanism seems particularly well-suited in explaining why the QBO affects MJO-related convection more than tropical mean convection. Clouds are known to be complex, and cirrus clouds in particular have

properties which are sensitive to the base state of the tropopause region (Davis et al. (2013); Tseng and Fu (2017)), which could further explain why, as the tropopause warms or cools as part of the annual cycle, the MJO-QBO link may change on a seasonal timescale. More work on the role of clouds in the MJO-QBO context is currently underway (Chidong Zhang, personal communication), including a recent study suggesting that QBO-caused high-cloud changes to the diurnal cycle of convection around the Maritime Continent could play a role in modulating the MJO (Sun et al. (2019)).

Another possible mechanism is related to QBO wind anomalies. Gray et al. (1992a, 1992b) and Collimore et al. (2003) suggested that QBO wind anomalies may influence tropical convection via changes in the TTL vertical wind shear, which may shear off convecting cloud tops or otherwise affect convection. Apart from this type of mechanism, which couples QBO wind anomalies to convection locally, QBO wind changes can be expected to alter the propagation and dynamics of transient waves excited by the MJO, such as vertically propagating gravity or Kelvin waves. As modulation of vertically propagating waves in the stratosphere through varying vertical wind shear is central to the mechanism of the QBO itself, it is conceivable that changes to the propagation characteristics of waves in the stratosphere could play a role in the MJO-QBO interaction. No more descriptive mechanism of this type has been set forth in the literature, however, and no detailed modeling or observational work has looked closely at these types of questions. The role of winds locally is examined more in Chapter 3.

Other mechanisms are, of course, possible and plentiful. However, the above discussion represents the present description of the major mechanisms published to date. No specific mechanism which explains all aspects of the MJO-QBO relationship has been proposed that the community at large has accepted as correct yet. In part, this is due to the difficulty in modeling the MJO-QBO connection, for without modeling studies it is difficult to separate the many effects the QBO has simultaneously in the real world (to clouds, temperatures, winds, etc.). In the next section we review modeling efforts which complement the work

discussed here. As this modeling is central to our work, the individual chapters have more detail as necessary regarding specific findings where relevant.

2.4.4 Modeling Efforts

To date modeling studies on the MJO-QBO relationship have been relatively limited – the primary goal of our research during this thesis has been to address this area and attempt to fill that gap in the literature. However, a series of studies that helped lay the foundation for several of our projects deserve mention at the outset.

While simulating the MJO-QBO link is a challenge, in several studies forecast models have demonstrated a strong MJO-QBO connection (Marshall et al. (2017), Lim et al. (2019), Wang et al. (2019b), Abhik and Hendon (2019)). However, it is difficult in a forecast model to know whether an apparent MJO-QBO link is merely due to the initial conditions or due to the effects of the stratosphere in the model. This will be addressed in detail in Chapter 4, but briefly the literature is somewhat divided on this question. Our results in Chapter 4, as well as findings of Wang et al. (2019b) and Kim et al. (2019), indicate that the stratosphere in forecast models has little direct effect on the MJO. This work suggests that the tropospheric initial conditions are important for the change in MJO behavior seen in those models. As those initial conditions are determined by observations, the connection seen in models is difficult to attribute to any model process with relevance to the observed MJO-QBO link.

However, Abhik and Hendon (2019) took a different approach using two versions of the Australian forecast model. They first grouped MJO events in QBOE and QBOW so that they had similar starting amplitudes despite the difference in the stratosphere. They showed that even controlling for initial amplitude, the MJO displayed differences, for several weeks into the simulations, in different QBO phases, with stronger MJO events in QBOE relative to QBOW (see Fig. 2.25). We have further confirmed that the results of Abhik and Hendon (2019) seem to generalize to all the S2S models (see Appendix A). This might suggests that the stratosphere in the model has an impact, but it is also possible that subtler differences

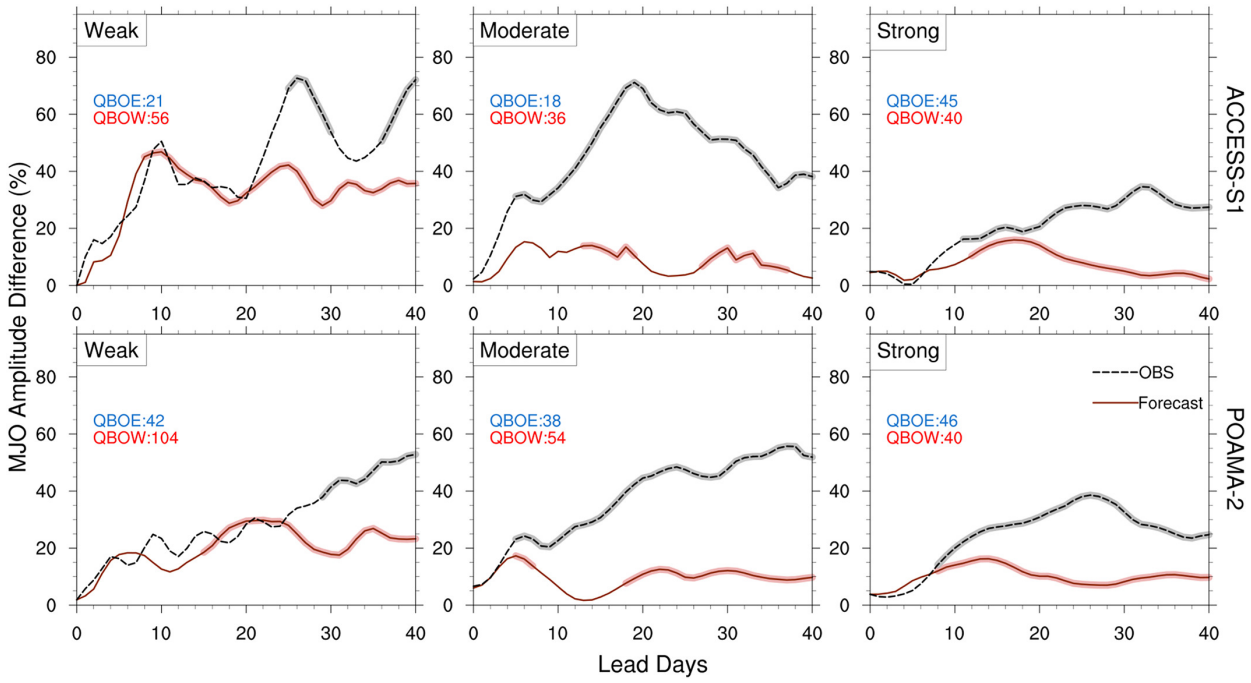

Figure 2.25: From Abhik and Hendon (2019) Figure 3, mean RMM percentage amplitude difference between QBOE and QBOW computed using individual ensemble members from two Australian forecast models: ACCESS-S1 (solid curve top panels) and POAMA-2 (solid curve bottom panels). The observed mean amplitude difference is dashed. Differences significantly different from zero at 5% level (see Abhik and Hendon (2019)) are highlighted in light brown (forecasts) and gray (observed). Three subsets are based on (left) weak initial MJO amplitude ($|RMM(0)| < 1.0$), (middle) moderate initial amplitude ($1.0 \leq |RMM(0)| \leq 1.5$), and (right) strong initial amplitude ($|RMM(0)| > 1.5$). The number of start times in each QBO phase is indicated in top left (blue for QBOE and red for QBOW). RMM = real-time multivariate MJO (Wheeler and Hendon (2004)); POAMA-2 = Predictive Ocean Atmosphere Model for Australia version 2; ACCESS-S1 = Australian Community Climate and Earth-System Simulator-Seasonal prediction system version 1.

in the MJO initial conditions exist in QBOE versus QBOW that simply binning by initial amplitude do no include (see Chapter 4).

In addition to forecast models, the MJO-QBO link in GCMs has also been examined. As simulating the MJO and the QBO individually in these models is difficult, even finding an appropriate model can be a challenge. And, even while current simulations of the QBO have improved, biases in the lowest part of the stratosphere remain which, if this region is key for the MJO-QBO link, represent a major challenge. An early result which showed that a GCM with a reasonably good representation of the MJO and the QBO had no MJO-QBO connection was by Lee and Klingaman (2018), who showed no MJO-QBO link in 75 years of simulation with a MetOffice GCM. Lee and Klingaman (2018) hypothesized that, among other issues, the lack of an MJO-QBO connection in their model may stem from a lack of realistic QBO representation in the lower stratosphere, where temperature anomalies in particular were found to be too weak. More recently, similar work has shown that these results generalize to the CMIP5 models (Seok-Woo Son, personal communication) and CMIP6 models (Kim et al. (2020a)). Kim et al. (2020a) showed that while no CMIP6 model had an MJO-QBO link, all models (with one exception) show biases in the QBO signals around the tropopause. These results are discussed more in Chapter 5. The literature on modeling work on this topic outside of global models is limited to cloud-resolving studies such as Nie and Sobel (2015) and our work presented in Chapter 3.

In general, the inability to model the MJO-QBO link represents a profound issue which challenges the robustness of the observed results, hampers attempts to better understand mechanisms, and suggests deficiencies in current generations of models. The cause of this modeling difficulty is a key theme of this work, and is discussed Chapters 3, 4, 5, and 7.

2.5 Conclusion

In this chapter we introduced the stratospheric quasi-biennial oscillation (QBO) and the intraseasonal Madden-Julian oscillation (MJO), two important modes of variability in the tropical atmosphere whose relationship to one another is the main topic of this thesis.

The QBO is a ∼28-month cycle in which the stratospheric zonal-mean zonal winds alternate between descending easterly (QBOE) and westerly (QBOW) states. These zonal winds changes are accompanied by a meridional overturning circulation as well as temperature anomalies which extend down to the tropopause. The MJO is a planetary-scale coupling between convection and circulation which propagates slowly to the east from the Indian ocean through the west Pacific. A basic theory for the MJO has not been settled upon to date, though progress has been made in recent decades in particular on the "moisture mode" hypotheses of the MJO. Via teleconnections, the MJO has a profound impact on weather and climate around the world, and is a key aspect of subseasonal predictions.

The impacts of the QBO on tropospheric weather and climate are less well-established than the MJO. After a brief discussion of the general ways in which the stratosphere and troposphere are coupled, we showed that the QBO in theory can influence the troposphere via three (not necessarily independent) pathways – a polar, subtropical, and tropical route. In general, the QBO impacts in the tropics, in particular on deep convection, seemed until recently to be relatively modest, and any mechanism through which the QBO might have a direct tropical impact is not well-established.

The study of the direct QBO effect on the tropics has experienced a renaissance in recent years thanks to the discovery of a strong relationship between the MJO and the QBO, first discovered by Kuma (1990) and then rediscovered by Yoo and Son (2016). The QBO is associated with almost 50% of the interannual variability in the strength and activity of the MJO (Son et al. (2017)) and modulates not only the MJO strength and behavior, but also MJO teleconnections and even MJO predictability. Several proposed mechanisms for the

MJO-QBO link have been put forth, but no coherent mechanism which explains the many nuances of the MJO-QBO connection (like why the link is only significant in boreal winter, why the MJO seems particularly affected, and why the link may only have emerged in recent decades) has emerged.

In part, this is due to a difficulty in modeling the MJO-QBO link. Until very recently, we showed that modeling the MJO and the QBO individually was a difficult challenge. Still, improvements in recent decades to comprehensive models allow some GCMs today to simulate both the MJO and the QBO together. However, biases in both phenomena still exist, and those deficiencies may be central to explaining the lack of an MJO-QBO connection in models. No GCM study in the literature to date shows an MJO-QBO connection. Forecast models do show an MJO-QBO link, but there difficulties separating the QBO's impact in the model on the MJO from the effect of the observed QBO on the model initial conditions make it difficult to use these models for mechanistic studies.

Chapters 3-5 present our work on modeling the MJO-QBO connection, building on all of the introductory material in this chapter. We present results using different model types – cloud-resolving models (Ch. 3), forecast models (Ch. 4), and free-running GCMs (Ch. 5) – because each has its own advantages and disadvantages for studying the problem at hand. Our overarching goal is to better understand the physical processes linking these two phenomena, but because ultimately all the models we consider are, to varying degrees, incapable of clearly capturing a strong MJO-QBO connection like that observed, it is difficult to draw firm conclusions about mechanisms.

In Chapter 6 we look more in more detail at QBO temperature anomalies in the light of the MJO-QBO link; the observational focus there provides a different perspective than the modeling work. This section is not as closely linked to the MJO-QBO connection as is our modeling work, but the MJO-QBO connection was the springboard from which that research began and the relevance of our findings there to the MJO-QBO relationship remains to be seen.

Chapter 7 concludes this thesis with a short summary of the main findings and some final, brief remarks which attempt to unify the various results and indicate potentially promising directions for future work.

* * *

Wide attention of the MJO-QBO link began around the winter of 2016-2017, when the MJO-QBO connection had just been discovered. At that time, the work of Nie and Sobel (2015), conducted just before the discovery of the MJO-QBO connection, was one of the few modeling studies that seemed well-suited for describing the physical mechanisms of how the MJO-QBO connection might work. However, Nie and Sobel (2015) focused on convection which is not necessarily related to the MJO. Fortuitously, another paper from our group, Wang et al. (2016b), had shown that it was possible to simulate convection associated with the MJO in a conceptually similar framework to that of Nie and Sobel (2015) (that is, a small domain cloud-resolving model with parameterized large-scale dynamics). It seemed natural therefore to attempt to combine the model of MJO convection by Wang et al. (2016b) with the general experimental design of Nie and Sobel (2015). Beginning around New Years of 2017, we began our first modeling project examining the MJO-QBO link in a cloud-resolving model.

Chapter 3

The Impact of the QBO on the MJO in an Idealized Cloud-Resolving Model

Note: This chapter has been published in very near its present form as "The impact of the QBO on MJO convection in cloud-resolving simulations" in *J. Atmos. Sci.* (2019), Vol. 76, pp. 669-688, doi: 10.1175/JAS-D-18-0179.1.[1] Minor edits have been made for clarity and length.

3.1 Introduction

The Madden-Julian oscillation (MJO) is the dominant mode of intra-seasonal variability in the tropical troposphere and is marked by a planetary-scale organization of deep convec-

[1]AUTHORS: Zane Martin[a]*, Shuguang Wang[a], Ji Nie[b], Adam Sobel[a,c]

[a] Department of Applied Physics and Applied Mathematics, Columbia University, New York, NY
[b] Department of the Atmospheric and Oceanic Sciences, Peking University, Beijing, China
[c] Lamont-Doherty Earth Observatory, Columbia University, Palisades, NY

* corresponding author: Zane Martin, zkm2102@columbia.edu

tion and circulation (Madden and Julian (1994); Zhang (2005)). Consisting of an "active" phase associated with increased convection and a corresponding "suppressed" phase associated with decreased convection, the MJO propagates eastward from the Indian Ocean through the West Pacific on timescales around 30 to 60 days. In contrast, the quasi-biennial oscillation (QBO) is the main source of inter-annual variability in the tropical stratosphere (Baldwin et al. (2001)). Its prevailing signal is an approximately 28-month cycle in which the tropical stratospheric zonal wind reverses direction, alternating between easterly (QBOE) and westerly (QBOW) phases. These alternating regimes form in the upper stratosphere and descend to the tropical tropopause layer (TTL) at a rate of around 1 km/month. The QBO also possesses a clear temperature signal in both tropical and extratropical regions that largely follows thermal wind balance (Baldwin et al. (2001)). Likely because they occur on different timescales and occupy largely distinct parts of the atmosphere, the MJO and QBO were considered independent by most until recent discoveries by Yoo and Son (2016) and others showed a strong MJO-QBO connection in boreal winter. Here, we present a modeling study aimed at understanding the physics of this connection.

A relationship between the QBO and the MJO was first noted by Kuma (1990), who found that the intensity of upper-tropospheric winds associated with the MJO was well correlated with the QBO. Little subsequent work was done until more recent studies, beginning with Yoo and Son (2016), spurred renewed interest in the topic (Yoo and Son (2016); Marshall et al. (2017); Son et al. (2017); Hood (2017); Nishimoto and Yoden (2017); Lee and Klingaman (2018); Zhang and Zhang (2018); Hendon and Abhik (2018); Wang et al. (2018)).

Yoo and Son (2016), through examining QBO and MJO indices, found a significant correlation indicating that the boreal winter MJO is stronger during QBOE and weaker in QBOW. Notably, the correlation was not significant in other seasons. Son et al. (2017) and Nishimoto and Yoden (2017) provided additional evidence for the MJO-QBO connection and described it in more detail. These and other studies have found that during QBOE winters, the MJO tends to propagate slower, last longer, and display stronger teleconnections (Son

et al. (2017); Nishimoto and Yoden (2017); Marshall et al. (2017); Wang et al. (2018)). Marshall et al. (2017) further showed that MJO prediction improved by approximately a week in QBOE versus QBOW. Recently, Zhang and Zhang (2018) have argued that the QBO does not directly modulate the strength of active MJO events; instead there are more active MJO days in QBOE and the MJO propagates more frequently through the Maritime Continent, often lasting longer.

None of these studies clearly establishes the physical mechanism connecting the two phenomena. Several such mechanisms have been proposed however, including a QBO temperature stratification effect, cloud-radiative feedbacks, and a QBO wind shear effect. Of these, the QBO temperature stratification effect is perhaps the most plausible (Hendon and Abhik (2018)). It asserts that QBO temperature anomalies modify the thermal stratification in the TTL, destabilizing the atmosphere during QBOE and promoting more vigorous deep convection (and vice versa during QBOW). A QBO temperature effect has also been proposed in studies on the QBO's effect on tropical convection more generally (Gray et al. (1992a); Gray et al. (1992b); Giorgetta et al. (1999); Collimore et al. (2003); Garfinkel and Hartmann (2011b); Liess and Geller (2012); Nie and Sobel (2015)).

In addition to the QBO's direct temperature stratification effect, cloud-radiative feedbacks may be a further driver of the MJO-QBO link. During QBOE, cold TTL temperatures are conducive to the formation of high-altitude cirrus clouds, whereas warm TTL temperatures are less conducive (e.g. Son et al. (2017)). Such cirrus clouds may feedback on existing QBO temperature anomalies and may increase large-scale ascent and precipitation (i.e. Nie and Sobel (2015); note this is opposite to strict radiative-convective equilibrium regimes, in which a reduction in radiative cooling implies a decrease in precipitation, as here we account for the effects of a large-scale circulation). As cloud-radiative feedbacks are potentially important for the maintenance of the MJO (e.g. Bony and Emanuel (2005); Sobel and Maloney (2012); Sobel and Maloney (2013); Crueger and Stevens (2015)), this mechanism seems particularly well-suited in explaining why the QBO affects MJO-related convection more than

tropical mean convection (e.g. Son et al. (2017), their Figure 1).

Another possible mechanism is related to QBO wind anomalies. Gray et al. (1992a), Gray et al. (1992b), and Collimore et al. (2003) suggested that QBO wind anomalies may influence tropical convection via changes in the TTL vertical wind shear, which may shear off convecting cloud tops or otherwise affect convection. Apart from this type of mechanism, which couples QBO wind anomalies to convection locally, QBO wind changes can be expected to alter the propagation and dynamics of transient waves excited by the MJO, such as vertically propagating gravity or Kelvin waves. Modulation of vertically propagating waves in the stratosphere through varying vertical wind shear is central to the mechanism of the QBO itself (Lindzen and Holton (1968), Holton and Lindzen (1972); Plumb and McEwan (1978)), and it is conceivable that changes to the propagation characteristics of waves in the stratosphere could play a role in the MJO-QBO interaction, to the extent that they can influence the troposphere. Such non-local mechanisms are not examined in this work.

This study models the MJO-QBO connection using a numerical model, and explores mechanisms that couple QBO temperature and wind anomalies directly to convection in the local column. We simulate the MJO in a limited-area, cloud-resolving model augmented with parameterized large-scale dynamics, following Wang et al. (2013) and Wang et al. (2016b), and then examine the impact of the QBO by imposing characteristic QBO anomalies in the simulation. An advantage of this approach is that cloud-resolving simulations avoid the large uncertainty due to convective parameterization in climate models. Additionally, imposing QBO anomalies allows us to focus on the QBO's impact on the MJO, and avoid issues simulating the QBO itself, which can cause difficulties in free-running global climate model simulations (e.g. Lee and Klingaman (2018)). Such an approach also allows us to examine QBO temperature and wind effects separately, which is difficult in a climate model due to the thermal wind balance constraint. Limitations include the assumptions and uncertainties associated with the parameterization of large-scale dynamics and the necessity of prescribing aspects of the large-scale flow, as described further in Section 3.2.1.

Following the modeling study of Wang et al. (2016b) (in this chapter, "W16"), we begin by simulating two consecutive, observed MJO events in our model. The specifics of our model configuration, the data and techniques we utilize, and our experimental design are described in Section 3.2. After establishing that our model reproduces the two observed MJO events with reasonable fidelity, we conduct several QBO experiments, loosely following the experimental design of Nie and Sobel (2015). These test whether various QBO temperature and/or wind anomalies influence the simulated convection. The results from these experiments are presented in Section 3.3. Discussion of our results is provided in Section 3.4, and a summary with our conclusions is laid out in Section 3.5.

3.2 Data, Methods, and Model

3.2.1 Data and Parameterized Large-Scale Dynamics

The observational data used in this study are from two sources: the Cooperative Indian Ocean Experiment on Intra-seasonal Variability in the Year 2011/Dynamics of the Madden-Julian Oscillation field campaign (CINDY/DYNAMO or simply DYNAMO; Yoneyama et al. (2013)) and the European Centre for Medium-Range Weather Forecasts' global interim reanalysis (ERA-Interim; Dee et al. (2011)). The DYNAMO data used here consist of six-hourly radiosonde measurements from October 1, 2011 through December 15, 2011, averaged horizontally over DYNAMO's Northern Sounding Array (NSA), a large region in the central equatorial Indian Ocean marked by four sounding sites (Johnson and Ciesielski (2013); Sobel et al. (2014); Johnson et al. (2015)). As the DYNAMO data do not extend above around 21 km, ERA-Interim reanalysis is utilized to capture the state of the lower to mid stratosphere up to around 29 km. To combine these two data sets, the DYNAMO data are linearly merged with six-hourly ERA-Interim data, which are horizontally averaged over 0-6°N and 73-80°E (a region closely corresponding to the NSA). Explicitly, at heights z between approximately

18 km and 21 km, a generic variable, say $X(z)$, is expressed as

$$X(z) = \frac{X_{DYN}(z)(21-z)}{(21-18)} + \frac{X_{ERA}(z)(z-18)}{(21-18)},$$

where X_{DYN} and X_{ERA} are the horizontally-averaged values of X in the DYNAMO and ERA-Interim data sets, respectively. This linear merging is done for both the wind and the temperature fields. We do not account for any bias within the ERA-Interim data, as we are primarily interested in the response in our model to QBO anomalies. For ease of reference, this combined ERA-Interim/DYNAMO data set is referred to simply as "the DYNAMO data."

Figure 3.1 shows the vertical velocity, precipitation, zonal wind, and horizontal moisture advection from the DYNAMO data. During the fall and early winter of 2011, two MJO events passed through the NSA. The active phases of these events are evident both in the strong ascent through the troposphere and the increased precipitation centered around days 25 and 55. Additionally, the suppressed phase from around days 30 to 50 shows decreased precipitation and weak descent. Also notable in Figure 3.1 are the QBO signals in stratospheric zonal wind: the QBO at 50hPa ($\sim$21 km) was westerly in October and November, and neutral by December 2011 (see further at Section 3.4).

The DYNAMO data is coupled to our cloud-resolving model following a method outlined in W16. The key step is to derive the large-scale vertical velocity using the weak temperature gradient approximation (WTG) discussed below (Sobel and Bretherton (2000); Raymond and Zeng (2005); Sessions et al. (2010); Wang and Sobel (2011)). The model is also constrained by the DYNAMO data in other aspects. The horizontally-averaged model zonal and meridional wind are relaxed uniformly at each model level towards the DYNAMO wind profile with a relaxation time of one hour. The lower boundary condition of the model is a horizontally uniform daily sea surface temperature taken from OAFlux, a product which uses optimal analysis to combine both reanalysis and satellite products (Yu and Weller (2007); Yu et al.

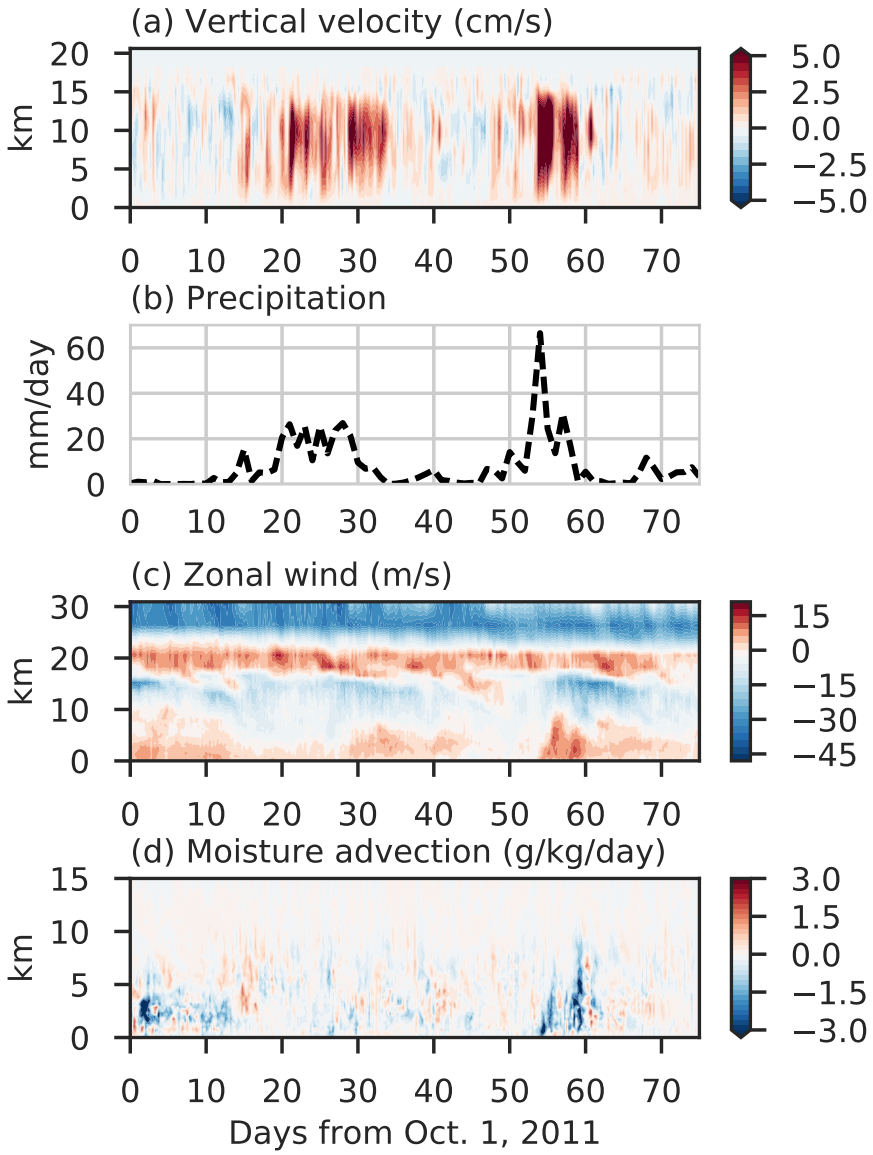

Figure 3.1: The DYNAMO/ERA-Interim linearly-merged data (as described in Section 3.2.1). Plotted are (a) vertical velocity, (b) precipitation (from NSA-derived data), (c) zonal wind, and (d) horizontal moisture advection. All fields are averaged over the DYNAMO Northern Sounding Array, or in ERA-Interim from 0-6°N and 73-80°E. Horizontal moisture advection is plotted only up to 15 km, as it is set to zero above that point (per Section 3.2.3). Days are relative to 10/01/2011; the last day is 12/15/2011.

(2008)). The horizontal advection of moisture into the model domain implied by the large-scale zonal and meridional flow is specified by imposing an additional tendency term to the moisture budget consistent with this advection (Figure 3.1d), at times forcing the model with significant low-level drying associated with westerly-winds (Sobel et al. (2014)). This large-scale horizontal moisture advection is held fixed regardless of the parameterized large-scale vertical velocity. While methods for parameterizing the large-scale horizontal moisture advection have been used occasionally in other modeling studies (Raymond and Zeng (2005); Sobel et al. (2007)), W16 showed that such methods were insufficient in this context (W16; their Appendix A).

3.2.2 Spectral Weak Temperature Gradient based on Vertical Structure

Limited-area cloud-resolving simulations are typically driven by prescribing the large-scale vertical wind and the vertical advective tendencies, a method that is useful for studying convective characteristics (e.g. Grabowski et al. (1996); Wu et al. (1998); Tao et al. (2004); Blossey et al. (2007); Wang et al. (2015); Li et al. (2018)). However, as specifying these fields may misrepresent causality related to convection and circulation (Mapes and Zuidema (1996); Mapes (2004)), methods have been developed to parameterize the large-scale vertical velocity and vertical tendencies (e.g. Sobel and Bretherton (2000); Raymond and Zeng (2005); Kuang (2008); Romps (2012b), Romps (2012a); Wang et al. (2013); Herman and Raymond (2014); Edman and Romps (2015); Nie and Sobel (2015); W16). An intercomparison using two such methods with many different models in idealized simulations can be found in Daleu et al. (2015) and Daleu et al. (2016). Following in particular W16 and Herman and Raymond (2014), here we utilize one such technique, known as the vertical-mode based, spectral weak temperature gradient method (SWTG).

Horizontal temperature gradients in the tropical troposphere are small because local temperature anomalies are quickly removed by gravity waves (Charney (1963); Held and

Hoskins (1985); Bretherton and Smolarkiewicz (1989)). The WTG method for single-column and limited-domain cloud-resolving modeling (Sobel and Bretherton (2000); Raymond and Zeng (2005)) assumes that the large-scale vertical velocity, w, maintains this homogeneity in temperature by restoring the virtual potential temperature, θ, to some reference profile θ_{ref}. Mathematically, this can be represented via a truncation of the temperature equation as:

$$\overline{w}\frac{\partial\overline{\theta}}{\partial z} = \frac{\overline{\theta} - \overline{\theta}_{ref}(z,t)}{\tau} \tag{3.1}$$

where the overbar indicates horizontal averaging. Here τ is a relaxation timescale, usually on the order of hours, associated with how quickly gravity waves propagate through the domain. For this study we set $\tau = 1$ hour. Note in Equation 3.1, $\overline{\theta}_{ref}$ is a function of height, as is typical, but is also time dependent. While this is not often the case in WTG experiments, several recent studies have demonstrated its viability (e.g. Wang et al. (2013); Sentić et al. (2015); W16; Sessions et al. (2016)). Following W16, $\overline{\theta}_{ref}$ is not taken directly from the DYNAMO data, but is calculated from a model run with imposed vertical velocity, as this improves simulations by explicitly considering model bias (Edman and Romps (2014); W16). Within the model, Equation 3.1 is solved for w throughout the free troposphere, and the resulting large-scale or "WTG" vertical velocity is used to advect moisture and temperature. In this way, we capture the effects of the large-scale circulation on these fields, and allow convection to vary during the simulation in a realistic way.

Here we use the spectral weak temperature gradient method developed by Herman and Raymond (2014) as modified by W16. We solve Equation 3.1 by first decomposing the vertical velocity into a sum of vertical modes, each with an associated vertical structure and phase speed. We then assume that WTG holds for each mode, and further that the ith mode has a characteristic time-scale, say τ_i, inversely proportional to its phase speed. Following W16 (their Section 2.2.3), we calculate these modes from the vertical profile of the Brunt-Vaisala frequency by solving a vertical structure equation with specified boundary conditions (e.g. Fulton and Schubert (1985); Wu et al. (2000); Bergman and Sardeshmukh

(2004); Mapes (2004); Tulich et al. (2007)). Once the modes are calculated, the right-hand side of Equation 3.1 is projected onto the vertical modes, and the large-scale vertical velocity field is then obtained by solving Equation 3.1 for each mode and then summing over the modes to obtain the total w.

We utilize this vertical-mode based SWTG methodology because it is conceptually appealing, produces smooth vertical velocity profiles, and leads to the most realistic structures of large-scale ascent and rain in the DYNAMO MJO events compared to other large-scale parameterizations (W16). The N^2 profile used to calculate the modes is the time-mean from the DYNAMO data. We use the first 20 modes, and assume a rigid lid boundary condition in the vertical velocity at 20 km. The sensitivity to the rigid lid height is explored in Appendix B where it is set to 16 km.

3.2.3 Numerical Model and Forcing

Our cloud-resolving simulations use the WRF model V3.5.1 (Skamarock et al. (2008)), the same model and version as W16. The set-up also largely follows W16 and is broadly similar to other WTG studies (e.g. Wang et al. (2013); Sentić et al. (2015); Edman and Romps (2014)). The horizontal domain is 64 by 64 km with a 1 km resolution and doubly periodic lateral boundary conditions. To better represent the lower stratosphere, we improve upon W16 by raising the model top to around 29 km with 89 vertical levels (from the ∼22 km used in W16). Following Nie and Sobel (2015), these levels are not uniformly spaced, but vary to include more levels near the surface and the tropopause. There are 20 levels below 5 km with a linearly-increasing step size from 75 m to 500 m; above 5 km the resolution is 500 m, except from 12 km to 20 km where it is 250 m.

We use the Morrison microphysics scheme, which predicts the mixing ratio and number concentration of rain, cloud water, cloud ice, snow, and graupel (Morrison et al. (2009)). The radiative fluxes are calculated via the RRTMG longwave scheme (Iacono et al. (2008)) and the Goddard shortwave scheme (Chou and Suarez (1999); Matsui et al. (2007); Shi et al.

(2010)). Insolation at 76°E 3°N, including the diurnal cycle, is specified uniformly over the domain. An implicit damping is used in the top 6 km of the model domain to suppress gravity wave reflection off the top boundary (Klemp et al. (2008)). Subgrid scale turbulent mixing by eddies are parameterized using the 3-D Smagorinsky first-order closure scheme (Skamarock et al. (2008)). To ensure conservation of moisture, we utilize the implicit vertical diffusion scheme from W16 and similar to Hong et al. (2006). The Coriolis parameter is set to zero, as the NSA is close to the equator and the domain is small relative to the equatorial deformation radius. The model simulation is sampled four-times daily.

Following W16, all runs analyzed are initialized on October 10, 2011. In runs initialized on October 1, the model settles into an unrealistically dry state with no precipitation. This sensitivity to initial moisture leading to "multiple equilibria" has been found in other WTG simulations (Sobel et al. (2007); Sessions et al. (2010)). Examining the transition behavior of w in such states suggests that the dry equilibrium originates from an ascent/descent couplet in the middle troposphere (e.g. day 10 in Figure 3.3d; Anber et al. (2017)). This couplet grows and descends because of interaction between radiation and temperature anomalies under WTG (Mapes and Zuidema (1996); Emanuel et al. (2014)). More importantly, it removes moisture from the column, and the system settles into the dry state. In our tests, initialization on October 10 largely avoids this issue, though non-precipitating states occur in one experiment discussed below. Model initial conditions of moisture, temperature, winds, and geopotential heights are created with an observed sounding averaged over the NSA and including ERA-Interim data in the lower stratosphere. To break symmetry, uniformly distributed random noise of magnitude 2 K is added to the initial potential temperature field in the bottom ten levels. This also permits us to carry out ensembles of integrations to better distinguish signal from noise. As a result, the individual convective systems simulated differ across ensemble members (not shown). This method does not, on the other hand, generate a large spread in horizontally-averaged quantities (e.g. rain rate or vertical profile of temperature), presumably due to lack of spread in the domain-mean forcing. The ensemble

spread generated should not be taken to represent the full dynamical uncertainty in the way that ensemble forecasts using global models can.

Two additional modifications were made from W16 due to our higher model top. First, the temperature and winds in the stratosphere (above 20 km) are relaxed on a one-hour timescale towards the reference virtual potential temperature to prevent unrealistic drift. Additionally, large-scale horizontal advection of moisture above 15 km is set to zero, as in some integrations the imposed drying lead to unphysical negative moisture values. As the actual forcing is already near zero at these levels, this change has a negligible effect on the simulations without negative moisture values.

3.2.4 Experimental Design

We track the QBO using ERA-Interim monthly zonal-mean zonal wind at 50 hPa (U50), averaged over the tropics (10°N-10°S and all longitudes) from January 1979 to June 2017. Months when U50 is greater than or less than half of its standard deviation are defined as QBOW and QBOE, respectively, following Yoo and Son (2016) and Son et al. (2017). During the DYNAMO period, the QBO was westerly during October and November and neutral by December 2011. Note too that the DYNAMO events studied here occurred in the fall and early winter, whereas the observed MJO-QBO relationship seems limited to December-February (Yoo and Son (2016); Son et al. (2017)). Despite both the existing QBO state and the season, we treat the simulated DYNAMO MJO events as a "control" simulation.

We now describe the QBO anomalies we impose upon this control simulation. We first composited vertical profiles of tropical-averaged zonal-mean temperature and zonal wind in QBOE and QBOW from ERA-Interim monthly data. The anomalies relative to the time mean are plotted in Figure 3.2. Following Nie and Sobel (2015), we then create idealized temperature and wind anomalies as parabolas with a peak amplitude approximately equal to the observed QBO signal, written as:

$$A'_{u,t}(z) = \begin{cases} \pm M_{u,t}\left(1 - \frac{z-z_0}{H}\right)^2 & \text{if } z_0 - H < z < z_0 + H \\ 0 & \text{otherwise} \end{cases} \tag{3.2}$$

Here $A'_{u,t}$ is the anomaly, $M_{u,t}$ is the amplitude of the anomaly, and the subscript denotes zonal wind or temperature. The $\pm$ indicates positive or negative anomalies, though in some cases the magnitude of the QBOE and QBOW anomalies are not symmetric. For the QBO wind anomalies, the values of M_u used are -15 m/s and 10 m/s for QBOE/W respectively. For the temperature anomalies, the values of M_t are symmetric and are either $\pm$1 K, $\pm$ 0.5 K, or $\pm$ 2 K, where indicated below; in most runs $M_t = \pm 1$ K. The anomaly peaks at height z_0, and it is symmetric in the vertical between $z_0 - H$ and $z_0 + H$, so that H is the half depth of the QBO anomaly. The peak height of the anomaly varies across different runs: QBO temperature anomalies vary z_0 from 16 km to 20 km, and QBO wind anomalies vary z_0 from 18 km to 22 km, both in 1 km increments. In all our experiments the half depth is fixed at $H = 4$ km. Note that observed QBO signals in the middle to upper stratosphere are not included in our idealized anomalies, as it seems unlikely that such high-altitude anomalies could affect convection (see Section 3.3.3.1 for validation).

Although the observed QBO anomalies are not strictly parabolic with height, we calculated approximate values of $M_{u,t}$ and z_0 from the ERA-Interim data to facilitate comparison with our input model values. To do this, we found both the minimum/maximum amplitude of the QBOE/W anomalies in the TTL (i.e. < 24 km) and the height at which those extrema occurred, quantities somewhat analogous to $M_{u,t}$ and z_0. For ERA-Interim, $z_0 = 18.6$ km for temperature and 20.6 km for wind, though the vertical resolution of ERA-Interim in the TTL is coarse (varying between $\sim$1-3 km from 14 km to 23 km). M_t is 0.81 K for QBOW and -0.78 K for QBOE, and M_u is -15.8 m/s for QBOE and 9.8 m/s for QBOW.

To impose the idealized QBO states, we add the QBO anomalies, derived as described above, to the DYNAMO large-scale forcing data during the entire simulation period. While

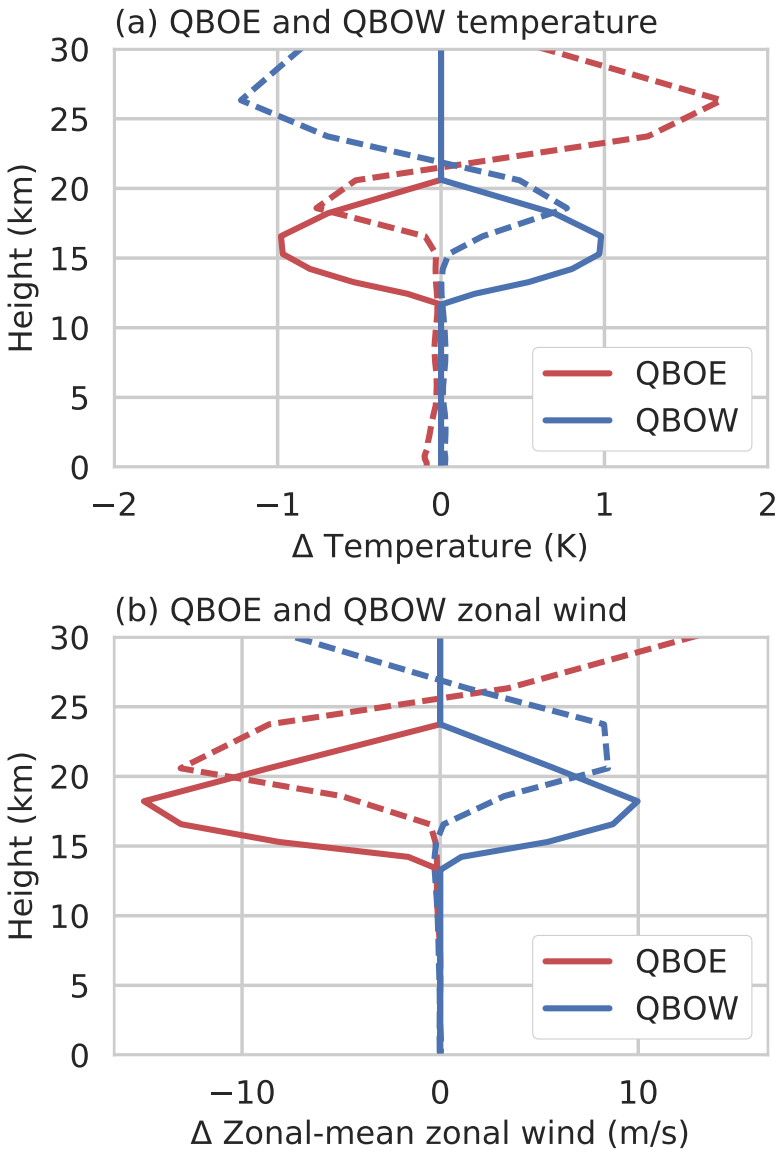

Figure 3.2: Idealized (solid) and observed (dashed) (a) QBO temperature and (b) zonal wind anomalies averaged over the tropics (10°N to 10°S and all longitudes). The observed anomalies are calculated using a 50 hPa QBO index based on ERA-Interim monthly data, as described in Section 3.2.4. The idealized anomaly is parabolic per Equation 3.2; here the peak is plotted at 16 km for the temperature anomaly and 18 km for the wind anomalies. The idealized anomaly is plotted after interpolation onto the DYNAMO forcing levels, which accounts for the vertical asymmetry about the peak in panel (b).

observed QBO anomalies descend at a rate of around 1 km/month, our anomalies are fixed during each simulation. The QBO anomalies were not added to the initial conditions in the results shown here, as this sometimes led to the model's settling into the non-precipitating state discussed above (not shown). While this itself suggests that conditions in the TTL can influence MJO-related convection, these dry states preclude comparison to other runs and thus are not considered.

We design three types of experiments to test the mechanisms discussed in the introduction: (1) those in which only the large-scale temperature field is modified with QBOE/W signals, (2) those in which only the large-scale wind is modified, and (3) those in which QBO temperature and wind signals are both included. In each set of experiments, we impose QBOE and QBOW anomalies by adding them to the DYNAMO data (which recall is weakly QBOW to QBO neutral during the integration period) and analyze how the model responds. To explore the sensitivity to the height and amplitude of the QBO anomaly, in Section 3.3.3 we consider a range of values for M_t and z_0. This sensitivity testing accounts in part for differences in the shape of the QBO anomaly that may be depend on, for example, our particular QBO index, reanalysis product, lack of bias correction, etc.. A summary of all the experiments presented in this paper is provided in Table 3.1.

3.3 Results

3.3.1 Control Runs

Our control runs are comparable to W16's simulations with interactive radiation (their Section 3.2), albeit with a higher model top and higher vertical resolution. Figure 3.3 shows the results from control simulations with five ensemble members, with ensemble spread (shading in Figs. 3.3a,b) due to the white noise in the initial temperature field. Comparisons of the model and observations in Figure 3.3 shows that the control runs simulate the two MJO active phases with reasonable fidelity. The model reproduces both periods of increased pre-

Type	z_0 **(km)**	$M_{u,t}$	**Ensemble size**	**Section**
Control	–	–	5	3.3.1
Temperature	16	±1 K	5 QBOE/W	3.3.2
Temperature	16,17,18,19,20	±1 K	1 QBOE/W per height	3.3.3.1
Temperature	18	±1 K	5 QBOE/W	3.3.3.1
Wind	18, 19, 20, 21, 22	10 and -15 m/s	1 QBOE/W per height	3.3.3.1
Temperature and wind	16/18, 17/19, 18/20,19/21,20/22	±1 K, 10 and -15 m/s	1 QBOE/W per height	3.3.3.1
Temperature	16	±0.5, ±2 K	1 QBOE/W per amplitude	3.3.3.2
16-km rigid lid: Control	–	–	5	B
16-km rigid lid: Temperature	16	±1 K	5 QBOE/W	B

Table 3.1: List of experiments. The first column indicates what type of QBO anomaly was imposed; control indicates no anomaly. The second and third columns correspond to the height of the anomaly's peak z_0 and its amplitude $M_{u,t}$ per Eq. 3.2. Commas indicate separate experiments. For temperature and wind experiments, the height is listed in the form: "temperature anomaly peak height"/"wind anomaly peak height." The fourth column lists the number of ensemble members. The final column indicates the main section where the run is discussed.

cipitation associated with the active phases, though the large observed spike of precipitation around day 55 is missed in the model, and the second MJO event develops later in the model than in observations. The dry, suppressed phase is also well-simulated, and evident from around day 35 to day 50.

The SWTG vertical velocity is in good agreement with the observed (Figs. 3.3c,d): the model captures the periods of ascent during the active phases and the weak descent in the suppressed phase. The magnitude of the SWTG vertical velocity is often larger than the observed however, and the structure is more top-heavy. The model displays a descending couplet (ascent in the upper troposphere and descent in the lower troposphere) around day 45, a feature that is inconsistent with the observations and can lead to unusually strong precipitation and/or low OLR. W16 and Anber et al. (2017) noted this feature in their simulations with interactive radiation as well.

Unlike the precipitation and vertical velocity, the model OLR differs more substantially from the observations (Fig. 3.3b), especially during the first MJO event, where the disagree-

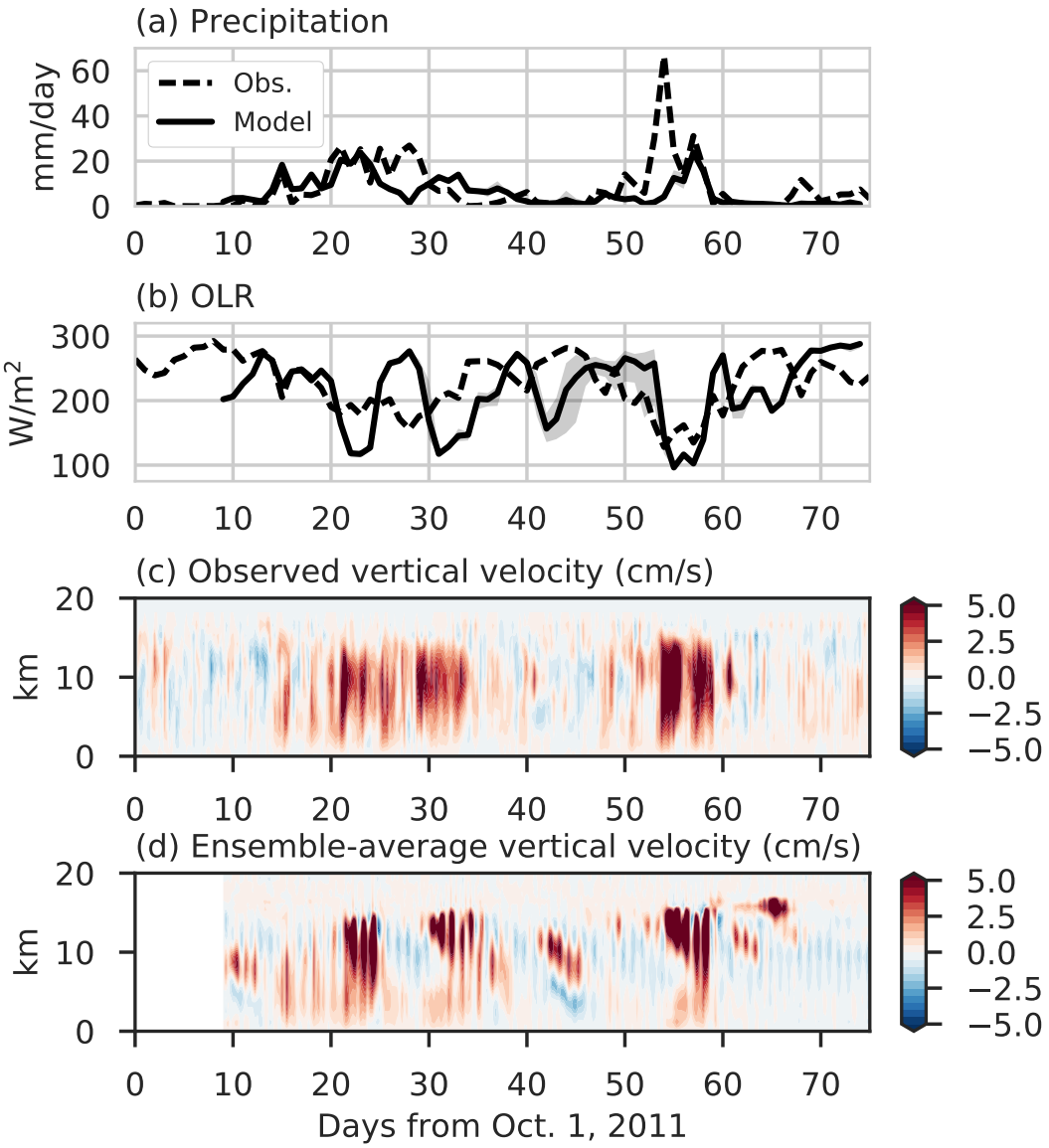

Figure 3.3: Control simulations compared to observations for horizontally-averaged (a) precipitation (mm/day), (b) OLR (W/m^2) and (c/d) vertical velocity (cm/s). In (a) and (b), shading denotes the spread among ensemble members, defined throughout as the minimum and maximum value across all ensemble members at each timestep. The solid black line is the model ensemble average and dashed line is the observed. The model is initialized on 10/10/2011 per Section 3.2.3; hence the white space preceding day 9.

ment reaches tens of W/m^2. The model OLR during the second MJO event is in closer agreement with the observations, though again the model MJO active phase begins later than the observed. The OLR also has an unrealistic dip in the model around day 40-45 corresponding to the descending couplet. We conclude that the model reproduces the observed MJO events reasonably well despite the discrepancies described above. Our results are not substantially different from those of W16 despite our modifications to the model and experimental setup.

3.3.2 QBO Experiments

In this section we present results from simulations in which we impose various QBOE/W anomalies. We begin by only modifying the temperature field, before discussing the wind-only experiments and then the combined wind and temperature experiments. We first impose a QBOE/W anomaly with amplitude $M_t = \pm 1$ K, with a peak z_0 at 16 km, extending down to 12 km and up to 20 km. These QBOE and QBOW idealized anomalies are shown in Figure 3.2.

The idealized temperature anomalies in this section are lower in altitude by around 2.5 km than those observed and have larger values of the vertical depth, H. The sensitivity of our results to these differences is explored more in Section 3.3.3, but in brief, it is likely that both the QBO forcing and the model response in these runs are stronger than in observations. We nevertheless include this stronger QBO temperature forcing, in large part because of the clearer MJO response shown below. Sections 3.3 and 3.4 discuss this issue in more detail.

As with the control, the QBOE and QBOW simulations are each performed with five ensemble members. The results are shown in Figures 3.4-3.6. These temperature-only experiments generally demonstrate an MJO response to the QBO that is qualitatively consistent with the observed MJO-QBO link: the model shows stronger MJO-associated convection in QBOE compared to QBOW. Figure 3.4 shows the time series of precipitation and OLR for the three QBO states: QBOE, QBOW, and the control. The OLR is consistently lower

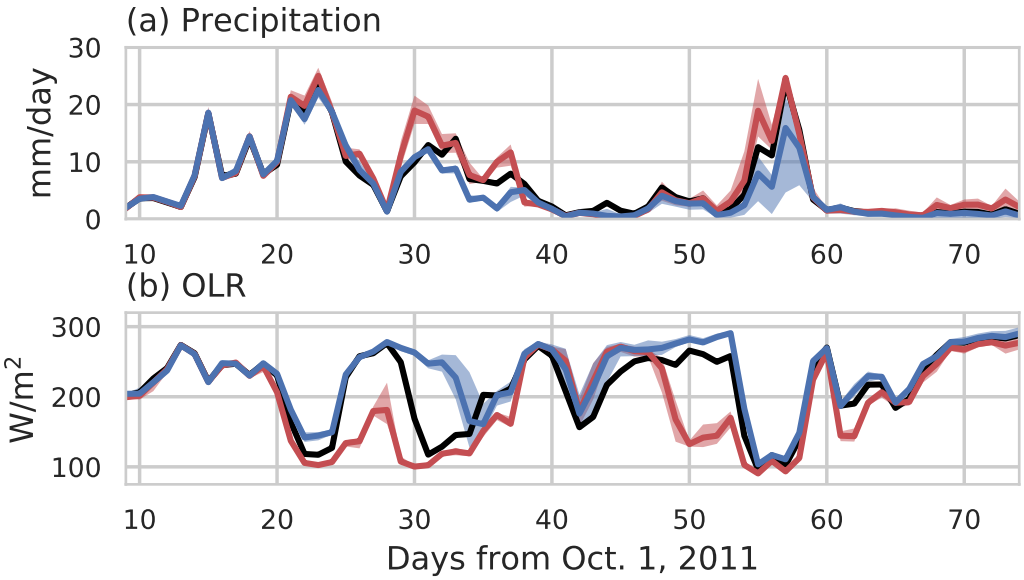

Figure 3.4: Precipitation (top) and OLR (bottom) from model integrations with no QBO anomaly (black), a QBOE temperature anomaly (red) and a QBOW temperature anomaly (blue). As before, the shading denotes ensemble spread and the bold is the ensemble average; the spread in the control is not shown. The QBO temperature anomaly is imposed with $z_0 = 16$ km and $M_t = \pm 1$ K as shown in Figure 3.2 and described in Section 3.2.4. No QBO wind signal is added.

in QBOE and higher in QBOW, while the precipitation is higher in QBOE and lower in QBOW; both are in keeping with enhanced convection during QBOE. The large-scale vertical velocity and cloud fraction are also consistent with stronger MJO convection during QBOE, as shown in Figure 3.5. The time-mean quantities show that from around 5 km to 15 km the vertical velocity is stronger in QBOE and weaker in QBOW. The same can be said of the cloud fraction; in particular, the changes to high clouds are in keeping with the observed MJO-QBO interaction (e.g. Son et al. (2017)). Figure 3.5 also shows a downward sloping pattern in the QBOE-QBOW changes to cloud fraction, indicating that changes to high clouds precede deeper, mid-tropospheric cloud changes (see days 25-35 and days 45-55).

Across all variables, the time series show that QBOE-QBOW differences are most pronounced during the MJO active phases, while differences are typically small during the suppressed phase. This suggests, as one might expect, that only convection capable of reaching the level of the QBO anomaly is modulated by the temperature changes. The pronounced

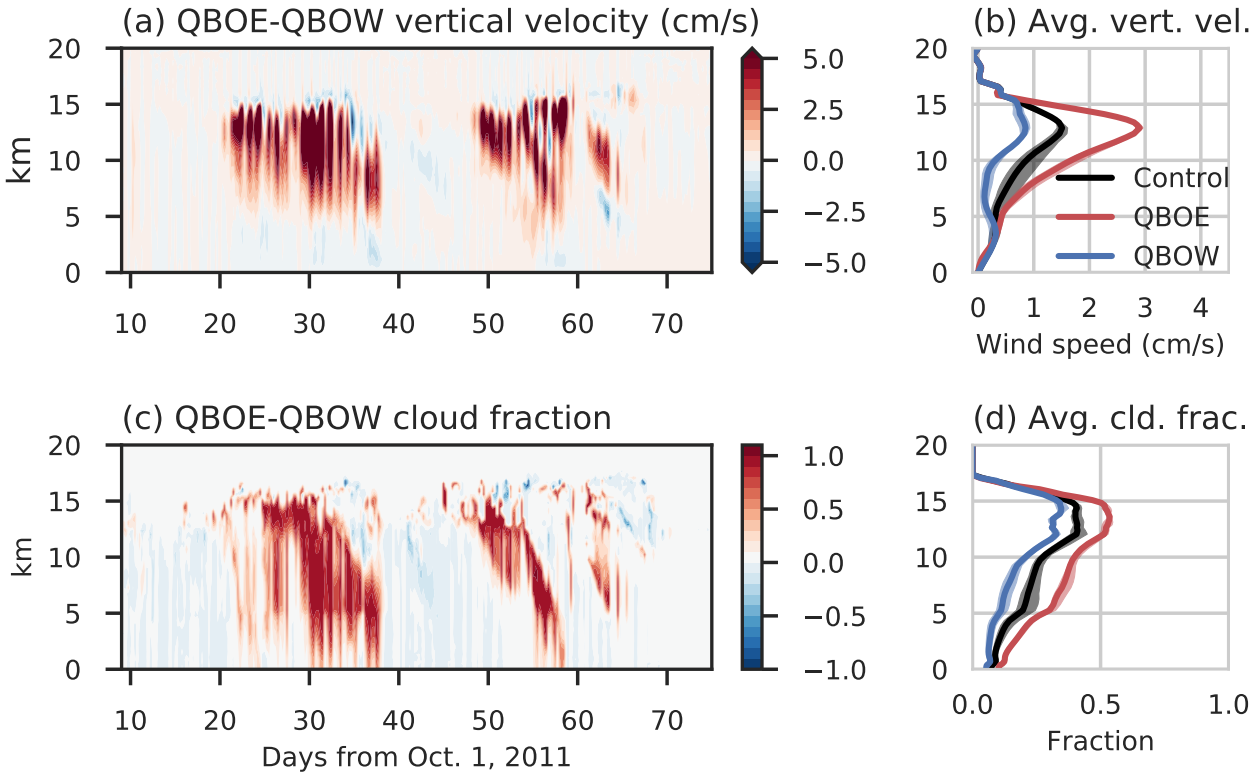

Figure 3.5: From the same QBO temperature experiment as in Figure 3.4, showing vertical velocity (top) and cloud fraction (bottom). The left panels are the ensemble-averaged, horizontally-averaged QBOE-QBOW difference (red indicates QBOE > QBOW). The right panels show the time-mean for QBOE, QBOW, and the control; the shading indicates ensemble spread. Here and throughout cloud fraction is calculated as the fraction of grid points with cloud-water content (cloud water vapor, ice, rain, snow, hail, and graupel) exceeding the minimum of .01 g/kg or 1% of its saturation value.

changes in the active phase and lack of change in the suppressed phase also demonstrate that QBO temperature anomalies modulate not only the model's mean state, but the amplitude of the variability associated with the MJO, as discussed more below.

Figure 3.6 shows the ensemble-averaged QBOE-QBOW potential temperature in the simulations; panel (b) compares the model time-mean to the input idealized QBO potential temperature anomaly (note here we plot potential temperature, not temperature as in Figure 3.2). The model potential temperature difference in the time mean is stronger (i.e. more negative) than the input anomaly around the tropopause by around 0.4 K, which amounts to $\sim$10 % of the time mean value (around -4 K). This suggests that some process in the tropopause region acts to enhance the imposed QBO anomaly. The time series in Figure 3.6a further shows that these enhanced temperature signals are largest during MJO active phases, as evident around day 20-35 and day 50-60 where difference reach a minimum of around -13 K. These results show that the imposed QBO temperature anomalies enhance coupling between large-scale velocity and convection in such a way as to reinforce the QBO temperature anomalies. These results may also be in keeping with Hendon and Abhik (2018), who examined the MJO's vertical structure under different phases of the QBO and found that the cold cap around the tropopause associated with the MJO is strengthened by around 0.5 K during QBOE, and similarly weakened during QBOW.

In contrast to the QBO temperature-only simulations, results from experiments in which the wind field was modified with QBO anomalies showed no substantial change across any of the fields of interest, even for lower-than-observed altitude anomalies. Further evidence that wind anomalies have little to no effect on convection is evident in the combined wind and temperature experiments, in which QBO anomalies in both variables were added. Results from these experiments are very similar to the temperature-only experiments, with minor differences that are indistinguishable from noise. Because these differences are small in general, results from both the wind-only and the temperature and wind results are presented only briefly in the following section (see Figures 3.7 and 3.8). This lack of an influence

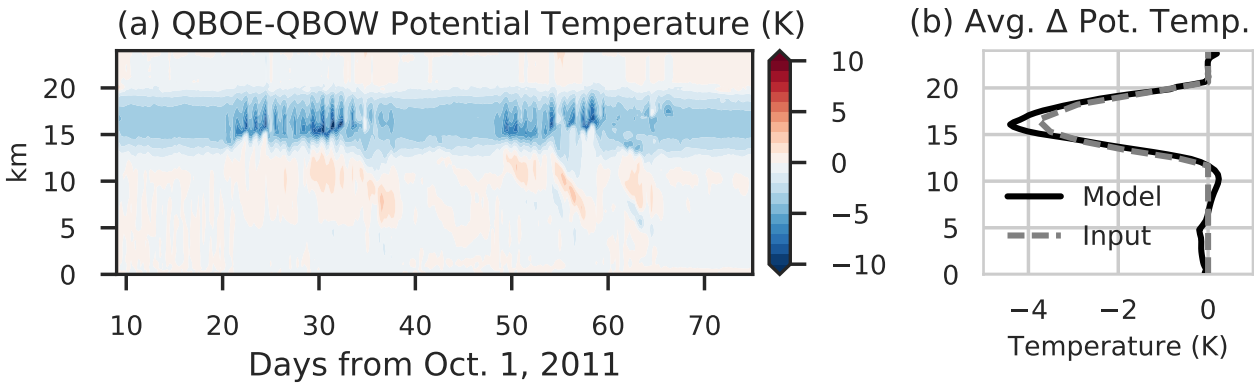

Figure 3.6: From the same QBO temperature experiment as in Figures 3.3 and 3.5, showing the potential temperature difference in QBOE versus QBOW. The left panel shows the ensemble-averaged, horizontally-averaged difference. The right panel shows the time-mean difference (black, solid) as well as the idealized QBOE-QBOW temperature anomaly added into the model (grey, dashed). Note we plot potential temperature as opposed to temperature, which is shown in Figure 3.2. Results are shown up to the level where the model damping begins (24 km).

suggests that QBO wind anomalies do not have a direct influence on MJO convection.

3.3.3 Sensitivities to the Shape of QBO Temperature Anomalies

In this section we explore the sensitivity of our results to the height and amplitude of the QBO temperature anomaly. As in Nie and Sobel (2015), both parameters are found to be important in determining the strength of the QBO influence on the simulated MJO. We also briefly present results from the QBO wind-only and QBO wind and temperature experiments to contrast the relatively small effects of wind anomalies on the simulated MJO convection, compared to the effects of temperature anomalies.

3.3.3.1 Height of the QBO Anomalies

We first perform a series of one-member integrations in which the height of the QBO anomalies in wind and temperature are varied in 1 km increments. QBO temperature anomalies in these simulations have peak heights z_0 from 16 km to 20 km and QBO wind anomalies vary z_0 from 18 km to 22 km. The vertical width of the anomaly H in all cases is 4 km;

the observed width of the anomaly tends to become thinner as it descends to lower levels, but for simplicity we hold it fixed. The amplitude of the anomalies is also held fixed at ± 1 K for temperature and at -15 m/s or 10 m/s for QBOE/W wind. When imposed together, the wind anomaly peaks 2 km above the temperature anomaly, roughly consistent with the observed peak-height difference per ERA-Interim. Figures 3.7 and 3.8 show the results of the integrations.

Figure 3.7 shows the QBOE-QBOW difference in the time-mean large-scale vertical velocity and cloud fraction for various experiment types and values of z_0. The similarity between the temperature-only simulations and the temperature and wind simulations is immediately apparent, as is the lack of a QBO signal in the wind-only integrations. Of more interest is the relationship between the height of the QBO temperature anomaly and the MJO response (Figs. 3.7a,b). Figures 3.7a and 3.7b clearly show that the QBO influence lessens dramatically as the height of the QBO anomaly increases: QBO-induced changes to cloud fraction and vertical velocity decrease in amplitude and lose a coherent structure as the height of the anomaly increase. The simulations with z_0 equal to 19 km and 20 km in particular lack an obvious QBO response. The run with $z_0 = 18$ is subtler to diagnose, as it shows a weak but detectable signal. This experiment is discussed in more detail below (see also Figs. 3.9-3.11). In addition to the weakening of the QBO influence as z_0 increases, note that the peak of the QBOE-QBOW difference in vertical velocity and cloud fraction shifts upward for higher anomalies and signals in the mid to lower troposphere weaken. This suggests that the QBO influence is increasingly confined locally as the temperature anomaly moves to higher altitudes.

Figure 3.8 shows the QBOE-QBOW differences in the time mean and standard deviation of precipitation and OLR as functions of z_0 for the three types of QBO experiment. The x-axis indicates the height of the anomaly's peak and the y-axis indicates the QBOE-QBOW difference. The OLR results (Figs. 3.8b,d) are fairly consistent with the cloud fraction and vertical velocity changes described above: there is a small change in the wind experiments,

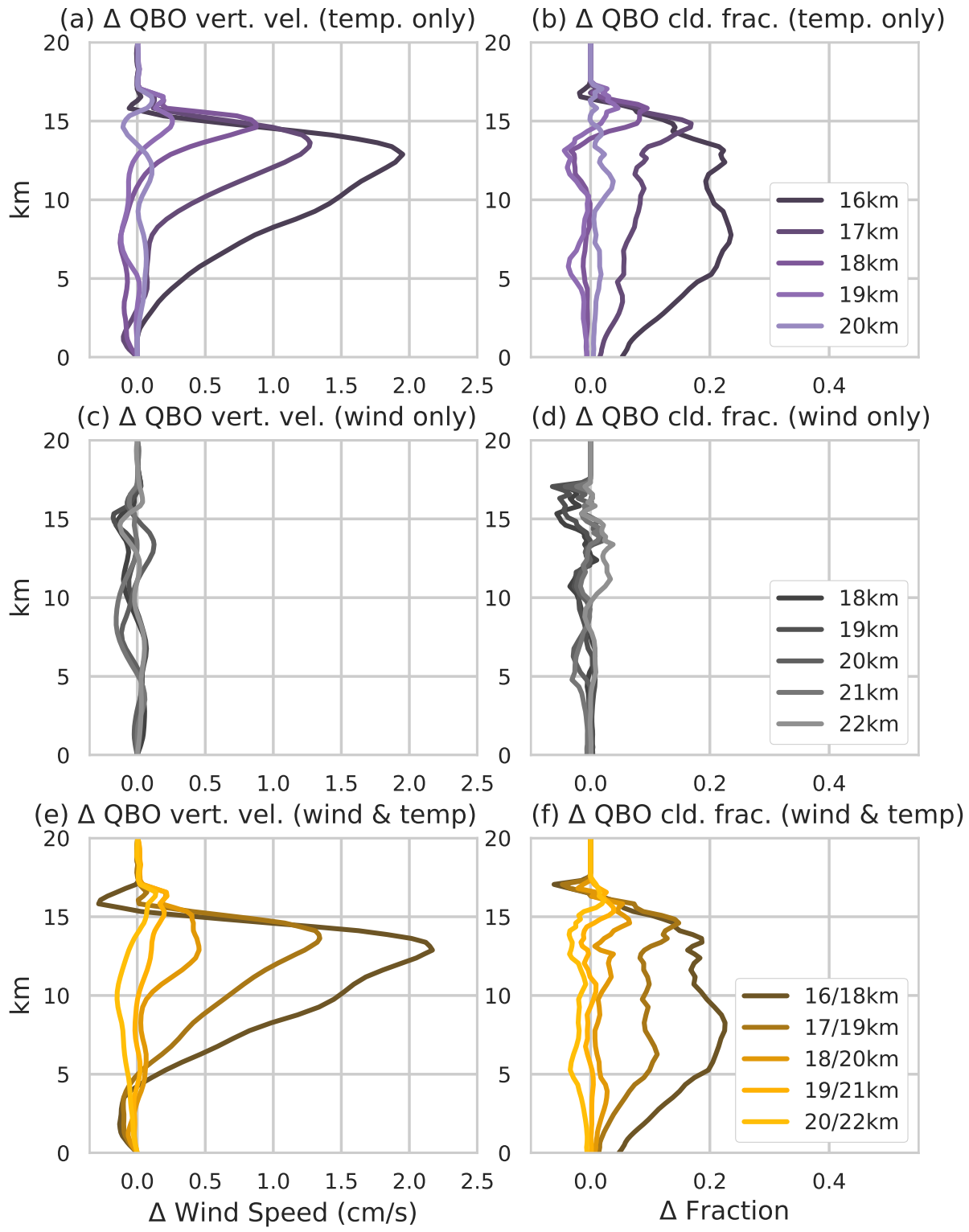

Figure 3.7: Time-mean, horizontal-mean QBOE-QBOW differences in vertical velocity (left) and cloud fraction (right). The top row is temperature-only experiments (purple), the center row is wind-only experiments (grey), and the bottom row is combined wind and temperature experiments (gold). Darker colors indicate lower-peaked anomalies; the legend indicates the altitude of the peak of the anomaly (z_0). For the combined temperature and wind experiments, the legend indicates first the height of the peak of the temperature anomaly, then that of the wind anomaly.

a similarity between the temperature-only and the temperature and wind experiments, and a monotonic relationship between the height of the QBO anomaly and the strength of the MJO convective response. This is true both in the time mean and standard deviation.

Precipitation changes display a less clear or consistent relationship as z_0 is varied, compared to changes in other fields (Figs. 3.8a,c). Only in the temperature-only experiment with the lowest-altitude forcing (z_0 =16 km) are precipitation signals clearly seen in the time mean or standard deviation. In all the higher-altitude forcing experiments it is difficult to detect a clear QBO-induced signal and the precipitation displays a lack of monotonicity with respect to forcing altitude. We conclude that no precipitation signal is clearly present in these QBO experiments. Possible reasons why the MJO-QBO relationship is less apparent in precipitation than in other variables are discussed more in Section 3.4.

To further explore forcing the model with more realistic altitude QBO anomalies, we repeat the 18km-peaked temperature anomaly simulation including five ensemble members each for QBOE and QBOW. This allows us to better assess the strength of the signal in the case where the MJO response is small. The results are shown in Figures 3.9-3.11.

Compared to the 16km-peaked runs, the changes in the model to the 18km-peaked QBO temperature anomaly are at times difficult to distinguish from noise. In particular, there no longer seems to be a robust or recognizable QBO signal for precipitation in the mean or the time series (Figs. 3.9 and 3.11). The QBO influence on OLR, while also much smaller than in the 16km-peaked temperature experiments, is more consistent across ensemble members, and typically shows a decrease during the MJO active phases in QBOE relative to QBOW (i.e. Fig. 3.9b from day 30-35 and day 50-55), and a small increase in the suppressed phase. Both vertical velocity and cloud fraction changes are clearer than OLR or precipitation, and are especially evident during MJO active phases. In the time mean, the changes have the same sign as the 16km-peaked results, albeit with a smaller magnitude (Figure 3.10). In addition, the signal is more localized to the upper troposphere compared to the 16 km run, and is near zero below 10 km in both cloud fraction and vertical velocity.

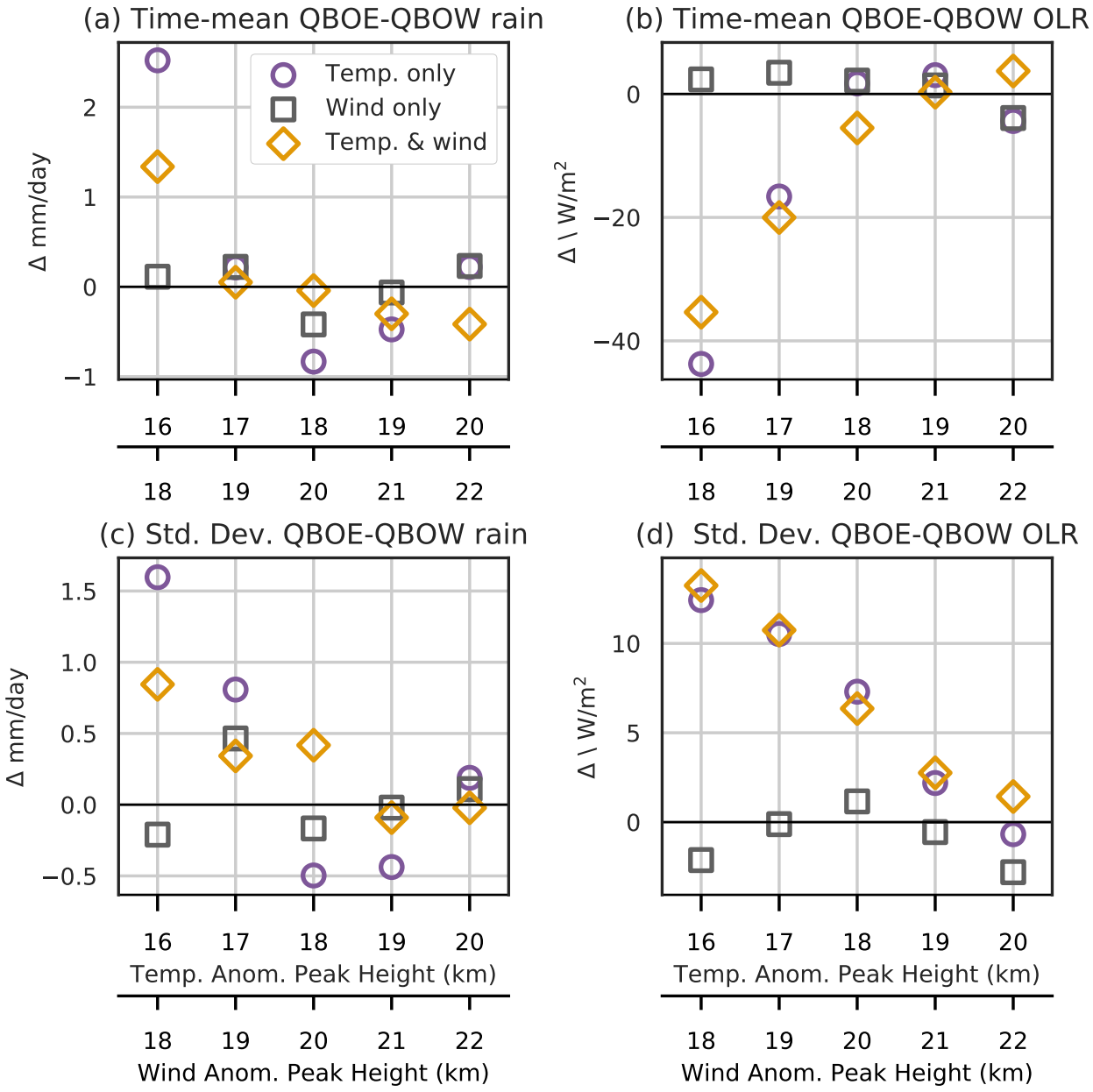

Figure 3.8: QBOE-QBOW differences in the time-mean (top row) and standard deviation (bottom row) of rain (a,c) and OLR (b,d) from the same experiments as in Figure 3.7. The y-axis shows the magnitude of the difference. The x-axis is the altitude (in km) of the peak of the QBO temperature or wind anomaly: farther right corresponds to higher altitudes. The results are shown for temperature-only experiments (purple, circles), wind-only experiments (grey, squares), and temperature and wind experiments (gold, diamonds).

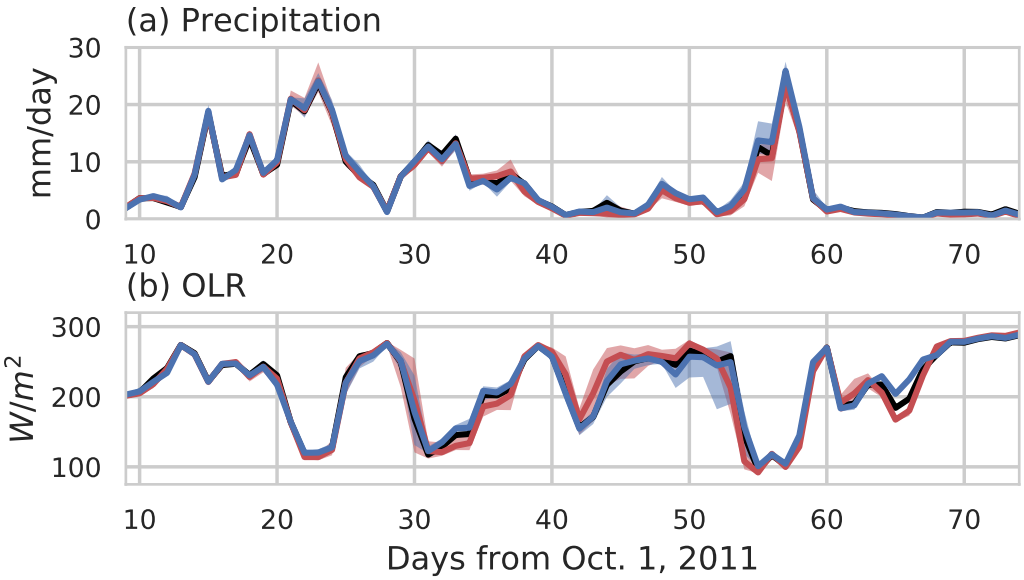

Figure 3.9: Horizontally-averaged precipitation (top) and OLR (bottom) from integrations with QBO temperature anomalies which peak at 18 km, as opposed to the 16 km shown in Figure 3.4. As in Figure 3.4, the shading indicates spread among ensemble members and the bold is the ensemble average; note that the control spread is not shown.

Figure 3.11 compares the ensemble QBOE-QBOW spread in the time mean and standard deviation of OLR and precipitation between the 16km-peaked and 18km-peaked runs. This establishes that while time-mean QBOE precipitation is always higher than QBOW precipitation in the 16km-peaked runs, the ensemble spread is fairly large; the precipitation signal is absent in the 18km-peaked simulations. The time-mean QBOE-QBOW OLR changes across ensemble members are also near zero in the 18km-peaked integrations. However, the 18 km runs do display a signal in the standard deviation of OLR, with an ensemble-mean QBOE-QBOW difference in standard deviation of approximately 5 W/m^2 (Fig. 3.11d). In this regard, the 18km-peaked runs may be more consistent with the observed relationship, with a small change in the mean but a larger signal in the standard deviation (e.g. Son et al. (2017)). However, care should be taken in interpreting this result, as it may simply be fortuitous and attributable to the small magnitude of the changes or the short integration period. Additionally, interpretation of this result is complicated by the lack of agreement between simulated and observed OLR, especially during the suppressed phase.

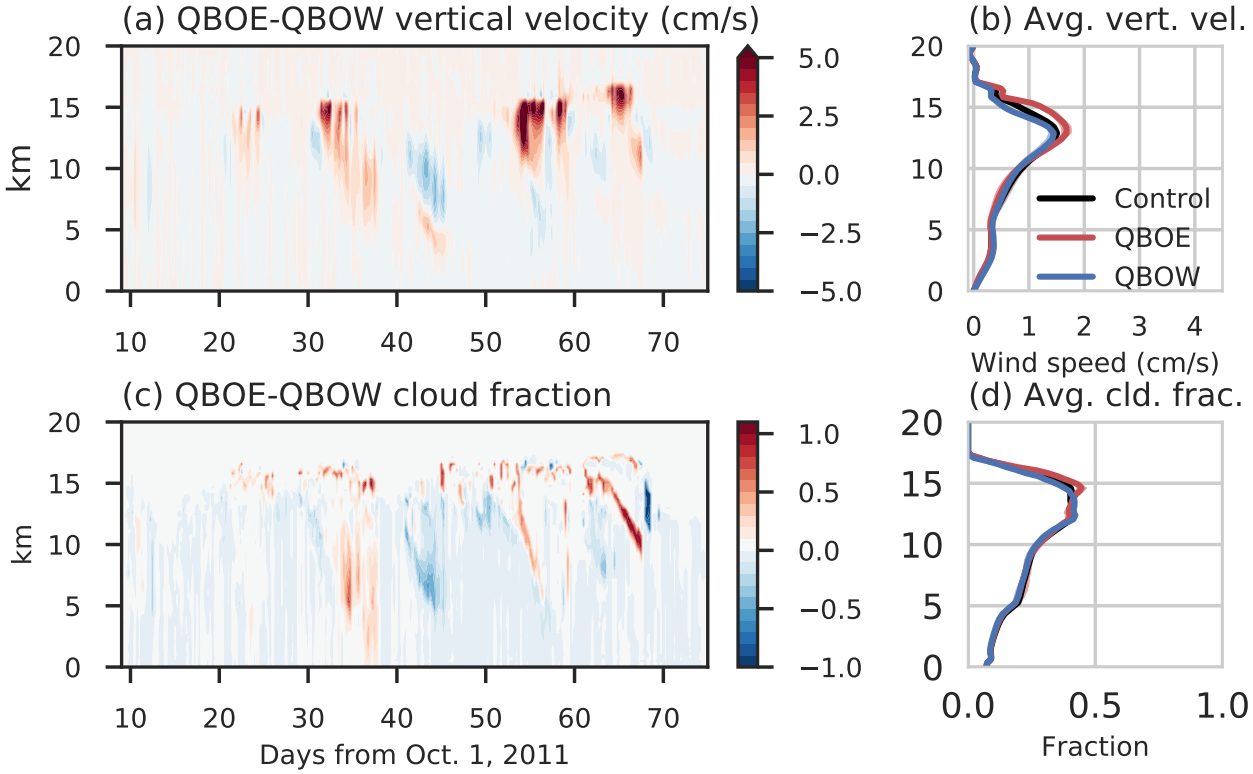

Figure 3.10: From the same experiment as in Figure 3.9, showing the horizontally-averaged, ensemble-averaged QBOE-QBOW difference in vertical velocity (top) and cloud fraction (bottom). As in Figure 3.5, the right panels show the time-mean for the control, QBOE, and QBOW runs, with shading indicating ensemble spread.

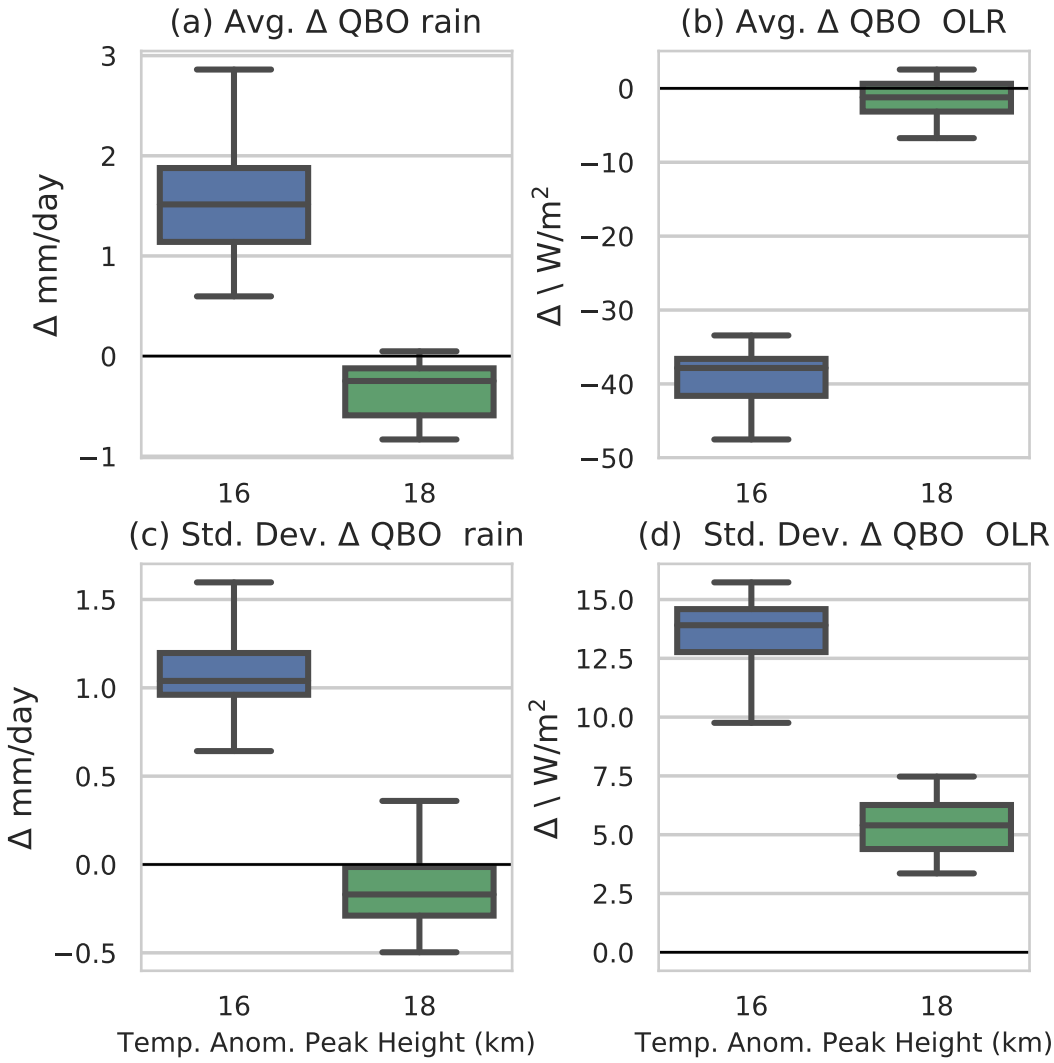

Figure 3.11: QBOE-QBOW changes in the mean (top) and standard deviation (bottom) of domain-averaged rain (a,c) and OLR (b,d) in the 16km-peaked and 18km-peaked temperature experiments. To capture the spread, the difference in the respective quantities was calculated for all 25 pairs of the 5 QBOE and 5 QBOW ensemble members. The box plots mark the median (center line), the upper and lower quartile (box), and the range (whiskers).

3.3.3.2 Amplitude of the QBO Temperature Anomalies

In this section we examine the effect of changing the amplitude of the QBO temperature anomalies. We repeat the simulations from Section 3.3.2 where $z_0 = 16$ km but include additional experiments either doubling or halving QBO temperature anomaly. Each experiment is conducted with a single ensemble member. The results (Figures 3.12 and 3.13 and Table 3.2) indicate a monotonic relationship between the amplitude of the QBO temperature anomaly and the strength of the MJO convective response. The QBOE integrations with the greatest amplitude ($M_t = -2$ K, approximately double the observed amplitude) show the lowest OLR, strongest vertical velocity, and highest cloud fraction, while those with the strongest QBOW amplitude ($M_t = 2$ K) show the highest OLR, the weakest vertical velocity and cloud fraction, and the lowest precipitation. The QBOE-QBOW temperature anomalies with $M_t = \pm 0.5$ K by contrast have the weakest response relative to the control, while the "realistic" amplitude temperature anomalies with $M_t = \pm 1$ K have a response in between the ± 0.5 K and ± 2 K results.

Despite being monotonic, the results do not appear strictly linear. For example, the QBOE-QBOW difference in vertical velocity, cloud fraction, and OLR is larger when comparing the 2 K QBOE run to the control run than when comparing the 1 K QBOE and QBOW runs to one another (not shown). This is despite the fact that the total QBOE-QBOW anomaly is identical in each case. This suggests that the MJO response to the same QBO forcing may be stronger when the TTL is colder, i.e. that the MJO response may depend on the base state of the tropopause region. However, given that the literature on the MJO-QBO relationship has not addressed the issue of the TTL base state, and that this may simply be an artifact of our limited number of integrations or idealized model, we defer further exploration of this question to future work.

While the time-mean precipitation response is monotonic (Table 3.2), the time series in Figure 3.12 shows that precipitation generally varies in a more complex manner across these integrations. The 2 K QBOE run, for example, rarely rains more than the 1 K and 0.5 K

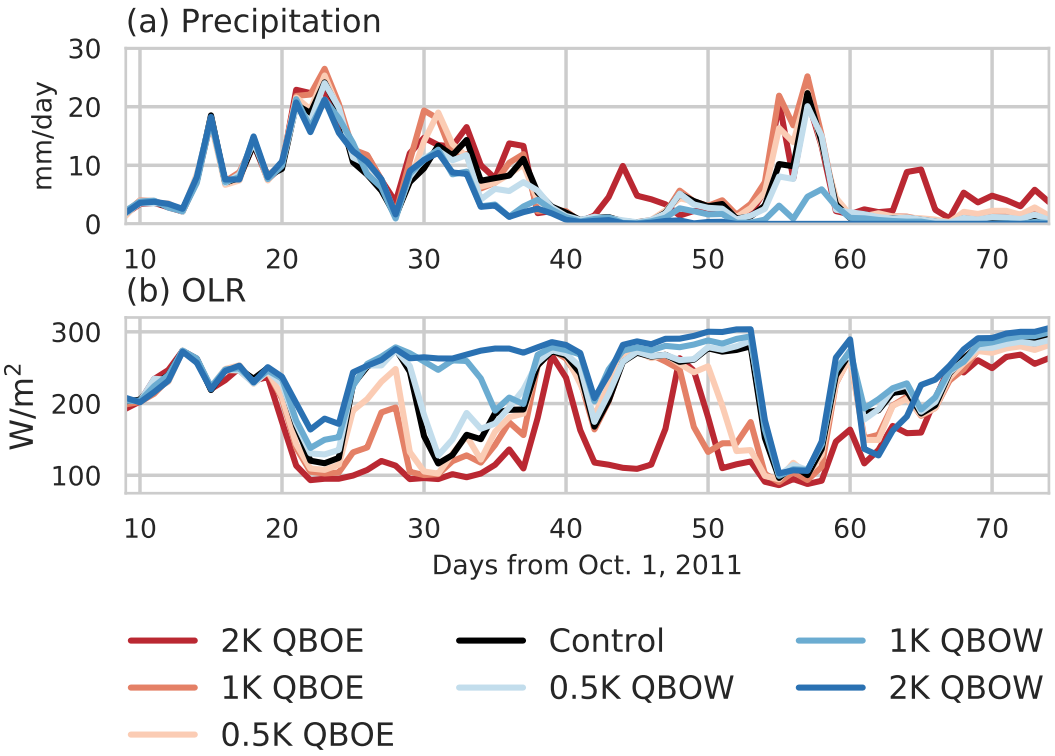

Figure 3.12: Horizontally-averaged precipitation (top) and OLR (bottom) from simulations varying the amplitude of the QBO temperature anomaly (all with $z_0 = 16$ km). Here darker red indicates a stronger QBOE anomaly and darker blue indicates stronger QBOW. The legend indicates the phase of the QBO and the magnitude of the QBO amplitude ($|M_t|$). The control, 2K QBOE, and 2K QBOW runs are not the ensemble average as in Figure 3.4, but a particular run chosen randomly from the five ensemble members, to facilitate comparison.

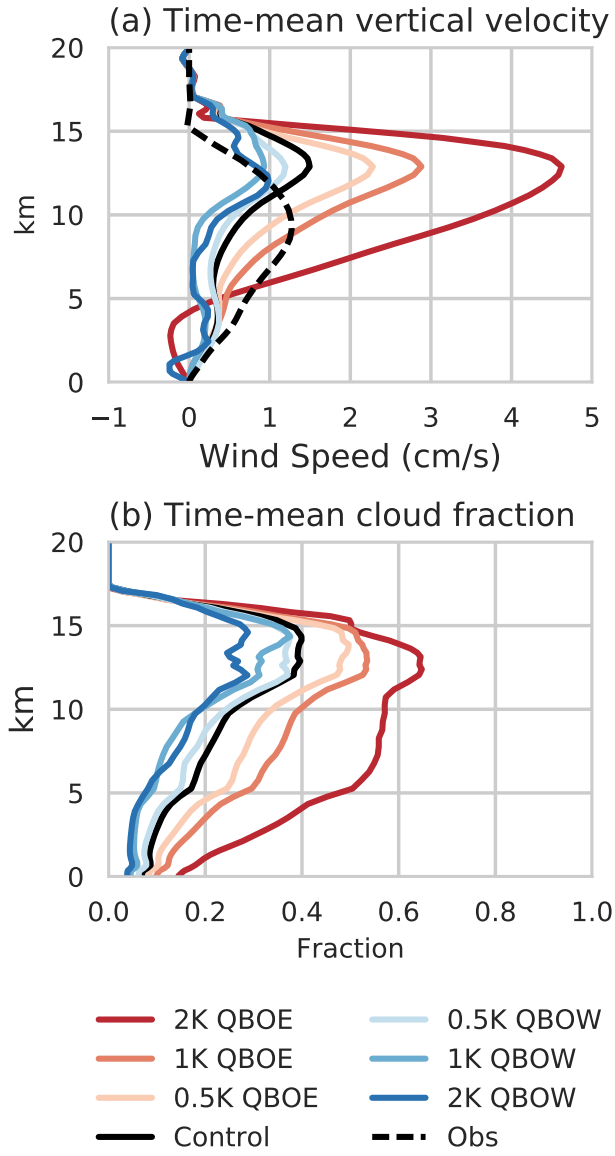

Figure 3.13: As in Figure 3.12; showing the time-mean vertical velocity and cloud fraction. The observed vertical velocity is also shown in dashed black.

QBOE runs, except in the periods following the MJO active phases. More significantly, the 2 K QBOW run completely misses the second MJO event, settling into the non-precipitating state discussed in Section 3.2.3 (see Fig. 3.12a at day 45). While the dry state is inconsistent with the DYNAMO data and prohibits comparison to some degree, it is indicative of the ability of temperatures in the TTL to exert an influence on the troposphere (if too strongly so). That the precipitation time series across these experiments are less monotonic than other variables is consistent with findings already noted.

List of experiments	**Precipitation (mm/day)**	**OLR (W/m^2)**
QBOE ($M_t = -2$K)	7.51	165
QBOE ($M_t = -1$K)	7.02	193
QBOE ($M_t = -0.5$K)	6.50	203
Control	5.97	220
QBOW ($M_t = 0.5$K)	5.76	224
QBOW ($M_t = 1$K)	4.49	237
QBOW ($M_t = 2$K)	3.98	243

Table 3.2: Time-mean, domain-averaged precipitation and outgoing longwave radiation for the seven experiments varying the amplitude of the QBO temperature anomaly. The first column indicates the amplitude of the QBO temperature anomaly, per Eq. 3.2.

3.4 Discussion

Our results suggest that QBO-induced temperature anomalies in the tropical tropopause region can influence convection associated with the MJO, providing a likely pathway for the MJO-QBO relationship seen in observations. Our sensitivity experiments demonstrate that the height and the amplitude of the QBO temperature anomaly substantially affect the strength of the MJO convective response. These sensitivities are consistent qualitatively with Nie and Sobel's (2015) results on the QBO influence on convection in a statistically

steady state, though their focus was not on the MJO. Both the pronounced sensitivity to the height of the temperature anomaly and the stronger model response to the QBO during the MJO active phases suggest that the QBO exerts an influence on the MJO primarily through an influence on convection sufficiently deep that it reaches the QBO temperature anomalies. This is consistent with other studies that show the QBO modulates convection in regions where such convection is already strong (e.g. Collimore et al. (2003); Liess and Geller (2012)). It may also offer insight into why the MJO-QBO link only manifests in boreal winter, as MJO convection is known to be strongest during that season (e.g. Zhang (2013)). This sensitivity of the QBO impact to the depth of convection could further explain why the observed QBO influence on the MJO seems strongest around the Maritime Continent (e.g. Son et al. (2017); Zhang and Zhang (2018)). Our study, which is centered over the Indian Ocean, may under-estimate the effect of the QBO on the MJO for this same reason, though we have not explored this possibility here.

Our results also show a sensitivity to the amplitude of the QBO temperature anomaly. This finding may be particularly applicable to the recent work by Lee and Klingaman (2018), who examined the MJO-QBO relationship in a GCM and found no significant link between the two phenomena. One of their hypotheses was that the GCM-simulated QBO temperature anomalies were too weak: less than one-fourth the magnitude of the observed anomaly (their Figure 4). Our results here lend additional support to that hypothesis.

As seen in Section 3.3 and in Appendix B, the response of MJO-related precipitation to the QBO state in our model is sensitive to the model configuration, and displays less monotonicity than other variables to variations in the height and amplitude of the QBO temperature anomaly. Precipitation also shows the greatest degree of variability between QBOE and QBOW. Given that Son et al. (2017) found a strong QBO signal in precipitation, this lack of a clear signal is difficult to reconcile with observations. However, Nie and Sobel (2015) found in their study imposing similar QBO anomalies in an idealized model that the QBOE-QBOW precipitation change was a non-monotonic function of sea-surface

temperature. This non-monotonicity resulted from a competition between changes in the gross moist stability (associated with changes in the vertical structure of the large-scale vertical motion) and radiative feedbacks, and suggests that precipitation changes may be more delicate than changes in other variables are. This may explain why, for example, in Figure 3.7 we observe cases with notable changes to the vertical velocity and cloud fraction but small changes in precipitation. In these cases, changes to the radiative heating (for example, warming due to an increase in high clouds) and changes in the amplitude and structure of the vertical velocity (e.g. towards a more top-heavy vertical velocity profile) may counteract one another. For a more nuanced discussion of the implications of these types of changes on precipitation, readers are referred to Nie and Sobel (2015; their Section 3c).

Zhang and Zhang (2018) also looked more specifically at the question of the QBO influence on MJO-related precipitation in their observational study. They noted that in the Indian Ocean, QBO changes to total precipitation were insignificant due to cancelling effects of precipitation associated with the MJO and non-MJO precipitation: non-MJO precipitation shows increases in QBOE whereas MJO precipitation decreases in QBOE. These results, in conjunction with our study, suggest the relationship between the QBO and MJO precipitation associated with the MJO deserves more careful study.

Other observational evidence further suggests it is important to distinguish between QBO changes to tropical mean convection and QBO changes to convection associated with the MJO. Son et al. (2017) showed that QBO changes to tropical mean OLR were not statistically significant, whereas QBO changes to the variance of OLR on MJO timescales were significant (their Fig. 1; Fig. 2.21). As other studies have found evidence for QBO changes to mean convection (i.e. Collimore et al. (2003); Liess and Geller (2012), Nie and Sobel (2015), Jie Nie and Adam Sobel, personal communication), more observational studies on this issue are needed.

In all our simulations in which the QBO has an influence on the MJO, that influence is

strongest during the MJO active phase, and weaker or of opposite sign during the suppressed phase. This strengthening of MJO convection primarily during the active phase leads to an increase in the variance on MJO timescales. Whether the mean state also changes due to the QBO depends on the relative sign and magnitude of changes in the active and suppressed phases. In several of our runs, especially the 16km-peaked temperature experiment, we observe a change in the time-mean of all the variables we consider, including OLR and precipitation. This seems inconsistent with the results of Son et al. (2017). However, our 65-day time period of integration makes separation of the mean state and MJO difficult. It may be that for longer integrations that simulate more MJO events changes to the mean state like those seen in our study would be averaged out. Additionally, the 16km-peaked and 17km-peaked runs have a larger QBO forcing than observed, making direct comparison with observations difficult. In runs with smaller forcing, such as the 18km-peaked temperature experiments, the increase in the active phase is smaller, and is balanced in the mean by the decreases during the suppressed phase, leading to less change in the mean-state while still allowing for a change in variance (i.e. Figure 3.11).

3.5 Conclusion

In this study we examine the MJO-QBO relationship using a cloud-resolving model coupled to parameterized large-scale dynamics. The goal is to explore whether the model can reproduce aspects of the observed MJO-QBO relationship; in particular, a strengthening (weakening) of MJO convection during the easterly (westerly) phase of the QBO. We also seek to identify likely pathways through which the QBO modulates the MJO. After establishing that our model reasonably reproduces two observed MJO events (Figure 3.3), we conduct three types of experiments: (1) adding only QBOE/W temperature signals to the large-scale forcing; (2) adding only QBOE/W zonal wind signals; and (3) adding QBOE/W temperature and wind signals together. These experiments were designed to isolate particu-

lar pathways of potential QBO influence. In addition, we conducted sensitivity experiments modifying the height and amplitude of the QBO anomalies (see Table 3.1). Our main results can be summarized as follows:

1. Forcing the model with idealized QBO temperature anomalies in the tropopause region (without the accompanying QBO wind anomalies) influences the simulated MJO convection in a manner qualitatively consistent with the observed MJO-QBO relationship: strengthening the MJO convection during QBOE and weakening it during QBOW (Figs. 3.4 and 3.5). This is evident across several variables, including cloud fraction, vertical velocity, precipitation, and outgoing longwave radiation.

2. QBO wind anomalies do not have a large effect on the model MJO convection (e.g. Fig. 3.7), either on their own or in combination with temperature anomalies, indicating that the dominant influence of the QBO on the simulated MJO convection is that due to QBO temperature anomalies.

3. The MJO response to the QBO depends significantly on the height and amplitude of the QBO temperature anomaly. Higher altitude or smaller amplitude temperature anomalies lead to a weaker MJO response (e.g. Figs. 3.8 and 3.13). For "realistic" heights of the QBO temperature anomalies, the QBO influence on simulated MJO convection is smaller than that in cases with lower-than-observed anomalies, and for some variables (e.g. precipitation) is inconclusive (Fig. 3.11).

Taken as a whole, our results suggest that the QBO-induced temperature anomalies could play a role in driving the MJO-QBO interaction. However, our results do not entirely explain the observed MJO-QBO relationship, and several caveats deserve further study. First, while the MJO response is clear and of the correct sign for larger-than-observed forcing, more realistic QBO temperature anomalies induce a smaller signal that is difficult to detect. Additionally, the model's precipitation response to the QBO is at times either absent or of the opposite sign to that initially expected (i.e. higher during QBOW than QBOE).

Precipitation also displays non-monotonic behavior with respect to QBO forcing parameters in our sensitivity testing, and the response is sensitive to the model configuration (Appendix B). Finally, in several simulations we observe QBO-induced changes not only to the variance of MJO convection, but also to the mean state. This seems inconsistent with the results of Son et al. (2017), though it is possible that this difference is due to our short integration period ($\sim$2.5 months) which makes separation of MJO and climatological timescales difficult.

* * *

In the concluding paragraph of Martin et al. (2019) we noted: "Additional work is needed to verify our results, especially modeling studies that simulate more complex pathways of QBO influence or a more realistic interplay between the MJO and QBO." The desire to move to a more complex model was in part due to the fickle nature of the cloud-resolving model presented here[2] and in part because this modeling framework was still fairly idealized. Forecast modeling studies conducted both before (e.g. Marshall et al. (2017)) and during (e.g. Wang et al. (2019b)) our cloud-resolving modeling work had further demonstrated that those models were capable of simulating an MJO-QBO connection. This, therefore, seemed like a promising framework to move towards, and within our group collaborations and resources for such a project were fortunately already in place. In particular, connections at ECMWF would allow us to make use of a model with an exceptionally good MJO, hopefully maximizing the chance that an MJO-QBO link would emerge. Around Halloween of 2017, we embarked on our next modeling project looking at the MJO-QBO link in a forecast model.

[2]The model enjoyed settling into pathological states which made extending this work sometimes somewhat of a chore.

Chapter 4

The Impact of the QBO on the MJO in a Forecast Model

Note: This chapter has been published in very near its present form as "The impact of the stratosphere on the MJO in a forecast model" in *J. Geophys. Res.: Atmos.* (2020), Vol. 125, e2019JD032106, doi: 10.1029/2019JD032106.[1] Minor edits have been made for clarity and length.

4.1 Introduction

The Madden-Julian oscillation (MJO; Madden and Julian (1971); Madden and Julian (1994); Zhang (2005)) and stratospheric quasi-biennial oscillation (QBO; Baldwin et al. (2001)) are important oscillatory modes of variability in the tropical atmosphere. The MJO, characterized by eastward-propagating, planetary-scale anomalies in convection and winds, is the

[1]AUTHORS: Zane Martin[a]*, Frederic Vitart[b], Shuguang Wang[a], Adam Sobel[a,c]

[a] Department of Applied Physics and Applied Mathematics, Columbia University, New York, NY
[b] European Centre for Medium-Range Weather Forecasting, Reading, UK
[c] Lamont-Doherty Earth Observatory, Columbia University, Palisades, NY

* corresponding author: Zane Martin, zkm2102@columbia.edu

main source of subseasonal (∼30-60 day) variability and predictability in the tropics, and has global impacts via teleconnections (Zhang (2013)).

The QBO occurs on longer timescales and higher in the atmosphere than the MJO does; it is characterized by a ∼28-month cycle in which the stratospheric zonal mean zonal wind reverses sign. The easterly and westerly wind regimes form in the upper stratosphere and descend to near the tropical tropopause layer (TTL; Fueglistaler et al. (2009)) with a speed of around 1 km/month (Baldwin et al. (2001)). Through thermal wind balance, QBO winds are accompanied by temperature anomalies that also reach the TTL.

The influence of the QBO on the troposphere has been studied for some time (Giorgetta et al. (1999); Collimore et al. (2003); Liess and Geller (2012)), but recent results have demonstrated a striking association between the QBO and the boreal winter MJO (Yoo and Son (2016); Son et al. (2017); Nishimoto and Yoden (2017)). The QBO accounts for roughly 50% of the inter-annual variation in MJO strength, with a stronger MJO when the QBO winds (defined at 50 hPa) are easterly and the TTL is anomalously cold (Son et al. (2017)). The QBO phase also exhibits statistical relationships with the propagation speed (Son et al. (2017)), teleconnection strength (Wang et al. (2018)), and predictability of the MJO (Marshall et al. (2017); Lim et al. (2019); Wang et al. (2019b)), as well as the tendency of the MJO to propagate through the Maritime continent (Zhang and Zhang (2018); Densmore et al. (2019)). However, the mechanism by which the QBO modulates the MJO remains unclear.

Any explanation of the QBO influence on the MJO needs to address several facts that render the observed relationship between them complex. First, the MJO-QBO link is only statistically significant in boreal winter, and by some metrics has the opposite sign in boreal summer (Wang et al. (2019b)). Second, the QBO impact seems to favor certain MJO phases, namely those in which convection is enhanced around the Maritime Continent (Zhang and Zhang (2018); Densmore et al. (2019)). Third, the MJO appears to be more strongly influenced by the QBO than any other mode of variability in tropical convection is; Kelvin

waves, Rossby waves, mixed Rossby-gravity waves, and the tropical mean state all demonstrate little to no modulation by the QBO (Son et al. (2017); Abhik et al. (2019)). Finally, one recent study (Klotzbach et al. (2019)) indicates that the MJO-QBO relationship may have changed on longer timescales, with the emergence of a strong MJO-QBO correlation only since the 1980s.

A number of recent studies provide evidence that the QBO influence on MJO convection is linked to QBO temperature anomalies. Both observational (Hendon and Abhik (2018), Abhik and Hendon (2019)) and modeling studies (Nie and Sobel (2015); Martin et al. (2019)) have shown that cold QBOE temperature anomalies – which destabilize the troposphere to deep convection and may induce additional feedbacks (for example from cloud-radiative effects) – can strengthen MJO convection during easterly QBO periods, and vice versa during QBOW. The MJO may be particularly affected due to its relatively strong convective signature and its vertical structure (Hendon and Abhik (2018); Abhik et al. (2019)). However, the observational studies do not clearly demonstrate causality, nor separate QBO temperature anomalies from other possible pathways of MJO influence – including QBO variations in vertical wind shear, cloud-radiative forcing, or vertical wave propagation. Modeling studies using comprehensive global models have yet to demonstrate a clear QBO impact on the MJO (e.g. Lee and Klingaman (2018)).

Modeling work on the MJO-QBO link is vital for identifying or ruling out particular pathways of influence and key aspects of the relationship. However, as both the MJO and QBO are difficult to capture in global models (Lee and Klingaman (2018)), finding a suitable model presents a challenge. Any failure of a particular model to show an MJO-QBO link is difficult to attribute to a particular cause due to model biases in both phenomena.

Here we examine the MJO-QBO connection using a state-of-the-art forecast model. While most prior MJO-QBO studies using forecast models have focused primarily on how and why the QBO modulates the predictability of the MJO (Marshall et al. (2017); Lim et al. (2019); Wang et al. (2019b)), here we are more concerned with the physical mechanisms of the

apparent MJO-QBO link. As such, we perform numerical experiments in which we alter the initial conditions in the model stratosphere and examine how this changes the behavior of the MJO. These stratosphere-altering experiments allow us to separate the impacts of the QBO on the model MJO that are consequences of the model's initial tropospheric conditions (i.e. from the observations, in which the QBO affects the MJO) from those exerted directly by the model stratosphere during the simulation.

Our study is organized as follows: Section 4.2 presents details regarding the model, observational data, methodology, and experimental design. Section 4.3 demonstrates the viability of our QBO experiments, and presents results from both control simulations and experiments in which we alter the model stratosphere. Section 4.4 discusses our findings and offers directions for future work, and Section 4.5 summarizes and concludes the study.

4.2 Data, Methods, and Model

4.2.1 Model Details and Configuration

We use a global forecast model from the European Centre for Medium-Range Weather Forecasting (ECMWF), namely the Integrated Forecasting System, cycle 45r1, implemented in June 2018. The model utilizes a cubic octahedral grid with spectral truncation after 319 spherical harmonics, a resolution known as TCo319, corresponding to a horizontal grid spacing of ∼32km. In the vertical, the model has 137 levels with a model top at 0.01 hPa; it has a relatively "high top" which makes it well-suited for studying the stratosphere and QBO. The model atmosphere is coupled beginning on forecast day 1 to a dynamic, finite-differences ocean model with 0.25 degree grid spacing.

The model is integrated for 61 days, with initial conditions created from ECMWF's global interim reanalysis product (ERA-Interim; Dee et al. (2011)). The model output is sampled twice daily and results here are analyzed from days 0-55 to accommodate the construction of the MJO indices discussed in Appendix C.1. Results are considered on common vertical

levels for analysis and display: 1000, 850, 700, 500, 250, 200, 100, and 50 hPa (30, 10, and 1 hPa were output additionally for some experiments). To better capture internal variability and uncertainty in the initial conditions, each simulation contains 15 ensemble members, with ensemble spread generated by perturbing the atmospheric initial conditions using singular vectors and a 25-member ensemble of data assimilations (EDA), and by perturbing the model physics using stochastic physics (SPPT scheme; see Robertson and Vitart (2018) for more details).

4.2.2 Data and Methodology

We use ERA-Interim daily and monthly data for wind and temperature and NOAA's daily satellite data for outgoing longwave radiation (OLR; Liebmann and Smith (1996)) as observational targets to which we compare model results.

To track the QBO, we use monthly-mean ERA-Interim 50 hPa zonal-mean zonal wind, averaged over all longitudes and 10°N/S (U50 herein). As in previous studies (Yoo and Son (2016); Son et al. (2017)), we define westerly and easterly QBO phases as months when the index exceeds ± 0.5 standard deviation, respectively.

We track the MJO using two indices: the real-time multivariate MJO index (RMM; Wheeler and Hendon (2004)) and the real-time OLR-based MJO index (ROMI; Kiladis et al. (2014)). These two indices measure different aspects of the MJO. RMM primarily represents the wind anomalies associated with the MJO (e.g. Ventrice et al. (2013)), while OMI only tracks MJO convection.

The RMM index is formed using a multi-variate empirical orthogonal function analysis on meridionally averaged (15°N/S) anomalies of zonal wind at 850 and 200 hPa and OLR. To calculate the RMM indices, we follow a protocol similar to that in Gottschalck et al. (2010) and Rashid et al. (2011), as summarized in Appendix C.1.

ROMI is the real-time version of the OMI index that was developed to focus in particular on OLR (Kiladis et al. (2014)). OMI uses bandpass-filtered OLR to form a pair of 2-D

(latitude and longitude) EOFs that are functions of the day of the year and designed to isolate intra-seasonal convective signals. The standard OMI uses bandpass-filtered OLR, precluding it from being used in real-time, though a real-time version was also developed (Kiladis et al. (2014)). Because we consider hindcasts in this study, OMI could be used in principle, but we choose to use ROMI as a methodology for calculating the index in forecast models has been established (Wang et al. (2019a)) and there is high correspondence between OMI and ROMI (bivariate correlation > 0.9; Kiladis et al. (2014)). Our methodology for calculating ROMI (following Wang et al. (2019a)) is also outlined in Appendix C.1. Because ROMI uses a 9-day rolling mean centered on each day of the forecast, in this study we analyze simulations only up to day 55. Inclusion of results out to day 61 do not change the findings of this study.

We assess the strength of the MJO using the RMM/ROMI amplitude, $Amp(PC1, PC2; t)$, given principal components, $PC1(t)$ and $PC2(t)$, which are functions of time. This is calculated as:

$$Amp(PC1, PC2; t) = \sqrt{PC1(t)^2 + PC2(t)^2} \tag{4.1}$$

Given that we have 15 ensemble members on each initialization date, and that $Amp(PC1, PC2; t)$ is a nonlinear function of $PC1/2$, the MJO amplitude can be computed two distinct ways: as the amplitude of the ensemble-mean principal components or as the mean of the ensemble members' individual amplitudes. If we denote the ensemble mean of the principal components as $< PC1/2 >$ these are equivalent to:

$$Amp(< PC1 >, < PC2 >; t) \tag{4.2}$$

$$< Amp(PC1, PC2; t) > \tag{4.3}$$

Throughout this study we use Equation 4.3, the mean of the ensemble amplitudes. This is because the ensemble-mean amplitude (Eqn. 4.2) decays with time, even if the amplitudes in

the individual ensemble members do not, as positive and negative $PC1/2$ values tend to cancel each other at longer lead times. Equation 4.3 is well-suited for the stratosphere-altering experiments (described below) in which all the experiments form two super-ensembles, each ensemble with identical stratospheric initial condition, regardless of how it is perturbed (different initial dates, initial noise realizations, or physics).

4.2.3 Experimental Design

All model initialization dates are limited to December-February (DJF) because the MJO-QBO relationship is significant only in boreal winter (Son et al. (2017)). We chose three groups of initialization dates: each January 1st for all years from 1989-2016 (28 dates); dates during 1989-2016 DJFs in which MJO was strong and initially in RMM Phase 2 (25 additional dates); and dates in which the MJO was strong and initially in RMM Phase 4 (31 additional dates). This yields a total of 84 distinct initialization dates.

To select the precise Phase 2 and 4 initialization days, we required that an MJO event have initial RMM amplitude greater than 1.1, was in the preceding phase (i.e. Phase 1 or 3, respectively) on the previous day, and did not re-enter Phase 2 or 4, respectively, for 15 subsequent days (to exclude events which propagate opposite to what is typical). A list of all the initialization dates, sorted by the phase of the observed QBO during the month of their initialization, can be found in Table 4.1.

We then performed three types of model simulations:

1. Control experiments in which the model stratosphere is initialized from observations (i.e. is not altered in any way);

2. Imposed-QBOE (I-QBOE) experiments in which all initial conditions above 150 hPa are replaced with those from an arbitrarily chosen date in which the QBO was easterly (January 1, 2006); and

Dates with initial easterly QBO	**Dates with initial westerly QBO**	**Dates with initial neutral QBO**
1 January 1990, 1 January 1997, 1 January 1999, 1 January 2002, 1 January 2004, 1 January 2006, 1 January 2008, 1 January 2013, 1 January 2015, 25 December 1989a, 16 February 1990a, 13 January 1997a, 17 January 1999a, 12 January 2002a, 6 January 2006a, 20 February 2006a, 8 December 2007a, 25 January 2008a, 11 February 2013a, 13 January 1990b, 2 December 1994b, 13 December 1996b, 23 January 1999b, 27 January 2002b, 15 December 2003b, 2 February 2004b, 15 January 2006b, 22 December 2007b, 7 February 2008b, 3 January 2013b, 20 December 2014b	1 January 1989, 1 January 1991, 1 January 1994, 1 January 1996, 1 January 1998, 1 January 2000, 1 January 2003, 1 January 2005, 1 January 2007, 1 January 2009, 1 January 2011, 1 January 2014, 1 January 2016, 6 January 1989a, 10 December 1990a, 3 February 1994a, 14 January 1996a, 9 February 1998a, 18 December 2002a, 11 February 2003a, 30 January 2011a, 13 January 2016a, 22 January 1989b, 18 December 1990b, 22 January 1991b, 5 December 1993b, 20 December 1997b, 1 December 1999b, 13 January 2000b, 28 December 2002b, 2 January 2005b, 31 December 2006b, 4 December 2010b, 16 December 2013b, 12 December 2015b	1 January 1992, 1 January 1993, 1 January 1995, 1 January 2001, 1 January 2010, 1 January 2012, 19 December 1991a, 7 February 1992a, 2 December 1992a, 10 January 1993a, 26 December 2009a, 15 February 2012a, 13 February 1992b, 21 January 1993b, 13 January 1995b, 8 February 2001b, 2 December 2011b, 5 February 2016b

Table 4.1: Model initialization dates considered in this study, sorted by the observed QBO phase during the month of the initialization. "a" indicates dates when the MJO was strong and in Phase 2, and "b" indicates a strong Phase 4 MJO date, as described in Section 4.2.3.

3. Imposed-QBOW (I-QBOW) experiments in which all initial conditions above 150 hPa are replaced with a westerly QBO date (January 1, 2000).

The control experiments were only performed for the 28 simulations initialized on each January 1. A control was not run on other dates due to computational limitations, and because our focus is on how the imposed stratospheric states affect the MJO. The I-QBOE and I-QBOW experiments were each performed for all 84 start dates, for a total of 168 imposed-QBO experiments.

For the I-QBOE and I-QBOW experiments, we do not perform any smoothing of vertical discontinuities in the initial condition that replacing values above 150 hPa introduces. The advantage of this is that, for a given initialization date, below 150 hPa the I-QBOE and I-QBOW experiments at day 0 are identical. Any subsequent differences between the I-QBOE and I-QBOW simulations must therefore originate in the model stratosphere. Additionally, above 150 hPa all the I-QBOE experiments are initially identical: the same January 1, 2006 stratosphere is always imposed (and similarly for the I-QBOW experiments with the January 1, 2000 stratosphere). This means the initial I-QBOE minus I-QBOW stratospheric difference is the same for all imposed-QBO experiments, which clearly isolates the separate effects of tropospheric and stratospheric conditions on the model MJO. This allows us to better determine whether the QBO in this model has a direct effect on the troposphere during the simulations.

A drawback of this method is that we introduce vertical discontinuities between the troposphere and stratosphere. While the model adjusts quickly, there is likely a shock introduced by this mismatch in the I-QBOE/W experiments. We see likely evidence of such a shock during the first $\sim$4-5 days of these integrations, as discussed in Appendix C.2 and Section 4.3.3.1. We find that we can account for this shock and remove associated biases to some extent by re-calculating our MJO indices using different forecast climatologies for the I-QBOE and I-QBOW experiments, as discussed in Appendix C.2. The main results of this study are not sensitive to the methodology we use, suggesting that any shock has a limited

overall effect.

A second noteworthy feature of our methodology is that we do not include any nudging of the stratosphere after day 0. One may worry that without nudging, our I-QBOE/W states may not persist or may differ markedly from the observed or control QBO. However, Section 4.3.1.2 demonstrates that the persistence of our imposed-QBO states is largely comparable with the QBO's persistence in the control runs. Compared to observations, the imposed-QBO signals in the model, in particular the temperature signals, weaken with time. The implications of this are discussed more in Section 4.4. Still, given that the imposed-QBO state persists comparably to the control QBO, our experiments examine whether the stratospheric state in forecast models as they are typically run (i.e. without any nudging) have a measurable impact on MJO convection.

4.3 Results

4.3.1 Model QBO Performance

4.3.1.1 Control Simulations

The skill of the ECMWF model in simulating the MJO has been extensively studied (Vitart (2014), Vitart (2017); Kim et al. (2018); Lim et al. (2019); Wang et al. (2019b)), and the ECMWF model has by most metrics the greatest MJO prediction skill among all operational forecast models by a clear margin, with skill out to approximately five weeks lead time (Vitart (2017), Wang et al. (2019b)).

The ECMWF model is also able to simulate the QBO (Johnson et al. (2019); Lim et al. (2019)), though this metric is less well-documented. Recently Lim et al. (2019) found, using many more initialization dates than we consider (but without alterations to the stratosphere), that the correlation coefficient between the ECMWF model and the ERA-Interim QBO is .99 (their Table 2), indicating that the model does a good job of maintaining QBO wind

anomalies for subseasonal forecasts. On timescales longer than around two months, the QBO is not well-simulated in this version of the model (Johnson et al. (2019)) though changes to the gravity wave drag scheme can improve the QBO at longer, seasonal lead times. However, as these changes have little effect during the first two months of the simulation (Johnson et al. (2019)), they are not implemented here.

Figure 4.1 compares the model QBO in the control runs to observations. Dates are categorized as QBOE or QBOW based on the value of the U50 QBO index during the month of initialization. The top four panels show the QBOE minus QBOW zonally- and meridionally-averaged zonal wind and temperature as a function of lead time and height. Results are averaged over all the control simulations and compared to observations from the same periods. The bottom panels show the tropical averaged 50 hPa zonal wind and 100 hPa temperatures, composited over QBOE and QBOW periods separately from the control runs and observations.

Both QBO winds and temperatures decay with time in the model in a way that they do not in observations, though they still remain in good agreement for much of the run. The westerly and easterly winds retain their initial signs for all 61 days, and decay fairly linearly at $\sim$0.1 m/s per day. The temperature also shows relatively good agreement: at 100 hPa the model and observations match to within approximately $\pm$0.2K. No systematic bias in 100 hPa temperature seems to develop over time in the model compared to the observations, though the control simulation QBOE minus QBOW difference at 100hPa is smaller in magnitude than the observed at lead times longer than around 40 days.

Higher than 100 hPa, temperature differences decay with time more noticeably in the model than at 100 hPa (Fig. 4.1d), and even change sign in the control simulations after around 40 days (to anomalously warm in QBOE). However, in these simulations data were not output at 70 hPa: the level at which the peak in the QBOE minus QBOW temperature anomaly occurs in observations. Based on the biases in temperature relative to observations at other levels, we expect that the control runs maintain a negative anomaly at 70 hPa in

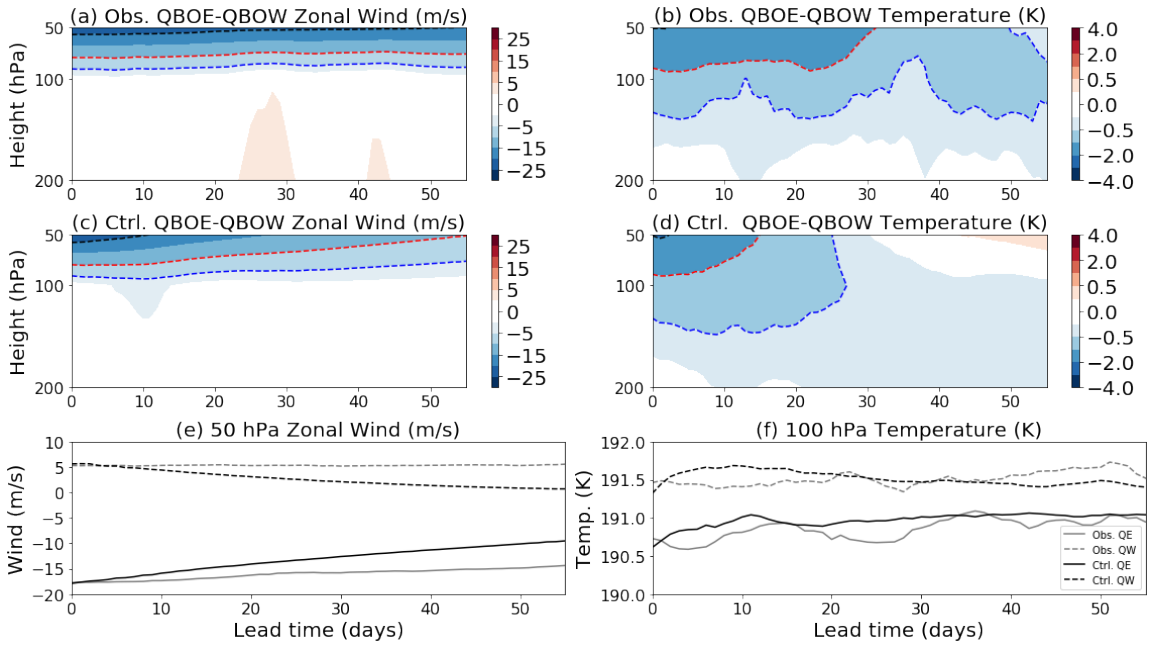

Figure 4.1: (a-d) QBOE minus QBOW zonal wind (left column) and temperature (right column) for observations (a,b) and control simulations (c,d). Contours are at -20 m/s (black), -10 m/s (red), and -5 m/s (blue) for zonal wind and -2K (black), -1K (red), and -0.5K (blue) for temperature. (e,f) QBO zonal wind at 50 hPa (e) and temperature at 100 hPa (f) shown separately for QBOE (solid) and QBOW (dashed). Observations are grey, and the control run is black. For all panels variables are averaged zonally and over 10° N/S. The observations have been linearly interpolated in height onto the coarser model grid.

these integrations, although we cannot demonstrate that with the data we have.

4.3.1.2 Imposed-QBO Experiments

We now examine the QBO in our imposed-QBO experiments. We find that the persistence of the imposed-QBO states is fairly consistent with the persistence of the control run QBO, as expected from long time scale of the QBO.

Figure 4.2 is similar to Figure 4.1, but the top panels now show the QBOE minus QBOW difference between the control runs initialized on January 1, 2006 and January 1, 2000, which are the dates we impose in the I-QBOE and I-QBOW experiments. The middle panels shows differences between the I-QBOE and I-QBOW experiments, averaged across all ensemble members for all 84 initialization dates in both the I-QBOE and I-QBOW runs. The bottom panels compare the 50 hPa zonal wind and 100 hPa temperature between the control (black), the imposed-QBO experiments (blue/red for I-QBOE/W) and the observations (grey). There, the mean across all experiments is the line, and shading represents the minimum and maximum for each initialization dates of the mean ensemble amplitude on each forecast day.

In general, the imposed-QBO experiments maintain their initial, altered stratospheric states above 150 hPa roughly as well as the control run maintains its un-altered stratospheric state. Below 150 hPa, differences in the control are due to the different tropospheric states on the selected control dates and are not representative of QBO impacts at lower levels. By design, the imposed QBO experiments have no differences in the initial conditions below 150 hPa.

The QBO wind signal in the imposed QBO simulation in particular is, on average, very similar to that in the control run, and imposed wind anomalies maintain their signs and approximate strengths for all 61 days. The bottom panel of Figure 4.2 shows the 50 hPa imposed-QBO wind is, on average, nearly identical between the control and imposed-QBO experiments (compare the black to the red/blue lines in panel (e)). The spread shows the

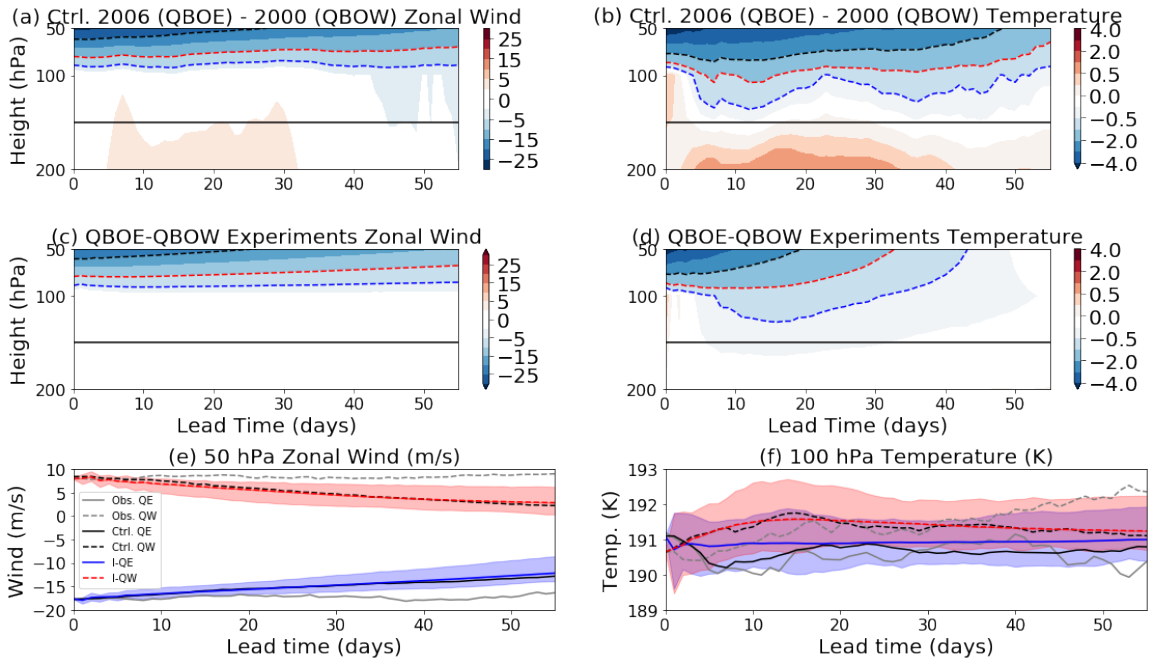

Figure 4.2: (a-d) QBOE minus QBOW zonal wind and temperature differences between (a,b) the Jan. 1, 2006 model control run (easterly QBO) and the Jan. 1, 2000 control run (westerly QBO) – the dates used for the imposed-QBO experiments. The middle panels (c,d) show the average difference between the I-QBOE and I-QBOW experiments averaged over all initialization dates. The black solid line is at 150 hPa, above which the model initial conditions are altered. Contours are as in Figure 4.1. (e,f) QBO zonal wind at 50 hPa (e) and temperature at 100 hPa (f) for the Jan. 1, 2000 QBOW control simulation (black dashed) and Jan. 1 2006 QBOE control simulations (black solid) as well as the same periods in observations (grey dashed/grey solid). The mean across all initialization dates from the imposed-QBOE simulations is shown in blue, and the mean from imposed-QBOW simulations is red. Shading shows the minimum to maximum range at each time step taken across all initialization dates.

I-QBOE and I-QBOW experiments have distinctly different stratospheres from one another for all lead times. This demonstrates that our methodology, with no additional nudging, is valid insofar as the model maintains the imposed QBO as well as it maintains the observed QBO.

The QBO temperature signal decays more quickly in the imposed-QBO experiments than in the control (panel (b) vs. (d)). At 100 hPa the I-QBOW and control QBOW temperatures show close correspondence, while the temperatures tend to be warmer in the I-QBOE experiments than the QBOE control or observations. There is also greater variability

in the temperatures across the imposed-QBO experiments: the ranges between the I-QBOE and I-QBOW experiments overlap to a considerable degree in panel (f).

Taking the I-QBOE minus I-QBOW 100 hPa temperature difference for each initialization date individually (not shown) we find that these temperature differences, after being positive for the first 1-2 days (a feature also seen in the control, but not the observations), are negative for all simulations from at least days 5-30. Thus, while there is more variability in the temperature compared to the wind, for a given start date the upper troposphere is always colder in the I-QBOE experiment relative to the I-QBOW experiment. This variability in the 100 hPa temperature and its implications for the MJO are examined more in Sections 4.3.3.1 and 4.4.

4.3.2 MJO-QBO Relationship: Control Runs

In this section we examine the MJO-QBO relationship from the control runs. While the sample size here is limited, our findings in general are consistent with other results (Marshall et al. (2017); Lim et al. (2019); Wang et al. (2019b); Abhik and Hendon (2019)), and we present them primarily for comparison to our imposed-QBO experiments in the following subsection.

For the control experiments the model has forecast skill using the RMM and ROMI indices out to 21 and 32 days respectively, measured via the bivariate correlation coefficient:

$$BCC(t) = \frac{\sum_i F_{1,i}(t)O_{1,i}(t) + F_{2,i}(t)O_{2,i}(t)}{\sqrt{\sum_i F_{1,i}(t)^2 + F_{2,i}(t)^2}\sqrt{\sum_i O_{1,i}(t)^2 + O_{2,i}(t)^2}} \tag{4.4}$$

F_1 and F_2 are the forecast ensemble-mean RMM1/2 or ROMI1/2 indices, O_1 and O_2 are the observed indices, and i denote the index of the reforecasts. The skill is measured as the time at which BCC drops below a threshold of 0.5. The forecast skill here is somewhat lower than in other recent studies (Lim et al. (2019), Wang et al. (2019b)), likely due to our relatively small sample size, which make the BCC somewhat noisy (not shown). Still, it

indicates that the model has significant MJO skill out to several weeks.

Also consistent with other forecast model studies (Marshall et al. (2017); Lim et al. (2019); Wang et al. (2019b); Abhik and Hendon (2019)), we find that the model shows stronger MJO events during QBOE compared to QBOW. Figure 4.3 shows the MJO amplitude in RMM/ROMI as a function of lead time for all forecasts (black), forecasts initialized in QBOE (blue), and initially QBOW forecasts (red). Observations are also shown in dashed lines. Plotted below the MJO amplitude are QBOE-QBOW differences in the model and observations.

Figure 4.3 shows that the model maintains the MJO amplitude as a function of lead time, though it is weaker than in observations (especially in QBOE). Thus, while the ensemble mean amplitude decays (not shown), individual ensemble members generally maintain the MJO's amplitude. This is potentially important, as weaker MJO events with shallower convection have been hypothesized to interact less with the QBO, since the shallower convection is unable to reach the levels in the upper troposphere where QBO has an influence (Hood (2017); Abhik and Hendon (2019); Martin et al. (2019)).

Figure 4.3 also indicates that on average the model MJO is stronger during QBOE than during QBOW, though there is a good deal of spread and the significance is hampered by a weaker-than-observed signal and small sample size. That the difference in the model is weaker than observed is consistent with Abhik and Hendon's (2019) finding that the QBO response in models tends to be too weak. Here our analysis differs from that of Abhik and Hendon (2019), who binned MJO events in QBOE and QBOW more stringently by their initial amplitude to control for the effects of the QBO in biasing the initial amplitude (towards stronger MJO events in QBOE). In this study, the relatively small sample size prohibits this approach.

The small sample size also means that differences are statistically significant only over a limited number of days. Here we measure significance using two methods. We first use a Welch's t-test (Welch (1947)) with a sample size consisting of the 9 QBOE and 13 QBOW

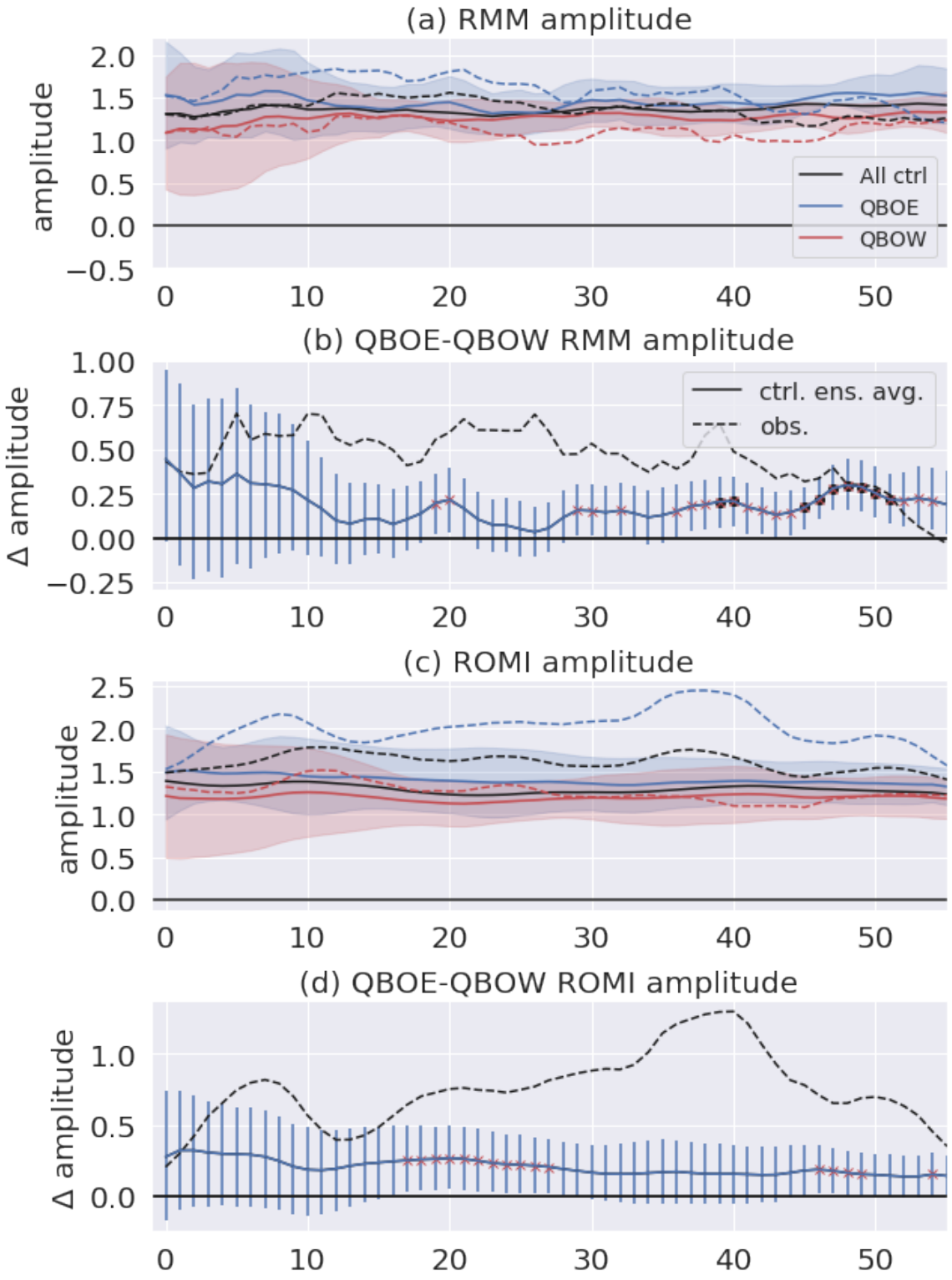

Figure 4.3: MJO amplitude calculated using the (a,b) RMM and (c,d) ROMI indices for all control integrations (black; solid), as well as those where the QBO is initially easterly (blue) or westerly (red). Shading in panels (a) and (c) represents one standard deviation. Corresponding observations are shown in dashed lines. Panels (b) and (d) show the QBOE-QBOW difference for the model (blue, solid) and observations (black, dashed). Model error bars are calculated using a bootstrapping re-sampling (Section 4.3), with significance at the 95% level shown with an "x". Significance using a t-test (Section 4.3.2) is shown with a black dot.

years, with a null hypothesis that the two samples do not differ and a 95% confidence level. Also shown are the results of a bootstrapping significance test: from the 28 control simulations we select 9 simulations at random without repetition and separately select 13 simulations randomly without repetition, matching the number of QBOE/W samples. We then calculate the MJO amplitude over these two sub-samples and difference them; we repeat this 1000 times from which we estimate the 95% confidence interval (the error bars shown in Fig. 4.2). In both cases, while the MJO is generally stronger in QBOE, we find only a few periods of significant increase.

If the amplitude of the ensemble mean is considered (calculated via Eqn. 4.2 as opposed to Eqn. 4.3), then the MJO amplitude decays with time, though the QBO difference is larger, with a stronger increase in MJO amplitude in QBOE relative QBOW. Calculating the difference this way also yields statistical significance on more days (not shown), though the overall conclusions are not materially different.

Figure 4.4 shows the MJO ensemble-mean amplitude binned by MJO phase. Grey bars indicate that all control simulations were considered, whereas blue and red bars show runs in which the QBO is initially easterly or westerly, respectively. Here we bin the data irrespective of the model lead time, and consider days from individual ensemble members as independent, which increases our sample size in the experiments. This is justified since both the initial conditions and physical parameterizations are perturbed by design to yield significant spread among the ensemble members that are independent of each other. Here the model shows a mean MJO amplitude comparable to the observed for RMM and ROMI (comparing the grey bars in panels (a/d) with panels (b/c)). The model MJO also demonstrates a significant QBO modulation in most phases, as seen in the rightmost panels (c/f). In both RMM and ROMI seven out of eight MJO phases show significantly stronger amplitude in QBOE than QBOW. This is consistent with observations, which also show significant increases in QBOE relative to QBOW, though the model QBO modulation is weaker than the observed. Why some MJO phases show stronger modulation than others is not clear.

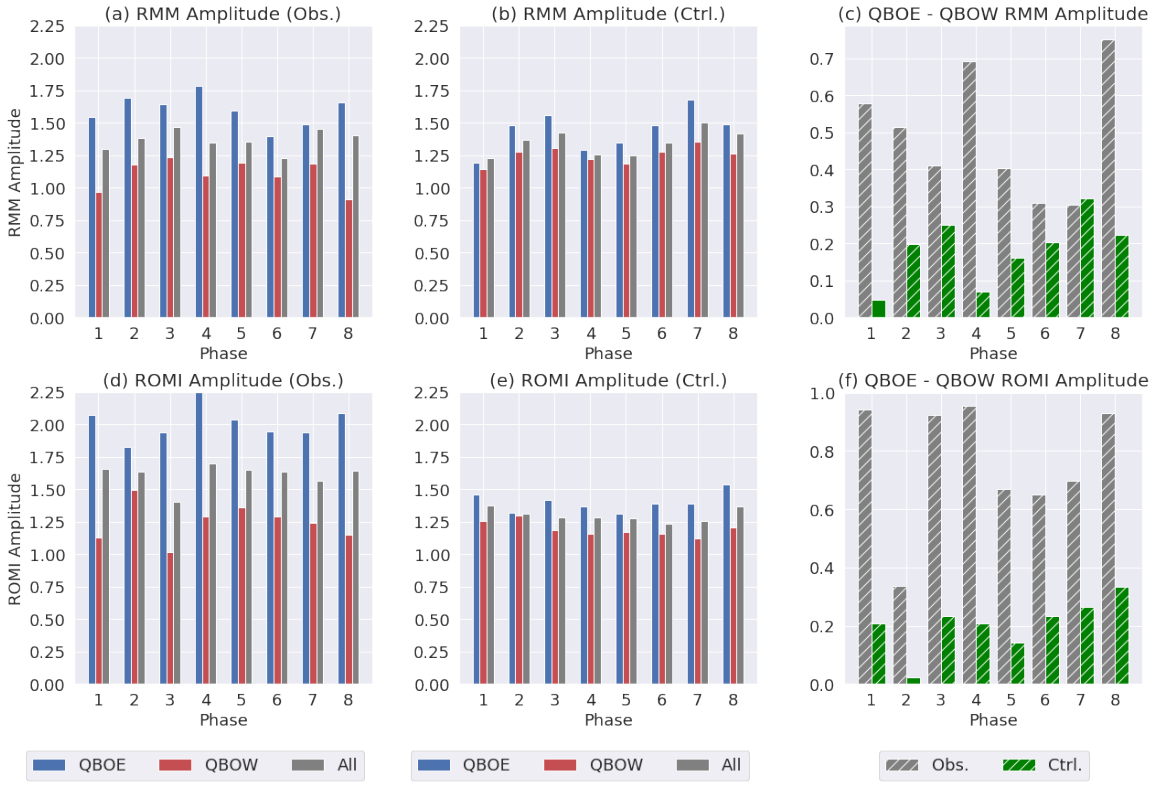

Figure 4.4: RMM (top) and ROMI (bottom) amplitude binned by MJO phase (irrespective of lead time). Grey bars are for all dates, and blue and red bars show dates where the QBO is initially easterly or westerly, respectively. The rightmost plot shows the QBOE-QBOW difference in observations (grey) and the model (green); hatching indicates significance at the 95% level, using a Welch's t-test with the degrees of freedom calculated as the number of days in each phase that are separated by at least 7 days, considering individual ensemble members and initialization dates as independent.

In addition to stronger MJO events during QBOE than QBOW, the model control runs displays greater predictability in QBOE, consistent with several previous results (Marshall et al. (2017); Lim et al. (2019); Wang et al. (2019b)). Using the BCC with a threshold of 0.5, the model MJO is more predictable in QBOE relative to QBOW by 15 days using ROMI (46 versus 31 days) and 6 days using RMM (23 versus 17 days). This is comparable to the results of Wang et al. (2019b) and Lim et al. (2019) who, using a larger sample size and a slightly different version of the ECMWF model from the Seasonal to Sub-seasonal prediction project (Vitart et al. (2017)), found a modulation of 10 days in ROMI (Wang et al. (2019b), their Fig. 2) and approximately 8 days in RMM (Lim et al. (2019), their Fig. 3).

While our results on predictability are comparable to previous studies, a recent study by Kim et al. (2019) calls into question more broadly the statistical robustness of QBO modulation of MJO predictability. They point out that in a range of forecast models, including the ECMWF model, differences in MJO predictability associated with the QBO are not statistically significant in most models or by most metrics. Amongst the models they consider, none have a QBO-induced difference in MJO predictability which is statistically significant after two weeks. Here our small number of control simulations makes meaningful statistics difficult, and as predictability is not necessarily the focus of our study, our results in this area should be taken in the context of the more comprehensive literature focused on that topic.

We conclude that the model MJO-QBO connection from the control simulations is similar to that in observations, although the model response is weaker than observed, making the signal difficult to detect given our small control run sample size. We turn now to the question of the mechanism by which the QBO affects the MJO in the model. Do the model MJO events tend to be stronger in QBOE simply because they were initialized as stronger events (or due to some other systematic aspect of the tropospheric initial conditions) or does the stratosphere in the model actually affect the simulated MJO?

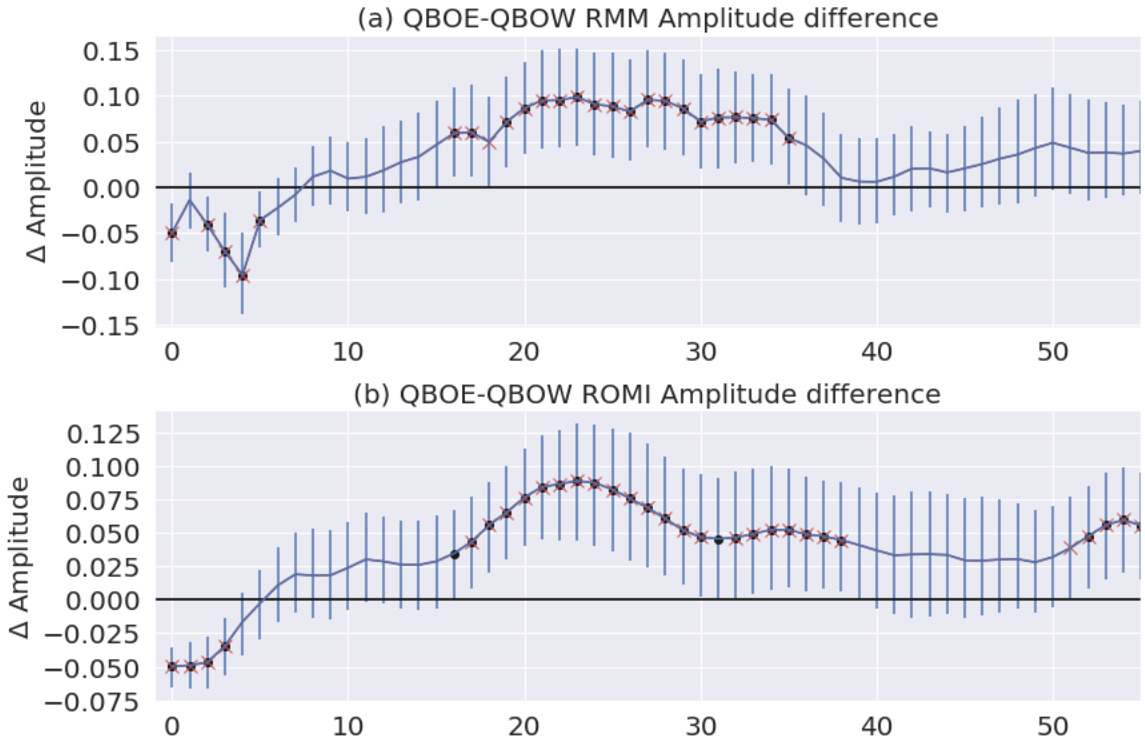

Figure 4.5: The MJO amplitude difference using the RMM (top) and ROMI (bottom) indices between all I-QBOE and I-QBOW experiments. Error bars are the 95% confidence level from a bootstrapping significant test (Section 3.3.1). Red "x's" indicate significance from the bootstrapping analysis, and black dots indicate significance using Welch's t-test.

4.3.3 MJO-QBO Relationship: Imposed-QBO Experiments

4.3.3.1 All Experiments

We now consider how the MJO responds in our imposed-QBO experiments. To take advantage of our experimental design, the MJO differences are examined by considering the I-QBOE minus I-QBOW behavior on each initialization date. This ensures that the only differences seen are due to the imposed QBO, because the initial state of the troposphere is unaltered and the I-QBOE minus I-QBOW stratospheric difference is identical at day 0.

Figure 4.5 shows the MJO amplitude difference between all the I-QBOE minus all the I-QBOW experiments. We do not differentiate based on the observed state of the QBO, so that the maximum number of I-QBO experiments (84 each for I-QBOE and I-QBOW) can be included. In general, we find a weak but significant modulation of the model MJO in the

first several weeks of the forecast, with a slightly stronger MJO under I-QBOE conditions compared to I-QBOW ones. Both the t-test and bootstrapping test demonstrate 10-20 days of near-contiguous, significantly stronger MJO activity in the I-QBOE experiments around weeks 2-4 using RMM and weeks 2-5 using ROMI: the robustness across indices suggests both wind and convection associated with the MJO are altered.

Significance here is calculated similarly to Section 4.3.2 with slight modifications: for the t-test we now take the 84 separate initialization dates as our sample size. For the bootstrapping test, we first take the amplitude difference between the I-QBOE and I-QBOW experiments on each initialization date, then randomly sample 84 dates with repetition from that population and calculate the mean difference to generate error bars at the 95% level.

While differences are significant for several days, note that the MJO amplitude difference is, at the most, approximately 0.1, a small value compared with the observed $\sim$0.5 amplitude difference or the $\sim$0.2 difference in the control. The use of the ensemble-mean amplitude does not meaningfully change these results; the difference is slightly smaller and the significance does not extend past 30 days in either RMM or ROMI.

Also evident in Figure 4.5 is a statistically significant difference in the first 4-5 days of the simulation: the MJO is significantly weaker in the I-QBOE experiments relative to the I-QBOW ones. This is in contrast to the behavior at longer lead times, and we believe may be due to a shock introduced by our method of changing the initial conditions. As discussed more in Appendix C.2, a small change in how the RMM/ROMI index were calculated removes this feature in the initial days, without materially changing the other aspects of Figure 4.5 (compare Fig. 4.5 to Appendix Fig. C.2) or other key results from this study. This suggests that the shock does not affect MJO behavior at later lead times. As these initial differences seem related to an issue with the experimental design rather than the observed MJO-QBO connection, we do not interpret them further.

Figure 4.6 shows the difference in MJO amplitude between the I-QBOE and I-QBOW experiments binned by MJO phase, similar to Figure 4.4. The left panel (a) shows the

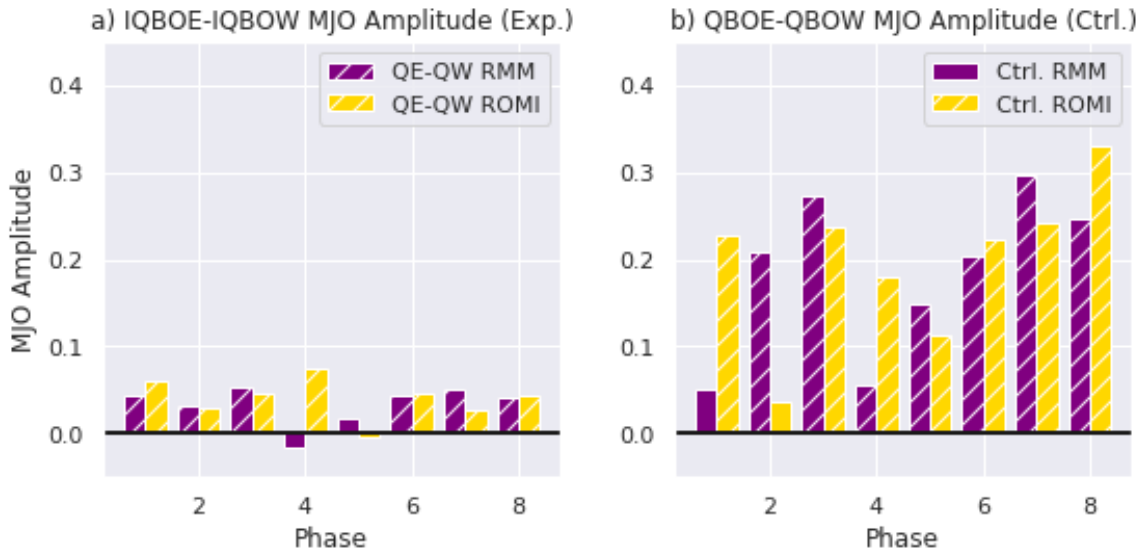

Figure 4.6: (a) Similar to Figure 4.4, but with the difference taken between all I-QBOE and all I-QBOW experiments (irrespective of the observed QBO initial state). Here the purple is RMM, gold is ROMI, and hatching indicates significance as in Figure 4.4. (b) Identical to the green bars in Figure 4.4(c/f); here we composite the control run over observed QBO easterly and westerly periods.

difference in MJO amplitude between all the I-QBOE and I-QBOW experiments as a function of MJO phase. As in Figure 4.4, we consider the phase irrespective of lead time, and treat ensemble members and initialization dates as independent to increase our sample size. In panel (a), all 84 initialization dates are considered regardless of the state of the observed QBO, and the difference shown is between I-QBOE and I-QBOW experiments. In contrast, panel (b) shows the QBOE minus QBOW difference in the control runs (identical to the green bars in Figure 4.4); such that the number of integrations is smaller (28 vs. 84 dates) and the QBOE/W composite in panel (b) is based on the *observed* initial state rather than an imposed state.

In the imposed-QBO experiments, we see a small increase in MJO amplitude in I-QBOE relative to I-QBOW, which is significant in most phases. However, the differences are again very small relative to the control, which is itself weaker than observed. Still, such differences are of the correct sign and statistically meaningful.

To further examine the relative impacts of the QBO on the model MJO via the initial

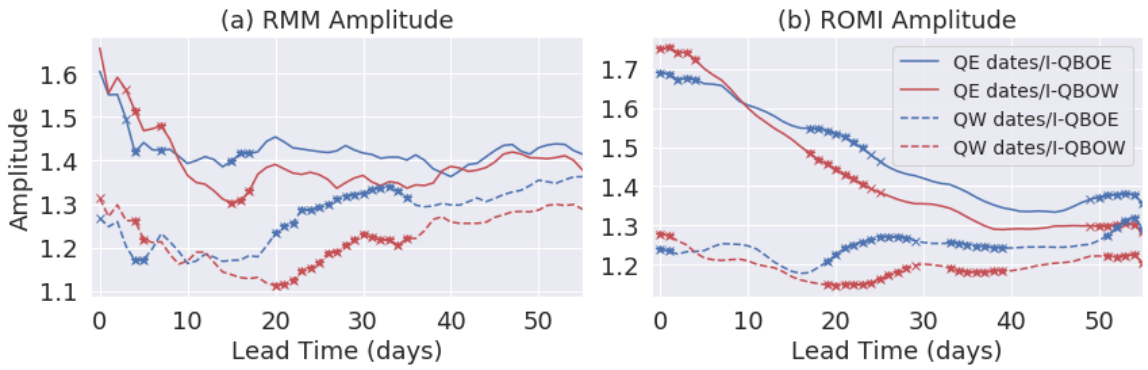

Figure 4.7: RMM (left) and ROMI (right) amplitude from simulations composited based on whether the observed QBO is initially easterly (solid curves) or westerly (dashed curves) per Table 4.1. The color of the curve denotes which imposed-QBO experiment is considered: the blue curves are I-QBOE experiments, and the red are I-QBOW experiments. An "x" indicates that the difference between the I-QBOE and I-QBOW experiments in a given observed QBO phase is significant using Welch's t-test at the 95% confidence level.

conditions versus via the model stratosphere, we can isolate the observed QBOE/W years in our imposed-QBO experiments. We did this by compositing imposed-QBO experiments by whether the observed QBO during the month of initialization was easterly or westerly. We then consider the I-QBOE and I-QBOW experiments' MJO amplitude during the observed QBOE and QBOW years separately.

Figure 4.7 shows the resulting MJO amplitudes. The solid and dashed lines are, respectively, the MJO amplitude from experiments during the observed QBOE and QBOW periods (see Table 4.1). The colors indicate which experiment is considered: I-QBOE is blue, and I-QBOW red. Days during which the I-QBOE minus I-QBOW MJO amplitude are significantly different from zero at the 95% confidence level using a t-test are indicated with an "x" on both curves.

In Figure 4.7, first note that the separation between observed QBOE and observed QBOW years is very clear for RMM and ROMI. Regardless of index or experiment type, solid curve remains substantially above the dashed during most of the integration, indicating that the model MJO is stronger when the observed QBO is easterly. Consistent with Abhik and Hendon (2019; their Figure S3), the initially strong, observed QBOE MJO events generally

decay in amplitude, whereas initially weak, observed QBOW MJO events tend to maintain or even increase in amplitude. This remains true in both the I-QBOE and I-QBOW experiments. It further suggests that the direct influence of the model stratosphere on the MJO is small compared to the differences in the initial conditions.

Still, there is a significant signal in the observed QBOW experiments from around day 20-35, when the I-QBOE runs are higher than the I-QBOW runs by around 0.1-0.15. The I-QBOE runs are also stronger than the I-QBOW runs during this time in the observed QBOE dates as well (solid blue/red), but they are not significant in RMM and not significant for as many days in ROMI. It is possible that the lack of significance is due in part to our method here of binning by the state of the observed QBO, which decreases the sample size to 31 observed QBOE and 35 observed QBOW dates, per Table 4.1.

What physical mechanisms may control this apparent, albeit small, increase in MJO amplitude? As discussed in Section 4.1, a key hypothesis supported by both modeling and observational evidence contends that QBO changes to temperatures in the tropopause region play a key role in modulating the MJO (Hendon and Abhik (2018); Abhik and Hendon (2019); Nie and Sobel (2015); Martin et al. (2019)). The spread in Figure 4.2f further demonstrates that, in our I-QBOE and I-QBOW experiments, despite starting with the same initial conditions the model maintains the imposed-QBO temperature signals differently across different runs. As Martin et al. (2019) demonstrated that the strength of the MJO response may be linked to the strength of these temperature anomalies, we might expect simulations with stronger QBO temperature differences to show stronger MJO response.

To explore this hypothesis, we calculated the 100 hPa temperature difference (averaged zonally and from 10°N to 10°S, as in Fig. 4.3) and MJO amplitude difference (as in Fig. 4.5) between the I-QBOE minus the I-QBOW experiments on each initialization date. We further averaged as a function of lead time over various 30-day periods: days 0-30, days 5-35 and days 10-40. Thus, for each initialization date we have one value representing the MJO amplitude change and one value representing the 100 hPa temperature change. We

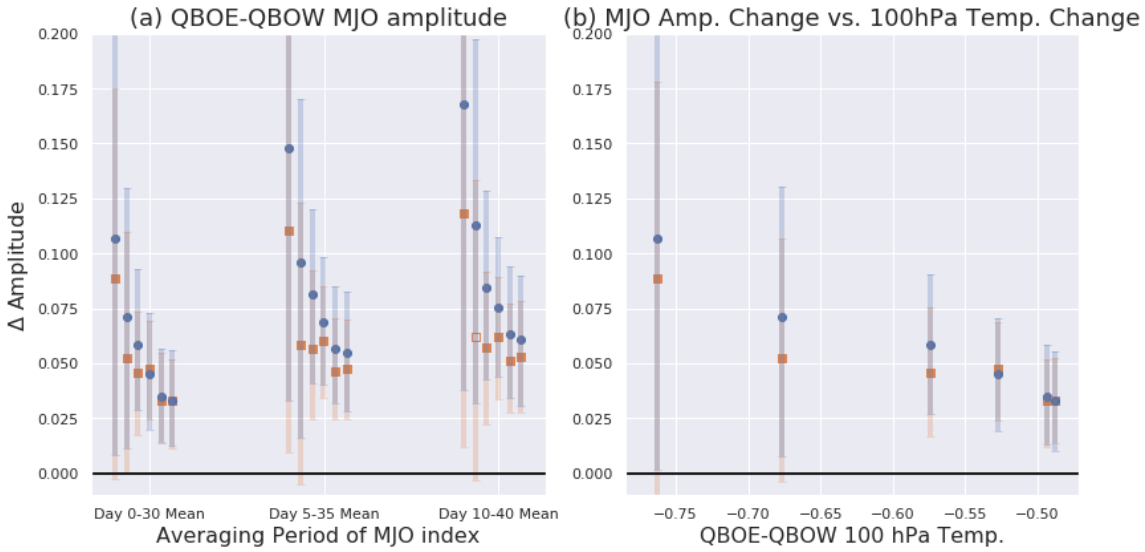

Figure 4.8: (a) (y-axis) The difference in MJO amplitude (RMM blue circles; ROMI orange squares) between the I-QBOE and I-QBOW experiments, as in Figure 4.5. The three clusters of points along the x-axis show the amplitude change averaged over different lead times: (from left to right) day 0-30, 5-35, and 10-40. Within each cluster, the rightmost point represents the amplitude difference from all runs. Subsequent points to the left within each cluster are the amplitude difference only composited over simulations where the 0-30 day mean 100 hPa temperature difference between I-QBOE and I-QBOW exceeds various thresholds of (from right to left) -0.3, -0.4, -0.5, -0.6, and -0.7 K as described in Section 4.3.3.1. Error bars are calculated using a bootstrapping method (Section 4.3.3.1) and filled points are statistically different from zero using a t-test. (b) As in (a), but only for the 0-30 day mean MJO amplitude change (leftmost cluster). The x-axis shows the 0-30 day mean I-QBOE minus I-QBOW 100 hPa temperature difference composited via the above threshold values.

then composited various simulations based on whether the 0-30 day 100 hPa temperature difference was less than a particular threshold. By choosing increasingly negative thresholds, we can select for only those simulations in which 100 hPa QBO temperature anomalies during the first month remain strong. We did this for temperature thresholds from -0.2K to -0.7K in -0.1K increments, chosen because this spans the range from including all 84 initialization dates (for -0.2K) to including no dates (the case for -0.8K). Correspondingly, sample size decreases with increasingly negative thresholds, and for the thresholds above are 84, 82, 66, 41, 11, and 4.

Figure 4.8a shows the I-QBOE minus I-QBOW change in MJO amplitude (y-axis) averaged over three lead time periods: days 0-30, days 5-35, and days 10-40 (i.e. the three

clusters of points along the x-axis). Individual points within each cluster represent the MJO amplitude difference given different 100 hPa temperature thresholds during day 0-30. The rightmost point in each cluster is the -0.2K temperature threshold and includes all experiments. Each point to the left represents subsets of experiments retaining only those with increasingly cold 100 hPa temperature differences via the thresholds listed above.

Figure 4.8b similarly shows the change in MJO amplitude averaged over the first 0-30 days (identical to the leftmost cluster in panel (a)) but the x-axis now shows the mean I-QBOE minus I-QBOW 100 hPa temperature difference, to demonstrate how the MJO amplitude increases as a function of the 100 hPa temperature difference. Significance in all cases is measured using a t-test (filled markers indicate significant differences) and bootstrapping tests identical to that used in Figure 4.5 (error bars).

Consistent with Figure 4.5, there is an approximately 0.03 increase in MJO amplitude during the first 30 days in both indices which is statistically significant, consistent with a small but measurable QBO impact. The amplitude increase in I-QBOE versus I-QBOW is also larger for later forecast periods: the 10-40 day mean for example shows an increase of greater than 0.05 in both indices.

As we restrict our analysis to subsets of simulations in which the 100hPa temperature difference remains increasingly colder during the first month, the MJO amplitude change in I-QBOE relative to I-QBOW becomes stronger. This is evident in the fact that all three clusters in Figure 4.8a show higher in MJO amplitude changes as one moves from right to left, corresponding to stronger QBO temperature anomalies. For the -0.7K threshold (leftmost points), the MJO amplitude increase is approximately 0.09 to 0.17, depending on the index or choice of averaging period, though the spread becomes large due to the small sample size. This may indicate that the model MJO responds to the imposed-QBO via a mechanism consistent with the observed relationship.

However, care should be taken in over-interpreting this response. The small sample size as we restrict ourselves to fewer dates with strong temperature anomalies means that the spread

grows very quickly even as the mean increases. The MJO amplitude increase with colder temperature differences is also not monotonic, especially for the ROMI index, though does have a general upward trend. Perhaps more significantly, this apparent relationship does not indicate clear causality: it may be that stronger MJO amplitude differences cause changes in 100 hPa temperatures. Hendon and Abhik (2018) showed that convective cold caps tend to overlay the active phase of the MJO at and around 100 hPa; these cold caps are understood theoretically as a response to diabatic tropospheric warming caused by increased convection (Holloway and Neelin (2007)). In that regard, one may expect such cold anomalies to grow stronger as the MJO amplitude increases, which may cause the apparent relationship seen in Figure 4.8. This cause and effect relationship could be explored in additional experiments in which QBO states are nudged rather than to evolve freely, as that can prevent the MJO from feeding back onto upper-level temperatures.

Taken as a whole, results from this subsection indicate that the QBO in the model has a direct impact on the MJO: we see significant increases in MJO strength of the correct sign relative to observations (stronger MJO in QBOE) by most metrics. Yet this change is small relative to both the change due to the initial conditions of the troposphere and to the observed QBO effect on the MJO. There also appears to be a link between the strength of the MJO response and the 100 hPa temperature anomalies associated with the imposed QBO: larger amplitude QBO temperature anomalies accompany a larger MJO response. However, this relationship in the model is not causal, appears somewhat non-monotonic, and is difficult to establish conclusively because the sample size becomes small. More broadly, the MJO changes in the imposed-QBO experiments are small in magnitude, significant only during limited periods, and a large sample size is needed to capture them. For example, remaking Figure 4.5 with only the 28 imposed-QBO January 1 simulations yields no significant differences, though an increase is still observed in imposed-QBOE relative to imposed-QBOW (not shown).

4.3.3.2 MJO Phase 2 and 4 Experiments

In this section we examine the imposed-QBO experiments where the MJO is initially strong and in Phase 2 or Phase 4 in greater detail. These experiments were designed to allow for many MJO events in similar starting conditions to be considered together. Additionally, observed results have suggested that the MJO-QBO link may depend strongly on the MJO phase (e.g. Zhang and Zhang (2018); Densmore et al. (2019)).

Figure 4.9 shows the RMM and ROMI indices averaged over all of the Phase 2 and Phase 4 I-QBOE and I-QBOW experiments, and plotted on a standard RMM phase diagrams (Wheeler and Hendon (2004)). Shown below each phase diagram is the amplitude difference between the imposed-QBO experiments, per Figure 4.5. As in Figure 4.5, the first 2-5 days show a behavior which is likely caused by a shock (Section 4.3.3.1 and Appendix C.2).

For the Phase 2 experiments; the only significant RMM impact is a decrease in MJO activity during the first ∼10 days of the simulation, which does not have an observational analog. There is a marginal increase in amplitude under ROMI around day 15-20, but it is a limited period and not significant in RMM. We conclude that these runs have no strong QBO link. In fact, these same Phase 2 events in observations, when composited by phase of the observed QBO during their initial conditions, show only a small QBOE-QBOW difference (not shown). This suggests, following previous studies (Zhang and Zhang (2018); Densmore et al. (2019)), that the observed MJO-QBO relationship may act preferentially in particular MJO phases: the observed MJO-QBO connection may not be particularly robust for MJO events which are strong and begin in Phase 2.

In the Phase 4 experiments, there is a larger difference in the I-QBOE/W experiments of the same sign as that observed, particularly after around 10 days. After around two weeks in the model there are significant differences for much of the rest of the simulation using both MJO indices, with a stronger MJO during I-QBOE around RMM phases 6-8. While the impacts are still small, the fact that amongst all of our simulations those initialized with an MJO around this region are most affected by our imposed-QBO states

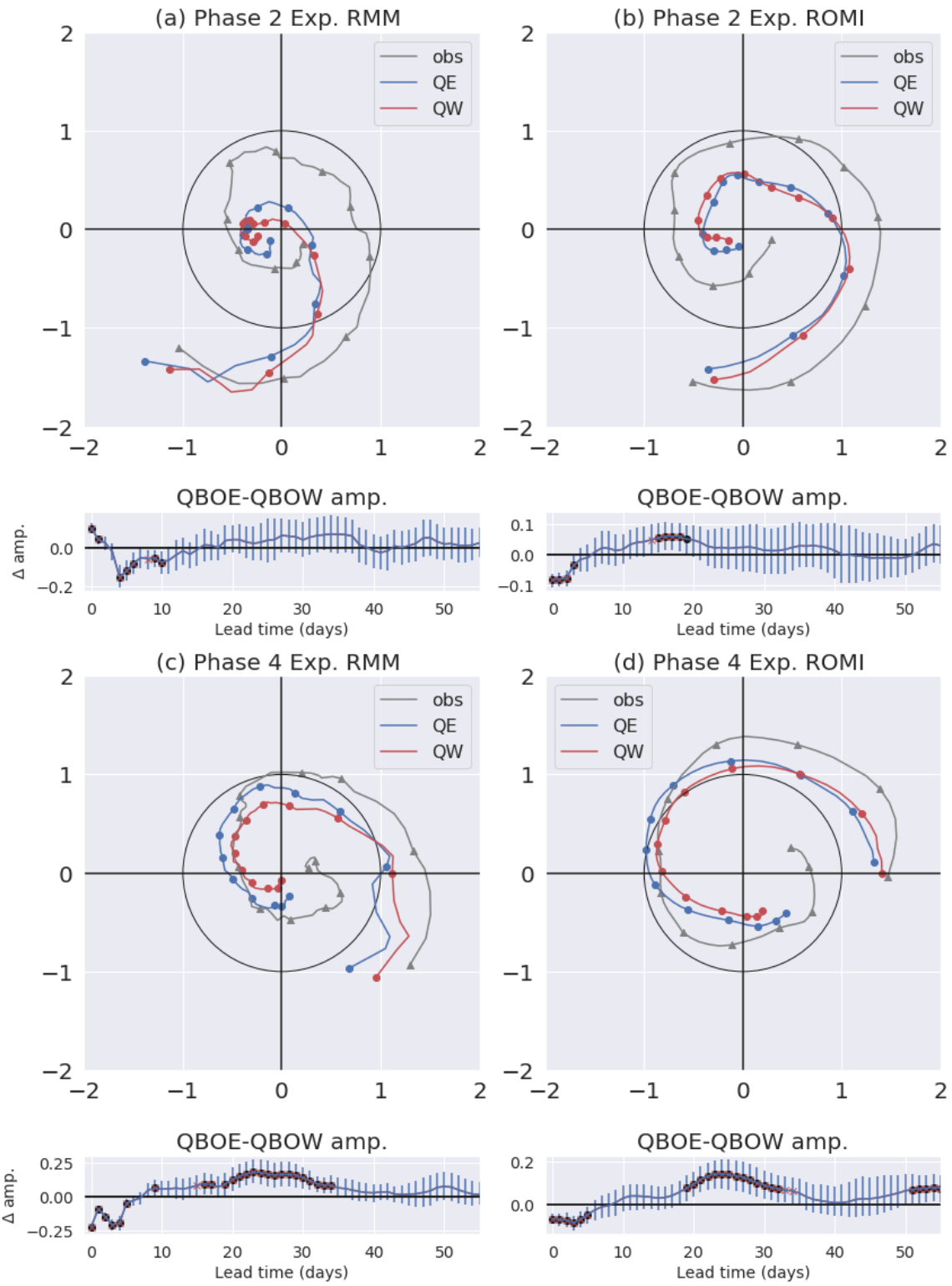

Figure 4.9: RMM (left) and ROMI (right) phase diagrams for the MJO Phase 2 (top) and MJO Phase 4 (bottom) experiments. Grey are observations, blue are I-QBOE, and red are I-QBOW. Dots/triangles denote every fifth day. Bottom panel shows the IQBOE-IQBOW MJO amplitude difference, calculated as in Figure 4.5.

seems at least consistent qualitatively with observational studies (Zhang and Zhang (2018); Densmore et al. (2019)).

To further examine the impact of the QBO specifically on MJO convection, we form reconstructed OLR anomalies from the ROMI index. This is motivated by the fact that RMM is known to be largely circulation-based (the mean contributions to RMM from OLR, 850 hPa zonal wind, and 200 hPa zonal wind during DJFM are, respectively, 0.16, 0.42, and 0.42; Ventrice et al. (2013); Harry Hendon, personal communication), and the QBO seems to affect MJO convection in particular (Son et al. (2017)). To reconstruct the OLR, we use the following formula:

$$OLR_{recon}(x, y, t) = ROMI1(t) \times EOF1(x, y, doy) + ROMI2(t) \times EOF2(x, y, doy) \quad (4.5)$$

where ROMI1/2 are the reforecast indices, and EOF1/2 are the ROMI EOFs, which are functions of latitude, longitude, and day of the year (doy).

Figure 4.10 shows the mean of the OMI-reconstructed OLR anomalies averaged from 20°N/S over all the Phase 4 I-QBOE and I-QBOW experiments, as well as the same dates from observations. The last panel shows the difference between the I-QBOE and I-QBOW experiments, with the I-QBOE mean contoured to facilitate comparison. Statistically significant differences using a t-test at each point are stippled. In general, the differences are small and initially of the opposite sign expected from observed (stronger in QBOW). However, at leads after around 10 days there are statistically significant differences indicating a strengthening of negative anomalies in the West Pacific. From days 20-30 we also see a stronger MJO active phase over the Indian Ocean and an enhancement of the suppressed phase around 100°E. There is a strengthening of the MJO active phase around 50-60 days that develops about 100°E, all of which is suggestive of a weak but significant enhancement of MJO convection associated with the imposed stratosphere. Similar signals can also be seen in the raw OLR fields, as well as in the 850 and 200 hPa zonal wind fields which comprise

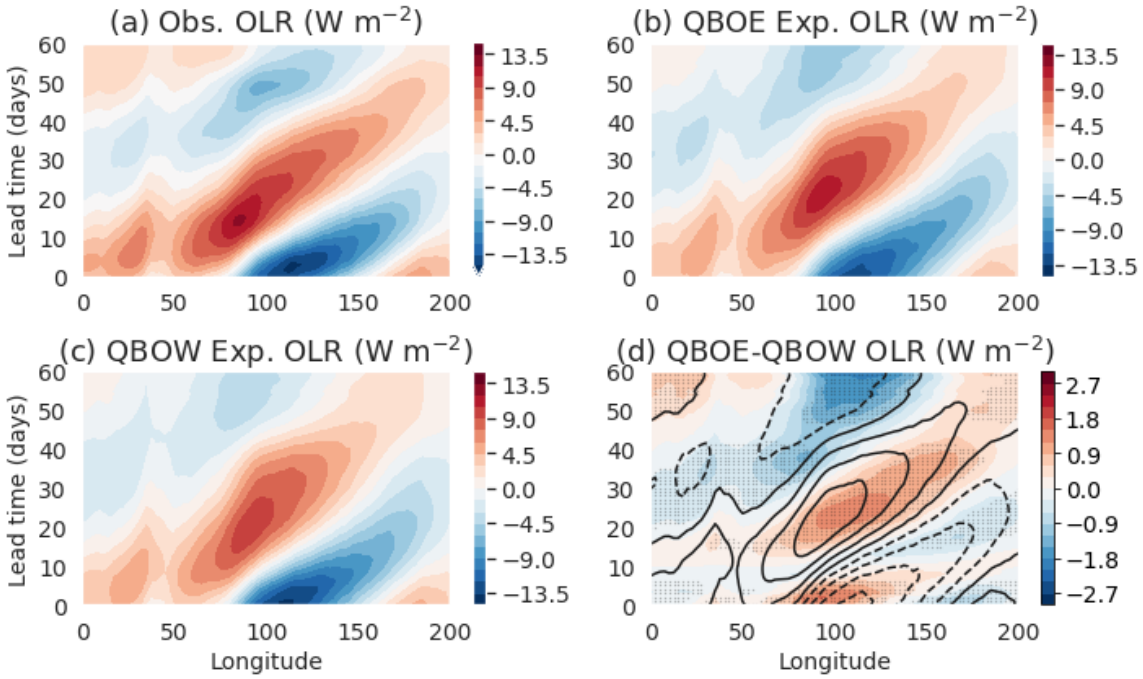

Figure 4.10: Reconstructed ROMI OLR anomalies (Equation 4.5) averaged over all MJO Phase 4 dates (see Table 4.1). Plotted are (a) observations, (b) I-QBOE experiments and (c) I-QBOW experiments. (d) The difference between the I-QBOE and I-QBOW experiments; black contours showing the I-QBOE experiment at 3 W/m^2 intervals from -12 to 12 W/m^2 (negative contours dashed), for comparison. In panel (d) the stippling indicates a statistically significant difference at the 95% confidence level using a Welch's t-test at each point.

the RMM index (not shown). This indicates that the circulation, not just the convection, is affected by the QBO, especially at upper levels where differences are larger and more significant than in the lower troposphere.

To elucidate to what degree differences in the Phase 4 experiments are due to tropospheric initial conditions, we computed differences in the reconstructed OLR between dates where the observed QBO was initially easterly or westerly similar to the methodology in Figure 4.7. Figure 4.11 shows the difference between dates in which the observed QBO is initially easterly or westerly. The left panel is observations, the center panel is I-QBOE, and the right panel is I-QBOW. The mean calculated over all initialization dates is contoured for comparison.

Figure 4.11 shows a striking similarity between the I-QBOE experiments, I-QBOW experiments and observations, demonstrating an enhancement of the MJO active and suppressed phases when the observed QBO is easterly versus westerly. Though the model response is weaker than the observed by about a factor of $\sim$2, these differences are much larger than those between the I-QBOE and I-QBOW experiments shown in Figure 4.10 (note the different color bar range). This suggests that the initial conditions in the troposphere are still the dominant driver of the simulated differences in MJO amplitude between QBOE and QBOW years.

4.4 Discussion

Our results indicate that the stratosphere has a significant but weak impact on MJO convection in the ECMWF model. The QBO-induced difference on the MJO is particularly notable at lead times of around 2-5 weeks. It may be that at shorter lead times, tropospheric conditions play too large a role for a direct stratospheric impact to be seen, whereas at longer lead times the MJO and/or QBO biases may explain the lack of a signal. The shock caused by our experimental design may also play a role in affecting the MJO response

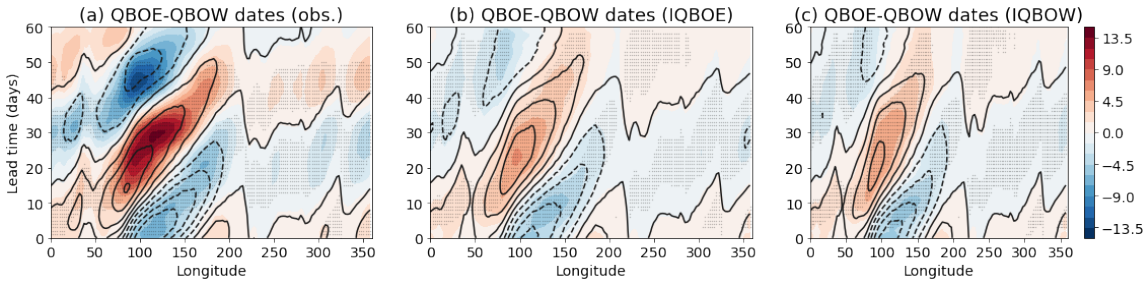

Figure 4.11: The difference in reconstructed ROMI OLR anomalies between the MJO Phase 4 dates where the observed QBO is easterly minus dates where the observed QBO is westerly per Table 4.1 (colored contours). Panel (a) is the observed difference, panel (b) is the difference from the I-QBOE experiments, and panel (c) is the difference from the I-QBOW experiments. Black contours show the mean reconstructed OLR from (a) the observations and (b/c) the I-QBOE/W experiments, respectively, at a 3 W/m^2 intervals from -12 to 12 W/m^2; dashed are negative. Stippling indicates a significant difference using a Welch's t-test at each point with 95% confidence and the number of observed QBOE/W years as the sample size.

during the first week. Our findings here are, however, consistent with other studies that show that the modeled MJO-QBO effect is much weaker than that observed (i.e. Lee and Klingaman (2018); Wang et al. (2019b); Abhik and Hendon (2019)). Abhik and Hendon (2019) found in their study, which uses a different methodology and does not directly alter the stratosphere to look at the QBO impact, that the QBO effects were most apparent and statistically significant after 1-2 weeks (see their Figure 2). Still, such a small stratospheric influence is difficult to reconcile with the large impact of the QBO on the observed MJO, since it leaves unanswered the question of how the differences in the tropospheric initial conditions developed in the first place.

We consider three main hypotheses regarding why the model experiments fail to show a strong QBO influence: (1) flaws in our experimental design, (2) the failure of the model to capture the observed operative MJO-QBO interaction mechanism, and (3) the possibility that the observed MJO-QBO link is not driven exclusively by stratospheric processes, or is not as statistically robust as current literature suggests.

It is possible that our experimental design has deficiencies that do not allow the QBO to exert a strong influence on the MJO. The model QBO drifts away from the imposed

initial condition (e.g. Figure 4.3), and the imposed QBO states in the stratosphere-altering experiments decay over a few weeks (Section 4.3.3). The drift of QBO temperature anomalies in particular may be a shortcoming of these experiments. Figure 4.12 shows the zonal mean temperature difference between the I-QBOE and I-QBOW experiments in the left panel, and the observed QBOE minus QBOW difference over the periods beginning on the two dates which we use as imposed-QBO states (January 1, 2006 and January 1, 2000). On the right is the difference between the experiments and observations; the rows represent the 15-day average for days 0-15, 15-30, and 30-45. This shows biases of several degrees between the observations and the model establish themselves relatively quickly and extend down to around 100 hPa. Since even small biases or changes in the height or amplitude of these TTL temperature anomalies may change whether there is a detectable response in the MJO (Martin et al. (2019); Klotzbach et al. (2019)), this could explain part of the weak response. In future work, we aim to extend our present results by nudging in the stratosphere to force the QBO anomalies to be better sustained through the simulations, and determine whether that increases the stratospheric influence on the MJO.

Second, it is possible that the model is incapable of generating a strong MJO-QBO link because the model fails to completely recreate the observed MJO-QBO mechanism, whatever that may be. We have discussed in particular model deficiencies in QBO temperature anomalies and presented some evidence that this mechanism plays a role in our model (e.g. Fig. 4.8). However, this mechanism is not yet clearly established as the causal link between the QBO and the MJO and it is conceivable that some other mechanisms or related feedbacks (say due to clouds) are operative in observations and not the model. In this regard a more detailed observational study of the observed MJO-QBO link would be of interest in helping guide modeling work or developing diagnostics for comparing models and observations. Relatedly, it is possible that QBO changes that affect the MJO may take longer to act than the two months of integration time we use. This could also potentially explain why the QBO impact seems strongest after 1-2 weeks in the model. Were the model run for longer and

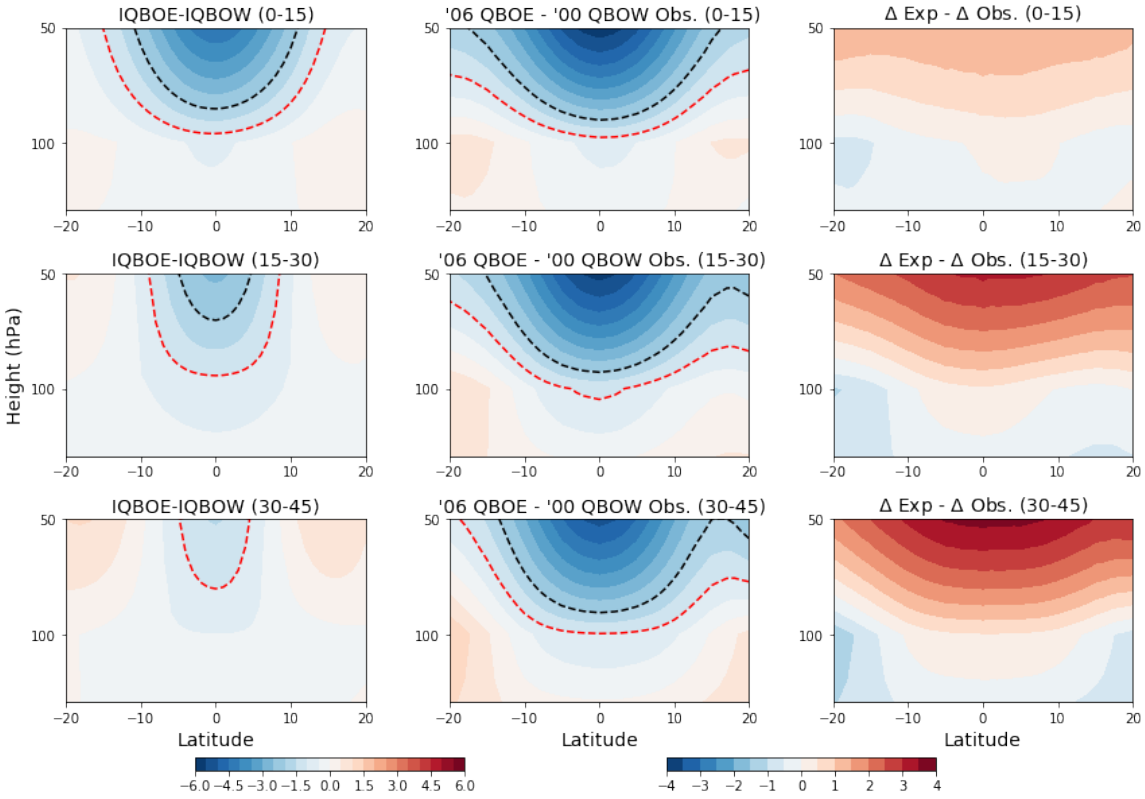

Figure 4.12: Zonal mean temperature difference (in degrees K) between (left) the mean I-QBOE minus mean I-QBOW experiments and (center) the observations between Jan. 1, 2006 (QBOE) and Jan. 1, 2000 (QBOW). Black and red contours indicate -2 K and -1 K. Rows indicate the average over days 0-15, 15-30, and 30-45 relative to the initialization date. The rightmost column shows the difference between the imposed-QBO experiments and the observations. The observations have been linearly interpolated onto the model vertical levels.

the effect of the initial condition allowed to disperse, the QBO impact from the stratosphere may be more apparent, though issues with MJO and QBO biases become more difficult to avoid. In this regard longer, free-running simulations may be a useful alternative to forecast models in examining this problem (Lee and Klingaman (2018)); while finding a model with a strong MJO and good QBO is difficult, this will also be explored in future work.

Third, it is possible that the strong observed MJO-QBO impact may not result exclusively from a stratospheric influence. Perhaps some other aspect of the climate system modulates both the MJO and QBO. Alternatively, perhaps the observed MJO-QBO link is a statistical fluke. Either would explain the small influence of the stratosphere on the model MJO and our difficulty simulating the MJO-QBO link. The observed MJO-QBO link has passed stringent statistical tests, however, (Yoo and Son (2016)) and been verified in several studies that all use somewhat different metrics to define the MJO and the QBO (Son et al. (2017); Nishimoto and Yoden (2017); Marshall et al. (2017); Zhang and Zhang (2018); Lee and Klingaman (2018); Densmore et al. (2019)). Still, several confounding aspects of the MJO-QBO link – namely, that it only holds in a particular season, may only have emerged in recent decades, and seems to affect only the MJO and not other convectively coupled tropical modes (Yoo and Son (2016); Son et al. (2017); Klotzbach et al. (2019); Abhik et al. (2019)) – remain largely unexplained. Previous literature has shown that correlations between the QBO and tropical tropospheric phenomena can change on longer timescales, e.g., in the case of tropical cyclones (Camargo and Sobel (2010)). Further, Wang et al. (2019b) examined the QBO impact on the boreal summer intra-seasonal oscillation (BSISO; the boreal summer counterpart of the MJO) and showed decadal variations in the strength and sign of the QBO influence on the BSISO. Even in modeling studies that show the potential for a QBO impact (Martin et al. (2019)), stronger-than-observed QBO anomalies were needed to see a substantial result.

At this stage it seems premature to conclude that the observed result is spurious, especially given the fact that we find some influence, though a weak one, in our simulations. Additional modeling studies should be carried out that more rigorously consider other as-

pects of the MJO-QBO relationship, including the potential for an upward impact of the MJO onto the QBO, and more targeted studies that fix the QBO to examine the downward stratospheric impact where model biases in the upper troposphere/lower stratosphere can be minimized.

4.5 Conclusion

In this study we examine the MJO-QBO relationship using a state-of-the-art version of the ECMWF forecast model. The model is integrated for 61 days with 15 ensemble members, and initialized on 84 dates in northern winters from 1989-2016. The goal is to determine whether the model can reproduce the observed MJO-QBO relationship, and in particular to distinguish between the role of the tropospheric initial conditions and the model stratosphere in determining the MJO behavior under different QBO phases. After running 28 "control" simulations initialized on every January 1 from 1989-2016 without any changes to the model stratosphere, we performed a series of imposed-QBOE and imposed-QBOW experiments where the stratospheric initial conditions (i.e. the state of all variables above 150 hPa) were altered to either an easterly or westerly QBO state. The imposed-QBOE/W states were taken from the initial conditions on January 1, 2006 and January 1, 2000, respectively; the troposphere below 150 hPa was not changed. We increased our sample size by choosing additional DJF dates when the MJO was initially strong and in either phase 2 or phase 4 (without a control run).

In the results from these altered-stratosphere experiments, we examined how the MJO responded to the imposed-stratosphere compared to both the control runs and the observations. Our main results can be summarized as follows:

1. In the control runs, the model is capable of simulating a stronger MJO during the observed easterly phase of the QBO than during the westerly phase, as measured using the amplitude of the RMM and ROMI MJO indices. While our relatively small sample

size of control runs inhibits statistical significance, the model shows a modulation of the MJO by the QBO that is largely consistent with observations, though the model response is weaker (e.g. Fig. 4.3 and 4.4). This finding is, broadly speaking, consistent with other published work on the ability of forecast models to simulate a QBO impact on the MJO (e.g. Abhik and Hendon (2019); Marshall et al. (2017); Wang et al. (2019b); Lim et al. (2019)).

2. In experiments in which the stratosphere was altered and a particular QBO state was imposed, the model MJO shows a small but statistically meaningful increase in imposed-QBOE conditions compared to imposed-QBOW conditions. While small compared to observations and control runs, the results are significant for 2-3 weeks, beginning around 15 days after initialization (e.g. Fig. 4.5-4.7), and further are significant if the MJO amplitude is averaged over days 0-30 (Fig. 4.8).

3. The MJO amplitude change in the imposed-QBO experiments is stronger when the 100 hPa tropically-averaged temperature difference is larger (i.e. is colder in imposed-QBOE compared to imposed-QBOW; Fig. 4.8). This suggests, though does not conclusively show, that 100 hPa QBO-related temperature anomalies may drive the strengthening of the MJO, as has been proposed and supported by other studies (Son et al. (2017); Hendon and Abhik (2018); Martin et al. (2019)).

4. In imposed-QBO experiments where the MJO is strong and initialized in RMM phase 4, there is still a weak but significant MJO response despite the smaller sample size, especially when the MJO is in phases 6-8 (Figs. 4.9-4.10). Differences in other subsets of experiments, such as strong, phase 2 MJO events, show no significant response (Fig. 4.9). This suggests the possibility that the MJO modulation by the QBO is stronger in certain phases than others in the model, potentially in keeping with observed results that show a dependence of QBO modulation on MJO phase (Zhang and Zhang (2018); Densmore et al. (2019)).

5. MJO differences due to tropospheric initial conditions still seem dominant compared to differences due to the model stratosphere acting on the MJO (e.g. Figs. 4.7,4.10). Compositing by the observed QBO state in the initial condition still shows a large effect on MJO behavior even in imposed-QBO experiments.

We discussed several interpretations of the relative weakness of the simulated MJO-QBO impact compared to observations, including (1) issues with our experimental design, (2) biases or deficiencies of the model MJO, QBO, or related elements of the climate system, and (3) the possibility that the observed MJO-QBO relationship may be driven or modulated by non-stratospheric processes or be a statistical fluke (Section 4). In particular we show that our experimental design leads to biases in the temperature structure in the upper troposphere/lower stratosphere that arise relatively early in the simulation and may decrease the strength of the model MJO response (c.f. Fig. 4.11). Modeling and observational work (Martin et al. (2019); Klotzbach et al. (2019); Lee and Klingaman (2018); Hendon and Abhik (2018)) has suggested that the MJO response to the QBO may be sensitive to the precise details of the QBO temperature anomalies in the TTL. This issue will be explored more in future work that attempts to force QBO temperature anomalies more directly in this modeling framework, as well as in free-running global models.

* * *

The next chapter presents results on the MJO-QBO link in a free-running global climate model. One of our goals in bringing this problem to a GCM is that it largely circumvents the issues raised in this chapter regarding the role of initial conditions. It would further allow us to carry out experiments in which we "nudged" the stratosphere to (ideally) overcome biases in QBO temperature anomalies in the lower stratosphere and upper troposphere that had plagued several other modeling studies. Finally, if a GCM demonstrated the MJO-QBO link (even with nudging) it would represent an important step forward on this problem, both showing it was possible to model the MJO-QBO connection and opening the door for experiments looking more at the physical mechanisms linking the MJO and QBO. Collaboration

with scientists at NASA GISS on this project, our final modeling work for this thesis, started around November of 2018.

Chapter 5

The Impact of the QBO on the MJO in Global Climate Models

Note: This chapter is in preparation for publication, pending additional analysis as discussed below and further improvements to the figures. Results presented in Section 5.3.1 on the MJO-QBO link in the 102-level model will likely be excluded from any final publication as they are consistent with published studies (Lee and Klingaman (2018); Richter et al. (2020)), and are shown here primarily for completeness and comparison.

5.1 Introduction

In this study we examine the link between two prominent modes of variability in the tropical atmosphere: the intraseasonal Madden-Julian oscillation (MJO) and the stratospheric quasi-biennial oscillation (QBO). The MJO is a planetary-scale, eastward propagating mode in the tropics in which circulation and convection are coupled on ∼30-60 day timescales (Madden and Julian (1971); Madden and Julian (1972); Zhang (2005)). MJO convection and circulation signals, which are primarily in the troposphere, extend from the Indian ocean through the West Pacific, though wind anomalies can circle the entire tropics (Zhang (2005)). Through teleconnections, the MJO can impact weather patterns and extreme events around

the globe (Stan et al. (2017)).

The quasi-biennial oscillation is a primarily stratospheric phenomena in which the zonal-mean zonal winds in the stratosphere alternate between descending easterly (QBOE) and westerly (QBOW) regimes with an ∼28-month period (Baldwin et al. (2001)). The QBO zonal wind oscillation is driven by upward propagating tropical waves (Lindzen and Holton (1968); Holton and Lindzen (1972)), including large-scale Kelvin and Rossby waves and smaller scale gravity waves. These waves interact with the mean flow and deposit momentum which drives the wind oscillation. The QBO zonal winds are also associated, through thermal wind balance, with temperature anomalies which can reach the tropopause.

A recent series of studies has revealed a strong link between the MJO and the QBO: the boreal winter MJO is more active, more predictable, and displays stronger teleconnections in QBOE relative to QBOW (Yoo and Son (2016); Son et al. (2017); Marshall et al. (2017)). This QBO connection has been confirmed and expanded upon in a series of recent observational (Nishimoto and Yoden (2017); Hood (2017); Zhang and Zhang (2018); Densmore et al. (2019); Hendon and Abhik (2018); Abhik et al. (2019); Klotzbach et al. (2019); Mundhenk et al. (2018); Mayer and Barnes (2019); Kim et al. (2020b)) and modeling works (Lee and Klingaman (2018); Abhik and Hendon (2019), Martin et al. (2019), Lim et al. (2019), Wang et al. (2019b), Kim et al. (2020a), Martin et al. (2020), Toms et al. (2020)). Observational results have confirmed that the MJO-QBO connection is statistically robust in boreal winter, and recently underscore the importance of the MJO-QBO link in modulating the strength of MJO teleconnections throughout the global troposphere (Son et al. (2017); Mundhenk et al. (2018); Mayer and Barnes (2019); Kim et al. (2020b); Toms et al. (2020)). Other studies have demonstrated several puzzling features of the MJO-QBO link: the MJO seems uniquely affected by the QBO compared to other types of tropical waves (Abhik et al. (2019)) and seems to have emerged only in recent decades (Klotzbach et al. (2019)).

These features are difficult to explain mechanistically, in particular because numerical models have struggled to show any MJO-QBO connection (Lee and Klingaman (2018);

Richter et al. (2020). This modeling difficulty represents a major obstacle for understanding how the MJO and the QBO are connected, as it is difficult to test hypothetical mechanisms without a modeling framework.

Some of the most promising modeling studies on the MJO-QBO connection have used forecast models, such as those associated with the Seasonal-to-Subseasonal (S2S) Prediction Project (Vitart et al. (2017)), to study the MJO-QBO interaction. This literature has shown that the majority of such models show an MJO-QBO link (Marshall et al. (2017); Abhik and Hendon (2019); Lim et al. (2019); Wang et al. (2019b); Kim et al. (2019); Martin et al. (2020)). However, it is difficult in those models to separate the direct effect of the QBO on the model MJO from the effect of the initial conditions, in which the observed MJO-QBO connection is present (Wang et al. (2019b); Kim et al. (2019); Abhik and Hendon (2019); Martin et al. (2020)). Among those studies that have attempted to isolate the direct impact of the QBO absent influences from initial conditions, the conclusion tends to be that the MJO-QBO connection is robust, albeit much weaker than observed (Abhik and Hendon (2019); Martin et al. (2020)). Coupled with the inability to neatly separate the QBO impact in these models from the initial condition impact, forecast models display issues which make it difficult to test particular mechanisms relevant to the observed link.

Free-running global climate models (GCMs) on the other hand are, in principle, some of the most promising models to study the MJO-QBO relationship because of they are less tethered to initial conditions than forecast models, and can simulate a wide range of climate processes which may be important for the MJO-QBO connection. However, to date no GCM demonstrates an MJO-QBO link. Lee and Klingaman (2018) found that a GCM with a reasonable representation of both the MJO and the QBO displayed no strong connection across three 25-year ensemble members. Kim et al. (2020a) looked more comprehensively at the MJO-QBO connection across many CMIP6 models (Eyring et al. (2016)), and found there too that no model simulated the strong MJO-QBO link that is observed. Sampling the interannual variability in the CMIP6 models from QBO neutral years, they found that

the models' MJO-QBO relationships were consistent with noise and not stratospherically driven.

A common issue across these studies are biases in QBO signals in the lower stratosphere, which is a common issue in models with internally generated QBOs (Richter et al. (2020)). In particular, biases to QBO temperature anomalies have been suggested by Lee and Klingaman (2018) and Kim et al. (2020a) as a potential source of error which may preclude the model from having an MJO-QBO connection. QBO temperature anomalies have been proposed as a viable mechanisms through which the QBO can alter the MJO by allowing deep convection to penetrate higher and more vigorously into the troposphere (Collimore et al. (2003); Nie and Sobel (2015); Son et al. (2017); Hendon and Abhik (2018); Martin et al. (2019); Martin et al. (2020)). Further interaction of the QBO temperature signals with MJO-associated "cold-cap" temperature anomalies were studied by Hendon and Abhik (2018), and in additional work Abhik et al. (2019) proposed that the MJO's vertical structure and deep convective signature explained why it is uniquely effected. Still, the specifics of this mechanism have yet to be fully explained. Whether or not these biases in GCMs' representations of QBO temperature anomalies around the tropopause can explain the lack of an MJO-QBO link in models is a central focus of this work. In this study, we set out to test the hypothesis that lower stratospheric temperature biases in GCMs, in particular associated with the QBO, are the primary reason why models fail to capture the observed MJO-QBO relationship.

After describing our model, data, methods, and experimental design in Section 5.2, we show in Section 5.3.1 that the NASA Goddard Institute for Space Studies (NASA GISS) Model E2.2 (the "middle atmosphere" configuration of the model; Rind et al. (2020)) with an internally-generated QBO and a reasonable MJO does not show any MJO-QBO connection, similar to the models in studies conducted by Lee and Klingaman (2018) and Kim et al. (2020a). We confirm that this model suffers from the same QBO temperature biases around the tropopause that other GCM studies have shown.

This motivates our main results in Section 5.3.2, in which we examine the MJO-QBO link

in the GISS Model E2.1 (Kelley et al. (2019)), a lower vertical resolution model, where the zonal and meridional winds in the upper troposphere and stratosphere are relaxed towards the observed QBO. The key advantage of this approach is it allows us to study the MJO-QBO connection in a model which has minimal QBO biases. We can then determine whether biases in QBO temperature and wind anomalies in the lower troposphere are a likely cause of model issues simulating the MJO-QBO link. Section 5.3.3 shows additional results from sensitivity tests varying the details of our nudging and the strength of the QBO. The final two Sections, 5.4 and 5.5, offer discussion of our findings and a summary of this work.

5.2 Data, Methods, and Model

5.2.1 Data and Methodology

We use several reanalysis and observed data products to compare, nudge, and verify our modeling results to. For zonal and meridional winds we use NASA's Modern-Era Retrospective Analysis for Research and Applications-2 (MERRA2) reanalysis (Gelaro et al. (2017)). For observed outgoing longwave radiation (OLR), we use NOAA daily satellite data (Liebmann and Smith (1996)).

To track the QBO, we use monthly-mean MERRA2 50 hPa zonal-mean zonal wind, averaged over all longitudes and from 10°N to 10°S (U50), which has been shown to accurately represent the QBO compared to observations (Coy et al. (2016)). As in previous studies (Yoo and Son (2016); Son et al. (2017)), we define westerly and easterly QBO phases (QBOW and QBOE) as months when the index exceeds ± 0.5 standard deviation, respectively. In some sections, we refer to other QBO indices such as "U70" – these are identical to U50 except that they consider a different pressure level indicated in the name (i.e. the 70 hPa QBO-winds are the U70 index, 30 hPa winds are U30, etc.).

We track the MJO in the model and in observations using the daily Real-time Multivariate MJO index (RMM; Wheeler and Hendon (2004)). RMM is a standard MJO index formed

using a pair of empirical orthogonal functions (EOFs) of OLR and zonal wind at 850 and 200 hPa in the tropics to form two principal component time series, often called RMM1 and RMM2. Together RMM1 and RMM2 track the strength and location of the MJO; their phase angle represents the MJO's location, and the amplitude (measured as $\sqrt{\text{RMM1}^2 + \text{RMM2}^2}$) represents the MJO's strength. The observed RMM index is available from the Australian Bureau of Meterology (available at http://www.bom.gov.au/climate/mjo/graphics/rmm.74toRealtime.txt) which is available from June 1974 and updated in near realtime. For the model RMM index, the model's OLR and zonal winds are processed after being output to remove the seasonal cycle and interannual variability following the same procedure as in Wheeler and Hendon (2004). These fields are projected onto the observed EOFs as calculated in Wheeler and Hendon (2004), rather than the model EOFs, to facilitate better comparison with observations.

We examine the MJO-QBO relationship primarily through three metrics: (1) the MJO amplitude differences in QBOE and QBOW, (2) the correlation between RMM and the various QBO indices, and (3) the difference in the standard deviation of DJF MJO-filtered OLR over the warm pool region in QBOE versus QBOW. The details of each of these techniques are:

1. The observed or model MJO is divided into eight phases as defined in Wheeler and Hendon (2004), corresponding to where the MJO is in its life cycle. Note no amplitude threshold is used to define the MJO activity level, so even weak MJO days are assigned a phase 1-8. The mean in each MJO phase is then calculated from all days in December-February, to measure the overall amplitude, and the calculation is then repeated for QBOE and QBOW months in DJF.

2. For each year in observations or the model, we calculate the DJF-mean RMM amplitude and DJF-mean of a QBO index (usually U50). We then calculate the correlation between these two datasets over all years.

3. We first calculate "MJO-filtered" OLR (similar to Wheeler and Kiladis (1999); Yoo and Son (2016); Son et al. (2017); and Kim et al. (2020a)). To do this, we band-pass filter the observed or model OLR data retaining only the 20-100 day component using a kaiser window and Python's filtfilt operation to ensure zero phase shift (see Wang (2020)). We further Fourier transform the data in space and filter it to retain only the eastward propagating, wavenumber 1-5 signals. We then calculate the standard deviation of the MJO-filtered OLR during DJF to measure MJO activity. To measure QBO impacts, we calculate the difference of this standard deviation between QBOE minus QBOW months in DJF. We also take the mean of this difference over the warm pool, defined following Kim et al. (2020a) as 50-170°E and 20°S-5°N.

5.2.2 Model Configurations

We use the current generation version of the NASA Goddard Institute for Space Studies (GISS) GCM ModelE for the experiments conducted in this study. This includes configurations using both the standard lower vertical resolution model E2.1 (Kelley et al. (2019)) and the "Middle Atmosphere" version, model E2.2 (Rind et al. (2020)), both of which have been contributed to CMIP6.

Model E2.1 has 40 vertical levels, a $2^\circ \times 2.5^\circ$ degree horizontal resolution, and a model top at 0.1 hPa. Compared to the CMIP5 version of ModelE (E2; Schmidt et al. (2014))), E2.1 has notable improvements, as discussed in Kelley et al. (2019). This includes a more credible representation of the MJO, which was achieved via modifications to the cumulus parameterization, as described in Kim et al. (2012), that improve MJO strength and propagation. These improvements are especially evident in the coupled version, which has a state-of-the-art MJO for a GCM (Kelley et al. (2019), Rind et al. (2020)).

Model E2.2 has the same horizontal resolution as E2.1, but a higher (102-level) vertical resolution (especially in the upper troposphere and lower stratosphere) as well as a higher model top at 0.002 hPa. Another major change to E2.2 from E2.1, which is important for

simulation of the QBO, is modification to the model's non-orographic gravity wave drag parameterization to include gravity wave drag due to convection and shear processes. E2.1, by comparison only has orographic gravity wave forcing and does not simulate a QBO (Orbe et al. (2020); Kelley et al. (2019)). In addition, while the underlying physics code is identical to that of E2.1, there are a few changes that were made to the convective parameterization in E2.2 in an attempt to better optimize certain aspects of the stratospheric circulation. Notably, one such change was the decision to disable evaporation of rain above the cloud base generated during a (parameterized) moist convective event, which results in a slightly weaker MJO in E2.2 compared to in the coupled version of E2.1 (Rind et al. (2020)).

For both models E2.1 and E2.2, we utilize both the atmosphere-only ("AMIP") configuration with prescribed sea surface temperature (SST) and sea ice fraction during the historical period (Rayner et al. (2003)) as well as a coupled configuration in which the atmosphere model is coupled to the GISS Ocean v1 (GO1; in the CMIP6 notation, versions E2.1/2-G, or in CMIP5 notation version E2/2–R). Versions of E2.1/2 coupled to the 'HYCOM' ocean model (E2.1/2-H) also exist and have been submitted to CMIP6, but for the sake of brevity we do not consider these HYCOM versions. See Schmidt et al. (2014) for a discussion of these two ocean models.

The atmosphere-only integrations considered in this study begin on January 1 1980, and are integrated through November 30 2017 ($\sim$ 37 years). Because the processing of the MJO indices we use involves removal of a 120-day running mean, all analysis is conducted beginning on May 1 1980. The observational data is pulled over the corresponding period, so that the length of the record is the same.

In the coupled version, the ocean is not initialized from observations, but, rather, from a year randomly chosen from a preindustrial control run. This allows ensemble members of the coupled run to be conducted by choosing different initial ocean restarts spaced 20 years apart from a 150 year preindustrial control. Note that this means that ensemble members' initial ocean states can be quite different from one another (due to interannual variability

such as ENSO) as discussed in Section 5.3.2.2. The coupled model is integrated for $\sim$ 36 years, and as with the AMIP run the processing of the MJO index precludes the first 120 days from analysis.

5.2.3 Nudging Experimental Design

A novel aspect of this work compared to previous GCM studies of the MJO-QBO connection is the use of nudging in the stratosphere. This helps to minimize biases in the QBO, as discussed more in Section 5.3.1. Nudging, sometimes also called "specified dynamics," is not a new technique (e.g. Jeuken et al. (1996)), and has been used in many climate modeling studies to look at effects including stratospheric ozone variability (Solomon et al. (2015); Ball et al. (2017)), the chemical and climate effects of volcanoes (Löffler et al. (2016); Schmidt et al. (2018)), dynamical coupling between stratospheric sudden warmings and the troposphere (Hitchcock and Simpson (2014)), stratospheric residual circulation (Chrysanthou et al. (2019)), or atmospheric predictability (Douville (2009), Jung et al. (2010)). In particular, nudging in the GISS ModelE framework has been developed and utilized in previous studies (e.g. Bauer et al. (2013), Shindell et al. (2013)). We briefly discuss the general way in which nudging is implemented in this model, before outlining our experimental design.

In this study we nudge the model's zonal and meridional wind towards MERRA2 reanalysis values. The nudging is carried out by adding a tendency term at each model timestep to the zonal and meridional wind, calculated as the difference between the model and the observations. For a generic time-step $N+1$, this additional tendency ($\frac{\Delta x_{\text{nudge}}}{\Delta t}$) is calculated implicitly as:

$$\frac{\Delta x_{\text{nudge}}}{\Delta t} = \frac{x_{N+1} - x_N}{\Delta t} = \frac{x_{\text{obs}} - x_{N+1}}{\tau} \tag{5.1}$$

where x is a generic variable (here zonal and meridional wind), x_{obs} is the reanalysis value, Δt is the model timestep and τ is a nudging relaxation timescale. Equation 5.1 is solved for x_{N+1}, the updated variable including the effects of nudging. The nudging timescale τ

controls how much the model value is allowed to stray from the observed value – for shorter timescales the model remains closer to the observations. In our study τ is 12 hours, though in Section 5.3.3 we conduct sensitivity tests with with $\tau = 30$ minutes and $\tau = 1$ week.

Our goal in nudging is to ensure that the model stratospheric biases are reduced. We do not seek to nudge the model MJO towards observations because, if the MJO were nudged, the model may show an MJO-QBO relationship simply because the observations contain an MJO-QBO link. As our goal is to test whether the model shows an emergent MJO-QBO link when the QBO is accurately represented, we only nudge the upper troposphere and stratosphere at the levels where any MJO signal is weak. This is done by only implementing the nudging in Equation 5.1 above a certain model pressure level, varying the nudging timescales linearly with height through the transition region from no nudging below to nudging at timescale τ at all levels above. For most runs, the transition region is 150-100 hPa, with full nudging above 100 hPa and no nudging below 150 hPa. Sensitivity tests in Section 5.3.3 lower the transition region to 200-150 hPa. For all nudging, the values in the reanalysis are first interpolated to the model levels. While it differs in the vertical, horizontally the nudging is spatially uniform and global.

We use two different implementations of the nudging. The first, which we call "grid-point" nudging, relaxes the model values at each latitude, longitude, and relevant pressure level to the reanalysis value at that same latitude, longitude, and relevant pressure level. In the context of Equation 5.1, $x_{N,N+1,\text{obs}}$ are functions of latitude, longitude, and pressure. The second implementation, "zonal-mean" nudging, relaxes the model zonal mean winds towards the observed zonal mean value – the only change in Equation 5.1 is that the model and observed zonal mean are calculated before the nudging is applied, and $x_{N,N+1,\text{obs}}$ are no longer functions of longitude. In the zonal-mean nudging, the nudging tendency added at a given pressure level, latitude, and timestep is the same at each longitudinal grid cell.

The advantage of the zonal-mean nudging is that the zonal structure of any vertically propagating waves from the troposphere into the stratosphere are not damped. In the grid-

point nudging, where the synoptic state of the stratosphere is primarily determined by the reanalysis and not the model values, given our short nudging timescale, these tropospheric waves will have less of an impact. The advantage of the grid-point nudging is that the model retains the same zonal structure in the stratosphere as the reanalysis (to the extent possible). Since the QBO is fairly zonally symmetric, this impact may not be of central importance, though Densmore et al. (2019) discussed a possible link between the MJO-QBO relationship and zonal asymmetries in QBO temperature anomalies. On the other hand, vertically propagating waves related to the MJO have been theorized as potentially important in driving the MJO-QBO link (Hendon and Abhik (2018)), so *a priori* the zonal-mean nudging seems more appealing. Using both nudging types balances the pros and cons of each approach.

Finally, in most runs we nudge to MERRA2 assimilated reanalysis fields, which represents observations as faithfully as a reanalysis product can. However, to explore whether increasing or decreasing the magnitude of the QBO has an effect on our results, for some sensitivity tests in Section 5.3.3 we multiply the meridional and zonal wind by a factor of 1.5 or 0.5 to look at whether stronger or weaker stratospheric winds have an noticeable impact on the MJO. Table 5.1 provides a summary of our experiments in this study across model versions and nudging strategies.

5.3 Results

5.3.1 Control Runs (without Nudging)

In this section, we examine the MJO-QBO relationship in the non-nudged control run versions of the coupled and AMIP models E2.1 and E2.2. Our analysis here is primarily on the 102-level version, as it simulates its own QBO without nudging. We first assess the representation of the MJO and QBO in each model, and then briefly show results from the 102-level model on the MJO-QBO relationship (or lack thereof). Our findings in that sec-

Model Version	**Ocean State**	**Nudging Style**	**Nudging Timescale (τ)**	**Nudging Transition Height**	**QBO Strength**	**Ens. Size**
E2.2	AMIP	None	–	–	Model QBO	1
E2.2	Coupled	None	–	–	Model QBO	1
E2.1	AMIP	Grid-point	12 hrs.	150-100hPa	Obs. QBO	1
E2.1	AMIP	Zonal-mean	12 hrs.	150-100hPa	Obs. QBO	1
E2.1	Coupled	Grid-point	12 hrs.	150-100hPa	Obs. QBO	1
E2.1	Coupled	Zonal-mean	12 hrs.	150-100hPa	Obs. QBO	5
E2.1	Coupled	Zonal-mean	30 min.	150-100hPa	Obs. QBO	1
E2.1	Coupled	Zonal-mean	1 wk.	150-100hPa	Obs. QBO	1
E2.1	Coupled	Zonal-mean	12 hrs.	200-150hPa	Obs. QBO	1
E2.1	Coupled	Zonal-mean	12 hrs.	150-100hPa	1.5 $\times$ Obs. QBO	1
E2.1	Coupled	Zonal-mean	12 hrs.	150-100hPa	0.5 $\times$ Obs. QBO	1

Table 5.1: List of experiments considered in this study per the modeling and nudging versions and parameters described in Section 5.2. The columns describe the model version (E2.2=102-level, E2.1=40-level); whether the model ocean state is specified ("AMIP") or coupled; whether the grid-point or zonal-mean nudging is used (see Sect. 5.2.3); the nudging timescale (τ in Eqn. 5.1); the nudging transition region (no nudging below the region, and full nudging at τ above the region); the strength of the QBO (if the QBO is internally-generated, "Model QBO"); and the size of the ensemble. Runs beneath the horizontal in the center of the table are the sensitivity tests discussed in Section 5.3.3.

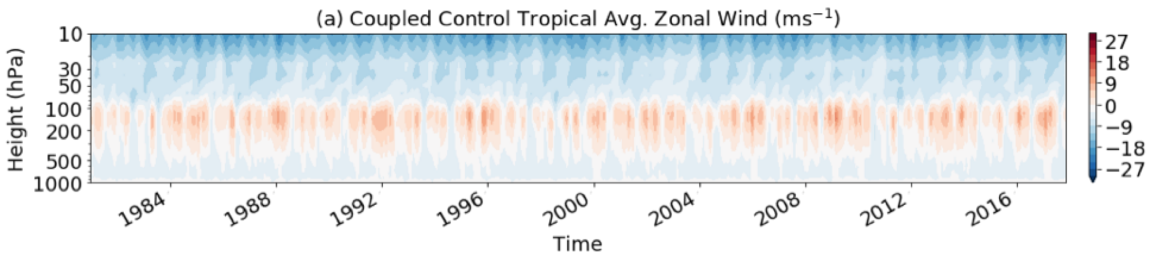

Figure 5.1: The zonal-mean, 10°N/S averaged monthly zonal wind from the 40-level version of the GCM (coupled version; AMIP not shown). No QBO is evident in this model.

tion are largely consistent with other published modeling work (Lee and Klingaman (2018), Kim et al. (2020a)) on the MJO-QBO relationship in free-running models with internally-generated QBOs.

5.3.1.1 MJO and QBO Performance

A major deficiency of the 40-level model as it is typically run without nudging is that, as shown in Figure 5.1, this model does not produce a QBO in either an AMIP or coupled configuration. This is not a surprise, as low vertical resolution is known to make simulating a QBO difficult and the necessary adjustments to the gravity wave drag scheme have also not been made to this version. For the purposes of this section this precludes us from analyzing this model's MJO-QBO relationship.

However, an important feature of the 40-level model is that the MJO is well-represented for a GCM of this resolution (Kelley et al. (2019), Rind et al. (2020)), especially in the coupled version. In particular, this is evident in Figure 5.2 which shows MJO convective signals. This longitude-time regression plot is formed by taking the 20-100 day bandpass filtered OLR averaged over 10°N/S, and regressing each longitude for leads/lags of ±50 days against the 60°-90°E/W mean (similar to Lee and Klingaman (2018)). The regression coefficient is plotted in Figure 5.2.

Figure 5.2 shows observations (left), the AMIP version of the model (center) and the coupled version of the model (right). In both model versions, the period of the MJO is close to that of observations, and the propagation is partially evident in the AMIP version and

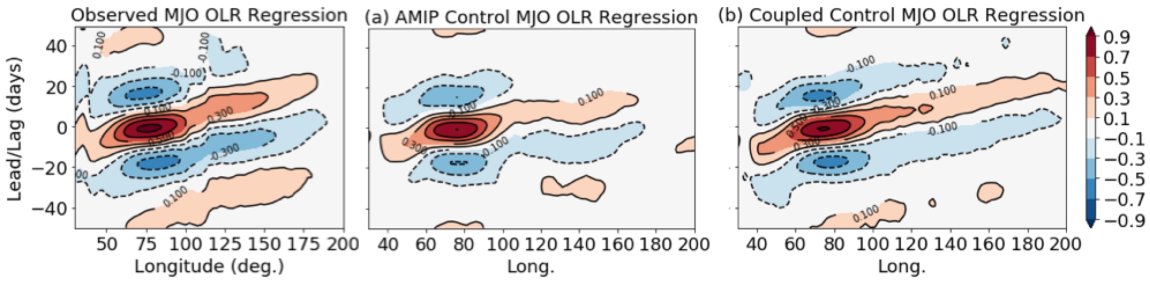

Figure 5.2: Longitude-time OLR regression in the 40-level control runs. Regression of the 10°N/S averaged, 20-100 day filtered OLR are taken at each longitude and at leads/lags of ±50 days versus the values averaged from 60°-90°E for (left) observations, (center) the AMIP model and (right) the coupled runs.

very good in the coupled version. Other studies of the E2.1 coupled model have confirmed in more detail that it captures a very good representation of the MJO amplitude, propagation, and phase speed (Daehyun Kim, personal communication).

Analogous plots to Figures 5.1 and 5.2 are shown in Figures 5.3 and 5.4 for the QBO and MJO in the 102-level model. Figure 5.3 clearly shows that the model has oscillating stratospheric winds consistent with the observed QBO, a product of the high vertical resolution and tuned gravity wave scheme. The accurate representation of the QBO was a goal in this model's development, though some deficiencies exist. First, while the period of the QBO in the model is comparable to the QBO in MERRA2 reanalysis, the model QBO is too regular, especially with regards to the downward propagation of the easterly phase. Also evident are biases in the tropopause region, where the model simulates stronger easterly winds than observed and lacks the clear modulation due to the QBO seen in observations. Other aspects of the deficiency simulating the QBO will be noted in the next section. Despite these issues, relative to other GCMs (Richter et al. (2020)) the QBO in the 102-level model is consistent with state-of-the-art simulations in comprehensive models.

We also examined the MJO in the 102-level model using the same filtered OLR regression as in Figure 5.2. The results are shown in Figure 5.4. Here unlike the 40-level version the AMIP and coupled versions of the model look relatively similar. The propagation is not as well-represented and the phase speed is also too low, especially compared to the coupled

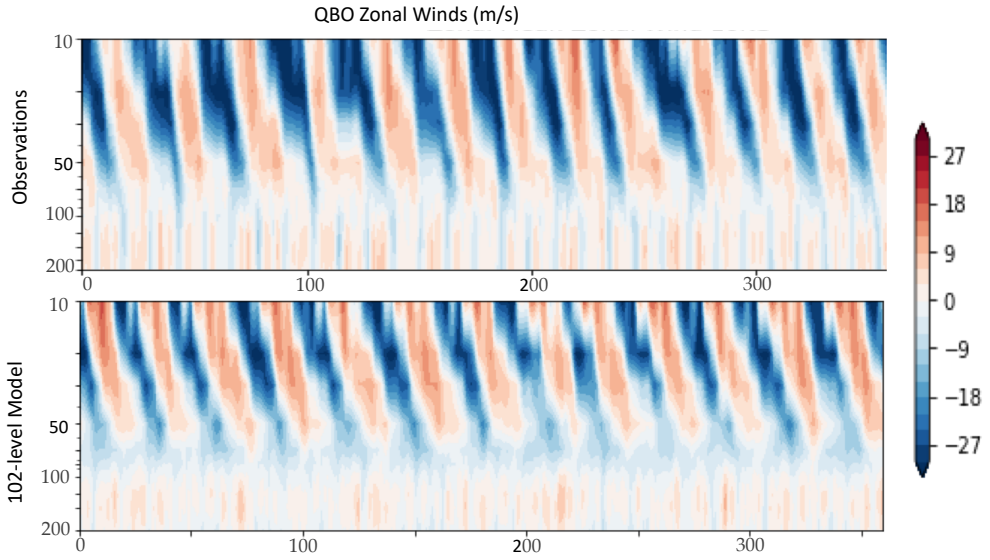

Figure 5.3: Similar to Figure 5.1, but for observations (top) and the 102-level model (bottom; coupled-version). Note the x-axis is the time in units of number of months since Jan. 1 1980, and the y-axis shows only the upper troposphere and stratosphere.

40-level model. Studies disagree on how much, in general, higher vertical resolution improves representation of the MJO (Inness and Slingo (2003); Crueger et al. (2013)); as discussed in the introduction of this chapter changes in the convective parameterization in E2.2 were made which improved the stratosphere but at the expense of the MJO. Still, because the 102-level version of the model has both a reasonable representation of the MJO and the QBO, we can examine the MJO-QBO link.

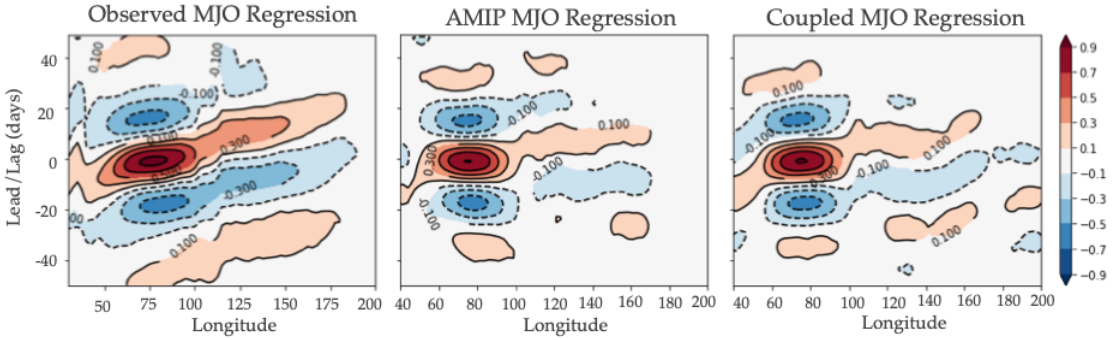

Figure 5.4: As in Figure 5.2 but for the 102-level model.

5.3.1.2 MJO-QBO Relationship

There is no strong MJO-QBO connection in the 102-level model in either the AMIP or coupled configuration. This can be seen clearly in Figure 5.5. The top panels show the MJO-QBO correlation during DJF periods in observations and in the AMIP and coupled models. The observations show, consistent with Yoo and Son (2016), a strong and significant anti-correlation of the MJO and the QBO. In contrast, the model shows no significant correlation in either version. Note that the QBO and MJO amplitudes evident in these panels are similar in the model and observations, indicating the model's ability to capture both processes. Additional correlation analyses between the QBO winds at 10, 30, 50, and 70 hPa and RMM do not show any strong or significant correlations across both model versions. Further, correlations in other seasons (not just DJF) do not change these result.[1]

The bottom panels in Figure 5.5 show the boreal winter MJO amplitude in QBOE and QBOW. This is similar to the analysis in Yoo and Son (2016) (see Figure 2.19d; differences are due to a different index for the MJO, a slightly different QBO index, and a difference in the time period). In observations a strong and clear separation between the MJO in QBOE versus QBOW is evident, with larger MJO amplitude in QBOE. In contrast, the two model types show no strong modulation. More analysis comparing the OLR linear regression plots (as in Figures 5.2 and 5.4) separately for QBOE and QBOW and the MJO-filtered OLR differences (not shown) lead us to conclude that there is no MJO-QBO connection.

A host of possibilities for why the model does not display an MJO-QBO link exist, as discussed in Section 5.4 (and other chapters, including Chapter 7). One popular hypothesis proposed in the literature (Lee and Klingaman (2018); Kim et al. (2020a)) is that models tend to under-estimate the strength of QBO temperature anomalies in the tropopause region. Figure 5.6 shows that our 102-level model is no exception, and has weaker than observed

[1]Without a coherent theory for why the observed MJO-QBO link should fall in DJF, it is possible the model may show the link in other seasons, though this is not the case here.

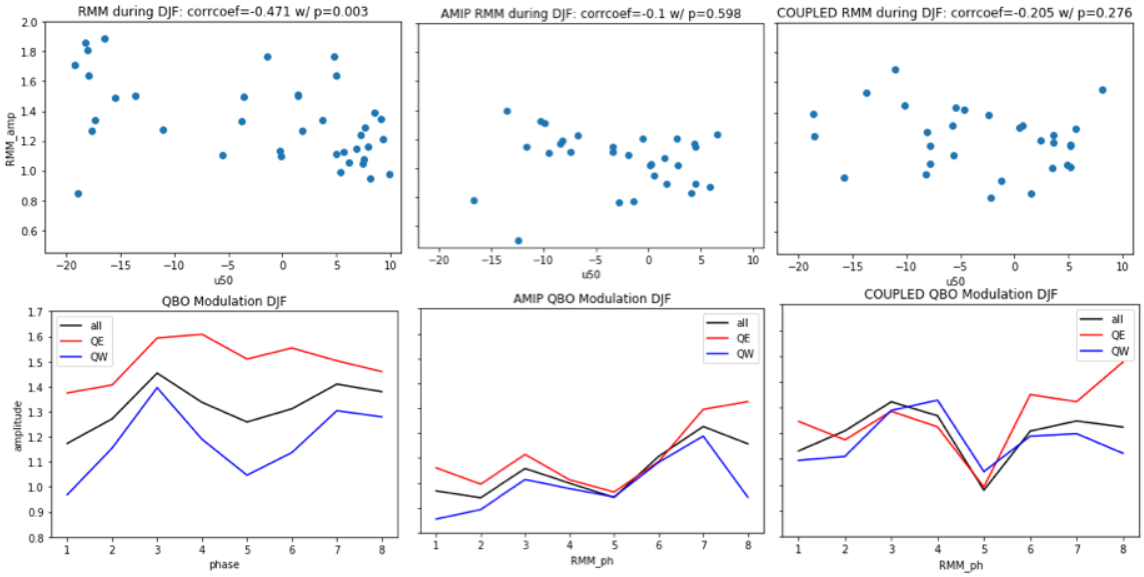

Figure 5.5: (Top panels) The DJF-mean U50 QBO value (x-axes) and RMM amplitude (y-axes) for (left) observations, (center) the AMIP model, and (right) the coupled model. Correlation coefficients and p-values shown in the title. (Bottom panels) The DJF MJO amplitude as a function of MJO phase for all winters (black), QBOE winters (red), and QBOW winters (blue) – observations and the two models are as in the top row.

QBO temperature signals. Comparing the QBOE minus QBOW temperature anomalies in the upper troposphere and lower stratosphere in observations (left) and the model (center), it is clear model anomalies are too weak by a factor of ∼2-3, especially near the tropopause. The rightmost panel shows the difference between the model and observations, confirming that the model does not show a strong enough variability in this region.

This deficiency in the model's representation of QBO temperature signals seems to be a promising candidate to explain the lack of an MJO-QBO link. More broadly, model biases in the simulation of the QBO, or of the stratosphere in general, could contribute to a lack of an MJO-QBO relationship. In that regard, reducing stratospheric biases can help determine whether simulation of model processes around the tropopause is a central and important feature of capturing the MJO-QBO link or not. This is the main motivation for the nudging experiments in the next section, where (as much as possible) we reduce biases in the simulation of the QBO. Another advantage of this method is we can make use of versions of the model (like the 40-level coupled version) which have very good representations of the

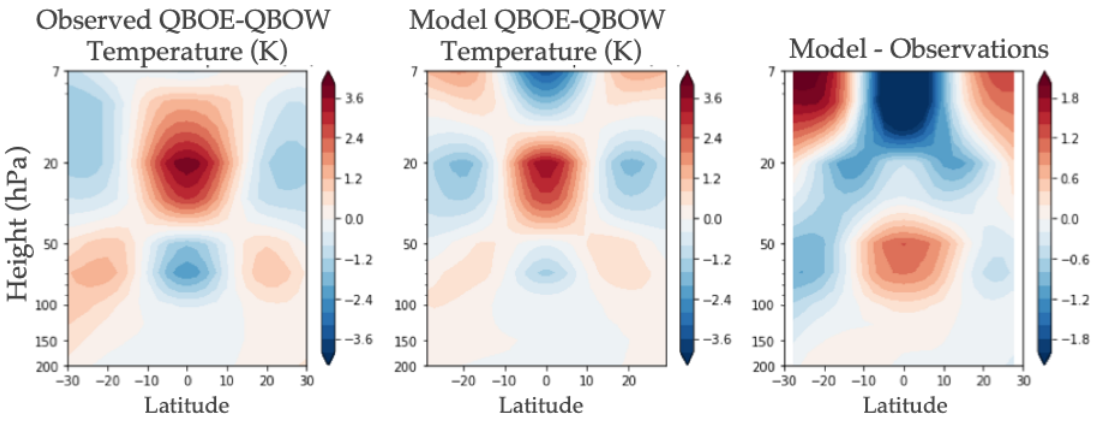

Figure 5.6: Zonal-mean, QBOE minus QBOW temperature anomalies (in K) as a function of latitude and height in the upper troposphere and stratosphere. Left panel shows observations, the center shows the coupled 102-level model control simulation (the AMIP version looks similar) and the right shows the model minus observed difference. Here observations have been linearly interpolated onto the model grid.

MJO but no inherent QBO signals.

5.3.2 Nudging Experiments

5.3.2.1 MJO and QBO Performance

In this section we present results from our nudging experiments, as described in Section 5.2.3. We first examine the QBO behavior in various versions of the model, before looking more at the MJO-QBO relationship.

We consider four configurations of the 40-level model: the AMIP configuration with grid-point and zonal-mean nudging and the coupled configuration with grid-point and zonal-mean nudging. Because of promising initial results the coupled, zonal-mean nudged model has four additional ensemble members, formed per Section 5.2.3 with different initial ocean states. Additional coupled, zonal-mean nudged experiments varying the nudging and increasingly or decreasing the strength of the QBO are presented in Section 5.3.3. Note no results in this section utilize the 102-level version of the model, in part because its representation of the MJO is worse than the 40-level version, but more significantly because for unresolved

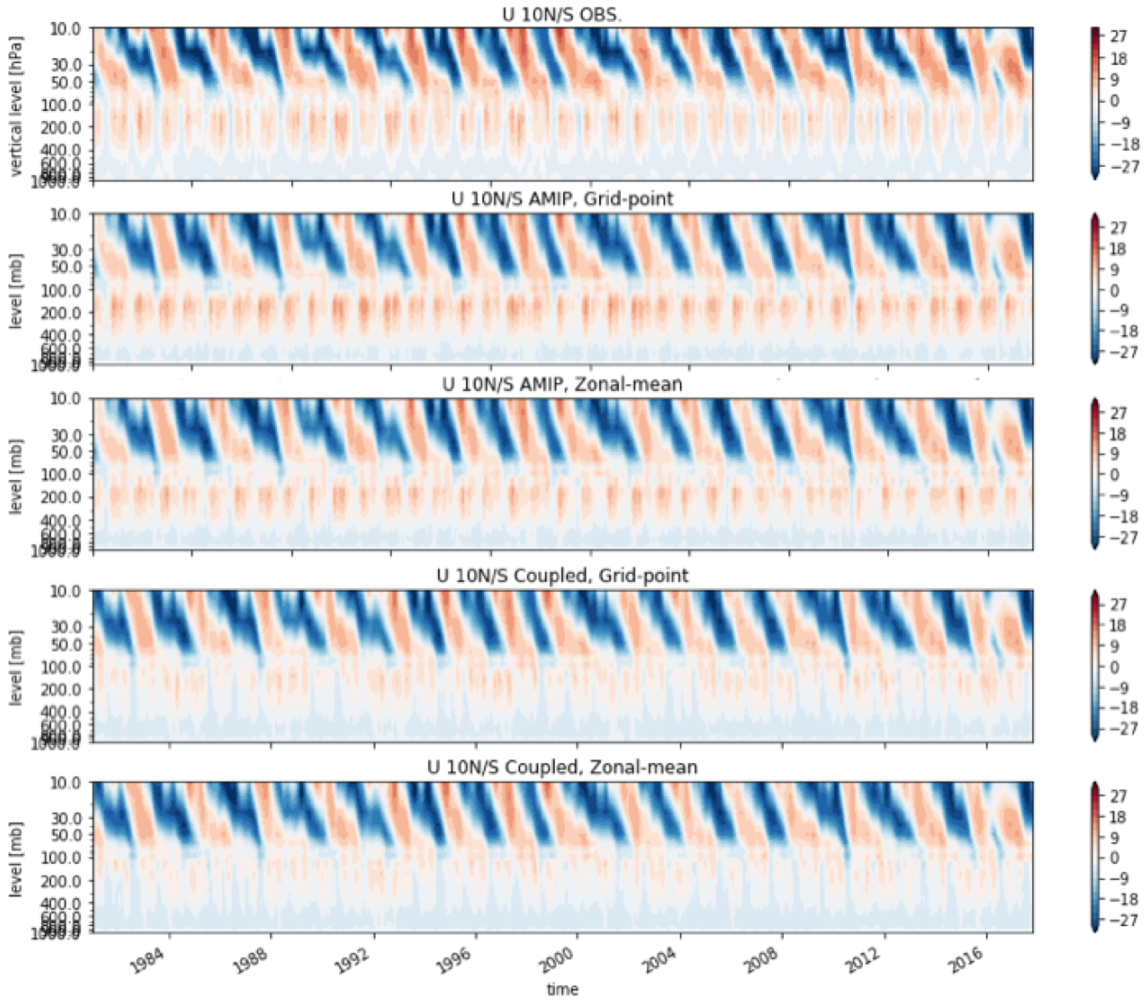

Figure 5.7: Identical to Figure 5.1, but for (top to bottom) observations, the AMIP grid-point nudged model, the AMIP zonal-mean nudged model, the coupled grid-point nudged model, and the coupled zonal-mean nudged model.

technical reasons nudging was not able to be implemented in that configuration.

Figure 5.7 shows the zonal winds in observations and the nudged versions of the model. With the nudging the QBO is well-represented compared to observations and looks essentially identical in the stratosphere across the four model variants. In the troposphere, the AMIP version displays a stronger annual cycle than observations or the coupled version, as well as in general stronger upper tropospheric flow than observed or compared to the coupled model.

Even though model temperatures are not nudged (for technical reasons), the nudging of

the winds and the constraint of thermal wind balance lead to realistic QBO temperature anomalies in the model. Figure 5.8 shows the QBOE minus QBOW temperature differences for the nudged versions, demonstrating that observed temperature anomalies in the tropopause region are well-represented in the model. That this occurs without needing to nudge the temperature is encouraging. If anything the variability associated with the QBO is slightly too large in the model compared to observations (e.g. the negative anomalies around the tropopause in the lower panels), which might encourage a stronger MJO-QBO connection (as seen in Martin et al. (2019)). The off-equatorial warm anomalies are also captured in the model with approximately the right magnitude, which suggests the QBO meridional circulation is also present in the model. Higher up (above 30 hPa) the model temperature signals are weaker than observed, but it is unlikely that temperatures at those levels play a strong role in the MJO-QBO link (Martin et al. (2019)).

Additional comparison of the model QBO wind and temperature versus observations can be seen in Figure 5.9, which shows the U50 zonal wind and the temperature at 100 hPa (T100; processed the same way as the 50 hPa zonal wind). The zonal wind is essentially identical across the four model versions, likely due to the short nudging timescale and the fact that 50 hPa is well into the region of the stratosphere where the nudging is applied. The zonal wind is also in close agreement between the model and observations, with a correlation of approximately 0.9. In general, the model has a stronger easterly phase than observed, and in some cases the precise timing of the westerly to easterly transition is earlier in the model than it is in observations (easterly to westerly transitions are well-captured).

The model temperature anomalies at 100 hPa show more variability in the model across different configurations. This is likely in part due to the fact that the temperature is not nudged. Also, since the wind below 100 hPa is being nudged less stringently, there is more variability in the vertical structure of the zonal wind around the tropopause, and therefore in the precise temperature anomalies on the equator due to thermal wind. The tropospheric wind differences for example between the AMIP and coupled versions may play a role in

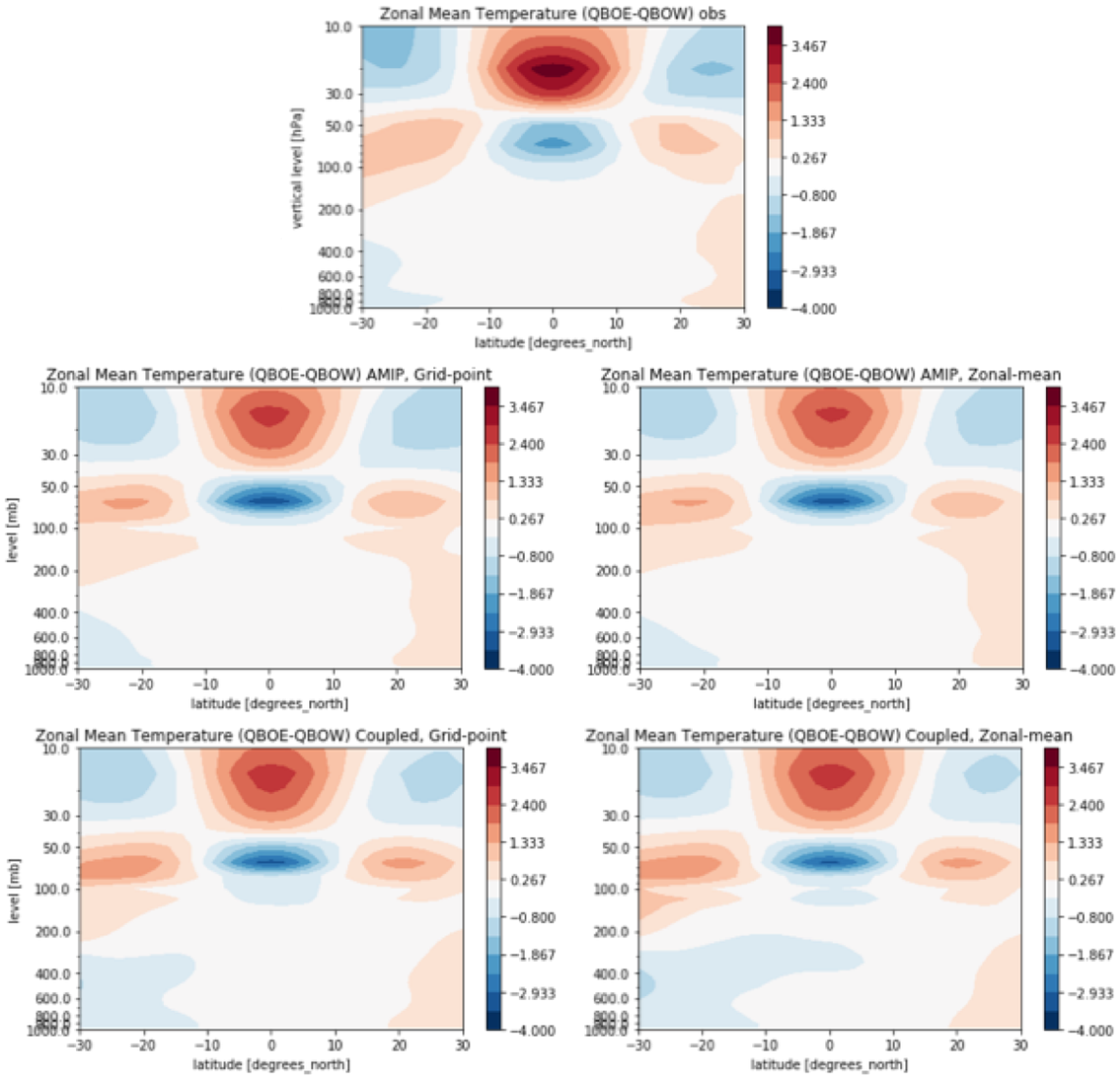

Figure 5.8: Zonal-mean QBOE minus QBOW temperature difference as in Figure 5.6, but shown from the surface to 10 hPa. The top shows the observed differences, whereas the bottom shows (clockwise from the top-left): the AMIP grid-point nudged, AMIP zonal-mean nudged, coupled grid-point nudged, and coupled zonal-mean nudged models. Here the model values are not interpolated to the observed levels.

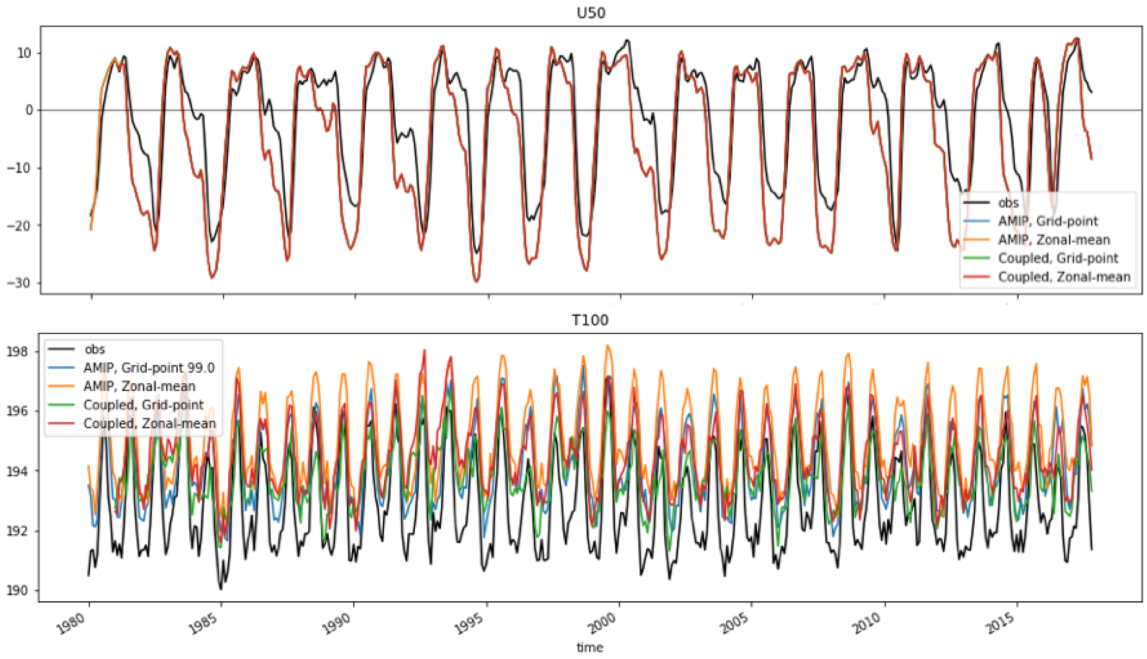

Figure 5.9: (top) The U50 QBO index described in Section 5.2.1 for MERRA2 (black) and the four nudged configurations (colored). Note the lack of coupled model data early in the record is due to the different initialization date. (bottom) The temperature at 100 hPa (T100), processed identically to the U50 index except for the change of variable and pressure level.

contributing to the small spread seen here. Also note that the main mode of variability evident in T100 is due to the annual cycle, not the QBO. While Figure 5.8 indicated that temperature anomalies associated with the QBO may be stronger than observed, the T100 time series in Figure 5.9 shows that the model is biased warmer than observations, and the coldest 100 hPa points reached in observations are not present in the model. Because nudging the temperature in this model is technically difficult to implement we are unable to resolve these biases further. The two grid-point nudged versions (green and blue) are often somewhat colder than their zonal-mean counterparts in QBOE periods, whereas the AMIP zonal-mean often shows the warmest values of T100 throughout the integration.

We now examine whether these major changes in the stratosphere and upper troposphere have an impact on the MJO. In particular, since we capture the strength of the variability associated with both QBO winds and temperatures, we might expect the model to display a strong MJO-QBO connection. We will see this is not the case.

5.3.2.2 MJO-QBO Relationship

We first examine the MJO-QBO connection in a single ensemble member run from the four different model configurations: AMIP grid-point, AMIP zonal-mean, coupled grid-point, and coupled zonal-mean. We assess the MJO-QBO link via the metrics described in Section 5.2.1: QBO changes to MJO amplitude, MJO-QBO correlation, and QBO changes to MJO-filtered OLR activity.

First, we assessed the MJO amplitude as a function of MJO phase in QBOE and QBOW, similar to Figure 5.5. Here we test the statistical significance of the model and observed results using both a Welch's t-test (Welch (1947)) and bootstrapping. For the t-test, the null hypothesis is that there is no difference between the QBOE and QBOW periods; the degrees of freedom are the number of days in each MJO phase and QBO phase that are separated by at least seven days (following Garfinkel et al. (2012)). For the bootstrapping test, for each MJO phase let N_{QE} and N_{QW} be the number of days in QBOE and QBOW,

respectively. From the group of all MJO days in a given phase, we randomly select two groups of size N_{QE} and N_{QW}, then calculate the MJO amplitude difference between those two groups, repeating this process 1000 times. Significance for both tests is defined at the 95% confidence level. The results are shown in Figure 5.10.

The topmost panel in Figure 5.10 shows observations, which demonstrates a strong, significant, and consistent modulation of the MJO by the QBO. The bottom four panels show model results. None of the models indicates a consistent MJO-QBO link across all phases. In some cases one or two phases show a significant difference, but it seems equally likely that in a given phase the MJO is stronger in QBOW than it is that the MJO is stronger in QBOE. This suggests that any QBO modulation is not related to the observed MJO-QBO link.

To examine the impact on MJO convection more specifically, in Figure 5.11 we plot the QBOE minus QBOW difference in MJO-filtered OLR activity. Also shown, in contours, is the DJF climatological MJO-filtered OLR activity. In observations, there is a clear increase in the MJO activity in QBOE relative to QBOW over the warm pool region, where the MJO is climatologically most active. The four model version show much weaker signals. Most model configurations show essentially no change, or if anything appear to have a slightly weaker MJO in QBOE versus QBOW. The exception is the coupled zonal-mean nudged model, which shows a modest enhancement over the warm pool region.

Averaging the differences in Figure 5.11 over the warm pool yields the values shown in Table 5.2. While observations shows a strong change of more than two and a half standard deviations, the model runs, with the exception of the coupled zonal-mean simulation, show a change of less than one standard deviation in amplitude. The change is marginal in the coupled zonal-mean run, but at least has the correct sign and a moderately strong amplitude.

Also shown in Table 5.2 are the results of the correlation between the DJF-mean RMM amplitude and the U50 index. None of the models shows a significant correlation, though consistent with other metrics the 40-level, coupled zonal-mean nudged version shows at least

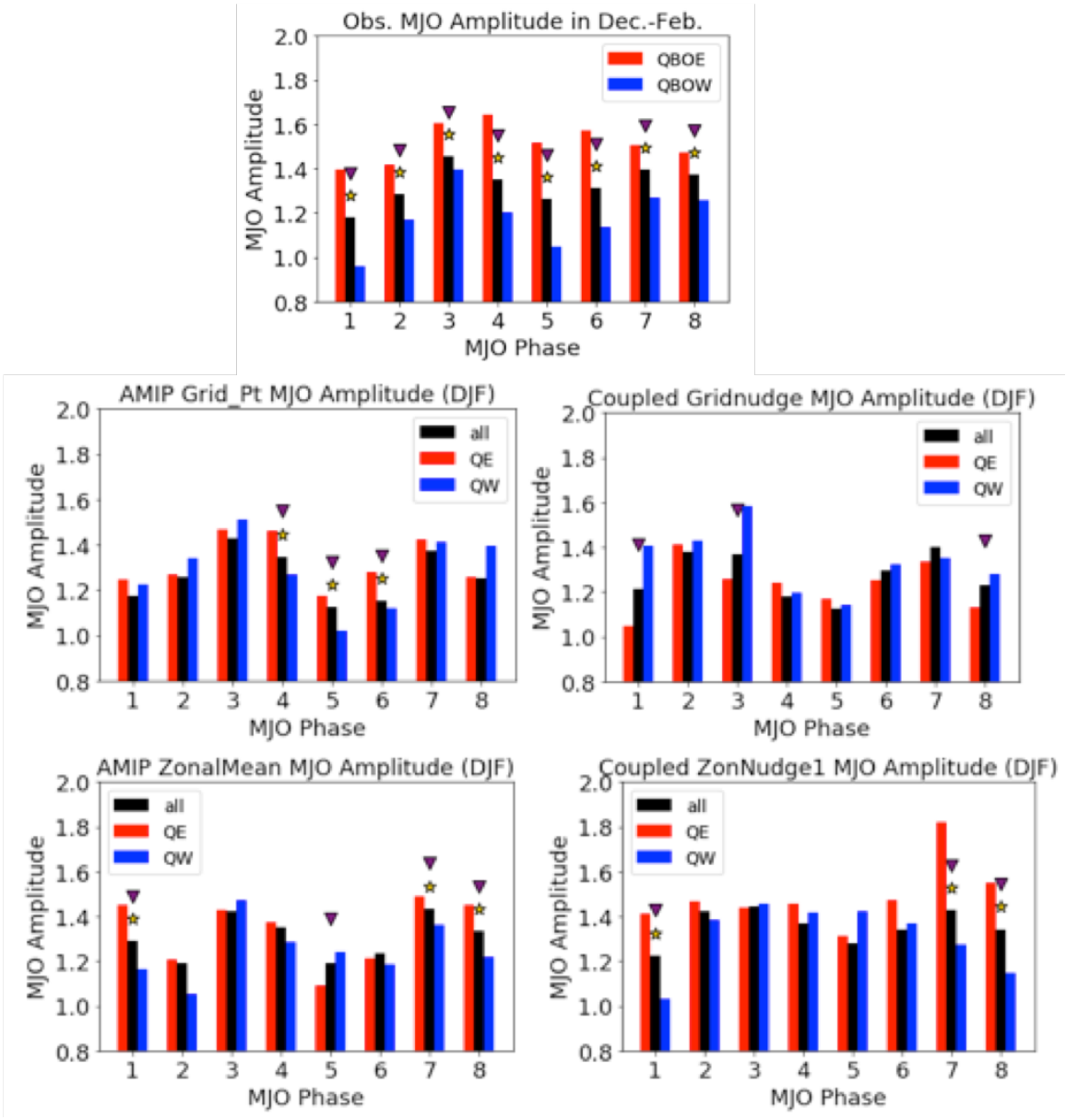

Figure 5.10: MJO amplitude as a function of MJO phase in all DJF periods (black), QBOE months (red) and QBOW months (blue). The top panel is observations, and the bottom four are (clockwise from the top-left): the AMIP grid-point nudged, coupled grid-point nudged, AMIP zonal-mean nudged, and coupled zonal-mean nudged models. Gold stars denote significance using a t-test, and purple triangles denote the significance with a bootstrapping test, as described in Section 5.3.2.2.

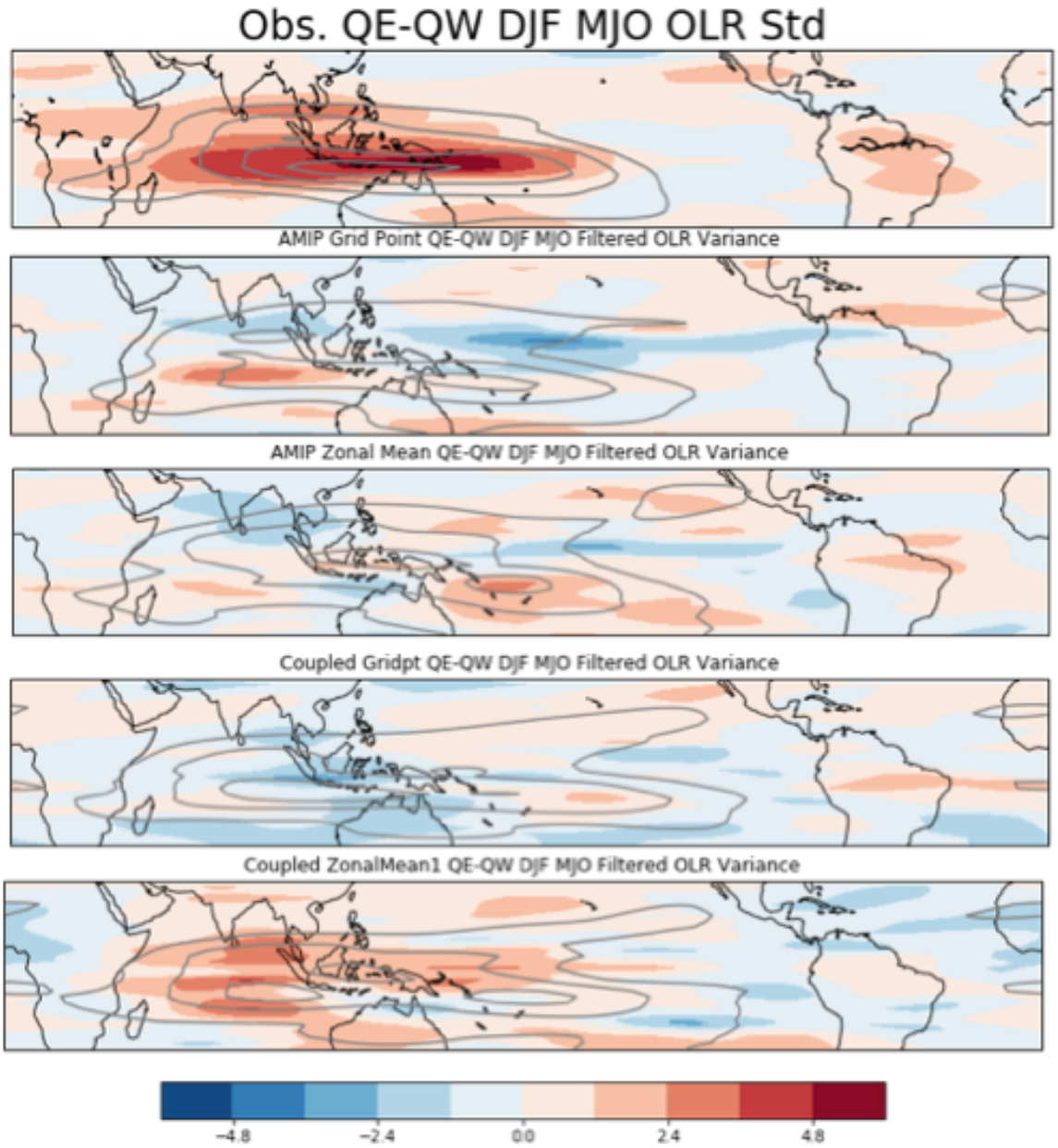

Figure 5.11: The QBOE minus QBOW difference in the standard deviation of MJO-filtered (20-100 day, eastward propagating wave number 1-5) OLR, as described more in Section 5.2.1. Panels are (top to bottom) observations, and the AMIP grid-point nudged, AMIP zonal-mean nudged, coupled grid-point nudged, and coupled zonal-mean nudged models. Grey contours show the DJF climatology of the standard deviation of MJO-filtered OLR from observations or the model. The contour intervals are from 9 to 24 W/m^2 at intervals of 3 W/m^2 .

Data Source	**QBOE-QBOW MJO-OLR Std.**	**MJO-QBO Corr. (p-value)**
Observations	2.57	-0.45 (.004)
AMIP Grid-point	0.12	0.16 (.43)
AMIP Zonal-mean	0.10	-0.20 (.24)
Coupled Grid-point	-0.79	0.20 (.25)
Coupled Zonal-mean	1.40	-0.24 (.17)

Table 5.2: MJO-QBO relationships metrics for observations and each model configuration. "QBOE-QBOW MJO-OLR Std." is the QBOE minus QBOW difference in the standard deviation of MJO-filtered OLR during DJF over the warm pool region, as defined in more detail in Section 5.2.1 and shown in Figure 5.11. "MJO-QBO Corr." is the U50/RMM amplitude correlation in DJF, with the p-value in parenthesis.

a relationship of the correct sign, albeit of weaker amplitude. Examination of the correlation in other seasons showed no stronger results.

While none of the models show as strong an MJO-QBO link as observed the coupled zonal-mean nudged version has somewhat promising initial results. To further investigate the model, we repeated over analysis excluding the first 10 years of data, because some theories for the MJO-QBO relationship (e.g. Klotzbach et al. (2019)) have suggested that it only emerged since the mid-to-late 1980s. Figure 5.12, the same MJO amplitude plots as in Figure 5.10 but from 1991 onward, show an even stronger signal in the model, with a statistically significant increase in the MJO amplitude when the QBO is easterly versus westerly in most model phases. Over this nearly 30-year period the MJO-QBO link in the model looks fairly comparable to observations.

To expand upon these somewhat promising results, we ran four additional simulations which are identical to the coupled, zonal-mean simulations except that the initial conditions of the ocean is different. The additional ensemble runs suggest that in fact, the apparent changes in the model MJO seen in the first ensemble member are not due to the QBO. This

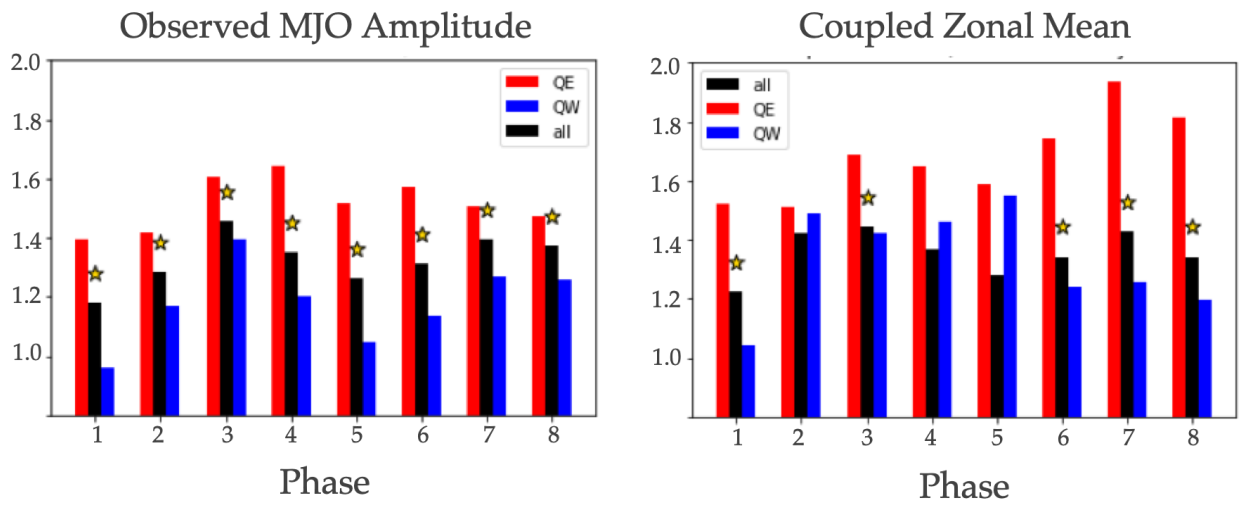

Figure 5.12: As in Figure 5.10, but only for the observations and the coupled, zonal-mean nudged model, and using only data from 1991 onward instead of 1981 (e.g. excluding the first 10 years). Here no bootstrap test was conducted.

seems to conclusively prove that the model does not have a strong MJO-QBO relationship. For example, Figure 5.13 shows the MJO amplitude modulation in QBOE and QBOW. There we see broadly different behavior across various ensemble members despite the fact that the nudging keeps the stratospheric winds and temperatures nearly identical across the different simulations. In general no consistent QBO modulation is evident. Restricting the analysis to the period 1991 onward (as in Figure 5.12) does not change the results.

The MJO-filtered OLR differences across ensemble members, Figure 5.14, supports the conclusion that the various ensemble members do not show an MJO-QBO connection. Some ensemble members show what appears to be decrease in MJO activity during QBOE (e.g. Member 3), whereas others show what looks like noise (Members 2, 4), and some show what appear to be strong local changes in various ocean basins (Members 1,5). The spatially confined increases in MJO activity in Members 1 and 5 seem more likely based on oceanic, rather than stratospheric, variability – a hypothesis that will be examine more in future work.

From this we conclude that even the coupled, zonal-mean nudged version of the 40-level model has no MJO-QBO link. The weak relationship in certain ensemble members is likely

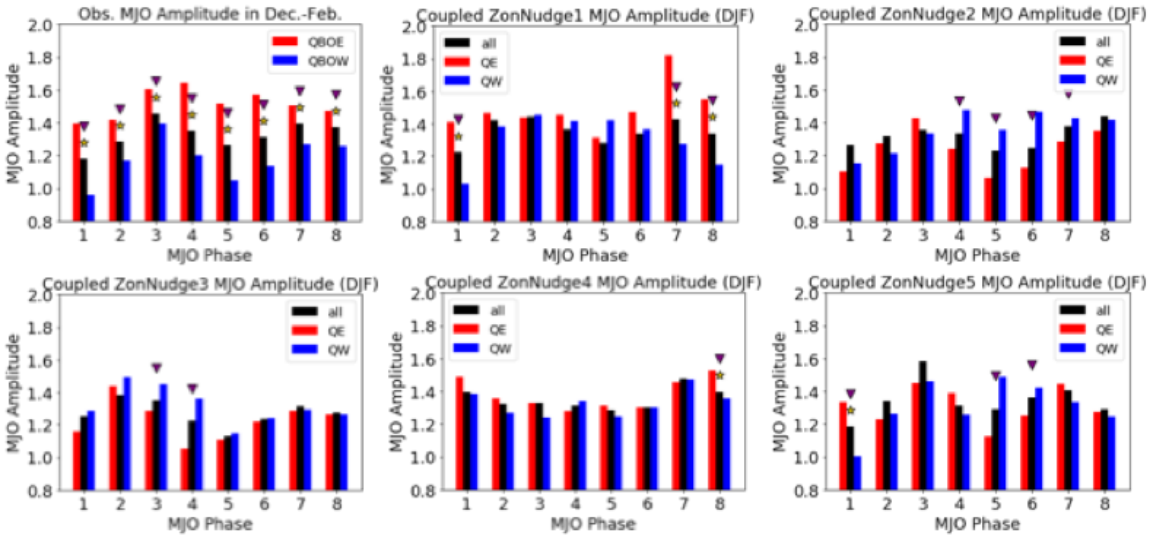

Figure 5.13: As in Figure 5.10, but for the five ensemble members of the coupled, zonal-mean nudged model (Member 1 identical to what is shown in Figure 5.10). Observations (top left) also shown for reference.

due to noise, or due to variability of some other element of the climate system unrelated to the stratosphere, such as ENSO.[2] It is worth stressing that the apparent weaker-than-observed relationship in Member 1 indicates that care should be taken in modeling studies of the MJO-QBO link to run sufficiently long period, as even in ∼30 years of data (e.g. Figure 5.12) apparent MJO-QBO connections can appear which do not seem significant when extended to longer timescales or ensembles.

We leave for future work the cause of differences in the MJO-QBO behavior across ensemble members. However, one hypothesis we can likely rule out at this stage is that the difference comes from the stratosphere, as the QBO winds among the ensemble members are essentially identical and temperature changes at 100 hPa are small (not shown).[3]

Figure 5.15 looks at whether the MJO itself is different between the different ensemble members. This does not appear to be the case. All ensemble members capture the seasonal

[2]This will be examined in future work looking more at SST signals in different ensemble members in QBOE versus QBOW.

[3]Additional work with an 11-member ensemble (simulations complete, analysis ongoing) will look more into whether any small changes in temperatures in the upper troposphere/lower stratosphere seem related to the MJO-QBO link, but given the sensitivity results in Section 5.3.3 this seems unlikely.

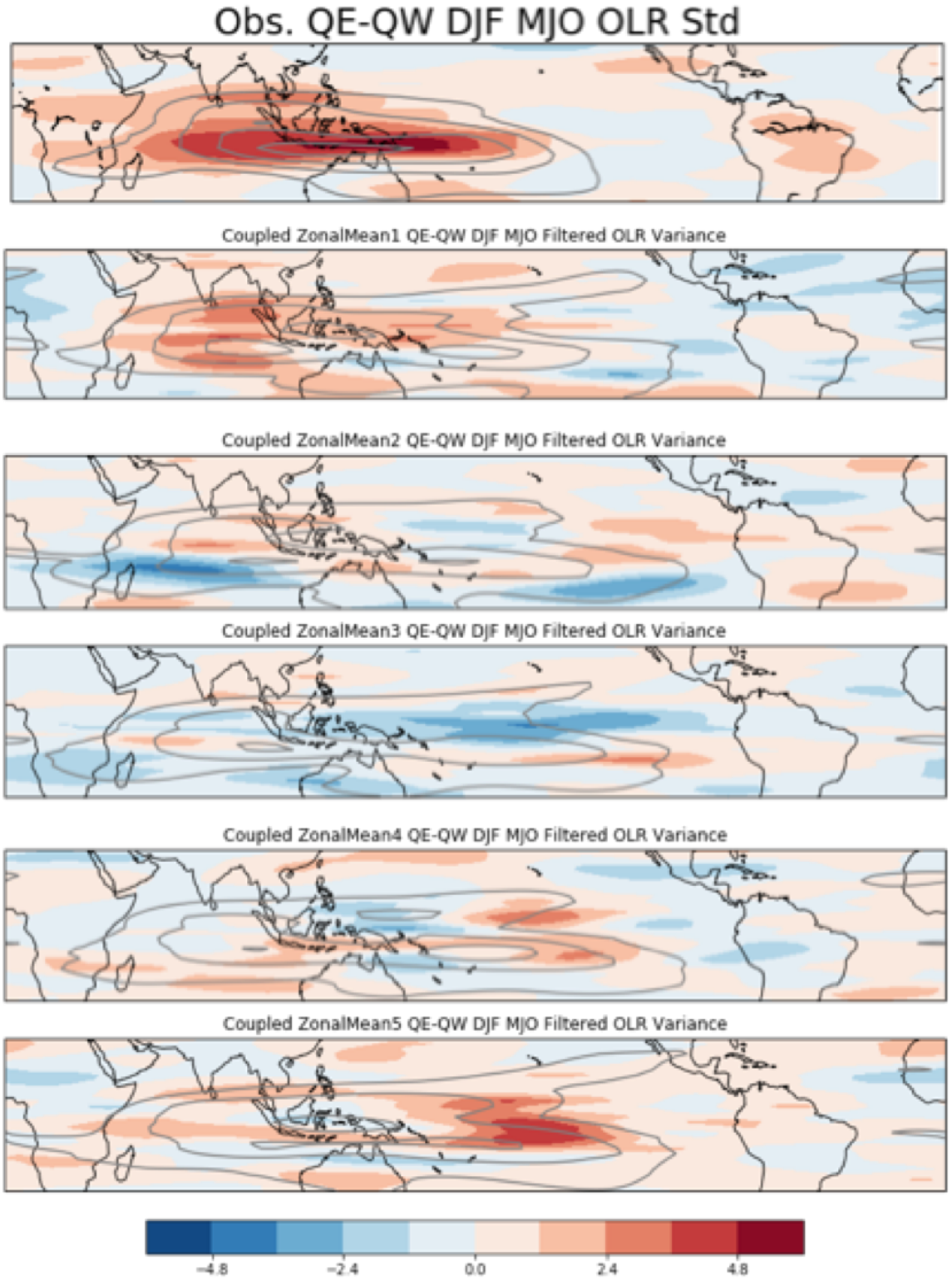

Figure 5.14: As in Figure 5.11 but for the coupled zonal-mean ensemble members.

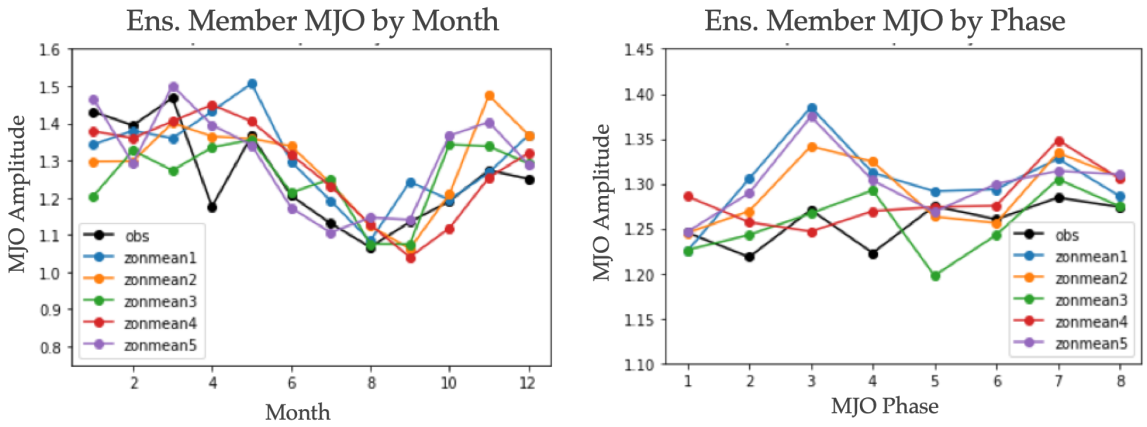

Figure 5.15: MJO amplitude binned by month (left) and MJO phase (right) in observations (black) and the five coupled zonal-mean nudged ensemble members (colors). Note the different y-axes in the two panels.

cycle of the MJO well compared to observations (left panel) and they show fairly consistent amplitudes across different MJO phases. In some cases (e.g. Members 1,2, and 5 in phase 3) there do appear to be differences in how strong the MJO is in a given phase. However our analysis found no connection between the amplitude of the MJO in a particular phase and ensemble member and the strength (or lack thereof) of the MJO-QBO connection in that member/phase. Additional analysis (not shown), including a comparison of climatological MJO-filtered OLR over the warm pool (e.g. Figure 5.14) and the OLR regressions of the MJO (e.g. Figure 5.2), support the conclusion that the behavior of the MJO is similar across different ensemble members.

5.3.3 Sensitivity Tests

In this section we show results from sensitivity tests to both the nudging parameters, as well as the strength of the QBO. These sensitivity test and their configuration are summarized in Table 5.1.

None of the sensitivity experiments show a strong MJO-QBO relationship. This suggests that the nudging parameters, at least over the ranges considered in this section, are not the crucial in the model's inability to show an MJO-QBO relationship. Further, we show here

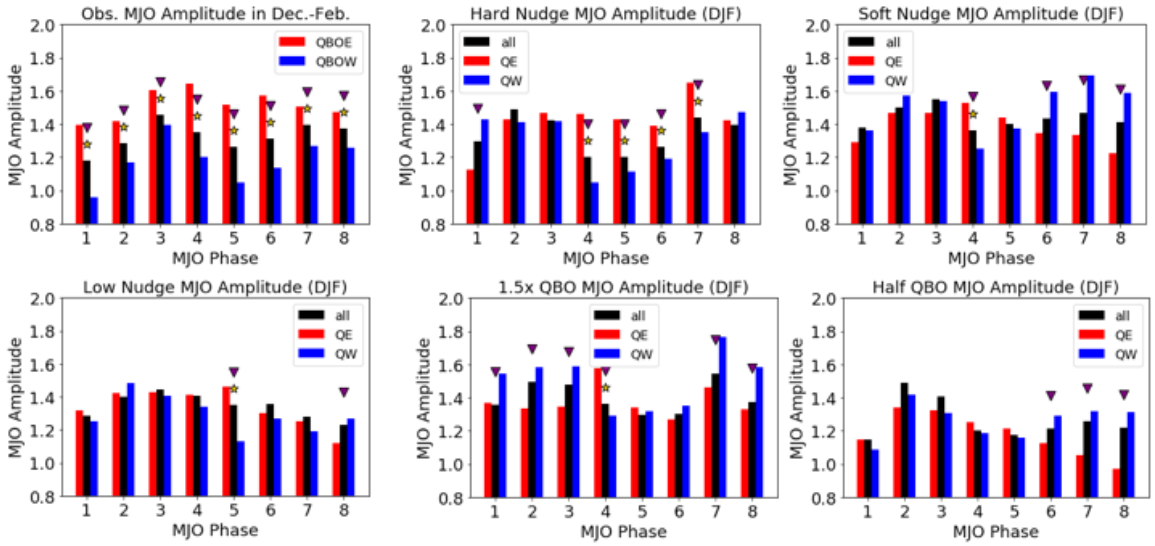

Figure 5.16: As in Figure 5.11 but for the sensitivity tests using zonal-mean nudging in the coupled model version. Clockwise from the top-left: observations; a shortened 30-minute nudging timescale; a lengthened 1-week nudging timescale; a lower (200-150 hPa) nudging transition region; a stronger 1.5×QBO; and a weaker 0.5×QBO.

that making the QBO artificially stronger via nudging does not lead to a strong MJO-QBO link, despite much stronger-than-observed temperature anomalies in the tropopause region. In all cases, the nudging is the zonal-mean implementation and the coupled version of the model is used. Figure 5.16 and Table 5.3 summarize the information from these sensitivity tests.

Altering the nudging timescale by extending it to 1 week or shortening it to 30 minutes does not lead to a stronger MJO-QBO link. While the shorter 30-minute nudging timescale does lead to a stronger MJO in QBOE relative to QBOW in phases 4-7 (see Fig. 5.16, top center) other MJO-QBO metrics from this run (Table 5.3) do not indicate a strong link in this version. The longer 1-week nudging timescale also shows no strong MJO-QBO connection. While the OLR activity (Table 5.3) increases by more than a 1-σ increase in QBOE relative to QBOW, other metrics do not show a strong MJO-QBO link. The amplitude analysis for example shows a stronger MJO in QBOW in several phases. Lowering the transition region of the nudging to 200-150 hPa has no clear impact on the MJO-QBO connection in viewed through any metric.

Data Source	**QBOE-QBOW MJO-OLR Std.**	**MJO-QBO Corr. (p-value)**
Observations	2.57	-0.45 (.004)
Shorter nudging timescale	0.11	-0.16 (.34)
Longer nudging timescale	1.13	0.15 (.39)
Lower nudging trans. region	0.32	-0.02 (.90)
1.5 × QBO	-0.45	0.15 (.37)
0.5 × QBO	-0.38	0.18 (.28)

Table 5.3: As in Table 5.2 but for the sensitivity experiments per Table 5.1 and Figure 5.16.

Note too that these changes to the nudging timescale or height have small effects on the representation of the QBO, per the top row of Figure 5.17. In this figure, which shows QBOE minus QBOW wind and temperature anomalies, all three of these nudging sensitivity tests look reasonably close to one another. Making the nudging timescale longer removes an odd kink around 100 hPa in the wind field, suggesting that the longer nudging timescale allows the model to smooth any discontinuities. However, the MJO-QBO link does not appear impacted, suggesting this feature does not influence our results.

Figure 5.17 does show that increasing or decreasing the QBO winds artificially leads to more striking differences in the wind and temperature differences. In particular, the 1.5×QBO run has much stronger QBO temperature anomalies in the lower stratosphere as well as in the upper troposphere, with cold anomalies reaching nearly twice the amplitude of their magnitude in the observations. Despite these much stronger temperature anomalies, no strong change is evident in the MJO. If anything the MJO looks stronger in QBOW in several of its phases in Figure 5.16, and the relationship viewed by other metrics (Table 5.3) is both too weak and of the opposite sign to what is observed.

The fact that making these striking changes to the stratospheric winds has only a marginal impact on the MJO makes it very unlikely that inability of this model to show an MJO-

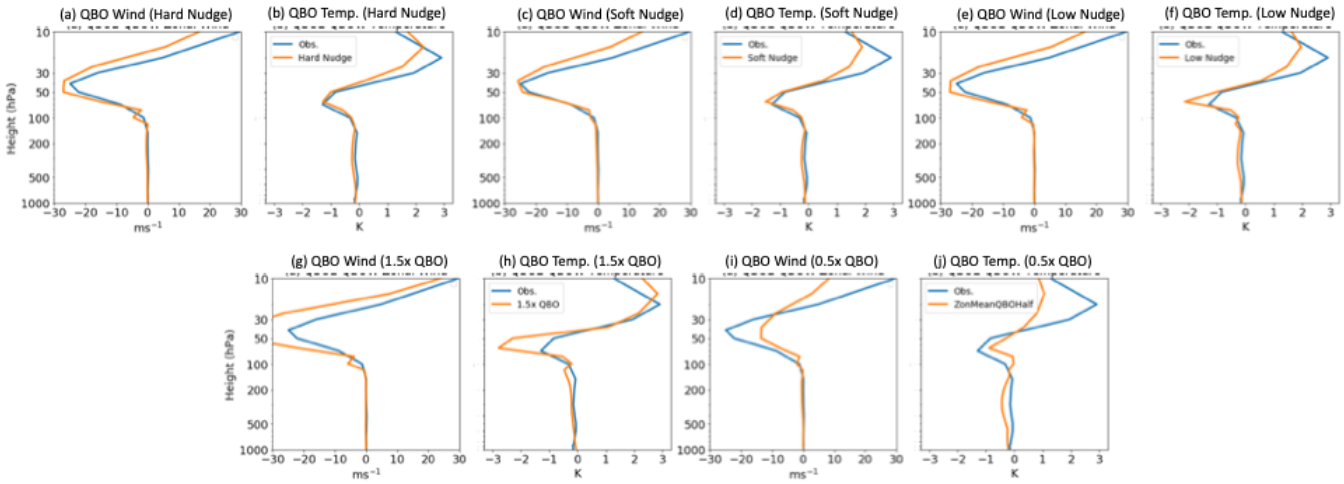

Figure 5.17: QBOE minus QBOW zonal-mean, 10°N/S averaged zonal wind and temperature anomalies for the sensitivity tests (orange) compared to observations (blue). Panels (a,c,e,g,i) show zonal wind differences for the 30-minute nudging timescale, 1-week nudging timescale, lower (150-200 hPa) nudging transition region, 1.5× QBO, and 0.5× QBO sensitivity experiments, respectively. Panels (b,d,f,h,j) show the temperature differences for those same tests.

QBO relationship is linked to something as subtle as the precise amplitude of tropopause layer temperature anomalies. Why then does the model not capture an MJO-QBO link? In general this question is difficult to conclusively answer, though next section discusses some possible deficiencies, some of which will be examined more rigorously in future work.

5.4 Discussion

Deficiencies capturing the MJO-QBO relationship can stem from four overlapping model issues: (1) biases in the QBO, (2) biases in the MJO, (3) biases in an unknown process(es) responsible for their coupling, or (4) the lack of an actual MJO-QBO connection in observations.

In this study, we have tried as much as possible to remove issues stemming from QBO biases by prescribing the QBO via nudging. Our results suggest, at least in this model, that biases of the QBO in models are not the exclusive reason why the MJO-QBO link is not represented. In particular, it does not appear to be the case that a model with correctly

captured QBO temperature anomalies in the tropopause region will have an MJO-QBO connection. We recognize there are still some issues with the nudged QBO – for example, the model is biased a little warm – which could in theory impact the result. Yet these biases seem fairly small. Other modeling studies similar to this work would be useful in confirming our results.

Biases in the MJO are more difficult to adjust for, as modeling of the MJO is still a challenge in many GCMs and it can be difficult to know which model parameters to tune in order to alter the MJO. In general, the coupled version of this model has a reasonably good MJO relative to other GCMs, which makes it a good candidate for ruling out MJO biases. The MJO amplitude in the coupled model is comparable to observations, as is the MJO seasonal cycle, two aspects of the oscillation which may be important for the MJO-QBO link (Hood (2017), Son et al. (2017), Hendon and Abhik (2018)). More subtle MJO properties, like its vertical structure will be diagnosed in future work. It may be that some feature which is key for the MJO-QBO connection is itself crucial for the model's MJO simulation. In that regard, work on the MJO-QBO relationship may in the future lead to improved MJO modeling or theory.

The model may also miss some other key feature which is vital to the MJO-QBO relationship. For example, the QBO is known to change high cirrus cloud amounts (Son et al. (2017)), which could be important to the MJO-QBO link and may missing in the model. The model high cloud changes due to the imposed QBO will be examined in future work. A myriad of other pathways which have been proposed for the MJO-QBO link, like QBO changes to wave propagation or QBO changes to the diurnal cycle over the Maritime Continent (Sun et al. (2019)), may be poorly simulated in the model. It is also possible that the MJO-QBO connection results from an upward impact of the MJO on the QBO, in which case nudging the stratosphere naturally will not assist with modeling the MJO-QBO link. This theory could be tested in a modeling framework, however additional evidence in favor of an upward effect of the MJO on the QBO in observations seems necessary before modelers

undertake a more detailed examination of this hypothesis.

Finally, the MJO-QBO link in observations may be less robust than it currently seems. Figure 5.12 shows that it is possible, in ∼30 years of model data, to observe what appears to be a strong MJO-QBO connection where there is no strong stratospheric mechanisms linking the MJO and QBO in the underlying model. Other processes in the climate system unrelated to the stratosphere could explain some or all of the observed QBO impact, for example longer inter-annual modes in the ocean like ENSO or the Pacific decadal oscillation. And the fact that other features of the climate system such as tropical cyclones and ENSO have shown QBO-related "relationships" which change on long timescales (Garfinkel and Hartmann (2007), Camargo and Sobel (2010)) challenges our concept of how strong the QBO impacts in the tropics is.

Still, the observed MJO-QBO link has passed stringent statistical tests, and is stronger in observations than any of the integrations, including ensemble members and sensitivity tests, that this model produces over an approximately four decade span (see also Kim et al. (2020a), who show this is further the case among the CMIP6 models). This suggests that the observed link *is* significant, and could not happen by chance. Because both the MJO and the QBO are still not straightforward to simulate in GCMs, it is not all that surprising that modeling the interaction between these two phenomena presents a stringent test which no GCM to date has passed.

5.5 Conclusion

In this study we examined the MJO-QBO relationship using several configurations of a global climate model. To date, no GCM has shown an MJO-QBO link like that observed, for reasons which are unknown. Here we consider two versions of the NASA GISS ModelE – one with 40 vertical levels (E2.1, Kelley et al. (2019) and one with 102 levels (E2.2; Rind et al. (2020)) – each of which is run in both a coupled ocean-atmosphere and a specified SST

("AMIP") configuration. The models are run for 37 years in the AMIP runs and 36 years in the coupled simulations.

In general, the model captures the MJO as well as or better than (in the case of the coupled, 40-level model) typical state-of-the art GCMs (Figs. 5.2, 5.4). The 40-level version shows a stronger MJO which propagates more realistically than the 102-level version due to changes in the convective scheme. All configurations capture approximately the correct MJO amplitude, and show a modulation of the MJO with the seasonal cycle (e.g. Fig. 5.15).

The model has an internally-generated QBO only in the 102-level setup (Fig. 5.3). This internal QBO resembles the observed QBO generally, but amongst other issues has a weaker-than-observed amplitude in the lower stratosphere/upper troposphere (Fig. 5.6). The 40-level version as it is typically run has no QBO (Fig. 5.1).

We examined the MJO-QBO relationship using several metrics, including the change in MJO amplitude in different QBO phases, the change in MJO-filtered OLR activity in different QBO phases, and the correlation of MJO and QBO indices. We focused our analysis in this work on boreal winter and on QBO defined at 50 hPa, but confirmed that our results generalize to other seasons and other QBO levels. Our main results can be summarized as follows:

1. The 102-level model version with the internally-generated QBO does not have a strong MJO-QBO link, consistent with other published work (Lee and Klingaman (2018), Richter et al. (2020)). Also consistent with those studies, our model displays QBO temperature biases around the tropopause that may be important in explaining the lack of an MJO-QBO connection (Figs. 5.5, 5.6).

2. Nudging the stratospheric zonal and meridional winds in the 40-level version of the model towards MERRA2 reanalysis allows the model to simulate the QBO with relatively little bias (Fig. 5.7). While no nudging was applied to the model temperature, the thermal wind constraint leads to realistic simulation of QBO temperature anomalies (Fig. 5.8). We implemented the nudging in two ways – once nudging the full

latitude/longitude structure of model stratospheric winds to reanalysis, and a second requiring only that the model zonal-mean winds match the observed zonal mean.

3. Even with nudging, no strong MJO-QBO link is evident in the AMIP versions of the model, or the coupled version with grid point nudging (Fig. 5.10, Tab. 5.2). The coupled model with zonal-mean nudging showed a weak and insignificant MJO-QBO link in a 36-year simulation that initially appeared promising, but additional ensemble simulations formed by changing the initial condition of the ocean model showed that in fact no strong MJO-QBO link is present (Figs. 5.13, 5.14).

4. Artificially increasing or decreasing the strength of the QBO, including multiplying the winds by a factor of 1.5 (which leads to much stronger-than-observed temperature anomalies), does not have an impact on the model MJO-QBO link, nor are our results sensitive to the nudging timescale or level above which we nudge (Fig. 5.16, Tab. 5.3).

This suggests that model biases to the QBO, and in particular to QBO temperature anomalies in the lower stratosphere, are not in and of themselves responsible for the lack of an MJO-QBO link in this model. Even when QBO biases are minimized through relatively strict nudging, the model fails to show a strong connection in many different configurations.

Several reasons why the model might fail to show a link were discussed. It seems most likely that the lack of an MJO-QBO link is due to biases simulating some presently unknown mechanism important for the MJO-QBO link, and in that regard more observational, theoretical, or modeling work on the MJO-QBO connection are needed. We also discussed potential issues with the robustness of the observed relationship, but at present the observed link is stronger than what is possible in the model due to chance, suggesting that the MJO-QBO link is in fact real (similar to Kim et al. (2020a)).

In future work finalizing this chapter for publication, additional diagnostics of why the model might fail to show an MJO-QBO connection will be examined and larger ensemble (11-members) of the coupled-zonal mean configuration will be examined. Further into the

future, we may coordinate nudging experiments across models to confirm these results, which could lend additional insights to support or refute the findings in this study.

* * *

This concludes our final chapter on our modeling work examining the MJO-QBO connection. The next chapter, work using observations, was nevertheless inspired by the modeling work we had conducted, in particular our findings presented in Chapter 3. There we showed that in the model, temperature anomalies around the tropopause associated with the QBO were increased relative to the model forcing (see Fig. 3.6). As stronger QBO temperatures in models (see results of Chapters 3 and 4) appear possibly linked to stronger MJO-QBO connections, we wondered whether, in observations, QBO temperature anomalies showed any strengthening during the periods when the MJO-QBO link was stronger (e.g. December-February). This motivated our work in the next chapter on variability of QBO temperature anomalies.

Chapter 6

Variability in QBO Temperature Anomalies on Annual and Interannual Timescales

Note: This chapter has been submitted for publication in the *Journal of Climate* as "Variability in QBO Temperature Anomalies on Annual and Decadal Timescales".[1]

6.1 Introduction

The tropical tropopause layer (TTL; Fueglistaler et al. (2009)) delineates the boundary between the troposphere and stratosphere. The TTL is crucial for setting the water budget of the stratosphere, has implications for ozone chemistry and tracer movement, and exhibits strong signatures of anthropogenic warming (Fueglistaler et al. (2009); Lin et al. (2017)).

[1]AUTHORS: Zane Martin[a]*, Adam Sobel[a,b] Shuguang Wang[a],

[a] Department of Applied Physics and Applied Mathematics, Columbia University, New York, NY
[b] Lamont-Doherty Earth Observatory, Columbia University, Palisades, NY

* corresponding author: Zane Martin, zkm2102@columbia.edu

Existing literature has further established that a number of modes of tropical variability in both the troposphere and stratosphere can influence TTL temperatures, including the Madden-Julian oscillation (MJO; Madden and Julian (1971); Madden and Julian (1972); Madden and Julian (1994); Zhang (2005); Son and Lee (2007); Virts and Wallace (2014)), the annual cycle (Gettelman et al. (2002); Jucker and Gerber (2017)), the stratospheric quasi-biennial oscillation (QBO; Baldwin et al. (2001); Huesmann and Hitchman (2001)), and the El Niño-Southern Oscillation (ENSO; Domeisen et al. (2019)).

The study of TTL temperatures has recently been reinvigorated by the discovery of a strong relationship between the QBO and the MJO (Yoo and Son (2016); Son et al. (2017); Nishimoto and Yoden (2017)). The QBO phase accounts for roughly 50% of the interannual variation in MJO strength during boreal winter – more than ENSO or any other mode of interannual variability – with a stronger MJO when the QBO winds (at 50 hPa) are easterly and the TTL is anomalously cold (Son et al. (2017)). In addition to modulating the strength of the MJO, the QBO also increases the amplitude and predictability of MJO teleconnections (Mundhenk et al. (2018); Mayer and Barnes (2019); Kim et al. (2020b), Toms et al. (2020)), and may enhance MJO predictability (Marshall et al. (2017); Lim et al. (2019); Wang et al. (2019a); Kim et al. (2019)). While a clear mechanism linking the MJO and QBO has not been established, an increasing body of work suggests that TTL temperature anomalies may be the primary cause (Nie and Sobel (2015); Yoo and Son (2016); Son et al. (2017); Hendon and Abhik (2018); Klotzbach et al. (2019); Martin et al. (2019)).

The most likely explanation for the observed and simulated relationships between TTL temperature and MJO amplitude is that colder TTL temperatures, such as those experienced in QBOE, allow convection to penetrate deeper into the troposphere more vigorously, whereas warmer TTL temperatures in QBOW have the opposite effect. As convection associated with the MJO is generally deep and vertically coherent, it is able to reach the level of QBO influence and is modulated accordingly (Hendon and Abhik (2018)), though the precise details of this destabilization have not been fully articulated and are difficult to capture in

global climate models (GCMs; Lee and Klingaman (2018); Kim et al. (2020a)). It is also not obvious why TTL temperature anomalies associated with the QBO should affect the MJO uniquely compared to other modes of tropical variability, as observations show to be the case (Abhik et al. (2019)). Abhik et al. (2019) suggested that the unique vertical structure of the MJO and its interaction with QBO temperature anomalies may explain the link, but more work is needed on how other equatorial waves may be impacted.

In an idealized cloud-resolving model, Martin et al. (2019) showed that anomalous temperatures in the upper troposphere and stratosphere could lead to modulations of MJO convection qualitatively consistent with observations. However, they found it necessary to impose temperature anomalies larger and lower than those observed in order to detect clear changes to MJO convection. The MJO convective response to QBO-like temperature anomalies was sensitive to the structure of these temperature anomalies around the TTL, and larger amplitude temperature anomalies were linked to stronger MJO responses. Additionally, studies using free-running GCMs or global forecast models have noted that model deficiencies in accurately capturing QBO temperature anomalies in the TTL may contribute to the lack of a strong direct impact of the QBO on the model MJO (Lee and Klingaman (2018); Martin et al. (2020); Kim et al. (2020a)).

Whether the TTL temperature mechanism is key for the MJO-QBO connection is still unsettled. However, if this mechanism is operative there are two key features of the MJO-QBO link it ought to explain: the seasonality and the long-term trend. On annual timescales, the MJO-QBO link is only statistically significant in boreal winter (December-February; Yoo and Son (2016)). On longer timescales, Klotzbach et al. (2019) showed that the MJO-QBO relationship has changed over the course of the 20th century, with the lack of a connection prior to the 1980s and emergence of a link only in recent decades. Inspired by those studies, here we examine TTL temperature signals associated with the QBO on both annual and decadal timescales.

This study is organized as follows: Section 6.2 describes reanalysis and observational

data we use to characterize TTL temperatures and the indices used to track various climate processes. Section 6.3 presents our results: the first sub-section examines TTL temperature signals generally, the second examines how QBO temperature anomalies change with the annual cycle, and the third considers QBO temperatures on decadal timescales. In Section 6.4 we discuss the implications of our work and offer direction for future research, and Section 6.5 summarizes and concludes this study.

6.2 Data and Indices

6.2.1 Data

This study makes use of seven reanalysis products, radiosonde observations from one site, and one radio occultation dataset. The consistency of our results across datasets is an indicator of the robustness of our findings. The data span roughly the period from January 1 1979 to December 31 2018, or as close to that period as possible given each product's availability. Additionally, one reanalysis product (JRA55, defined below) is examined starting from January 1 1958.

Recent initiatives using most of the reanalysis datasets we consider, including especially the SPARC Reanalysis Intercomparison Project (S-RIP; Fujiwara et al. (2017)), have examined the commonalities and differences across reanalysis products in particular in the stratosphere and upper-troposphere. Findings have shown in particular that more modern reanalysis products provide a good representation of TTL temperatures compared to observations (Tegtmeier et al. (2020)), which further helps lend credence to our findings and justifies our use of reanalysis as a stand-in for observations.

The reanalysis products we consider are the NCEP/NCAR Reanalysis 1 (R1; Kalnay et al. (1996); Kistler et al. (2001)), ERA-Interim reanalysis (Dee et al. (2011)), ERA-5 reanalysis (Hersbach et al. (2019)), NASA's Modern-Era Retrospective Analysis for Research and Applications (MERRA) reanalysis, including MERRA1 (Rienecker et al. (2011)) and

MERRA2 (Gelaro et al. (2017)), and the Japanese 55-year Reanalysis Project (JRA55; Kobayashi et al. (2015)). In addition to JRA55, we also utilize "JRA55C" (Kobayashi et al. (2014)) through 2012 (due to availability), which is a unique reanalysis product that is identical to JRA55 except that it excludes satellite data in its data assimilation. This allows one to examine whether particular features in the standard JRA55 reanalysis are attributable to changes in observing platforms. We retrieve monthly-mean data for all these datasets. We additionally retrieve daily data from MERRA2 and ERA5 to better examine MJO variability in Section 6.4.

In addition to reanalysis, we also use monthly and daily data from the Singapore sounding station, located at approximately 104°E and 1°N. Singapore was chosen because it has been a hallmark of QBO studies and has a long record of available data. Sounding data was retrieved through the Integrated Global Radiosonde Archive, version 2 (Durre et al. (2006); Durre and Yin (2008)).

Finally, we use the NASA Atmospheric Infrared Sounders and Advanced Microwave Sounding Unit (AIRS and AMSU; herein "AIRS" for ease of reference) dataset (Aumann et al. (2003)), available from September 2002 onward. Because this data has a shorter record, it is less suitable for considering interannual variability and is primarily used in Section 6.3.2.2. Again monthly mean data is utilized from the AIRS dataset. More details regarding the horizontal, vertical, and temporal resolution of the data we consider can be found in Table 6.1.

6.2.2 MJO, QBO, and ENSO Indices

We track the MJO using the daily Realtime Multivariate MJO index (RMM; Wheeler and Hendon (2004)). RMM is a standard MJO index formed using a pair of EOFs of OLR and zonal wind at 850 and 200 hPa averaged over the tropics to form two principal component time series, often called RMM1 and RMM2. Together these two components track the strength and location of the MJO: their phase angle represents the MJO's location, and the

Product Name	Product Type	Spatial Resolution	Temporal Resolution
NCEP-NCAR	Reanalysis	2.5°x2.5° — 17 levels: 1000, 925, 850, 700, 600, 500, 400, 300, 250, 200, 150, 100, 70, 50, 30, 20, 10	Monthly Jan. 1979 - Dec. 2018
ERA-Interim	Reanalysis	2.5°x2.5° — 37 levels: 1000 to 750 by 25hPa, 750 to 250 by 50 hPa, 200 to 100 by 25 hPa, 100, 70, 50, 30, 20, 10 7, 5, 3, 2, 1 hPa	Monthly Jan. 1979 - Dec. 2018
ERA5	Reanalysis	1°x1° — 22 levels: 1000 to 800 by 50 hPa, 800 to 300 by 100 hPa, 250 to 100 by 25 hPa 70, 50, 30, 20, 10 hPa	Monthly and daily Jan. 1979 - Dec. 2018
MERRA	Reanalysis	1°x1° — 31 levels: 1000 to 700 by 25 hPa, 700 to 100 by 50 hPa, 70, 50, 40, 30, 20, 10 hPa	Monthly Jan. 1979 - Feb. 2016
MERRA2	Reanalysis	1°x1° — 19 levels: 1000 to 800 by 50 hPa 800 to 200 by 100 hPa 150, 100, 70, 50, 40, 30, 20, 10 hPa	Monthly and daily Jan. 1980 – Dec. 2018
JRA55	Reanalysis	2.5°x2.5° — 18 levels 1000 to 800 by 50 hPa 800 to 200 by 100 hPa 150, 100, 70, 50, 30, 20, 10 hPa	Monthly Jan 1958 – Dec. 2019
JRA55C	Reanalysis	2.5°x2.5° — 18 levels 1000 to 800 by 50 hPa 800 to 200 by 100 hPa 150, 100, 70, 50, 30, 20, 10 hPa	Monthly Jan 1958 – Dec. 2012
Singapore	Sounding	N/A — 17 levels: Sfc., 1000, 925, 850, 700, 500, 400, 300, 250, 200, 150, 100, 70, 50, 30, 20, 10 hPa	Monthly and daily Jan. 1979 – Dec. 2018
AIRS	Occ.	1°x1° — 18 levels: 1000, 925, 850, 700 to 300 by 100 hPa, 250 to 100 by 50 hPa, 70, 50, 30, 20, 15, 10 hPa	Monthly and daily Sept. 2002 – Dec. 2018

Table 6.1: List of data products used in this study, as discussed in Section 6.2.1. Spatial resolution is given horizontally, followed by the vertical levels retrieved (in hPa). Not all available vertical levels were retrieved for all products, but the highest available resolution was selected in the TTL.

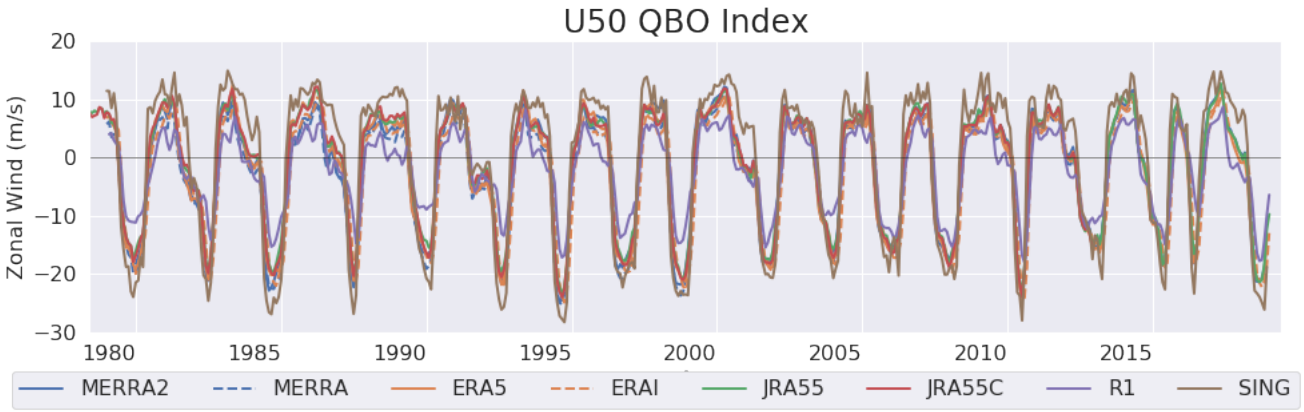

Figure 6.1: The monthly U50 QBO index (zonal-mean zonal wind at 50 hPa averaged 10°N to 10°S) for all datasets. For Singapore, no averaging is possible so monthly values at 50 hPa are used. The period shown (1979-2019) corresponds to the period over which most datasets overlap, though JRA55 and JRA55C extend back to 1958.

amplitude (measured as $\sqrt{RMM1^2 + RMM2^2}$) represents the MJO's strength. We use the RMM index available from the Australian Bureau of Meteorology. We do not recalculate RMM for various reanalysis products. We define strong and weak MJO months as periods when monthly-mean RMM amplitude is, respectively, greater than or less than a half standard deviation.

For ENSO we use the Hadley Centre Niño3.4 index, formed from by monthly averaging SST anomalies at 5°N-S and 170-120°W. El Niño and La Niña events are defined when the index value is, respectively, less than or greater than a standard deviation. To track the QBO in each dataset, we use the monthly-mean 50 hPa zonal-mean zonal wind, averaged from 10°N/S (U50) if available in that dataset. As in previous studies (Yoo and Son (2016); Son et al. (2017)) we define westerly and easterly QBO phases as months when the index exceeds ±0.5 standard deviations, respectively. For the AIRS dataset, which does not include wind, we use MERRA2's U50 to define QBO phases. For the Singapore sounding data, we use the value of the Singapore zonal wind at 50 hPa.

Figure 6.1 shows the QBO index from all datasets and indicates very good agreement representing the QBO, in particular among the reanalysis datasets. The correlation between

each reanalysis datasets and ERA5 is over 0.99. This is not surprising given that the QBO in this region of the atmosphere is the main source of variability, as well as the regularity of the QBO. The correlation between JRA55 and JRA55C is approximately 0.998, suggesting that changes in observing systems do not have a large impact on monthly 50 hPa winds. The Singapore U50 index (brown line in Figure 6.1) is noisier than the reanalyses, and has higher minimum and maximum value during some QBO peaks (though it still has a high correlation – $\sim$0.97 – with ERA5 and other reanalyses). This is likely due to the tropical averaging in the reanalysis calculations that smooths variability associated with a single point, and includes points farther from the equator where QBO signals are weaker. The R1 reanalysis is also an outlier in that it tends to underestimate the strength of the QBO in the easterly phase, where it displays values typically 5-10 m/s weaker than other datasets. Overall however, the period and timing of QBO transitions looks similar in all datasets.

6.3 Results

6.3.1 TTL Variability Across Timescales

The QBO, the annual cycle, ENSO, and the MJO all contribute to variability in TTL temperatures, as seen in Figure 6.2. We take the difference in TTL temperatures by compositing onto different phases of the four modes of variability we consider: for the annual cycle we consider winter minus summer; for ENSO we take El Niño minus La Niña; for the QBO we take QBOE minus QBOW; and for the MJO we subtract strong and weak MJO months (measured using the monthly mean RMM amplitude). The top two rows show, respectively, the zonal-mean difference and the zonal anomalies averaged from 10°N/S relative to the zonal-mean difference from MERRA2. The bottom row shows the tropical (i.e. zonal and 10N/S mean) differences for all datasets.

It is clear from Figure 6.2 that the annual cycle, ENSO, QBO, and MJO can all influence TTL temperatures. For example, it is evident that the TTL is colder in northern winter

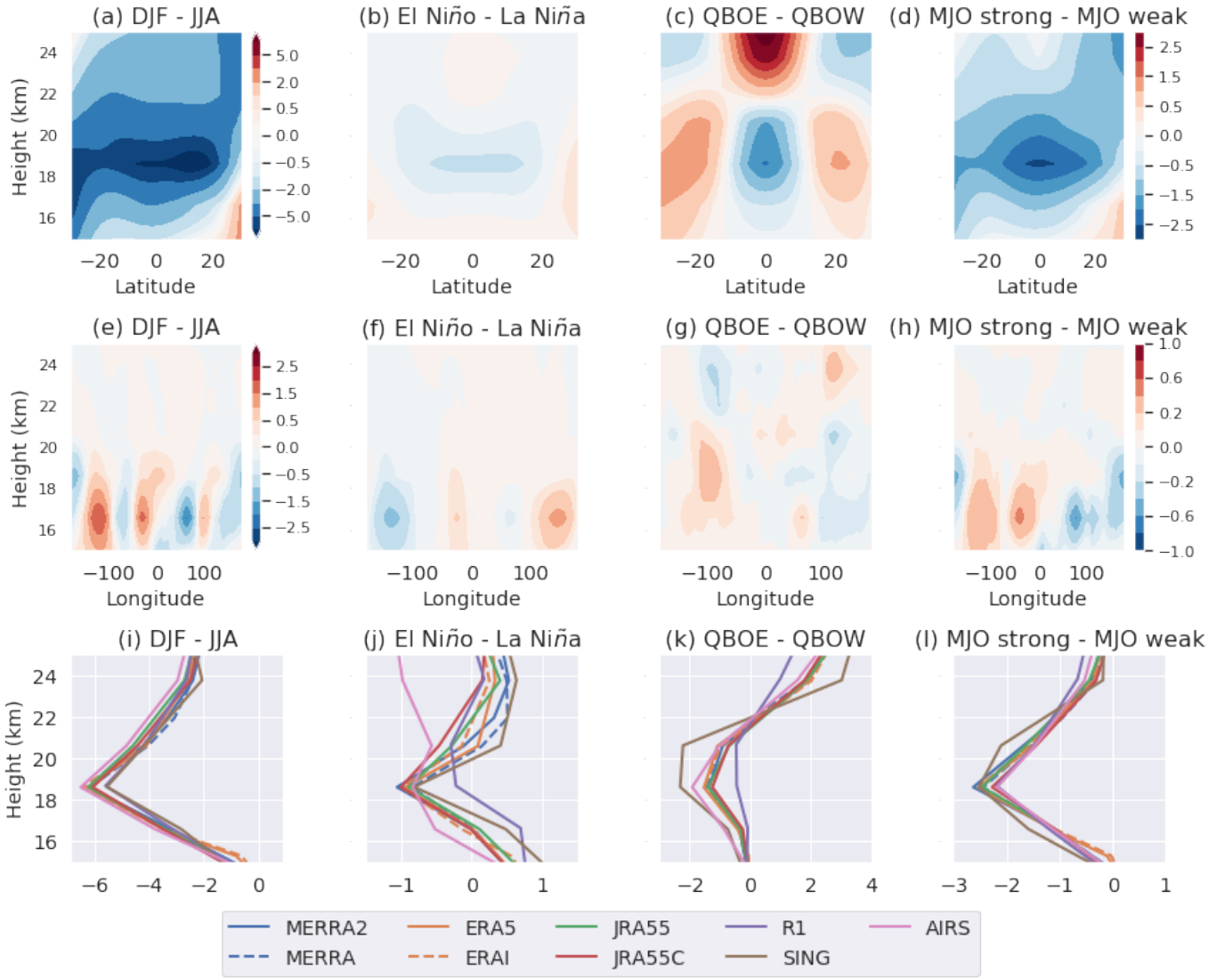

Figure 6.2: (a-d) MERRA2 zonal-mean temperature differences between (left to right) December-February and June-August periods; El Niño and La Niña periods; QBOE and QBOW periods; and strong and weak MJO periods as defined in Section 6.2.1. (e-h) MERRA2 anomalies for the same modes of variability as in the top row, but for the 10°N/S averaged zonal anomaly relative to the zonal mean. (i-l) The tropical mean (zonally and 10°N/S averaged) differences for the above modes, with various lines showing all datasets as defined in the legend and Table 6.1.

than in northern summer, as is well known (e.g. Fueglistaler et al. (2009) and older citations therein), though still not entirely well understood (Randel and Jensen (2013); Jucker and Gerber (2017)). The TTL is also colder during QBOE than QBOW, consistent with thermal wind balance given the differences in zonal wind which define QBOE and QBOW, and assuming constant meridional structure. For both the annual cycle and QBO, the zonal mean signal is fairly large, while zonal asymmetries are small.

In the case of ENSO, the zonal mean indicates relatively weak TTL cold anomalies in El Niño relative to La Niña, but a more nuanced look indicates that this small zonal-mean signature is the cancellation of two larger terms: there are larger cold anomalies centered over the east Pacific and warm anomalies approximately over the west Pacific (noted for example in Domeisen et al. (2019)).

The MJO signal in Figure 6.2d is quite strong, but some of this is an artifact of aliasing. The MJO is known to be strongest in boreal winter (Zhang (2005)) and is stronger in QBOE relative to QBOW. Thus, much of the cold anomaly in the TTL region in Figure 6.2d is due to sampling bias: strong MJO months correspond to TTL states taken in winter and during, whereas weak MJO months are typically summertime states occurring in QBOW. We confirmed this by differencing strong and weak MJO months, as in Figure 6.2, but controlling for both the season and QBO phase (not shown). This reduces these TTL anomalies substantially – anomalies at upper levels on the equator around 18 km are found to be less than 1 K.

Figure 6.2i-l show similar plots to the top two rows, but averaged over the whole tropics and taken from all the datasets. The results are comparable to the top panels in terms of the structure and magnitude of the temperature anomalies, though some diversity among datasets is seen. In the annual cycle, the Singapore and R1 products have a smaller annual magnitude than other sources. In the sounding data this is in part due to the lack of meridional and zonal averaging, which we confirmed by resampling the MERRA2 data at approximately the same point as Singapore (i.e. taking reanalysis values only at $\sim$104°E

and 1°N). This increases the similarity between these two datasets (not shown), though the reanalysis difference in the annual mean is still somewhat larger than the sounding data by approximately 0.5 K.

The weak R1 reanalysis signal is consistent with its behavior in general: it displays a weaker ENSO signal that peaks at higher levels than other datasets, as well as an almost non-existent QBO temperature change. Other studies have noted deficiencies this dataset's representation in particular of QBO temperature signals (Tegtmeier et al. (2020)) and have attributed issues to the low vertical resolution and the use of poorly-resolved satellite temperature retrievals (Fujiwara et al. (2017); Tegtmeier et al. (2020)).

Other reanalysis datasets agree well with regards to ENSO and QBO anomalies. The QBO anomalies are stronger in the Singapore soundings than the reanalyses, which is consistent again with the lack of zonal and meridional averaging and with the stronger wind anomalies noted in Figure 6.1. As previously, this was confirmed by resampling MERRA2 data from near the Singapore location, which leads to very similar QBO and ENSO anomalies between the reanalysis and sounding data. For AIRS, there is some ENSO difference, but this is in part due to the much shorter sampling period, which includes fewer events. For the MJO events, the datasets generally agree quite well, though the same aliasing issues that are noted for the upper panel still holds.

Having established that in general the four climate phenomena discussed above can impact the TTL, next we examine the variability in QBO temperature anomalies across the intra-seasonal to interannual timescales on which these various processes operate.

6.3.2 QBO Temperature Anomalies

6.3.2.1 QBO Boreal Winter Temperature Anomalies

Here we consider whether QBO temperature anomalies are stronger in boreal winter than other seasons, and how the annual cycle and the QBO interact. Figure 6.3 shows zonal-

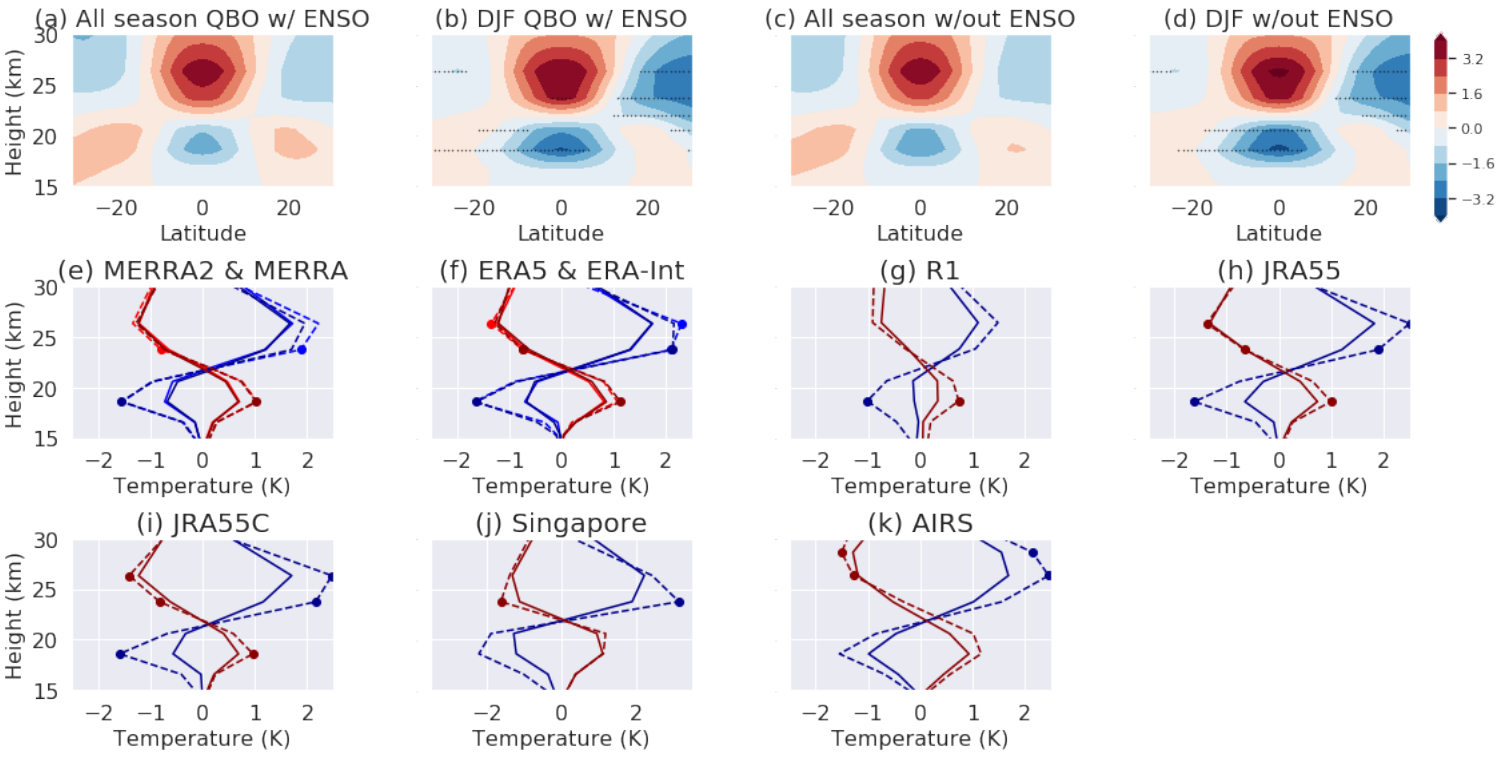

Figure 6.3: (top row) MERRA2 QBOE minus QBOW zonal-mean anomalies for (a) all months; (b) only DJF periods; (c) all months excluding strong ENSO periods; and (d) DJFs excluding strong ENSO periods. (bottom two rows) The QBOE (blue) and QBOW anomalies (red) in each dataset for all seasons (solid) and DJF only (dashed). Periods where the DJF difference is significant via a bootstrap (see Section 6.3.2.1) are labeled with stippling in panels (b,d) or a dot in (e-k). In panels (e) and (f) the lighter curves are the older reanalysis products, listed second in the title.

mean QBO anomalies in boreal winter versus those taken irrespective of season. The top row is similar to Figure 6.2c (Fig. 6.3a is identical), and shows the QBOE minus QBOW temperatures composited independent of season (Fig. 6.3a,c) and those in DJF (Fig 6.3b,d). We form these plots with and without strong ENSO months. MERRA2 data is used for the top row, whereas the bottom rows show the tropical mean over all the datasets.

It is evident from Figure 6.3 that TTL QBO temperature anomalies on the equator are stronger in boreal winter than other seasons. Whereas the QBOE minus QBOW difference in MERRA2 has a peak at around -1.5 K in all seasons, in boreal winter this maximum difference is -2.5 K. This influence is not due to ENSO: panels (c) and (d) show the same signals as (a) and (b), respectively, despite having active El Niño or La Niña months removed.

The average QBOE and QBOW temperature anomalies from 10°N to 10°S are shown in the bottom panels across all datasets. Here we plot the QBOE (blue) and QBOW (red) anomalies individually rather than the QBOE minus QBOW difference. The all-season the anomaly (solid curve) is calculated relative to the all-season climatology whereas the DJF anomaly (dashed) is relative to the DJF climatology to account for the mean state changes (e.g. Figure 6.1a).

Figure 6.3e-k demonstrates that all datasets show larger equatorial QBO temperature anomalies in boreal winter compared to the all-season mean, though the change is not significant across all datasets. We use a bootstrapping method to test significance. For each dataset, we let N_{QE} and N_{QW} be the number of months in DJF where the QBO is easterly and westerly, respectively. From the list of all QBOE months (independent of season) we select N_{QE} at random without replacement, and from all the QBOW months we select N_{QW}; we then difference the two sets and repeat this process 1000 times to build up a distribution. At each height (and also at each latitude in Fig. 6.3b,d), points where the DJF QBOE-QBOW difference is significant at the 95% level are marked with stippling (Fig. 6.3b,d) or with a dot on both the curves (Fig. 6.3e-k).

Differences in reanalyses are largest in the tropopause region, though higher in the strato-

sphere also shows significant differences. All reanalysis datasets show significantly stronger QBO anomalies from 10°N-10°S in both in the TTL around 18 km as well as at upper levels around 24 km. While QBO anomalies in DJF are stronger in the AIRS and Singapore data than the all-season values, the differences are not significant. In the AIRS data this seems likely due to the shorter period of the record – resampling the reanalysis and Singapore datasets over the more limited AIRS period yields no significance in these datasets (not shown). For Singapore, it appears that ENSO plays more of a role due to the physical location of the Singapore sounding site near a region where ENSO TTL anomalies are stronger. Removing ENSO periods from the Singapore record leads to slightly stronger and statistically significant DJF anomalies in Figure 6.3 (not shown).

Both the QBOE and QBOW anomalies are stronger in DJF, in the sense that the cold QBOE anomalies are colder and the warm anomalies are warmer than the all-season values. This suggests that whatever process acts to enhance the QBO in DJF represents a true increase in the QBO amplitude rather than being in part associated with a change in the mean. Also, while the all-season QBO anomalies are fairly symmetric, the DJF anomaly seems stronger in QBOE than in QBOW, suggesting that whatever acts to increase TTL variability associated with the QBO in DJF acts more strongly during the easterly phase than during the westerly phase.

While the equatorial QBO anomalies are stronger in DJF relative to other seasons, the off-equatorial QBO anomalies are, in contrast, weaker in DJF than other seasons, as shown in Figure 6.3a-d. In the all-season plots, warm anomalies of around 1 K are located around 20°N/S, whereas these anomalies are essentially zero in boreal winter. This feature is also found in the other datasets, as shown in Figure 6.4. Plotted there are zonal-mean QBOE and QBOW temperature anomalies, as in Figure 6.3e-k, but now as functions of latitude, taken at a fixed height of 70 hPa ($\sim$ 18.5 km). Dashed lines again show the DJF values, whereas solid lines show the all-season values. The on-equator strengthening is again evident, and is significant across all the reanalysis products (significance is measured using the same

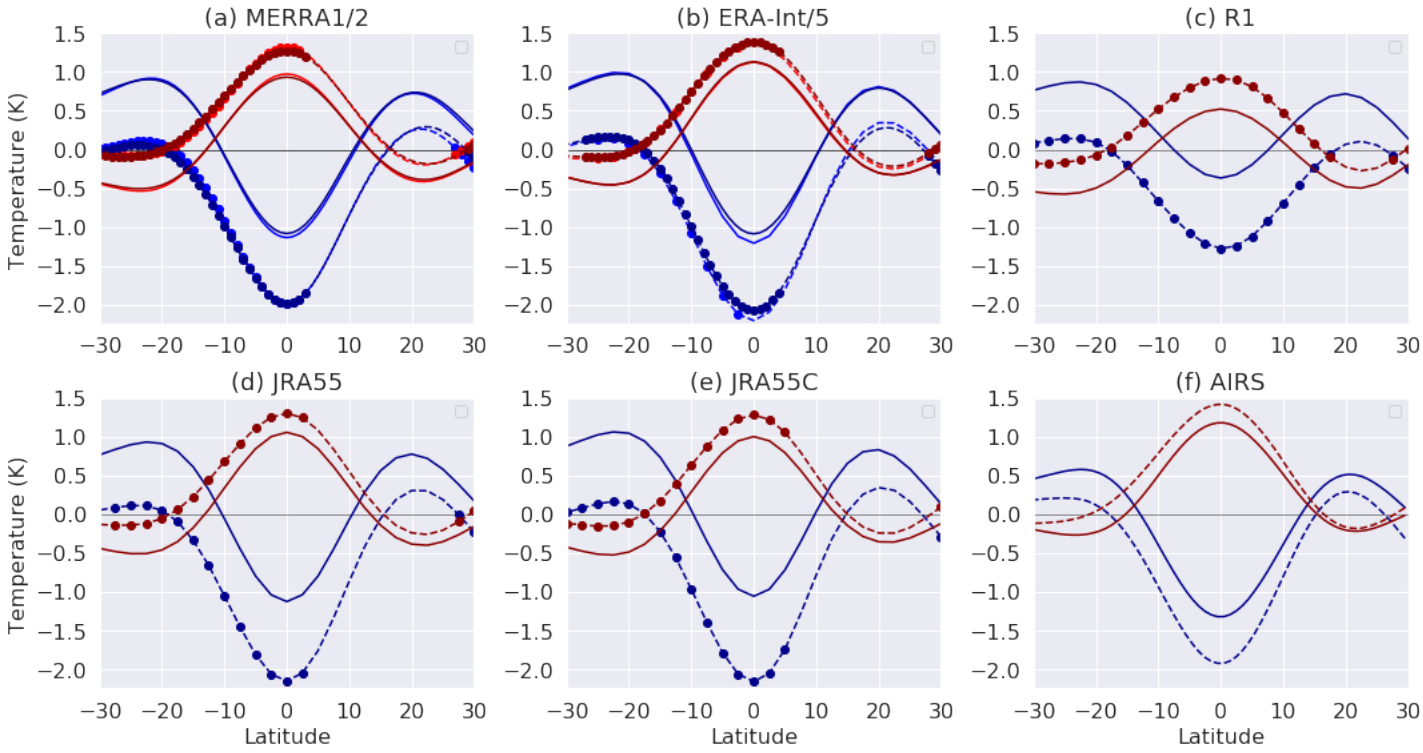

Figure 6.4: Zonal-mean QBOE and QBOW temperature anomalies at 70 hPa (18.5 km), as a function of latitude (x-axis). As in Figure 3, QBOE anomalies are in blue and QBOW anomalies are red – dashed lines are DJF and solid lines are all-seasons. Lighter curves in panels (a) and (b) are earlier reanalysis products. Points where the QBOE minus QBOW difference is significantly stronger or weaker in DJF relative to the all-seasons mean using the same bootstrap method as in Figure 3 are marked with a dot on both DJF curves.

bootstrap method as previously), but also evident are weaker off-equatorial anomalies in all the datasets. They are statistically significant in the southern hemisphere in all products, and while not significantly different are still weaker in the northern subtropical regions. The AIRS data show the same behavior, but as before the difference is not significant, perhaps because of the shorter sampling period.

The off-equatorial warm QBO anomalies have been attributed to a QBO meridional circulation (Baldwin et al. (2001)). The equatorial cold anomaly in the TTL during QBOE is driven by adiabatic ascent whereas at upper levels the warm anomaly is driven by descent. These vertical motions form the equatorial branch of a pair of meridional overturning cells with descent in the subtropics, and that descent causes the warm anomalies in QBOE. The same argument, but with opposite signs, holds in QBOW. It is not clear why these off-equatorial anomalies should weaken despite the stronger on-equator variability, though it is clear from Figure 6.4 that the overall meridional structure of the temperature fields between the DJF and all-season QBO anomalies are similar – the curves are merely shifted colder throughout the tropics and subtropics in QBOE and shifted warmer in QBOW.

The absence of a QBOE-QBOW difference in the meridional temperature structure in DJF is consistent, through thermal wind balance, with a similarly small change in the zonal wind field. Figure 6.5 is the same as Figure 6.3, but showing zonal wind anomalies, and indeed we see no change in the peak of the zonal wind anomalies between different seasons. There is a change in some datasets to the vertical shear of the wind at levels above around 23 km, which may account for small changes in the temperature structure, but overall signals are not as apparent in the wind as they are in temperature.

We also examined the zonal structure of QBO temperature anomalies. Figure 6.6 shows the 100 hPa and 70 hPa ($\sim$16.5 km and $\sim$18.5 km, respectively) QBOE minus QBOW differences from MERRA2 as functions of both longitude and latitude for all seasons compared to only boreal winter. Significant differences in DJF, using the same bootstrapping method as above, are stippled.

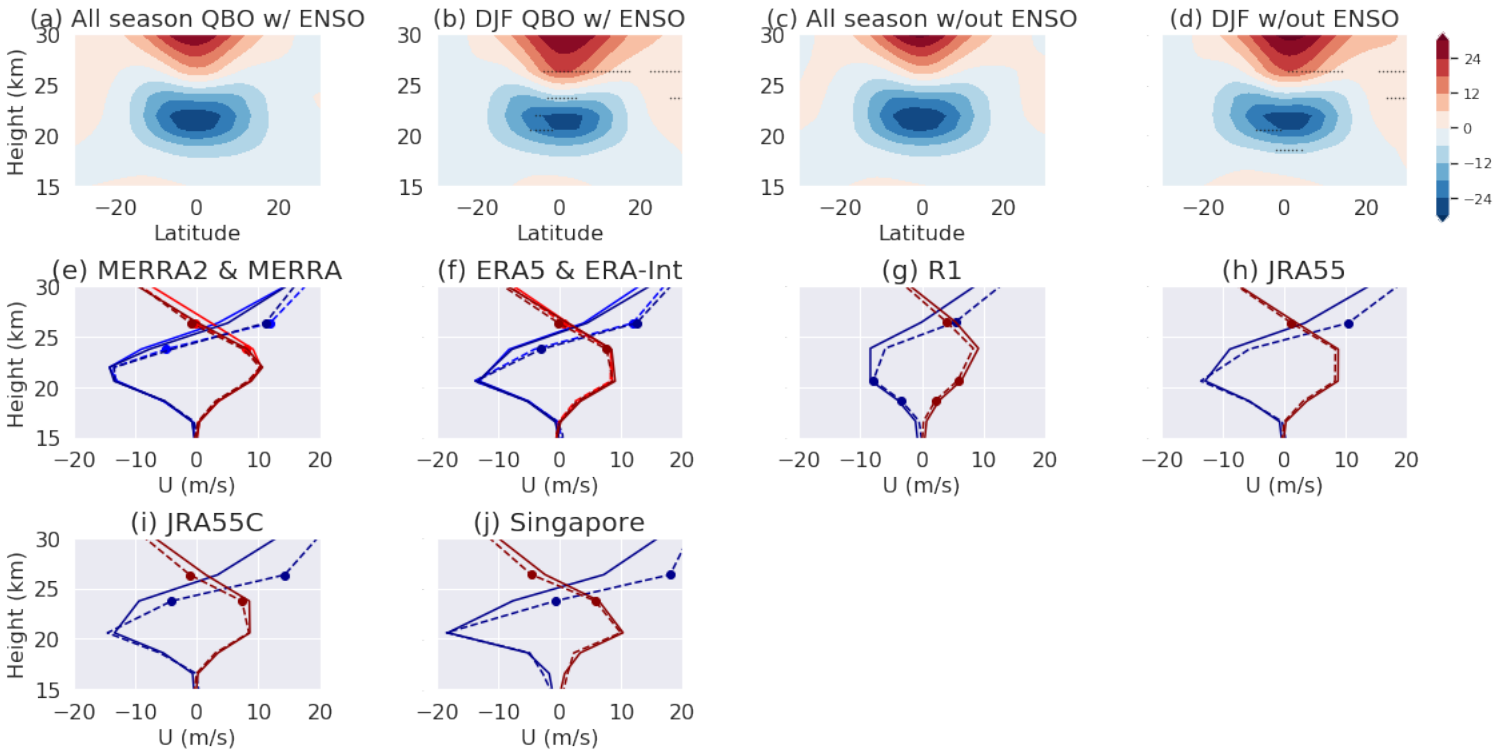

Figure 6.5: As in Figure 6.3 but for QBO zonal wind anomalies.

The overall strengthening of equatorial QBO anomalies in DJF relative to the all-season behavior is evident, as is the weakening in the off-equatorial warm anomalies, especially at 70 hPa. Interestingly, this plot also reveals differences in zonal structure. At 100 hPa, the DJF enhancement is more pronounced around the Maritime Continent, equatorial Africa, and the East Pacific (though not significantly so). At 70 hPa, the same pattern is somewhat evident, but the maximum region of DJF increase in temperature is over the West Pacific to the east of the Maritime Continent, where changes are strong and significant. Also evident at 70 hPa is significant weakening of anomalies in the southern hemisphere subtropics, particularly around the Indian Ocean and Pacific. Changes to the northern hemisphere subtropics, while also displaying a weaker temperature signal in DJF, are not significant, consistent with Figure 6.4.

This suggests that the QBO enhancement in DJF may be due to stronger characteristics locally at particular longitude regions, rather than a zonally symmetric increase. The Maritime Continent and warm pool region display some of the strongest and most persistent deep convection anywhere in the world, suggesting perhaps that some process linked to convection may be related to this enhanced temperature variability. This will be explored more in future work and discussed briefly in Section 6.4.

To further assess how equatorial QBO temperature anomalies change throughout the seasons, Figure 6.7 shows QBOE minus QBOW temperature anomalies binned by month from MERRA2, ERA5, Singapore, AIRS, R1, and JRA55. MERRA1 and ERAI are similar to their more modern counterparts, and JRA55 and JRA55C also do not differ markedly during the period in which they overlap. Figure 6.7 confirms the strengthening of equatorial QBO anomalies in DJF noted above, but shows a smaller local maximum around June-August (JJA). R1 shows weaker anomalies overall, but the same relative behavior can be seen. These plots indicate that QBO temperature anomalies undergo a semi-annual cycle in amplitude. At around 26 km, where the peak QBOE minus QBOW warm anomaly occurs, the phasing is somewhat different. Though there are still stronger warm anomalies around

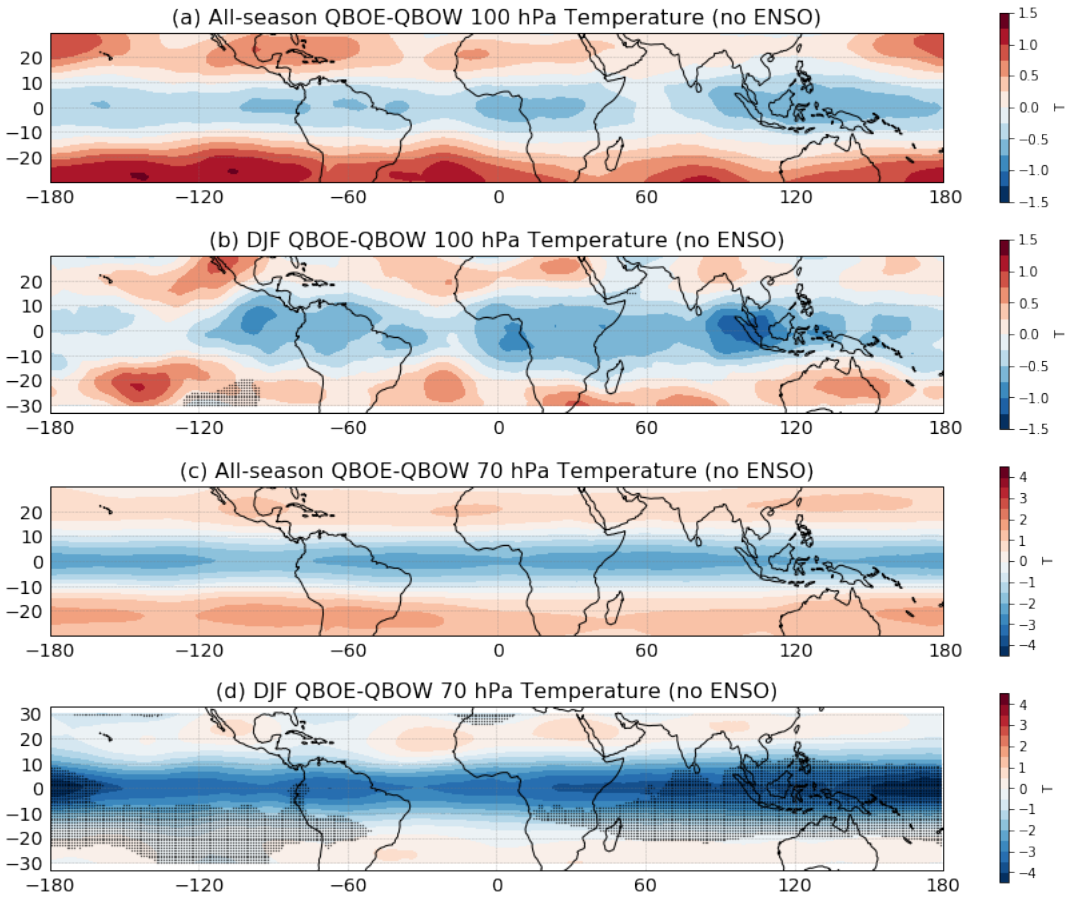

Figure 6.6: The MERRA2 QBOE minus QBOW temperatures at 100 hPa (a,b), and 70 hPa (c,d) with strong ENSO months removed. Panels (a,c) are the all-season QBO, and panels (b,d) are DJF, stippling on the DJF panels indicates significant changes relative to the all-season panels via a bootstrap.

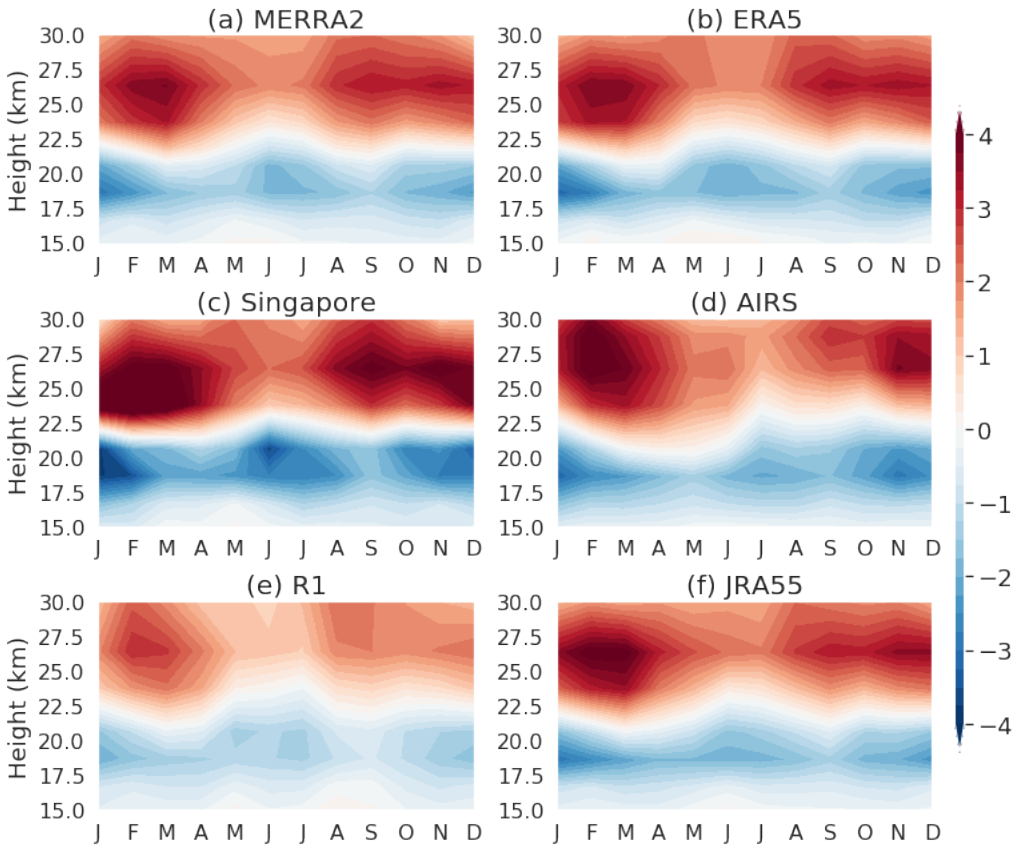

Figure 6.7: Upper troposphere/lower stratosphere QBOE minus QBOW temperature anomalies averaged over the tropics (zonally and between 10°N/S) binned by month of the year (January to December on the x-axis; height in km on y-axis) for the MERRA2, ERA5, Singapore sounding, AIRS, R1, and JRA55 datasets. ERAI and MERRA are similar to ERA5 and MERRA2, and JRA55C is similar to JRA55.

fall, late winter and into early spring, a peak in the strength of the warm in JJA appears absent.

The results described above show that during boreal winter, QBO temperature anomalies are colder in QBOE and warmer in QBOW on the equator, and anomalies are weaker off the equator. In terms of zonal structure, the QBOE-QBOW differences tend to be pronounced around the East Pacific and central America, over equatorial Africa, and in particular around the Maritime Continent and West Pacific. If TTL temperature anomalies are key to modulating the MJO, their greater amplitude in DJF may explain why the MJO-QBO relationship

is only significant in boreal winter. However, stronger than average anomalies are also evidence in boreal summer, when the MJO-QBO link is not significant. It remains possible that other factors also play a role in explaining the seasonality. One might be the amplitude of the MJO, which is greater in boreal winter than summer; another might be its meridional structure, as the MJO's activity tends to be closer to the equator in winter than summer.

6.3.2.2 QBO Decadal Temperature Anomalies

In this section we look at whether QBO temperature anomalies show longer-term trends or variability associated with the emergence of a strong MJO-QBO link beginning in the 1980s. To look at this, we consider the 40-year span of data from 1979-2019 and divide the record in half, considering the period before 1999 and the period after 1999 separately. 1999 was chosen so that the statistics are roughly the same in each period – changing the precise year does not change the results.

Figure 6.8 is similar to Figure 6.3, except that we now compare the period from 1979-1999 to the period from 1999-2019 rather than comparing DJF to all-season anomalies. For the analysis here we do not segregate by season. The bottom panels now show the QBOE minus QBOW difference, as the two phases show a similar and symmetric increase. The same patterns that appear in DJF also appear when comparing earlier and later periods: there is an enhanced equatorial QBO difference and a decreased off-equatorial QBO difference post-1999 compared to pre-1999. The bottom panels show that this is again robust across all datasets (earlier years are solid and later years are dashed): in general, the pre-1999 QBO anomalies are on the order of -1 K, whereas the post-1999 QBO anomalies are over or around -2 K. Similar to Figure 6.4, these changes in QBO temperature anomalies between decades shows the same broad shift throughout the tropics and subtropics relatively independent of latitude, with colder QBOE temperatures and warmer QBOW temperatures during the post-1999 period compared to the pre-1999 period in all reanalysis datasets.

For Singapore data, the difference is of the correct sign but not significant in the TTL,

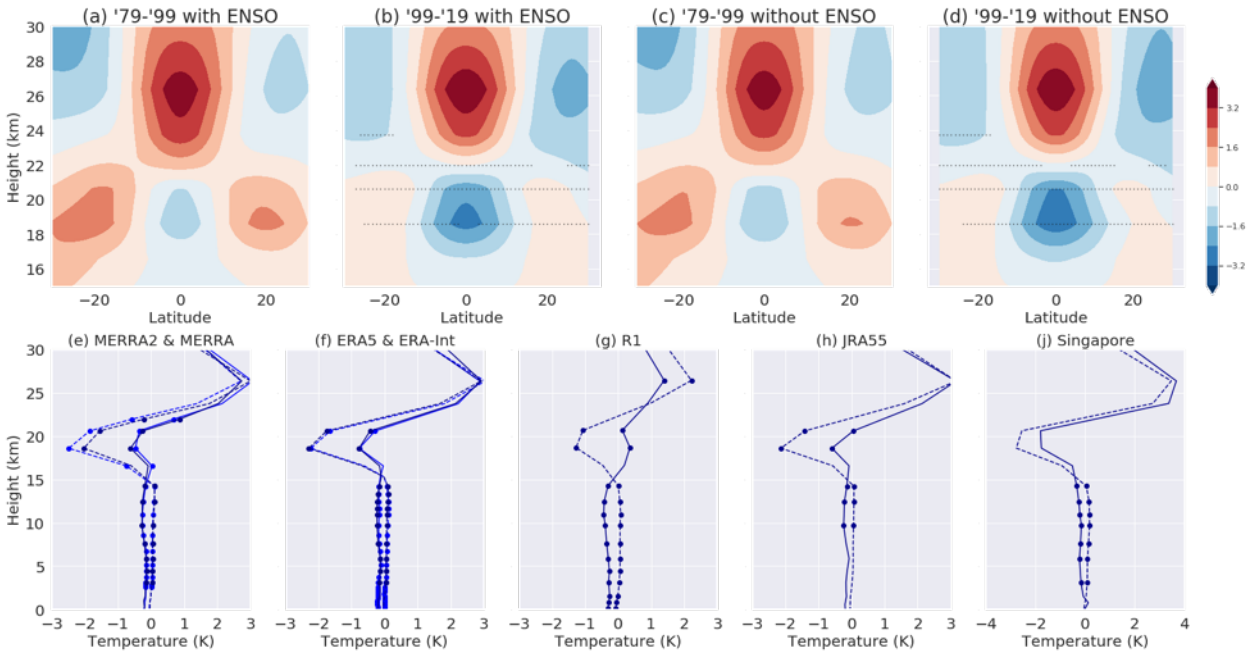

Figure 6.8: Similar to Figure 6.3, but now the top rows shows (a/c) the zonal-mean QBOE minus QBOW temperature anomaly in MERRA2 from 1979-1999 compared to (b/d) the anomaly from 1999-2019 (both independent of season). Panels (a/b) include strong ENSO periods, whereas (c/d) do not include strong ENSO months. The bottom row shows QBOE minus QBOW anomalies across all datasets in the early 1979-1990 period (solid) versus the late 1999-2019 period (dashed). Significance is marked with stippling or a dot and is calculated via the bootstrapping described in Section 6.3.2.1. As in Figure 6.3, in panels (e,f) the dark curve is the dataset listed first in the title and the lighter curve is the second one.

consistent with the previous section. Here we exclude AIRS from this analysis because it does not include data from the prior period. Significance is calculated similarly to the previous case via bootstrapping. We randomly split the QBOE and QBOW months from the whole period into two non-overlapping groups with size equal to the pre- and post-1999 period, then take the difference between these two random samplings, and repeat that process 1000 times to build our distribution.

In addition to the strengthening of the TTL anomalies post-1999, another interesting feature is the small but robust difference in the troposphere between the two periods. In the early period, QBOE phases tended to be accompanied by colder tropospheric states, while later in the record tropospheric temperature anomalies are nearer to zero. It is possible that this signal is caused by aliasing, but restricting the dataset to only ENSO neutral years or only the DJF season, while it reduces the sample size, does not change it. This strengthening of QBO temperature anomalies in Figure 6.8 also does not seem to be a product of changes in observing systems over these two periods: the same strengthening post 1999 is evident in both JRA55 to JRA55C over the period where the two datasets overlap (not shown).

Our finding here is somewhat at odds with analysis by Klotzbach et al. (2019) who looked at whether QBO temperature anomalies change on decadal timescales. There, they found via a linear trend analysis that there were no trends in 100 hPa temperature or stability from the period from 1960-2015. Here however, we consider primarily the temperatures at higher levels than 100 hPa, at global mean behavior rather than just the warm pool region, and rather than consider the linear trend look at the general QBOE minus QBOW difference in temperature. Additionally, Klotzbach et al. (2019) did find that the while both QBOE and QBOW years showed negative trends (consistent with a cooling overall of the TTL that seems robust across most reanalysis products; Tegtmeier et al. (2020)), QBOE years seem to be cooling faster than QBOW years, which would contribute to a stronger easterly minus westerly difference.

The JRA55 and Singapore datasets also allow us to perform analyses further back in

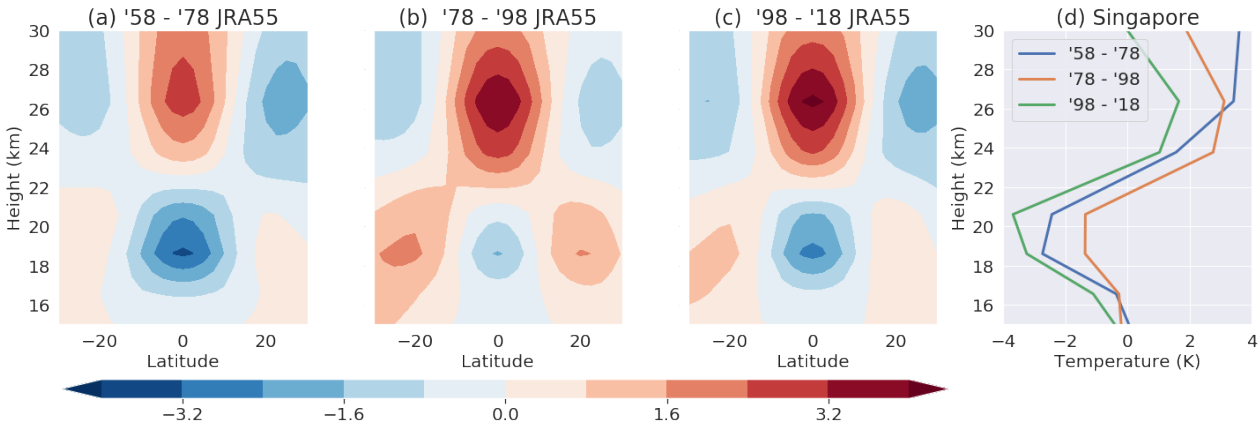

Figure 6.9: QBOE minus QBOW temperature difference, similar to Figure 6.8, but from the JRA55 datasets (a-c) and Singapore dataset (d) for the periods from 1958-1978, 1978-1998, and 1998-2018.

time, though the amount of observed data assimilated into the reanalysis is obviously greatly reduced in the pre-satellite era. Nevertheless, we perform a similar analysis using JRA55 and Singapore during the period from Jan. 1958 through Dec. 2018. We divide the record into three 20-year periods: 1958-1978, 1978-1998, and 1998-2018, and then calculate the QBOE minus QBOW anomaly in each period. The results are shown in Figure 6.9. Comparison of the 1978-1998 period to the 1998-2018 period yields results similar to those already discussed in this section: QBO anomalies on the equator are weaker from 1978-1998 relative to the 21st century. However, we additionally see strong equatorial QBO temperature anomalies in the earliest part of the record from 1958-1978. This suggests that the stronger QBO anomalies in recent decades may be oscillatory in nature rather than due to a trend. Both JRA55 and Singapore show similar behavior, adding confidence to the results (though JRA55 likely assimilates Singapore sounding data, meaning that the two datasets are not entirely independent).

Similar to the previous results, in this section we showed stronger QBO anomalies on the equator in more recent decades when the MJO-QBO relationship is stronger and significant (e.g. Klotzbach et al. (2019)). This is again consistent with the theory that the stronger

QBO temperature changes in the recent decades contributed to the stronger MJO-QBO link. However, we also find that the QBO temperature anomalies are strong in the two decades prior to 1979, although the MJO-QBO link is not significant then. This makes it difficult to state conclusively that there is a clear link between decadal QBO temperature anomalies and the MJO. It may, however, help explain why overall, Klotzbach et al. (2019) saw no trend when considering the 1960-2015 period, since the changes we find are not monotonic over that period. Changes to the QBO structure between decades, in particular, tropospheric differences and weaker off-equatorial temperature signals, are further suggestive of different regimes during the different periods we consider. The causes of these differences are not known, but the next section shows some evidence for or against different mechanisms and offers suggestions for future work.

6.4 Possible Mechanisms

At present it is not clear what causes the observed differences either seasonally or on longer timescales. Two hypotheses we explore are 1) whether the MJO plays an active role in generating the observed QBO temperature differences in the TTL, and 2) whether those differences are a by-product of phase locking between the QBO and the annual cycle. Neither of those seems to explain the observed changes to the QBO fully. We further discuss the additional hypothesis, which will be examined in future work, that changes to the QBO meridional circulation and QBO-related tropical upwelling may play a role.

To examine whether the MJO plays an active role in generating the QBO TTL signals described in the preceding sections, Figure 6.10 shows composites using daily data to look at periods when the MJO is strong or weak, controlling for the phase of the QBO and the season to avoid aliasing. We use daily data from Singapore, ERA5 and MERRA2. Figure 10 plots the anomalous TTL temperatures in DJF (relative to the DJF climatology) during QBOE and QBOW periods in blue and red, respectively. We further segregate the data

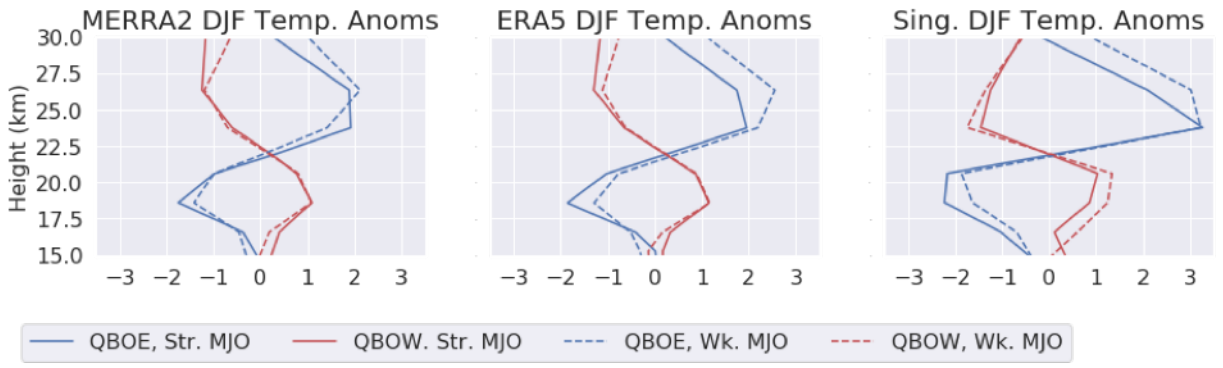

Figure 6.10: (left to right) MERRA2, ERA5, and Singapore temperature anomalies from daily data averaged zonally and from 10°N/S. Blue curves are anomalies composited over QBOE periods in DJF relative to the DJF mean. Red curves are similarly DJF anomalies during QBOW periods. The solid versus dashed lines are composites from days in DJF and the specified QBO phase on which the MJO was strong (solid) or weak (dashed) as defined in Section 6.2.1.

based on days when the MJO is strong (solid) and days when the MJO is weak (dashed).

Whether the MJO is strong or weak does not appear to explain the enhancement in QBO temperatures in DJF. QBOW temperature anomalies in Figure 6.10 are the same regardless of the strength of the MJO, such that stronger MJO events in DJF are likely not the cause of the enhanced anomalies. There is also not much change in QBOE: the TTL anomaly is slightly colder when the MJO is strong than when it is weak, but the change is smaller than the differences in DJF discussed in Section 6.3.2.1. Remaking these composites with monthly data shows stronger MJO signals, in particular indicating stronger cold anomalies in QBOE when the MJO is strong versus weak (not shown). However, due to the restrictive compositing by season, QBO phase, and MJO strength, the number of data points using monthly data is very limited and hampers statistical significance and meaningful interpretation.

Further analysis looking at correlations between MJO strength and the strength of QBO temperature anomalies did not reveal any strong link between the two (not shown). We also examined whether there is an overall trend in MJO strength from 1979-2018 and were

Figure 6.11: A histogram of the number of QBOE and QBOW peaks (left and right panels, with peaks identify per Section 6.4 that occurred per month (January-December on the x-axis) in the ERA5, MERRA2, JRA55, and Singapore sounding data. Note for JRA55 the full span of available dates beginning in 1958 was used.

unable to demonstrate any strengthening of the MJO during this period which may explain decadal changes. It therefore seems unlikely that changes to the MJO cause differences in QBO TTL temperature signals.

Another hypothesis for why the QBO demonstrates stronger temperature anomalies in DJF relative to other time periods is that it is a by-product of phase-locking between the QBO and the annual cycle. This phase-locking has been previously discussed in the literature (see a review in Baldwin et al. (2001) and more recently Rajendran et al. (2016)), and has established that the QBO tends to preferentially undergo transitions in phase (at 50 hPa) in the boreal spring. We can similarly assess in which months the approximate peak of the QBO occurs. We identify peaks in the data by looking for months containing local extrema. For example, for QBOE we find months in which the previous month's winds are stronger and the following month's winds are weaker (and vice versa for QBOW). We further require that the QBOE peaks are less than -14 m/s and the QBOW peaks are greater than 5 m/s in magnitude; these thresholds were chosen so that the peaks identified by the algorithm corresponded with those obvious by eye in the data. Finally, we required that the QBOE peaks be separated by 6 months and the QBOW peaks be separated by 18 months, to ensure different QBO events were sampled.

Once the peaks were identified, a histogram of the month during which they occurred was constructed for QBOE and QBOW. Results from ERA5, MERRA2, JRA55, and Singapore are shown in Figure 6.11. Note for JRA55, all data was included from 1958 onward to maximize the number of samples. Figure 6.11 shows a clear bimodal distribution of peaks centered roughly in the winter and summer seasons in both QBOE and QBOW, consistent with Figure 6.7. It is intuitive that the strongest temperature anomalies at lower levels should occur simultaneously with peaks in the 50 hPa wind, as the wind shear is likely strongest during these months and thus, by thermal wind balance, the temperature anomalies must be largest.

However, the more fundamental question of why the QBO sometimes phase locks to the annual cycle is not established. Examination of whether this phase locking may have changed on decadal timescales and could contribute to the signals noted in Section 6.3.2.2. yielded no conclusive results. Thus, a more detailed understanding of what drives the links between the QBO and the annual cycle would be useful.

It seems unlikely that either the MJO or the phase-locking of the QBO and the annual cycle entirely explain the results described in the previous section. It is therefore probable that other processes are responsible for the greater variability in this region during the solstice seasons compared to the equinoxes, and in the last two decades compared to the two before. Any mechanism should also explain the associated changes in the spatial structure QBO temperature anomalies in the TTL.

One possibility, given the fact that the shifts in the QBOE and QBOW temperature anomalies are approximately independent of latitude within a wide band encompassing the tropics and subtropics (e.g. Figure 6.4) is that the Brewer-Dobson circulation (BDC; Butchart (2014)) and associated large-scale upwelling in the TTL and lower stratosphere may be modified by the QBO in the solstice seasons (and especially DJF). Because the anomalous upwelling or downwelling associated with the BDC tends to be broad throughout the tropics, changes to this upwelling might explain why the temperature anomalies are

shifted more negative in QBOE and more positive in QBOW reasonably uniformly between ∼30°S-30°N.

A link between the QBO and the BDC and tropical upwelling has been proposed in other studies (Niwano et al. (2003); Fujiwara et al. (2010); Flury et al. (2013); Neu et al. (2014); Rao et al. (2019)), which generally find a stronger BDC in QBOE and a weaker BDC in QBOW. These changes could alter temperature anomalies consistent with what we observe. The Brewer-Dobson circulation in models strengthens under global warming (Butchart (2014)) and in observations tend to be strongest in DJF, which might be linked to why QBO temperature changes are observed on those two timescales. The mechanism by which the QBO and BDC are connected seems not to be firmly established, though Flury et al. (2013) and Neu et al. (2014) discuss possible mechanisms related to changes in the tropical pipe (Plumb (1996)) or to changes in the QBO meridional circulation.

Changes to the QBO's meridional circulation may also play a direct role in altering QBO temperature anomalies that is independent of their connection to a larger scale upwelling. The QBO meridional circulation shows a synchronization to the seasonal cycle (Jones et al. (1998); Kinnersley and Tung (1998); Kinnersley (1999); Kinnersley and Tung (1999); Peña-Ortiz et al. (2008)) such that it is less symmetric about the equator and extends deeper into the midlatitudes during solstice seasons. This change in the QBO meridional circulation could lead to larger temperature anomalies (Kinnersley (1999)), especially in boreal winter compared to boreal summer (Peña-Ortiz et al. (2008)). The cause of this change in QBO meridional circulation in the solstice seasons is also not clear: Kinnersley (1999) showed in a simple model that nonlinear advection of equatorial zonal winds may play a role, while more recently Peña-Ortiz et al. (2008) argued that seasonal changes in the Eliassen Palm flux and planetary wave forcing could be responsible.

It may be that these changes to the QBO meridional circulation induce stronger temperature signals in the solstice seasons like those we observe. However, the shifts observed here, e.g. in Figure 6.4, are not confined to one hemisphere, but are better described as a

shift across the whole tropical band. It is unclear whether the QBO meridional circulation changes in such a way as to completely explain this difference. Additionally, this process only explains the seasonality, and seems less well-suited to describe decadal changes.

6.5 Conclusions

This study examines TTL temperature anomalies, focusing especially on those associated with the QBO. We are motivated by the strong link between the QBO and the MJO, in which TTL temperature anomalies have been hypothesized to play a key role. In particular, we examined whether the seasonality of the MJO-QBO link (it is only significant in boreal winter; Yoo and Son (2016)) and its emergence only in recent decades (Klotzbach et al. (2019)) can be linked to changes in QBO temperature anomalies during these periods. We hypothesize that stronger QBO temperature anomalies could help explain the stronger MJO-QBO connection. We find that QBO temperature anomalies in the TTL are indeed modulated on both annual and decadal time scales, and our main results can be summarized as:

1. On annual timescales, QBO temperature anomalies on the equator are stronger (i.e. colder in QBOE and warmer in QBOW) in boreal winter relative to the all-season behavior (Fig. 6.3). Off-equatorial QBO temperature anomalies are also weaker in boreal winter than in the all-season mean (Figs. 6.3, 6.4, 6.6), with large differences in particular around the Maritime Continent and the West Pacific warm pool (Fig. 6.6). Thus, the strength of both the equatorial and off-equatorial QBO temperature anomalies are distinctly different in DJF. However, the difference can be viewed as a shift in DJF that is relatively independent of latitude within a broad range encompassing the subtropics. Thus, the meridional structure and (by thermal wind balance) the associated zonal wind anomalies do not show strong differences in DJF compared to the all-season mean.

2. QBO temperature anomalies in the TTL also tend to be stronger on the equator in boreal summer (Fig. 6.7) than the all-season mean (or the equinoctial seasons). QBO temperature anomalies thus display a semi-annual cycle in their magnitude, similar to annual cycle changes in QBO meridional circulation noted in previous literature (e.g. Jones et al. (1998); Kinnersley and Tung (1998); Kinnersley and Tung (1999); Kinnersley (1999); Peña-Ortiz et al. (2008)).

3. The same on-equatorial strengthening and off-equatorial weakening of QBO temperature anomalies occurs on decadal timescales. The period from 1999-2019 showed stronger equatorial QBO anomalies than the period from 1979-1999 (Fig. 6.8). In one reanalysis dataset which extends back to 1958 (JRA55), as well as in the Singapore sounding data, we further found that the period from 1958-1978 also had stronger equatorial QBO temperature anomalies relative to the period 1978-1998 (Fig. 6.9).

Comparison of JRA55 to JRA55C (a version of the reanalysis identical to JRA55 except that it does not assimilate satellite observations) shows similar behavior, suggesting that the decadal changes are not due to changes in observing systems.

We are unable to explain the cause of these changes to QBO temperature anomalies. It appears unlikely that an upward influence due to the MJO causes these changes (Fig. 6.10). We find, consistent with previous literature (e.g. Rajendran et al. (2016)) that the QBO winds at 50 hPa tend to phase-lock to the annual cycle and peak in the solstice seasons (Fig. 6.11), when temperature anomalies are strongest. But this argument cannot be causally disentangled without a mechanism explaining why either the temperature or the wind should synchronize with the annual cycle.

Our results may help explain some of the confounding features of the MJO-QBO connection and lend some credence to the idea that TTL temperature anomalies could influence tropical deep convection. These results also suggest that the upwelling in the TTL and lower stratosphere associated with the QBO or other larger-scale processes like the Brewer-Dobson circulation could display more intricate behavior than has previously been recognized. It is

also possible that processes we have not explored, such as ozone or cloud feedbacks, has a role in modulating QBO temperature anomalies, as changes to tropical upwelling also alter ozone amounts in the tropics.

Changes in the QBO meridional circulation or more broadly to tropical upwelling could influence other aspects of the climate system, and thus the circulation and dynamical implications of this study should be examined in more detail. In particular, a better understanding of whether the QBO might induce changes to the Brewer-Dobson circulation and large-scale upwelling in the TTL in DJF seems a promising avenue of further inquiry that will be examined.

Chapter 7

Summary and Final Remarks

This chapter summarizes the main results of this thesis, and concludes with a few final remarks on the broader context of this work.

Chapter 2 introduced the two processes central to this thesis: the stratospheric quasi-biennial oscillation (QBO) and the intraseasonal Madden-Julian oscillation (MJO). We reviewed the key observed features of each oscillation, discussed the basic (or proposed) theory, and reviewed historical efforts to model each process. We then discussed how, very generally, the stratosphere and troposphere are coupled, before reviewing the literature on how the QBO can or might affect the troposphere. We concluded Chapter 2 with a detailed discussion of the relationship between the MJO and the QBO. The main feature of this MJO-QBO connection is that the boreal winter MJO is more active and more predictable when the lower-stratospheric QBO winds are easterly versus westerly. The MJO-QBO link is the main focus of this thesis. At the conclusion of Chapter 2 we stressed the uncertainty regarding what physical mechanisms explain the MJO-QBO interaction, and highlighted both the lack of MJO-QBO modeling studies and the challenge of modeling the MJO-QBO interaction.

In Chapter 3, published as Martin et al. (2019), we studied the MJO-QBO link in an idealized, cloud-resolving model. We used the WRF model to simulate a small, 3D column

of atmosphere over a specified, homogeneous sea surface. Our model was run in a unique configuration with parameterized large-scale dynamics taken from observations as part of the DYNAMO field campaign. In particular, the model calculates a large-scale vertical velocity during the simulation using an implementation of the weak temperature gradient approximation. We showed that the model reproduces convection associated with two observed MJO events, before forcing the model with a variety of idealized temperature and wind perturbations similar to those associated with the QBO. An advantage of this method is that temperature and wind anomalies can be independently considered. This model also allows for more realistic representation of convection than models which must resort to cumulus parameterizations. In general we found that QBO wind anomalies had essentially no effect on MJO-convection, whereas QBO temperature anomalies affected simulated convection in a manner similar to the observed MJO-QBO link. However, lower-than-observed temperature anomalies were needed to show a strong response, and for observed temperature anomalies higher up in the tropopause region the model QBO impact was weak and difficult to detect. We concluded that it was possible that QBO temperature anomalies may play a role in driving the MJO-QBO connection, but recognized that in this framework it was difficult to conclusively say more.

In Chapter 4, published as Martin et al. (2020), we studied the MJO-QBO link in a forecast model. We used a model which is part of the European Centre for Medium-Range Weather Forecasting's (ECMWF) Integrated Forecasting System, which was chosen in part because it has an exceptionally good representation of the MJO. We examined the behavior of the MJO in many hindcast simulations during DJF periods from 1989-2016, integrated for approximately 2 months with many ensemble members. We first showed that, consistent with other literature, the model simulated stronger MJO events when initialized during QBO easterly months than during QBO westerly months. However, because our goal was to examine the effect of the model QBO on the model MJO during the simulations, we performed a series of "stratosphere-swapping" experiments in which the observed stratosphere in the

initial conditions was replaced by either a QBO easterly or QBO westerly state (without changing the troposphere). We then re-ran our simulations and examined the difference between the experiments with imposed QBO easterly and westerly stratospheres. We found that, while a QBO impact on the MJO was detected and was of the same sign as observed, the MJO changes due to changing the QBO were very small in the model. We provided some evidence suggesting that stronger QBO temperature anomalies in the model led to a stronger MJO response, but the causality and statistical significance of these results was difficult to confirm. We concluded with some discussion of why the QBO impact in the model was so small, including potential issues with our experimental design which led to weaker-than-observed QBO temperature anomalies in the model.

In Chapter 5, in preparation for publication, we studied the MJO-QBO link in a global climate model (GCM). We used a model developed at NASA's Goddard Institute for Space Studies (GISS), known as ModelE, in two configurations: a standard configuration with 40-vertical levels and a high vertical resolution configuration optimized for the middle atmosphere with 102-vertical levels. For both the 40- and 102-level versions, we examined a series of both specified sea-surface temperature runs ("AMIP" simulations) and fully coupled ocean-atmosphere runs integrated for approximately 40 years. We first showed in the 102-level version, which has an internally generated QBO and a reasonable MJO, that the model showed no MJO-QBO link in either the AMIP or coupled configuration. We noted, however, that in these simulations, QBO temperature signals showed biases in the lower stratosphere. To remedy this, we conducted a series of experiments in which "nudging" was applied in the stratosphere of the 40-level version of the model. This nudging was implemented as a relaxation of the model's zonal and meridional winds towards observations. We showed this led to a realistic simulation of the QBO, including QBO temperature anomalies around the tropopause. Despite the accuracy of the QBO, we showed that no versions of the nudged model ultimately showed a strong MJO-QBO link. This included versions with different implementations of the nudging, a series of ensemble runs, and simulations in which

the QBO was artificially strengthened to 1.5 times its observed values. We concluded with a discussion of why, even in the case when stratospheric biases were minimized, the observed MJO-QBO link was not captured in the model, and suggested that simply capturing strong QBO temperature anomalies around the tropopause does not lead to modulation of the MJO in this GCM.

In Chapter 6, in preparation for publication, we looked in more detail at QBO temperature anomalies across several observed datasets. Our work was motivated by the potential connection between these temperature anomalies and theories of the MJO-QBO link. We asked whether QBO temperature anomalies showed notable variability seasonally and decadally, motivated by literature showing that the MJO-QBO link is only significant in boreal winter and may only have emerged since the 1980s. We examined temperature anomalies associated with the QBO in seven reanalysis datasets, one sounding dataset, and one occultation dataset. We found that QBO temperature anomalies were generally stronger on the equator and weaker off the equator both in boreal winter relative to other seasons, and in recent decades (i.e. after 1999) relative to earlier decades (from 1979-1999). The cause of this strengthening was not clear, though we showed it was likely not due to an upward influence by the MJO, and possibly linked to synchronization between the QBO and the annual cycle.

Taken as a whole, Chapters 3-5 demonstrate that it is difficult to capture the MJO-QBO connection in models. First, it is difficult to find a model that is well-suited for this problem, due to the difficulties simulating both the MJO and QBO individually, let alone any subsequent coupling. To overcome this challenge, we attempted to work with many different types of models, with the hopes that the pros and cons of each setup would balance out and a coherent story would emerge. Yet each of the models we considered failed to show a strong MJO-QBO link like that observed. With regards to the failure of individual models, in each case experimental, methodological, or modeling limitations are apparent which must play a role in leading to weak or non-existent MJO-QBO connections. Still, the consistent

failure to model the MJO-QBO relationship underscores that small biases or subtle issues are likely not to blame. Rather, it seems likely either that models miss some fundamental pathway which couples the QBO to the MJO (and perhaps more broadly connects the tropical stratosphere to intraseasonal oscillations), or that the observed MJO-QBO relationship has some important feature which has not yet been discovered.

Without a strong modeling framework in which to examine this question, it is difficult to make strong claims about the physical mechanisms connecting the two phenomena. Based on our cloud-resolving modeling work in Chapter 3, it seems unlikely that the local effect of QBO wind anomalies on individual convective systems has a role in modulating the MJO. Yet it is certainly plausible that QBO changes to wave propagation in the stratosphere or more generally to the dynamics either of the stratosphere or the troposphere (or both) may be at the heart of the MJO-QBO link. If small-scale elements like gravity waves are important, (not an unreasonable assumption given their role in driving the QBO) it is further possible that models, which must resort to gravity wave parameterizations which are tuned and imperfect, might miss the MJO-QBO link. These types of dynamical pathways should be considered in the literature moving forward, at least to rule them out more definitively.

QBO temperature anomalies, and mechanisms related to the effects they might have on convection and the MJO, have been central to most of the work presented in this thesis. These temperature signals have been proposed as a potential pathway for QBO changes in the tropics since initial results dating back to Giorgetta et al. (1999) and Collimore et al. (2003), as well as in the modeling work of Nie and Sobel (2015), and more recent studies on the MJO-QBO link directly by Son et al. (2017), Hendon and Abhik (2018), and our own work in Chapters 3 and 4. But the details regarding how precisely these temperature anomalies actually impact convection have not been clearly and conclusively set forth. Chapter 3 shows that at least in principle temperature anomalies in the upper troposphere can impact convection associated with the MJO. But for the small anomalies high up near the tropopause in observations, that modeling study is much less convincing in

showing a significant impact. And our results in Chapter 5 seem to suggest that, at least in GCMs, too-weak QBO temperature anomalies are not in and of themselves the only reason models fail to capture the MJO-QBO link (though this does not mean they are not a factor altogether). Chapter 6 shows that QBO temperature signals undergo interesting modulation on a variety of timescales, but causality is difficult to deduce from this work and it is unclear to what extent the MJO is affected by these subtle changes in QBO strength and structure. This makes it hard to firmly say whether these temperature changes in and of themselves are important. It may be that their indirect impacts on other elements of the climate (like properties of high clouds) are more important than their direct impacts on the instability of the upper atmosphere to convection. More modeling and observational work along these lines should also be examined in the future.

Looming over the recent modeling literature on the MJO-QBO link, which has now shown a slew of negative or generally inconclusive modeling results, is the hypothesis that the entire MJO-QBO relationship may be somehow statistically a fluke, or due to some other mode of variability aliasing onto one or both of these oscillations. Indeed, since its rediscovery in 2016, several scientists have doubted the existence or robustness of the MJO-QBO link (personal communications and discussions at several meetings during my graduate work attest to this). Still, no work claiming to refute the observed connection has been published which might explain how this could be. The fact that the MJO-QBO link is significant only in certain seasons, and only in recent decades, has also made some doubt how robust the connection really is. And other apparent QBO connections, such as the QBO-ENSO and QBO-tropical cyclone relationship, have shown longer term modulation or decorrelation which defy explanation. But the MJO-QBO link has passed strict *a posteriori* statistical tests, which makes it difficult to dismiss out of hand. The results have been confirmed by many studies, and are independent of the precise definition of the MJO or QBO, or the dataset considered. An MJO-QBO relationship exists in forecast models (even if the reasons why remain elusive), and clearly impacts MJO predictability and teleconnections. And while

GCMs don't capture the connection, models also do not display an MJO-QBO signal which is anywhere near as strong as the observed link over a comparable 40-year period of time (per Chapter 5 and Richter et al. (2020)). Given all of this, as well as the many noted issues with models' ability to represent the MJO and the QBO, we believe it is more likely that models miss some important process than that the observed link is not real. More data, more thought, and more work will elucidate whether this hunch turns out to be true.

* * *

The MJO-QBO link is a feature of the present climate system which is observationally nuanced and theoretically stimulating, pushing the limits of our modeling capabilities and possessing real relevance to human society. Over the past four years, it has been a fickle, frustrating, and above all fascinating fixture in my daily work. As the results here demonstrate, it has proven more than a match to my understanding and creativity, and has similarly flummoxed many peers and colleagues much cleverer than me. Work on this problem has been in turns exasperating and exhilarating, as I suspect all good science should be. Rather than a culmination or conclusion, I hope that my work – on this problem, on others I have considered outside the confines of this thesis, and on problems I have not yet begun to imagine – is only just beginning.

If the conclusions here seem speculative and unfinished, it only underscores the ways in which this topic remains scientifically vibrant, evolving, profound, and unsettled. We leave our readers, therefore, not with a cogent and complete description of the interaction of the Madden-Julian oscillation and the quasi-biennial oscillation, but instead with the advice of Carl-Gustaf Rossby in a letter he wrote to Jule Charney:

"If all you do is to give them a faultless and complete and uninhabited architectural masterpiece, then you do not help them to become builders of their own."[1]

[1] Phillips (1994)

Bibliography

Abhik, S., Hendon, H.H., 2019. Influence of the QBO on the MJO during coupled model multiweek forecasts. Geophysical Research Letters 46, 9213–9221.

Abhik, S., Hendon, H.H., Wheeler, M.C., 2019. On the sensitivity of convectively coupled equatorial waves to the quasi-biennial oscillation. Journal of Climate 32, 5833–5847.

Adames, F., Kim, D., 2016. The MJO as a dispersive, convectively coupled moisture wave: Theory and observations. Journal of the Atmospheric Sciences 73, 913–941. doi:10.1175/JAS-D-15-0170.1.

Ahn, M.S., Kim, D., Kang, D., Lee, J., Sperber, K., Gleckler, P., Jiang, X., Ham, Y.G., Kim, H., 2020. MJO propagation across the Maritime Continent: Are CMIP6 models better than CMIP5 models? *submitted to Geophys. Res. Lett.* .

Ahn, M.S., Kim, D., Sperber, K.R., Kang, I.S., Maloney, E., Waliser, D., Hendon, H., et al., 2017. MJO simulation in CMIP5 climate models: MJO skill metrics and process-oriented diagnosis. Climate Dynamics 49, 4023–4045.

Anber, U., Wang, S., Sobel, A., 2017. Coupling with ocean mixed layer leads to intraseasonal variability in tropical deep convection: Evidence from cloud-resolving simulations. Journal of Advances in Modeling Earth Systems 9, 616–626.

Andersen, J.A., Kuang, Z., 2012. Moist static energy budget of MJO-like disturbances in the atmosphere of a zonally symmetric aquaplanet. Journal of Climate 25, 2782–2804.

Andrews, D., Mcintyre, M.E., 1976. Planetary waves in horizontal and vertical shear: The generalized Eliassen-Palm relation and the mean zonal acceleration. Journal of the Atmospheric Sciences 33, 2031–2048.

Andrews, D.G., Holton, J., Leovy, C., 1987. Middle Atmosphere Dynamics. Academic.

Aumann, H.H., Chahine, M.T., Gautier, C., Goldberg, M.D., Kalnay, E., McMillin, L.M., Revercomb, H., Rosenkranz, P.W., Smith, W.L., Staelin, D.H., et al., 2003. AIRS/AMSU/HSB on the Aqua mission: Design, science objectives, data products, and processing systems. IEEE Transactions on Geoscience and Remote Sensing 41, 253–264.

Baldwin, M.P., Dunkerton, T.J., 2001. Stratospheric harbingers of anomalous weather regimes. Science 294, 581–584. doi:10.1126/science.1063315.

Baldwin, M.P., Gray, L.J., Dunkerton, T.J., Hamilton, K., Haynes, P.H., Randel, W.J., Holton, J.R., Alexander, M.J., Hirota, I., Horinouchi, T., Jones, D.B.A., Kinnersley, J.S., Marquardt, C., Sato, K., Takahashi, M., 2001. The quasi-biennial oscillation. Reviews of Geophysics 39, 179–229. doi:10.1029/1999RG000073.

Ball, W.T., Alsing, J., Mortlock, D.J., Staehelin, J., Haigh, J.D., Thomas, P., Tummon, F., Stübi, R., Stenke, A., Anderson, J., et al., 2017. Continuous decline in lower stratospheric ozone offsets ozone layer recovery. Atmospheric Chemistry and Physics .

Barnston, A.G., Livezey, R.E., Halpert, M.S., 1991. Modulation of Southern Oscillation-Northern Hemisphere mid-winter climate relationships by the QBO. Journal of Climate 4, 203–217. doi:10.1175/1520-0442(1991)004<0203:MOSONH>2.0.CO;2.

Barton, C.A., McCormack, J.P., 2017. Origin of the 2016 QBO disruption and its relationship to extreme El Niño events. Geophysical Research Letters 44, 11,150–11,157. doi:10.1002/2017GL075576.

Bauer, S.E., Ault, A., Prather, K.A., 2013. Evaluation of aerosol mixing state classes in the GISS modelE-MATRIX climate model using single-particle mass spectrometry measurements. Journal of Geophysical Research: Atmospheres 118, 9834–9844. doi:10.1002/jgrd.50700.

Benedict, J.J., Maloney, E.D., Sobel, A.H., Frierson, D.M., Donner, L.J., 2013. Tropical intraseasonal variability in version 3 of the GFDL atmosphere model. Journal of Climate 26, 426–449.

Benedict, J.J., Randall, D.A., 2007. Observed characteristics of the MJO relative to maximum rainfall. Journal of the Atmospheric Sciences 64, 2332–2354.

Benedict, J.J., Randall, D.A., 2009. Structure of the Madden–Julian oscillation in the superparameterized CAM. Journal of the Atmospheric Sciences 66, 3277–3296.

Bergman, J.W., Sardeshmukh, P.D., 2004. Dynamic stabilization of atmospheric single column models. Journal of Climate 17, 1004–1021.

Blossey, P.N., Bretherton, C.S., Cetrone, J., Kharoutdinov, M., 2007. Cloud-resolving model simulations of KWAJEX: Model sensitivities and comparisons with satellite and radar observations. Journal of the Atmospheric Sciences 64, 1488–1508.

Boer, G.J., Hamilton, K., 2008. QBO influence on extratropical predictive skill. Climate Dynamics 31, 987–1000.

Bony, S., Emanuel, K.A., 2005. On the role of moist processes in tropical intraseasonal variability: Cloud–radiation and moisture–convection feedbacks. Journal of the Atmospheric Sciences 62, 2770–2789.

Boyd, J.P., 1976. The noninteraction of waves with the zonally averaged flow on a spherical earth and the interrelationships on eddy fluxes of energy, heat and momentum. Journal of the Atmospheric Sciences 33, 2285–2291.

Bretherton, C.S., Smolarkiewicz, P.K., 1989. Gravity waves, compensating subsidence and detrainment around cumulus clouds. Journal of the Atmospheric Sciences 46, 740–759.

Brewer, A.W., 1949. Evidence for a world circulation provided by the measurements of helium and water vapour distribution in the stratosphere. Quarterly Journal of the Royal Meteorological Society 75, 351–363. doi:10.1002/qj.49707532603.

Bushell, A., Anstey, J., Butchart, N., Kawatani, Y., Osprey, S., Richter, J., Serva, F., Braesicke, P., Cagnazzo, C., Chen, C.C., et al., 2019. Evaluation of the quasi-biennial oscillation in global climate models for the SPARC QBO-initiative. Quarterly Journal of the Royal Meteorological Society doi:https://doi.org/10.1002/qj.3765.

Butchart, N., 2014. The Brewer-Dobson circulation. Reviews of Geophysics 52, 157–184. doi:10.1002/2013RG000448.

Butchart, N., Anstey, J.A., Hamilton, K., Osprey, S., McLandress, C., Bushell, A.C., Kawatani, Y., Kim, Y.H., Lott, F., Scinocca, J., Stockdale, T.N., Andrews, M., Bellprat, O., Braesicke, P., Cagnazzo, C., Chen, C.C., Chun, H.Y., Dobrynin, M., Garcia, R.R., Garcia-Serrano, J., Gray, L.J., Holt, L., Kerzenmacher, T., Naoe, H., Pohlmann, H., Richter, J.H., Scaife, A.A., Schenzinger, V., Serva, F., Versick, S., Watanabe, S., Yoshida, K., Yukimoto, S., 2018. Overview of experiment design and comparison of models participating in phase 1 of the SPARC quasi-biennial oscillation initiative (QBOi). Geoscientific Model Development 11, 1009–1032. URL: https://www.geosci-model-dev.net/11/1009/2018/, doi:10.5194/gmd-11-1009-2018.

Camargo, S.J., Sobel, A.H., 2010. Revisiting the influence of the quasi-biennial oscillation on tropical cyclone activity. Journal of Climate 23, 5810–5825. doi:10.1175/2010JCLI3575.1.

Charlton, A.J., Polvani, L.M., 2007. A new look at stratospheric sudden warmings. Part I: Climatology and modeling benchmarks. Journal of Climate 20, 449–469. doi:10.1175/JCLI3996.1.

Charlton-Perez, A.J., Baldwin, M.P., Birner, T., Black, R.X., Butler, A.H., Calvo, N., Davis, N.A., Gerber, E.P., Gillett, N., Hardiman, S., Kim, J., Krüger, K., Lee, Y.Y., Manzini, E., McDaniel, B.A., Polvani, L., Reichler, T., Shaw, T.A., Sigmond, M., Son, S.W., Toohey, M., Wilcox, L., Yoden, S., Christiansen, B., Lott, F., Shindell, D., Yukimoto, S., Watanabe, S., 2013. On the lack of stratospheric dynamical variability in low-top versions of the CMIP5 models. Journal of Geophysical Research: Atmospheres 118, 2494–2505. doi:10.1002/jgrd.50125.

Charney, J.G., 1963. A note on large-scale motions in the tropics. Journal of the Atmospheric Sciences 20, 607–609.

Chipperfield, M.P., Bekki, S., Dhomse, S., Harris, N.R., Hassler, B., Hossaini, R., Steinbrecht, W., Thiéblemont, R., Weber, M., 2017. Detecting recovery of the stratospheric ozone layer. Nature 549, 211–218.

Chou, M.D., Suarez, M.J., 1999. A solar radiation parameterization (CLIRAD-SW) for atmospheric studies. NASA Tech. Memo 10460, 48.

Christiansen, B., Yang, S., Madsen, M.S., 2016. Do strong warm ENSO events control the phase of the stratospheric QBO? Geophysical Research Letters 43, 10,489–10,495. doi:10.1002/2016GL070751.

Chrysanthou, A., Maycock, A.C., Chipperfield, M.P., Dhomse, S., Garny, H., Kinnison, D., Akiyoshi, H., Deushi, M., Garcia, R.R., Jöckel, P., Kirner, O., Pitari, G., Plummer, D.A., Revell, L., Rozanov, E., Stenke, A., Tanaka, T.Y., Visioni, D., Yamashita, Y., 2019. The effect of atmospheric nudging on the stratospheric residual circulation in chemistry–climate models. Atmospheric Chemistry and Physics 19, 11559–11586. URL: https://www.atmos-chem-phys.net/19/11559/2019/, doi:10.5194/acp-19-11559-2019.

Claud, C., Terray, P., 2007. Revisiting the possible links between the quasi-biennial oscillation and the Indian summer monsoon using NCEP R-2 and CMAP fields. Journal of Climate 20, 773–787. doi:10.1175/JCLI4034.1.

Collimore, C.C., Hitchman, M.H., Martin, D.W., 1998. Is there a quasi-biennial oscillation in tropical deep convection? Geophysical Research Letters 25, 333–336. doi:10.1029/97GL03722.

Collimore, C.C., Martin, D.W., Hitchman, M.H., Huesmann, A., Waliser, D.E., 2003. On the relationship between the QBO and tropical deep convection. Journal of Climate 16, 2552–2568. doi:10.1175/1520-0442(2003)016<2552:OTRBTQ>2.0.CO;2.

Coy, L., Wargan, K., Molod, A.M., McCarty, W.R., Pawson, S., 2016. Structure and dynamics of the quasi-biennial oscillation in merra-2. Journal of Climate 29, 5339–5354. doi:10.1175/JCLI-D-15-0809.1.

Crueger, T., Stevens, B., 2015. The effect of atmospheric radiative heating by clouds on the Madden-Julian o scillation. Journal of Advances in Modeling Earth Systems 7, 854–864.

Crueger, T., Stevens, B., Brokopf, R., 2013. The Madden–Julian oscillation in ECHAM6 and the introduction of an objective MJO metric. Journal of Climate 26, 3241–3257.

Daleu, C.L., Plant, R.S., Woolnough, S.J., Sessions, S., Herman, M.J., Sobel, A., Wang, S., Kim, D., Cheng, A., Bellon, G., et al., 2015. Intercomparison of methods of coupling between convection and large-scale circulation: 1. Comparison over uniform surface conditions. Journal of Advances in Modeling Earth Systems 7, 1576–1601.

Daleu, C.L., Plant, R.S., Woolnough, S.J., Sessions, S., Herman, M.J., Sobel, A., Wang, S., Kim, D., Cheng, A., Bellon, G., et al., 2016. Intercomparison of methods of coupling between convection and large-scale circulation: 2. Comparison over nonuniform surface conditions. Journal of Advances in Modeling Earth Systems 8, 387–405.

Davis, S.M., Liang, C.K., Rosenlof, K.H., 2013. Interannual variability of tropical tropopause layer clouds. Geophysical Research Letters 40, 2862–2866.

Dee, D.P., Uppala, S.M., Simmons, A., Berrisford, P., Poli, P., Kobayashi, S., Andrae, U., Balmaseda, M., Balsamo, G., Bauer, d.P., et al., 2011. The ERA-Interim reanalysis: Configuration and performance of the data assimilation system. Quarterly Journal of the royal meteorological society 137, 553–597.

Densmore, C.R., Sanabia, E.R., Barrett, B.S., 2019. QBO influence on MJO amplitude over the Maritime Continent: Physical mechanisms and seasonality. Monthly Weather Review 147, 389–406.

Dobson, G.M.B., 1956. Origin and distribution of the polyatomic molecules in the atmosphere. Proceedings of the Royal Society of London. Series A. Mathematical and Physical Sciences 236, 187–193.

Dobson, G.M.B., Harrison, D., Lawrence, J., 1929. Measurements of the amount of ozone in the Earth's atmosphere and its relation to other geophysical conditions. Part III. Proceedings of the Royal Society of London. Series A, Containing Papers of a Mathematical and Physical Character 122, 456–486.

Domeisen, D.I., Garfinkel, C.I., Butler, A.H., 2019. The teleconnection of El Niño Southern Oscillation to the stratosphere. Reviews of Geophysics 57, 5–47. doi:10.1029/2018RG000596.

Douville, H., 2009. Stratospheric polar vortex influence on Northern Hemisphere winter climate variability. Geophysical Research Letters 36. doi:10.1029/2009GL039334.

Dunkerton, T.J., 1990. Annual variation of deseasonalized mean flow acceleration in the equatorial lower stratosphere. Journal of the Meteorological Society of Japan. Ser. II 68, 499–508. doi:10.2151/jmsj1965.68.4_499.

Dunkerton, T.J., 1997. The role of gravity waves in the quasi-biennial oscillation. Journal of Geophysical Research: Atmospheres 102, 26053–26076. doi:10.1029/96JD02999.

Dunkerton, T.J., Delisi, D.P., 1985. Climatology of the equatorial lower stratosphere. Journal of the Atmospheric Sciences 42, 376–396. doi:10.1175/1520-0469(1985)042<0376:COTELS>2.0.CO;2.

Durre, I., Vose, R.S., Wuertz, D.B., 2006. Overview of the integrated global radiosonde archive. Journal of Climate 19, 53–68.

Durre, I., Yin, X., 2008. Enhanced radiosonde data for studies of vertical structure. Bulletin of the American Meteorological Society 89, 1257–1262.

Ebdon, R., Veryard, R., 1961. Fluctuations in equatorial stratospheric winds. Nature 189, 791–793.

Edman, J.P., Romps, D.M., 2014. An improved weak pressure gradient scheme for single-column modeling. Journal of the Atmospheric Sciences 71, 2415–2429.

Edman, J.P., Romps, D.M., 2015. Self-consistency tests of large-scale dynamics parameterizations for single-column modeling. Journal of Advances in Modeling Earth Systems 7, 320–334.

Emanuel, K., Wing, A.A., Vincent, E.M., 2014. Radiative-convective instability. Journal of Advances in Modeling Earth Systems 6, 75–90.

Emanuel, K.A., 1987. An air-sea interaction model of intraseasonal oscillations in the tropics. Journal of the Atmospheric Sciences 44, 2324–2340.

Eyring, V., Bony, S., Meehl, G.A., Senior, C.A., Stevens, B., Stouffer, R.J., Taylor, K.E., 2016. Overview of the coupled model intercomparison project phase 6 (CMIP6) experimental design and organization. Geoscientific Model Development 9, 1937–1958. URL: https://www.geosci-model-dev.net/9/1937/2016/, doi:10.5194/gmd-9-1937-2016.

Feng, P.N., Lin, H., 2019. Modulation of the MJO-related teleconnections by the QBO. Journal of Geophysical Research: Atmospheres 124, 12022–12033. doi:10.1029/2019JD030878.

Flury, T., Wu, D.L., Read, W.G., 2013. Variability in the speed of the Brewer–Dobson circulation as observed by Aura/MLS. Atmospheric Chemistry and Physics 13, 4563–4575. URL: https://www.atmos-chem-phys.net/13/4563/2013/, doi:10.5194/acp-13-4563-2013.

Fuchs, Ž., Raymond, D.J., 2002. Large-scale modes of a nonrotating atmosphere with water vapor and cloud–radiation feedbacks. Journal of the Atmospheric Sciences 59, 1669–1679.

Fueglistaler, S., Dessler, A., Dunkerton, T., Folkins, I., Fu, Q., Mote, P.W., 2009. Tropical tropopause layer. Reviews of Geophysics 47.

Fujiwara, M., Vömel, H., Hasebe, F., Shiotani, M., Ogino, S.Y., Iwasaki, S., Nishi, N., Shibata, T., Shimizu, K., Nishimoto, E., Valverde Canossa, J.M., Selkirk, H.B., Oltmans, S.J., 2010. Seasonal to decadal variations of water vapor in the tropical lower stratosphere observed with balloon-borne cryogenic frost point hygrometers. Journal of Geophysical Research: Atmospheres 115. doi:10.1029/2010JD014179.

Fujiwara, M., Wright, J.S., Manney, G.L., Gray, L.J., Anstey, J., Birner, T., Davis, S., Gerber, E.P., Harvey, V.L., Hegglin, M.I., Homeyer, C.R., Knox, J.A., Krüger, K., Lambert, A., Long, C.S., Martineau, P., Molod, A., Monge-Sanz, B.M., Santee, M.L., Tegtmeier, S., Chabrillat, S., Tan, D.G.H., Jackson, D.R., Polavarapu, S., Compo, G.P., Dragani, R., Ebisuzaki, W., Harada, Y., Kobayashi, C., McCarty, W., Onogi, K., Pawson, S., Simmons, A., Wargan, K., Whitaker, J.S., Zou, C.Z., 2017. Introduction to the SPARC Reanalysis Intercomparison Project (S-RIP) and overview of the reanalysis systems. Atmospheric Chemistry and Physics 17, 1417–1452. URL: https://www.atmos-chem-phys.net/17/1417/2017/, doi:10.5194/acp-17-1417-2017.

Fulton, S.R., Schubert, W.H., 1985. Vertical normal mode transforms: Theory and application. Monthly Weather Review 113, 647–658.

Garfinkel, C.I., Feldstein, S.B., Waugh, D.W., Yoo, C., Lee, S., 2012. Observed connection between stratospheric sudden warmings and the Madden-Julian oscillation. Geophysical Research Letters 39. doi:10.1029/2012GL053144.

Garfinkel, C.I., Hartmann, D.L., 2007. Effects of the El Niño–Southern Oscillation and the quasi-biennial oscillation on polar temperatures in the stratosphere. Journal of Geophysical Research: Atmospheres 112. doi:10.1029/2007JD008481.

Garfinkel, C.I., Hartmann, D.L., 2011a. The influence of the quasi-biennial oscillation on the troposphere in winter in a hierarchy of models. Part I: Simplified dry GCMs. Journal of the Atmospheric Sciences 68, 1273–1289. doi:10.1175/2011JAS3665.1.

Garfinkel, C.I., Hartmann, D.L., 2011b. The influence of the quasi-biennial oscillation on the troposphere in winter in a hierarchy of models. Part II: Perpetual winter WACCM runs. Journal of the Atmospheric Sciences 68, 2026–2041. doi:10.1175/2011JAS3702.1.

Gates, W., 1992. AMIP: The Atmospheric Model Intercomparison Project. Program for Climate Model Diagnosis and Intercomparison: Revision 1. Technical Report. Lawrence Livermore National Lab., CA (United States).

Gelaro, R., McCarty, W., Suárez, M.J., Todling, R., Molod, A., Takacs, L., Randles, C.A., Darmenov, A., Bosilovich, M.G., Reichle, R., et al., 2017. The modern-era retrospective analysis for research and applications, version 2 (MERRA-2). Journal of Climate 30, 5419–5454.

Geller, M.A., Zhou, T., Yuan, W., 2016. The QBO, gravity waves forced by tropical convection, and ENSO. Journal of Geophysical Research: Atmospheres 121, 8886–8895. doi:10.1002/2015JD024125.

Gettelman, A., et al., 2002. A climatology of the tropical tropopause layer. Journal of the Meteorological Society of Japan. Ser. II 80, 911–924.

Gildor, H., Sobel, A.H., Cane, M.A., Sambrotto, R.N., 2003. A role for ocean biota in tropical intraseasonal atmospheric variability. Geophysical Research Letters 30. doi:10.1029/2002GL016759.

Gill, A.E., 1980. Some simple solutions for heat-induced tropical circulation. Quarterly Journal of the Royal Meteorological Society 106, 447–462.

Giorgetta, M., Manzini, E., Roeckner, E., Esch, M., Bengtsson, L., 2006. Climatology and forcing of the quasi-biennial oscillation in the MAECHAM5 model. Journal of Climate 19, 3882–3901.

Giorgetta, M.A., Bengtsson, L., Arpe, K., 1999. An investigation of QBO signals in the east Asian and Indian monsoon in GCM experiments. Climate Dynamics 15, 435–450.

Gottschalck, J., Wheeler, M., Weickmann, K., Vitart, F., Savage, N., Lin, H., Hendon, H., Waliser, D., Sperber, K., Nakagawa, M., et al., 2010. A framework for assessing operational Madden–Julian oscillation forecasts: A CLIVAR MJO working group project. Bulletin of the American Meteorological Society 91, 1247–1258.

Grabowski, W.W., Wu, X., Moncrieff, M.W., 1996. Cloud-resolving modeling of tropical cloud systems during Phase III of GATE. Part I: Two-dimensional experiments. Journal of the Atmospheric Sciences 53, 3684–3709.

Gray, L.J., 2013. Stratospheric Equatorial Dynamics. American Geophysical Union (AGU). pp. 93–107. doi:10.1002/9781118666630.ch5.

Gray, L.J., Anstey, J.A., Kawatani, Y., Lu, H., Osprey, S., Schenzinger, V., 2018. Surface impacts of the quasi-biennial oscillation. Atmospheric Chemistry and Physics 18, 8227–8247. URL: https://www.atmos-chem-phys.net/18/8227/2018/, doi:10.5194/acp-18-8227-2018.

Gray, L.J., Pyle, J.A., 1989. A two-dimensional model of the quasi-biennial oscillation of ozone. Journal of the Atmospheric Sciences 46, 203–220. doi:10.1175/1520-0469(1989)046<0203:ATDMOT>2.0.CO;2.

Gray, W.M., 1984a. Atlantic seasonal hurricane frequency. Part I: El Niño and 30 mb quasi-biennial oscillation influences. Monthly Weather Review 112, 1649–1668. doi:10.1175/1520-0493(1984)112<1649:ASHFPI>2.0.CO;2.

Gray, W.M., 1984b. Atlantic seasonal hurricane frequency. Part II: Forecasting its variability. Monthly Weather Review 112, 1669–1683. doi:10.1175/1520-0493(1984)112<1669:ASHFPI>2.0.CO;2.

Gray, W.M., Sheaffer, J.D., Knaff, J.A., 1992a. Hypothesized mechanism for stratospheric QBO influence on ENSO variability. Geophysical Research Letters 19, 107–110. doi:10.1029/91GL02950.

Gray, W.M., Sheaffer, J.D., Knaff, J.A., 1992b. Influence of the stratospheric QBO on ENSO variability. Journal of the Meteorological Society of Japan. Ser. II 70, 975–995. doi:10.2151/jmsj1965.70.5_975.

Guan, B., Waliser, D.E., Molotch, N.P., Fetzer, E.J., Neiman, P.J., 2012. Does the Madden–Julian oscillation influence wintertime atmospheric rivers and snowpack in the Sierra Nevada? Monthly Weather Review 140, 325–342.

Haigh, J.D., Blackburn, M., Day, R., 2005. The response of tropospheric circulation to perturbations in lower-stratospheric temperature. Journal of Climate 18, 3672–3685. doi:10.1175/JCLI3472.1.

Ham, Y.G., Kim, J.H., Luo, J.J., 2019. Deep learning for multi-year ENSO forecasts. Nature 573, 568–572.

Hamilton, K., 1998. Observations of tropical stratospheric winds before World War ii. Bulletin of the American Meteorological Society 79, 1367–1372. doi:10.1175/1520-0477(1998)079<1367:OOTSWB>2.0.CO;2.

Hand, E., 2015. The storm king. doi:10.1126/science.350.6256.22.

Hannah, W.M., Maloney, E.D., 2014. The moist static energy budget in NCAR CAM5 hindcasts during DYNAMO. Journal of Advances in Modeling Earth Systems 6, 420–440.

Hartmann, D.L., Holton, J.R., Fu, Q., 2001. The heat balance of the tropical tropopause, cirrus, and stratospheric dehydration. Geophysical research letters 28, 1969–1972.

Haynes, P.H., 1998. The latitudinal structure of the quasi-biennial oscillation. Quarterly Journal of the Royal Meteorological Society 124, 2645–2670. doi:10.1002/qj.49712455206.

Held, I.M., Hoskins, B.J., 1985. Large-scale eddies and the general circulation of the troposphere, in: Advances in geophysics. Elsevier. volume 28, pp. 3–31.

Hendon, H.H., 2000. Impact of air–sea coupling on the Madden–Julian oscillation in a general circulation model. Journal of the Atmospheric Sciences 57, 3939–3952.

Hendon, H.H., Abhik, S., 2018. Differences in vertical structure of the Madden-Julian oscillation associated with the quasi-biennial oscillation. Geophysical Research Letters 45, 4419–4428.

Hendon, H.H., Zhang, C., Glick, J.D., 1999. Interannual variation of the Madden–Julian oscillation during austral summer. Journal of Climate 12, 2538–2550. doi:10.1175/1520-0442(1999)012<2538:IVOTMJ>2.0.CO;2.

Herman, M.J., Raymond, D.J., 2014. WTG cloud modeling with spectral decomposition of heating. Journal of Advances in Modeling Earth Systems 6, 1121–1140.

Hersbach, H., Bell, W., Berrisford, P., Horányi, A., J., M.S., Nicolas, J., Radu, R., Schepers, D., Simmons, A., Soci, C., Dee, D., 2019. Global reanalysis: goodbye ERA-Interim, hello ERA5 , 17–24URL: https://www.ecmwf.int/node/19027, doi:10.21957/vf291hehd7.

Higgins, R.W., Schemm, J.K.E., Shi, W., Leetmaa, A., 2000. Extreme precipitation events in the Western United States related to tropical forcing. Journal of Climate 13, 793–820. doi:10.1175/1520-0442(2000)013<0793:EPEITW>2.0.CO;2.

Hitchcock, P., Simpson, I.R., 2014. The downward influence of stratospheric sudden warmings. Journal of the Atmospheric Sciences 71, 3856–3876. doi:10.1175/JAS-D-14-0012.1.

Ho, C.H., Kim, H.S., Jeong, J.H., Son, S.W., 2009. Influence of stratospheric quasi-biennial oscillation on tropical cyclone tracks in the western North Pacific. Geophysical Research Letters 36. doi:10.1029/2009GL037163.

Holloway, C.E., Neelin, J.D., 2007. The convective cold top and quasi equilibrium. Journal of the Atmospheric Sciences 64, 1467–1487.

Holton, J.R., Gettelman, A., 2001. Horizontal transport and the dehydration of the stratosphere. Geophysical Research Letters 28, 2799–2802. doi:10.1029/2001GL013148.

Holton, J.R., Haynes, P.H., McIntyre, M.E., Douglass, A.R., Rood, R.B., Pfister, L., 1995. Stratosphere-troposphere exchange. Reviews of Geophysics 33, 403–439. doi:10.1029/95RG02097.

Holton, J.R., Lindzen, R.S., 1972. An updated theory for the quasi-biennial cycle of the tropical stratosphere. Journal of the Atmospheric Sciences 29, 1076–1080. doi:10.1175/1520-0469(1972)029<1076:AUTFTQ>2.0.CO;2.

Holton, J.R., Tan, H.C., 1980. The influence of the equatorial quasi-biennial oscillation on the global circulation at 50 mb. Journal of the Atmospheric Sciences 37, 2200–2208. doi:10.1175/1520-0469(1980)037<2200:TIOTEQ>2.0.CO;2.

Holton, J.R., Tan, H.C., 1982. The quasi-biennial oscillation in the Northern Hemisphere lower stratosphere. Journal of the Meteorological Society of Japan. Ser. II 60, 140–148. doi:10.2151/jmsj1965.60.1_140.

Hong, S.Y., Noh, Y., Dudhia, J., 2006. A new vertical diffusion package with an explicit treatment of entrainment processes. Monthly Weather Review 134, 2318–2341.

Hong, Y., Liu, G., Li, J.L., 2016. Assessing the radiative effects of global ice clouds based on CloudSat and CALIPSO measurements. Journal of Climate 29, 7651–7674.

Hood, L.L., 2017. QBO/solar modulation of the boreal winter Madden-Julian oscillation: A prediction for the coming solar minimum. Geophysical Research Letters 44, 3849–3857.

Hood, L.L., Redman, M.A., Johnson, W.L., Galarneau, T.J., 2020. Stratospheric influences on the MJO-induced Rossby wave train: Effects on intraseasonal climate. Journal of Climate 33, 365–389. doi:10.1175/JCLI-D-18-0811.1.

Huang, B., Hu, Z.Z., Kinter, J.L., Wu, Z., Kumar, A., 2012. Connection of stratospheric QBO with global atmospheric general circulation and tropical SST. Part I: Methodology and composite life cycle. Climate Dynamics 38, 1–23.

Huesmann, A.S., Hitchman, M.H., 2001. The stratospheric quasi-biennial oscillation in the NCEP reanalyses: Climatological structures. Journal of Geophysical Research: Atmospheres 106, 11859–11874. doi:10.1029/2001JD900031.

Hung, M.P., Lin, J.L., Wang, W., Kim, D., Shinoda, T., Weaver, S.J., 2013. MJO and convectively coupled equatorial waves simulated by CMIP5 climate models. Journal of Climate 26, 6185–6214. doi:10.1175/JCLI-D-12-00541.1.

Iacono, M.J., Delamere, J.S., Mlawer, E.J., Shephard, M.W., Clough, S.A., Collins, W.D., 2008. Radiative forcing by long-lived greenhouse gases: Calculations with the AER radiative transfer models. Journal of Geophysical Research: Atmospheres 113.

Inness, P.M., Slingo, J.M., 2003. Simulation of the Madden–Julian oscillation in a coupled general circulation model. Part I: Comparison with observations and an atmosphere-only GCM. Journal of Climate 16, 345–364.

Jensen, E.J., Diskin, G., Lawson, R.P., Lance, S., Bui, T.P., Hlavka, D., McGill, M., Pfister, L., Toon, O.B., Gao, R., 2013. Ice nucleation and dehydration in the tropical tropopause layer. Proceedings of the National Academy of Sciences 110, 2041–2046. doi:10.1073/pnas.1217104110.

Jeuken, A., Siegmund, P., Heijboer, L., Feichter, J., Bengtsson, L., 1996. On the potential of assimilating meteorological analyses in a global climate model for the purpose of model validation. Journal of Geophysical Research: Atmospheres 101, 16939–16950.

Jiang, X., Adames, Á.F., Zhao, M., Waliser, D., Maloney, E., 2018. A unified moisture mode framework for seasonality of the Madden–Julian oscillation. Journal of Climate 31, 4215–4224.

Johnson, R.H., Ciesielski, P.E., 2013. Structure and properties of Madden–Julian oscillations deduced from DYNAMO sounding arrays. Journal of the Atmospheric Sciences 70, 3157–3179.

Johnson, R.H., Ciesielski, P.E., Ruppert Jr, J.H., Katsumata, M., 2015. Sounding-based thermodynamic budgets for DYNAMO. Journal of the Atmospheric Sciences 72, 598–622.

Johnson, S.J., Stockdale, T.N., Ferranti, L., Balmaseda, M.A., Molteni, F., Magnusson, L., Tietsche, S., Decremer, D., Weisheimer, A., Balsamo, G., et al., 2019. SEAS5: the new ECMWF seasonal forecast system. Geoscientific Model Development 12.

Jones, C., Carvalho, L.M.V., 2002. Active and break phases in the South American monsoon system. Journal of Climate 15, 905–914. doi:10.1175/1520-0442(2002)015<0905:AABPIT>2.0.CO;2.

Jones, D.B., Schneider, H.R., McElroy, M.B., 1998. Effects of the quasi-biennial oscillation on the zonally averaged transport of tracers. Journal of Geophysical Research: Atmospheres 103, 11235–11249.

Jucker, M., Gerber, E.P., 2017. Untangling the annual cycle of the tropical tropopause layer with an idealized moist model. Journal of Climate 30, 7339–7358. doi:10.1175/JCLI-D-17-0127.1.

Jung, T., Miller, M.J., Palmer, T.N., 2010. Diagnosing the origin of extended-range forecast errors. Monthly Weather Review 138, 2434–2446. doi:10.1175/2010MWR3255.1.

Kalnay, E., Kanamitsu, M., Kistler, R., Collins, W., Deaven, D., Gandin, L., Iredell, M., Saha, S., White, G., Woollen, J., et al., 1996. The NCEP/NCAR 40-year reanalysis project. Bulletin of the American meteorological Society 77, 437–472.

Kang, I.S., Kim, H.M., 2010. Assessment of MJO predictability for boreal winter with various statistical and dynamical models. Journal of Climate 23, 2368–2378.

Kang, I.S., Liu, F., Ahn, M.S., Yang, Y.M., Wang, B., 2013. The role of SST structure in convectively coupled Kelvin–Rossby waves and its implications for MJO formation. Journal of Climate 26, 5915–5930. doi:10.1175/JCLI-D-12-00303.1.

Kang, W., Tziperman, E., 2018. The MJO-SSW teleconnection: Interaction between MJO-forced waves and the midlatitude jet. Geophysical Research Letters 45, 4400–4409. doi:10.1029/2018GL077937.

Kelley, M., Schmidt, G.A., Nazarenko, L., Miller, R.L., Bauer, S.E., Ruedy, R., Russell, G.L., Aleinov, I., Bauer, M., Bleck, R., Canuto, V., Cesana, G., Cheng, Y., Clune, T.L., Cook, B., Cruz, C.A., Del Genio, A.D., Elsaesser, G.S., Faluvegi, G., Kiang, N.Y., Kim, D., Lacis, A.A., Leboissetier, A., LeGrande, A.N., Lo, K.K., Marshall, J.C., McDermid, S., Matthews, E.E., Mezuman, K., Murray, L.T., Oinas, V., Orbe, C., Pérez García-Pando, C., Perlwitz, J.P., Puma, M.J., Rind, D., Romanou, A., Shindell, D.T., Sun, S., Tausnev, N., Tsigaridis, K., Tselioudis, G., Weng, E., Wu, J., Yao, M., 2019. GISS-E2.1: Configurations and climatology. *Manuscript submitted for publication*.

Khouider, B., Majda, A.J., 2006. A simple multicloud parameterization for convectively coupled tropical waves. Part I: Linear analysis. Journal of the Atmospheric Sciences 63, 1308–1323.

Khouider, B., Majda, A.J., 2007. A simple multicloud parameterization for convectively coupled tropical waves. Part II: Nonlinear simulations. Journal of the Atmospheric Sciences 64, 381–400.

Kiladis, G.N., Dias, J., Straub, K.H., Wheeler, M.C., Tulich, S.N., Kikuchi, K., Weickmann, K.M., Ventrice, M.J., 2014. A comparison of OLR and circulation-based indices for tracking the MJO. Monthly Weather Review 142, 1697–1715.

Kiladis, G.N., Wheeler, M.C., Haertel, P.T., Straub, K.H., Roundy, P.E., 2009. Convectively coupled equatorial waves. Reviews of Geophysics 47. doi:10.1029/2008RG000266.

Kim, D., Ahn, M.S., Kang, I.S., Del Genio, A.D., 2015. Role of longwave cloud–radiation feedback in the simulation of the Madden–Julian oscillation. Journal of Climate 28, 6979–6994. doi:10.1175/JCLI-D-14-00767.1.

Kim, D., Maloney, E.D., 2016. Simulation of the Madden-Julian Oscillation Using General Circulation Models. chapter Chapter 9. pp. 119–130. doi:10.1142/9789813200913_0009.

Kim, D., Sobel, A.H., Del Genio, A.D., Chen, Y., Camargo, S.J., Yao, M.S., Kelley, M., Nazarenko, L., 2012. The tropical subseasonal variability simulated in the NASA GISS general circulation model. Journal of Climate 25, 4641–4659.

Kim, D., Sobel, A.H., Kang, I.S., 2011a. A mechanism denial study on the Madden-Julian oscillation. Journal of Advances in Modeling Earth Systems 3.

Kim, D., Sobel, A.H., Maloney, E.D., Frierson, D.M.W., Kang, I.S., 2011b. A systematic relationship between intraseasonal variability and mean state bias in AGCM simulations. Journal of Climate 24, 5506–5520. doi:10.1175/2011JCLI4177.1.

Kim, H., Caron, J., Richter, J., Simpson, I., 2020a. QBO-MJO connection in CMIP6 models. *submitted to Geophys. Res. Lett.* .

Kim, H., Richter, J.H., Martin, Z., 2019. Insignificant QBO-MJO prediction skill relationship in the SubX and S2S subseasonal reforecasts. Journal of Geophysical Research: Atmospheres 124, 12655–12666.

Kim, H., Son, S.W., Yoo, C., 2020b. QBO modulation of the MJO-related precipitation in East Asia. Journal of Geophysical Research: Atmospheres 125, e2019JD031929. doi:10.1029/2019JD031929.

Kim, H., Vitart, F., Waliser, D.E., 2018. Prediction of the Madden–Julian oscillation: A review. Journal of Climate 31, 9425–9443. doi:10.1175/JCLI-D-18-0210.1.

Kinnersley, J.S., 1999. Seasonal asymmetry of the low-and middle-latitude QBO circulation anomaly. Journal of the atmospheric sciences 56, 1140–1153.

Kinnersley, J.S., Tung, K.K., 1998. Modeling the global interannual variability of ozone due to the equatorial QBO and to extratropical planetary wave variability. Journal of the atmospheric sciences 55, 1417–1428.

Kinnersley, J.S., Tung, K.K., 1999. Mechanisms for the extratropical qbo in circulation and ozone. Journal of the atmospheric sciences 56, 1942–1962.

Kirtman, B.P., Min, D., Infanti, J.M., Kinter, J.L., Paolino, D.A., Zhang, Q., van den Dool, H., Saha, S., Mendez, M.P., Becker, E., Peng, P., Tripp, P., Huang, J., DeWitt, D.G., Tippett, M.K., Barnston, A.G., Li, S., Rosati, A., Schubert, S.D., Rienecker, M., Suarez, M., Li, Z.E., Marshak, J., Lim, Y.K., Tribbia, J., Pegion, K., Merryfield, W.J., Denis, B., Wood, E.F., 2014. The North American multimodel ensemble: Phase-1 seasonal-to-interannual prediction; Phase-2 toward developing intraseasonal prediction. Bulletin of the American Meteorological Society 95, 585–601. doi:10.1175/BAMS-D-12-00050.1.

Kistler, R., Kalnay, E., Collins, W., Saha, S., White, G., Woollen, J., Chelliah, M., Ebisuzaki, W., Kanamitsu, M., Kousky, V., et al., 2001. The NCEP–NCAR 50-year reanalysis: monthly means CD-ROM and documentation. Bulletin of the American Meteorological society 82, 247–268.

Klemp, J., Dudhia, J., Hassiotis, A., 2008. An upper gravity-wave absorbing layer for NWP applications. Monthly Weather Review 136, 3987–4004.

Klingaman, N.P., Woolnough, S.J., 2014. The role of air–sea coupling in the simulation of the Madden–Julian oscillation in the Hadley Centre model. Quarterly Journal of the Royal Meteorological Society 140, 2272–2286. doi:10.1002/qj.2295.

Klotzbach, P., Abhik, S., Hendon, H., Bell, M., Lucas, C., Marshall, A., Oliver, E., 2019. On the emerging relationship between the stratospheric quasi-biennial oscillation and the Madden-Julian oscillation. Scientific reports 9, 1–9.

Klotzbach, P.J., 2007a. Recent developments in statistical prediction of seasonal Atlantic basin tropical cyclone activity. Tellus A: Dynamic Meteorology and Oceanography 59, 511–518.

Klotzbach, P.J., 2007b. Revised prediction of seasonal Atlantic basin tropical cyclone activity from 1 August. Weather and Forecasting 22, 937–949. doi:10.1175/WAF1045.1.

Knaff, J.A., 1993. Evidence of a stratospheric QBO modulation of tropical convection. M.S. Thesis, Coloardo State Univ. Paper No. 520.

Kobayashi, C., Endo, H., Ota, Y., Kobayashi, S., Onoda, H., Harada, Y., Onogi, K., Kamahori, H., 2014. Preliminary results of the JRA-55C, an atmospheric reanalysis assimilating conventional observations only. Sola 10, 78–82.

Kobayashi, S., Ota, Y., Harada, Y., Ebita, A., Moriya, M., Onoda, H., Onogi, K., Kamahori, H., Kobayashi, C., Endo, H., Miyaoka, K., Takahashi, K., 2015. The JRA-55 reanalysis: General specifications and basic characteristics. Journal of the Meteorological Society of Japan. Ser. II 93, 5–48. doi:10.2151/jmsj.2015-001.

Kuang, Z., 2008. Modeling the interaction between cumulus convection and linear gravity waves using a limited-domain cloud system–resolving model. Journal of the Atmospheric Sciences 65, 576–591.

Kuma, K.I., 1990. A quasi-biennial oscillation in the intensity of the intra-seasonal oscillation. International Journal of Climatology 10, 263–278.

Labitzke, K., Loon, H.V., 1988. Associations between the 11-year solar cycle, the QBO and the atmosphere. Part I: The troposphere and stratosphere in the northern hemisphere in winter. Journal of Atmospheric and Terrestrial Physics 50, 197 – 206. doi:https://doi.org/10.1016/0021-9169(88)90068-2.

Lau, K., Peng, L., 1987. Origin of low-frequency (intraseasonal) oscillations in the tropical atmosphere. Part I: Basic theory. Journal of the Atmospheric Sciences 44, 950–972.

Lau, W.K., Waliser, D.E., Sperber, K., Slingo, J., Inness, P., 2012. Modeling intraseasonal variability, in: Intraseasonal Variability in the Atmosphere-Ocean Climate System. Springer, pp. 399–431.

Lavender, S.L., Matthews, A.J., 2009. Response of the West African monsoon to the Madden–Julian oscillation. Journal of Climate 22, 4097–4116. doi:10.1175/2009JCLI2773.1.

Lawrence, D.M., Webster, P.J., 2002. The boreal summer intraseasonal oscillation: Relationship between northward and eastward movement of convection. Journal of the Atmospheric Sciences 59, 1593–1606.

Lee, J.C., Klingaman, N.P., 2018. The effect of the quasi-biennial oscillation on the Madden–Julian oscillation in the Met Office Unified Model Global Ocean Mixed Layer configuration. Atmospheric Science Letters 19, e816.

Li, X., Janiga, M.A., Wang, S., Tao, W.K., Rowe, A., Xu, W., Liu, C., Matsui, T., Zhang, C., 2018. Evolution of precipitation structure during the November DYNAMO MJO event: Cloud-resolving model intercomparison and cross validation using radar observations. Journal of Geophysical Research: Atmospheres 123, 3530–3555.

Liebmann, B., Hartmann, D.L., 1984. An observational study of tropical–midlatitude interaction on intraseasonal time scales during winter. Journal of the Atmospheric Sciences 41, 3333–3350. doi:10.1175/1520-0469(1984)041<3333:AOSOTI>2.0.CO;2.

Liebmann, B., Smith, C.A., 1996. Description of a complete (interpolated) outgoing longwave radiation dataset. Bulletin of the American Meteorological Society 77, 1275–1277.

Liess, S., Bengtsson, L., Arpe, K., 2004. The intraseasonal oscillation in ECHAM4 Part I: coupled to a comprehensive ocean model. Climate Dynamics 22, 653–669.

Liess, S., Geller, M.A., 2012. On the relationship between QBO and distribution of tropical deep convection. Journal of Geophysical Research: Atmospheres 117. doi:10.1029/2011JD016317.

Lim, Y., Son, S.W., Marshall, A.G., Hendon, H.H., Seo, K.H., 2019. Influence of the QBO on MJO prediction skill in the subseasonal-to-seasonal prediction models. Climate Dynamics 53, 1681–1695.

Lin, P., Paynter, D., Ming, Y., Ramaswamy, V., 2017. Changes of the tropical tropopause layer under global warming. Journal of Climate 30, 1245–1258.

Lindzen, R.S., 1990. Dynamics in Atmospheric Physics. Cambridge University Press, Cambridge.

Lindzen, R.S., Holton, J.R., 1968. A theory of the quasi-biennial oscillation. Journal of the Atmospheric Sciences 25, 1095–1107. doi:10.1175/1520-0469(1968)025<1095:ATOTQB>2.0.CO;2.

Liu, F., Wang, B., 2013. An air–sea coupled skeleton model for the Madden–Julian oscillation. Journal of the Atmospheric Sciences 70, 3147–3156.

Löffler, M., Brinkop, S., Jöckel, P., 2016. Impact of major volcanic eruptions on stratospheric water vapour. Atmospheric Chemistry and Physics (ACP) 16, 6547–6562.

van Loon, H., Labitzke, K., 1987. The Southern Oscillation. Part V: The anomalies in the lower stratosphere of the northern hemisphere in winter and a comparison with the quasi-biennial oscillation. Monthly Weather Review 115, 357–369. doi:10.1175/1520-0493(1987)115<0357:TSOPVT>2.0.CO;2.

Lu, H., Bracegirdle, T.J., Phillips, T., Bushell, A., Gray, L., 2014. Mechanisms for the Holton-Tan relationship and its decadal variation. Journal of Geophysical Research: Atmospheres 119, 2811–2830. doi:10.1002/2013JD021352.

Ma, Z., Fei, J., Huang, X., Cheng, X., 2015. A potential problem with the application of moist static energy in tropical cyclone studies. Journal of the Atmospheric Sciences 72, 3009–3019. doi:10.1175/JAS-D-14-0367.1.

Madden, R.A., 1986. Seasonal variations of the 40-50 day oscillation in the tropics. Journal of the Atmospheric Sciences 43, 3138–3158. doi:10.1175/1520-0469(1986)043<3138:SVOTDO>2.0.CO;2.

Madden, R.A., Julian, P.R., 1971. Detection of a 40–50 day oscillation in the zonal wind in the tropical Pacific. Journal of the Atmospheric Sciences 28, 702–708.

Madden, R.A., Julian, P.R., 1972. Description of global-scale circulation cells in the tropics with a 40–50 day period. Journal of the Atmospheric Sciences 29, 1109–1123. doi:10.1175/1520-0469(1972)029<1109:DOGSCC>2.0.CO;2.

Madden, R.A., Julian, P.R., 1994. Observations of the 40–50-day tropical oscillation — A review. Monthly Weather Review 122, 814–837.

Majda, A.J., Biello, J.A., 2004. A multiscale model for tropical intraseasonal oscillations. Proceedings of the National Academy of Sciences 101, 4736–4741.

Majda, A.J., Stechmann, S.N., 2009. The skeleton of tropical intraseasonal oscillations. Proceedings of the National Academy of Sciences 106, 8417–8422.

Maloney, E.D., Adames, Á.F., Bui, H.X., 2019. Madden–Julian oscillation changes under anthropogenic warming. Nature Climate Change 9, 26–33.

Maloney, E.D., Hartmann, D.L., 2000. Modulation of hurricane activity in the Gulf of Mexico by the Madden-Julian oscillation. Science 287, 2002–2004.

Maloney, E.D., Hartmann, D.L., 2001. The Madden–Julian oscillation, barotropic dynamics, and North Pacific tropical cyclone formation. Part I: Observations. Journal of the Atmospheric Sciences 58, 2545–2558.

Mapes, B.E., 2004. Sensitivities of cumulus-ensemble rainfall in a cloud-resolving model with parameterized large-scale dynamics. Journal of the Atmospheric Sciences 61, 2308–2317.

Mapes, B.E., Zuidema, P., 1996. Radiative-dynamical consequences of dry tongues in the tropical troposphere. Journal of the Atmospheric Sciences 53, 620–638.

Marshall, A.G., Hendon, H.H., Son, S.W., Lim, Y., 2017. Impact of the quasi-biennial oscillation on predictability of the Madden–Julian oscillation. Climate Dynamics 49, 1365–1377.

Martin, Z., Vitart, F., Wang, S., Sobel, A., 2020. The impact of the stratosphere on the MJO in a forecast model. Journal of Geophysical Research: Atmospheres 125, e2019JD032106. doi:10.1029/2019JD032106.

Martin, Z., Wang, S., Nie, J., Sobel, A., 2019. The impact of the QBO on MJO convection in cloud-resolving simulations. Journal of the Atmospheric Sciences 76, 669–688.

Maruyama, T., 1997. The quasi-biennial oscillation (QBO) and equatorial waves. Papers in Meteorology and Geophysics 48, 1–17. doi:10.2467/mripapers.48.1.

Maruyama, T., Yanai, M., 1967. Evidence of large-scale wave disturbances in the equatorial lower stratosphere. Journal of the Meteorological Society of Japan. Ser. II 45, 196–199.

Matsui, T., Tao, W., Shi, R., 2007. Goddard radiation and aerosol direct effect in Goddard WRF, in: NASA/UMD WRF Workshop.

Matsuno, T., 1966. Quasi-geostrophic motions in the equatorial area. Journal of the Meteorological Society of Japan. Ser. II 44, 25–43.

Matsuno, T., 1971. A dynamical model of the stratospheric sudden warming. Journal of the Atmospheric Sciences 28, 1479–1494. doi:10.1175/1520-0469(1971)028<1479:ADMOTS>2.0.CO;2.

Mayer, K.J., Barnes, E.A., 2019. Subseasonal midlatitude prediction skill following QBO-MJO activity. Weather and Climate Dynamics Discussions 2019, 1–21. URL: http://www.weather-clim-dynam-discuss.net/wcd-2019-13/, doi:10.5194/wcd-2019-13.

Morrison, H., Thompson, G., Tatarskii, V., 2009. Impact of cloud microphysics on the development of trailing stratiform precipitation in a simulated squall line: Comparison of one-and two-moment schemes. Monthly Weather Review 137, 991–1007.

Mundhenk, B.D., Barnes, E.A., Maloney, E.D., Baggett, C.F., 2018. Skillful empirical subseasonal prediction of landfalling atmospheric river activity using the Madden–Julian oscillation and quasi-biennial oscillation. NPJ Climate and Atmospheric Science 1, 1–7.

Neelin, J.D., Yu, J.Y., 1994. Modes of tropical variability under convective adjustment and the Madden–Julian oscillation. Part I: Analytical theory. Journal of the Atmospheric Sciences 51, 1876–1894.

Neu, J.L., Flury, T., Manney, G.L., Santee, M.L., Livesey, N.J., Worden, J., 2014. Tropospheric ozone variations governed by changes in stratospheric circulation. Nature Geoscience 7, 340–344.

Newchurch, M., Yang, E.S., Cunnold, D., Reinsel, G.C., Zawodny, J., Russell III, J.M., 2003. Evidence for slowdown in stratospheric ozone loss: First stage of ozone recovery. Journal of Geophysical Research: Atmospheres 108.

Nie, J., Sobel, A.H., 2015. Responses of tropical deep convection to the QBO: Cloud-resolving simulations. Journal of the Atmospheric Sciences 72, 3625–3638. doi:10.1175/JAS-D-15-0035.1.

Nishimoto, E., Yoden, S., 2017. Influence of the stratospheric quasi-biennial oscillation on the Madden–Julian oscillation during austral summer. Journal of the Atmospheric Sciences 74, 1105–1125.

Niwano, M., Yamazaki, K., Shiotani, M., 2003. Seasonal and QBO variations of ascent rate in the tropical lower stratosphere as inferred from UARS HALOE trace gas data. Journal of Geophysical Research: Atmospheres 108. doi:10.1029/2003JD003871.

Orbe, C., Roekel, L.V., Adames, Á.F., Danabasoglu, G., Dezfuli, A., Fasullo, J., Gleckler, P.J., Lee, J., Li, W., Nazarenko, L., Schmidt, G.A., Sperber, K.R., Zhao, M., 2020. Representation of modes of variability in 6 U.S. climate models. J. Climate Submitted (see https://pubs.giss.nasa.gov/abs/or01200v.html).

Osprey, S.M., Butchart, N., Knight, J.R., Scaife, A.A., Hamilton, K., Anstey, J.A., Schenzinger, V., Zhang, C., 2016. An unexpected disruption of the atmospheric quasi-biennial oscillation. Science 353, 1424–1427. doi:10.1126/science.aah4156.

Pegion, K., Kirtman, B.P., Becker, E., Collins, D.C., LaJoie, E., Burgman, R., Bell, R., DelSole, T., Min, D., Zhu, Y., Li, W., Sinsky, E., Guan, H., Gottschalck, J., Metzger, E.J., Barton, N.P., Achuthavarier, D., Marshak, J., Koster, R.D., Lin, H., Gagnon, N., Bell, M., Tippett, M.K., Robertson, A.W., Sun, S., Benjamin, S.G., Green, B.W., Bleck, R., Kim, H., 2019. The Subseasonal Experiment (SubX): A multimodel subseasonal prediction experiment. Bulletin of the American Meteorological Society 100, 2043–2060. doi:10.1175/BAMS-D-18-0270.1.

Peña-Ortiz, C., Ribera, P., García-Herrera, R., Giorgetta, M., García, R., 2008. Forcing mechanism of the seasonally asymmetric quasi-biennial oscillation secondary circulation in ERA-40 and MAECHAM5. Journal of Geophysical Research: Atmospheres 113.

Phillips, N.A., 1994. Jule Gregory Charney, in: Biographical Memoirs: Volume 65 - National Academy of Sciences. National Academies Press, pp. 81–113.

Plumb, R., McEwan, A., 1978. The instability of a forced standing wave in a viscous stratified fluid: A laboratory analogue of the quasi-biennial oscillation. Journal of the Atmospheric Sciences 35, 1827–1839.

Plumb, R.A., 1977. The interaction of two internal waves with the mean flow: Implications for the theory of the quasi-biennial oscillation. Journal of the Atmospheric Sciences 34, 1847–1858. doi:10.1175/1520-0469(1977)034<1847:TIOTIW>2.0.CO;2.

Plumb, R.A., 1996. A "tropical pipe" model of stratospheric transport. Journal of Geophysical Research: Atmospheres 101, 3957–3972. doi:10.1029/95JD03002.

Plumb, R.A., Bell, R.C., 1982. A model of hte quasi-biennial oscillation on an equatorial beta-plane. Quarterly Journal of the Royal Meteorological Society 108, 335–352.

Polvani, L.M., Kushner, P.J., 2002. Tropospheric response to stratospheric perturbations in a relatively simple general circulation model. Geophysical Research Letters 29, 18–1–18–4. doi:10.1029/2001GL014284.

Pritchard, M.S., Bretherton, C.S., 2014. Causal evidence that rotational moisture advection is critical to the superparameterized Madden–Julian oscillation. Journal of the Atmospheric Sciences 71, 800–815.

Quiroz, R.S., 1983. Relationships among the stratospheric and tropospheric zonal flows and the Southern Oscillation. Monthly Weather Review 111, 143–154. doi:10.1175/1520-0493(1983)111<0143:RATSAT>2.0.CO;2.

Rajendran, K., Moroz, I.M., Read, P.L., Osprey, S.M., 2016. Synchronisation of the equatorial QBO by the annual cycle in tropical upwelling in a warming climate. Quarterly Journal of the Royal Meteorological Society 142, 1111–1120.

Randel, W.J., Jensen, E.J., 2013. Physical processes in the tropical tropopause layer and their roles in a changing climate. Nature Geoscience 6, 169–176.

Rao, J., Yu, Y., Guo, D., Shi, C., Chen, D., Hu, D., 2019. Evaluating the Brewer–Dobson circulation and its responses to ENSO, QBO, and the solar cycle in different reanalyses. Earth and Planetary Physics 3, 166–181. doi:10.26464/epp2019012.

Rashid, H.A., Hendon, H.H., Wheeler, M.C., Alves, O., 2011. Prediction of the Madden–Julian oscillation with the POAMA dynamical prediction system. Climate Dynamics 36, 649–661.

Raymond, D.J., 2001. A new model of the Madden–Julian oscillation. Journal of the Atmospheric Sciences 58, 2807–2819.

Raymond, D.J., Zeng, X., 2005. Modelling tropical atmospheric convection in the context of the weak temperature gradient approximation. Quarterly Journal of the Royal Meteorological Society 131, 1301–1320.

Rayner, N., Parker, D.E., Horton, E., Folland, C.K., Alexander, L.V., Rowell, D., Kent, E., Kaplan, A., 2003. Global analyses of sea surface temperature, sea ice, and night marine air temperature since the late nineteenth century. Journal of Geophysical Research: Atmospheres 108.

Reed, R.J., Campbell, W.J., Rasmussen, L.A., Rogers, D.G., 1961. Evidence of a downward-propagating, annual wind reversal in the equatorial stratosphere. Journal of Geophysical Research (1896-1977) 66, 813–818. doi:10.1029/JZ066i003p00813.

Richter, J., Anstey, J., Butchart, N., Kawatani, Y., Meehl, G., Osprey, S., Simpson, I., 2020. Progress in simulating the quasi-biennial oscillation in CMIP models. *submitted to J. Geophys. Res. Atmos.* .

Riddle, E.E., Stoner, M.B., Johnson, N.C., L'Heureux, M.L., Collins, D.C., Feldstein, S.B., 2013. The impact of the MJO on clusters of wintertime circulation anomalies over the North American region. Climate Dynamics 40, 1749–1766.

Rienecker, M.M., Suarez, M.J., Gelaro, R., Todling, R., Bacmeister, J., Liu, E., Bosilovich, M.G., Schubert, S.D., Takacs, L., Kim, G.K., Bloom, S., Chen, J., Collins, D., Conaty, A., da Silva, A., Gu, W., Joiner, J., Koster, R.D., Lucchesi, R., Molod, A., Owens, T., Pawson, S., Pegion, P., Redder, C.R., Reichle, R., Robertson, F.R., Ruddick, A.G., Sienkiewicz, M., Woollen, J., 2011. MERRA: NASA's modern-era retrospective analysis for research and applications. Journal of Climate 24, 3624–3648. doi:10.1175/JCLI-D-11-00015.1.

Rind, D., Orbe, C., Jonas, J., Nazarenko, L., Zhou, T., Kelley, M., Lacis, A., Shindell, D., Faluvegi, G., Russell, G., Bauer, M., Schmidt, G., Romanou, A., Tausnev, N., 2020. GISS Model E2.2: A climate model optimized for the middle atmosphere. Part 1: Model structure, climatology, variability and climate sensitivity.

Robertson, A., Vitart, F., 2018. Sub-seasonal to Seasonal Prediction: The Gap Between Weather and Climate Forecasting. Elsevier.

Romps, D.M., 2012a. Numerical tests of the weak pressure gradient approximation. Journal of the Atmospheric Sciences 69, 2846–2856.

Romps, D.M., 2012b. Weak pressure gradient approximation and its analytical solutions. Journal of the Atmospheric Sciences 69, 2835–2845.

Schenzinger, V., Osprey, S., Gray, L., Butchart, N., 2017. Defining metrics of the quasi-biennial oscillation in global climate models. Geoscientific Model Development 10, 2157–2168. URL: https://www.geosci-model-dev.net/10/2157/2017/, doi:10.5194/gmd-10-2157-2017.

Schmidt, A., Mills, M.J., Ghan, S., Gregory, J.M., Allan, R.P., Andrews, T., Bardeen, C.G., Conley, A., Forster, P.M., Gettelman, A., Portmann, R.W., Solomon, S., Toon, O.B., 2018. Volcanic radiative forcing from 1979 to 2015. Journal of Geophysical Research: Atmospheres 123, 12491–12508. doi:10.1029/2018JD028776.

Schmidt, G.A., Kelley, M., Nazarenko, L., Ruedy, R., Russell, G.L., Aleinov, I., Bauer, M., Bauer, S.E., Bhat, M.K., Bleck, R., et al., 2014. Configuration and assessment of the GISS ModelE2 contributions to the CMIP5 archive. Journal of Advances in Modeling Earth Systems 6, 141–184.

Sentić, S., Sessions, S.L., Fuchs, Ž., 2015. Diagnosing DYNAMO convection with weak temperature gradient simulations. Journal of Advances in Modeling Earth Systems 7, 1849–1871.

Sessions, S.L., Sentić, S., Herman, M.J., 2016. The role of radiation in organizing convection in weak temperature gradient simulations. Journal of Advances in Modeling Earth Systems 8, 244–271.

Sessions, S.L., Sugaya, S., Raymond, D.J., Sobel, A.H., 2010. Multiple equilibria in a cloud-resolving model using the weak temperature gradient approximation. Journal of Geophysical Research: Atmospheres 115.

Shepherd, T.G., 2002. Issues in stratosphere-troposphere coupling. Journal of the Meteorological Society of Japan. Ser. II 80, 769–792. doi:10.2151/jmsj.80.769.

Shi, J., Tao, W., Matsui, T., Cifelli, R., Hou, A., Lang, S., Tokay, A., Wang, N., Peters-Lidard, C., Skofronick-Jackson, G., et al., 2010. WRF simulations of the 20–22 January 2007 snow events over eastern Canada: Comparison with in situ and satellite observations. Journal of Applied Meteorology and Climatology 49, 2246–2266.

Shindell, D., Pechony, O., Voulgarakis, A., Faluvegi, G., Nazarenko, L., Lamarque, J.F., Bowman, K., Milly, G., Kovari, B., Ruedy, R., et al., 2013. Interactive ozone and methane chemistry in GISS-E2 historical and future climate simulations. Atmos. Chem. Phys 13, 2653–2689.

Simpson, I.R., Blackburn, M., Haigh, J.D., 2009. The role of eddies in driving the tropospheric response to stratospheric heating perturbations. Journal of the Atmospheric Sciences 66, 1347–1365. doi:10.1175/2008JAS2758.1.

Skamarock, W.C., Klemp, J.B., Dudhia, J., Gill, D.O., Barker, D.M., Wang, W., Powers, J.G., 2008. A description of the Advanced Research WRF version 3. NCAR Technical note-475+ STR .

Slingo, J., Sperber, K., Boyle, J., Ceron, J.P., Dix, M., Dugas, B., Ebisuzaki, W., Fyfe, J., Gregory, D., Gueremy, J.F., et al., 1996. Intraseasonal oscillations in 15 atmospheric general circulation models: results from an AMIP diagnostic subproject. Climate Dynamics 12, 325–357.

Sobel, A., Maloney, E., 2012. An idealized semi-empirical framework for modeling the Madden–Julian oscillation. Journal of the Atmospheric Sciences 69, 1691–1705.

Sobel, A., Maloney, E., 2013. Moisture modes and the eastward propagation of the MJO. Journal of the Atmospheric Sciences 70, 187–192.

Sobel, A., Wang, S., Kim, D., 2014. Moist static energy budget of the MJO during DYNAMO. Journal of the Atmospheric Sciences 71, 4276–4291. doi:10.1175/JAS-D-14-0052.1.

Sobel, A.H., 2014. Storm surge: Hurricane Sandy, our changing climate, and extreme weather of the past and future. Harper Wave.

Sobel, A.H., Bellon, G., Bacmeister, J., 2007. Multiple equilibria in a single-column model of the tropical atmosphere. Geophysical Research Letters 34.

Sobel, A.H., Bretherton, C.S., 2000. Modeling tropical precipitation in a single column. Journal of Climate 13, 4378–4392.

Sobel, A.H., Kim, D., 2012. The MJO-Kelvin wave transition. Geophysical Research Letters 39. doi:10.1029/2012GL053380.

Sobel, A.H., Nilsson, J., Polvani, L.M., 2001. The weak temperature gradient approximation and balanced tropical moisture waves. Journal of the Atmospheric Sciences 58, 3650–3665.

Solomon, S., 1999. Stratospheric ozone depletion: A review of concepts and history. Reviews of Geophysics 37, 275–316. doi:10.1029/1999RG900008.

Solomon, S., Kinnison, D., Bandoro, J., Garcia, R., 2015. Simulation of polar ozone depletion: An update. Journal of Geophysical Research: Atmospheres 120, 7958–7974.

Son, S.W., Lee, S., 2007. Intraseasonal variability of the zonal-mean tropical tropopause height. Journal of the Atmospheric Sciences 64, 2695–2706. doi:10.1175/JAS3982A.1.

Son, S.W., Lim, Y., Yoo, C., Hendon, H.H., Kim, J., 2017. Stratospheric control of the Madden–Julian oscillation. Journal of Climate 30, 1909–1922.

Song, L., Wu, R., 2020. Modulation of the westerly and easterly quasi-biennial oscillation phases on the connection between the Madden–Julian oscillation and the Arctic Oscillation. Atmosphere 11, 175.

Sperber, K.R., Annamalai, H., 2008. Coupled model simulations of boreal summer intraseasonal (30–50 day) variability, Part 1: Systematic errors and caution on use of metrics. Climate Dynamics 31, 345–372.

Stan, C., Straus, D.M., Frederiksen, J.S., Lin, H., Maloney, E.D., Schumacher, C., 2017. Review of tropical-extratropical teleconnections on intraseasonal time scales. Reviews of Geophysics 55, 902–937. doi:10.1002/2016RG000538.

von Storch, H., Xu, J., 1990. Principal oscillation pattern analysis of the 30-to 60-day oscillation in the tropical troposphere. Climate Dynamics 4, 175–190.

Straus, D.M., Lindzen, R.S., 2000. Planetary-scale baroclinic instability and the MJO. Journal of the Atmospheric Sciences 57, 3609–3626. doi:10.1175/1520-0469(2000)057<3609:PSBIAT>2.0.CO;2.

Sun, L., Wang, H., Liu, F., 2019. Combined effect of the QBO and ENSO on the MJO. Atmospheric and Oceanic Science Letters 12, 170–176. doi:10.1080/16742834.2019.1588064.

Taguchi, M., 2010. Observed connection of the stratospheric quasi-biennial oscillation with El Niño–Southern Oscillation in radiosonde data. Journal of Geophysical Research: Atmospheres 115. doi:10.1029/2010JD014325.

Takahashi, M., 1996. Simulation of the stratospheric quasi-biennial oscillation using a general circulation model. Geophysical Research Letters 23, 661–664. doi:10.1029/95GL03413.

Takahashi, M., Boville, B.A., 1992. A three-dimensional simulation of the equatorial quasi-biennial oscillation. Journal of the Atmospheric Sciences 49, 1020–1035. doi:10.1175/1520-0469(1992)049<1020:ATDSOT>2.0.CO;2.

Tao, W., Johnson, D., Shie, C., Simpson, J., 2004. The atmospheric energy budget and large-scale precipitation efficiency of convective systems during TOGA COARE, GATE, SCSMEX, and ARM: Cloud-resolving model simulations. Journal of the Atmospheric Sciences 61, 2405–2423.

Tegtmeier, S., Anstey, J., Davis, S., Dragani, R., Harada, Y., Ivanciu, I., Pilch Kedzierski, R., Krüger, K., Legras, B., Long, C., Wang, J.S., Wargan, K., Wright, J.S., 2020. Temperature and tropopause characteristics from reanalyses data in the tropical tropopause layer. Atmospheric Chemistry and Physics 20, 753–770. URL: https://www.atmos-chem-phys.net/20/753/2020/, doi:10.5194/acp-20-753-2020.

Tippett, M.K., 2018. Robustness of relations between the MJO and U.S. tornado occurrence. Monthly Weather Review 146, 3873–3884. doi:10.1175/MWR-D-18-0207.1.

Toms, B.A., Barnes, E.A., Maloney, E.D., van den Heever, S.C., 2020. The global teleconnection signature of the Madden-Julian oscillation and its modulation by the quasi-biennial oscillation. Journal of Geophysical Research: Atmospheres n/a, e2020JD032653. doi:10.1029/2020JD032653.

Tseng, H.H., Fu, Q., 2017. Temperature control of the variability of tropical tropopause layer cirrus clouds. Journal of Geophysical Research: Atmospheres 122, 11,062–11,075. doi:10.1002/2017JD027093.

Tulich, S.N., Randall, D.A., Mapes, B.E., 2007. Vertical-mode and cloud decomposition of large-scale convectively coupled gravity waves in a two-dimensional cloud-resolving model. Journal of the Atmospheric Sciences 64, 1210–1229.

Ventrice, M.J., Wheeler, M.C., Hendon, H.H., Schreck III, C.J., Thorncroft, C.D., Kiladis, G.N., 2013. A modified multivariate Madden–Julian oscillation index using velocity potential. Monthly Weather Review 141, 4197–4210.

Virts, K.S., Wallace, J.M., 2014. Observations of temperature, wind, cirrus, and trace gases in the tropical tropopause transition layer during the MJO. Journal of the Atmospheric Sciences 71, 1143–1157. doi:10.1175/JAS-D-13-0178.1.

Vitart, F., 2014. Evolution of ECMWF sub-seasonal forecast skill scores. Quarterly Journal of the Royal Meteorological Society 140, 1889–1899.

Vitart, F., 2017. Madden—Julian oscillation prediction and teleconnections in the S2S database. Quarterly Journal of the Royal Meteorological Society 143, 2210–2220.

Vitart, F., Ardilouze, C., Bonet, A., Brookshaw, A., Chen, M., Codorean, C., Déqué, M., Ferranti, L., Fucile, E., Fuentes, M., Hendon, H., Hodgson, J., Kang, H.S., Kumar, A., Lin, H., Liu, G., Liu, X., Malguzzi, P., Mallas, I., Manoussakis, M., Mastrangelo, D., MacLachlan, C., McLean, P., Minami, A., Mladek, R., Nakazawa, T., Najm, S., Nie, Y., Rixen, M., Robertson, A.W., Ruti, P., Sun, C., Takaya, Y., Tolstykh, M., Venuti, F., Waliser, D., Woolnough, S., Wu, T., Won, D.J., Xiao, H., Zaripov, R., Zhang, L., 2017. The Subseasonal to Seasonal (S2S) prediction project database. Bulletin of the American Meteorological Society 98, 163–173. doi:10.1175/BAMS-D-16-0017.1.

Waliser, D., 2005. Predictability and forecasting, in: Intraseasonal variability in the atmosphere-ocean climate system. Springer, pp. 389–423.

Waliser, D.E., Jones, C., Schemm, J.K.E., Graham, N.E., 1999a. A statistical extended-range tropical forecast model based on the slow evolution of the Madden–Julian oscillation. Journal of Climate 12, 1918–1939.

Waliser, D.E., Lau, K., Kim, J.H., 1999b. The influence of coupled sea surface temperatures on the Madden–Julian oscillation: A model perturbation experiment. Journal of the Atmospheric Sciences 56, 333–358.

Wallace, J.M., Chang, F.C., 1982. Interannual variability of the wintertime polar vortex in the Northern Hemisphere middle stratosphere. Journal of the Meteorological Society of Japan. Ser. II 60, 149–155. doi:10.2151/jmsj1965.60.1_149.

Wang, B., 1988. Dynamics of tropical low-frequency waves: An analysis of the moist Kelvin wave. Journal of the Atmospheric Sciences 45, 2051–2065.

Wang, B., 2005. Theory, in: Intraseasonal variability in the atmosphere-ocean climate system. Springer, pp. 389–423.

Wang, B., Liu, F., 2011. A model for scale interaction in the Madden–Julian oscillation. Journal of the Atmospheric Sciences 68, 2524–2536.

Wang, B., Liu, F., Chen, G., 2016a. A trio-interaction theory for Madden–Julian oscillation. Geoscience Letters 3, 1–16.

Wang, B., Rui, H., 1990. Synoptic climatology of transient tropical intraseasonal convection anomalies: 1975–1985. Meteorology and Atmospheric Physics 44, 43–61.

Wang, J., Kim, H.M., Chang, E.K.M., Son, S.W., 2018. Modulation of the MJO and North Pacific storm track relationship by the QBO. Journal of Geophysical Research: Atmospheres 123, 3976–3992. doi:10.1029/2017JD027977.

Wang, S., 2020. A precipitation-based index for tropical intraseasonal oscillations. Journal of Climate 33, 805–823. doi:10.1175/JCLI-D-19-0019.1.

Wang, S., Sobel, A.H., 2011. Response of convection to relative sea surface temperature: Cloud-resolving simulations in two and three dimensions. Journal of Geophysical Research: Atmospheres 116.

Wang, S., Sobel, A.H., Fridlind, A., Feng, Z., Comstock, J.M., Minnis, P., Nordeen, M.L., 2015. Simulations of cloud-radiation interaction using large-scale forcing derived from the CINDY/DYNAMO northern sounding array. Journal of Advances in Modeling Earth Systems 7, 1472–1498.

Wang, S., Sobel, A.H., Kuang, Z., 2013. Cloud-resolving simulation of TOGA-COARE using parameterized large-scale dynamics. Journal of Geophysical Research: Atmospheres 118, 6290–6301.

Wang, S., Sobel, A.H., Nie, J., 2016b. Modeling the MJO in a cloud-resolving model with parameterized large-scale dynamics: Vertical structure, radiation, and horizontal advection of dry air. Journal of Advances in Modeling Earth Systems 8, 121–139.

Wang, S., Sobel, A.H., Tippett, M.K., Vitart, F., 2019a. Prediction and predictability of tropical intraseasonal convection: seasonal dependence and the Maritime Continent prediction barrier. Climate Dynamics 52, 6015–6031.

Wang, S., Tippett, M.K., Sobel, A.H., Martin, Z.K., Vitart, F., 2019b. Impact of the QBO on prediction and predictability of the MJO convection. Journal of Geophysical Research: Atmospheres 124, 11766–11782.

Waugh, D.W., Sobel, A.H., Polvani, L.M., 2017. What is the polar vortex and how does it influence weather? Bulletin of the American Meteorological Society 98, 37–44. doi:10.1175/BAMS-D-15-00212.1.

Webster, P.J., 1972. Response of the tropical atmosphere to local, steady forcing. Mon. Wea. Rev 100, 518–541.

Welch, B.L., 1947. The generalization of Student's problem when several different population variances are involved. Biometrika 34, 28–35.

Wheeler, M., Kiladis, G.N., 1999. Convectively coupled equatorial waves: Analysis of clouds and temperature in the wavenumber–frequency domain. Journal of the Atmospheric Sciences 56, 374–399.

Wheeler, M.C., Hendon, H.H., 2004. An all-season real-time multivariate MJO index: Development of an index for monitoring and prediction. Monthly Weather Review 132, 1917–1932. doi:10.1175/1520-0493(2004)132<1917:AARMMI>2.0.CO;2.

Wu, X., Grabowski, W.W., Moncrieff, M.W., 1998. Long-term behavior of cloud systems in TOGA COARE and their interactions with radiative and surface processes. Part I: Two-dimensional modeling study. Journal of the Atmospheric Sciences 55, 2693–2714.

Wu, Z., Sarachik, E., Battisti, D.S., 2000. Vertical structure of convective heating and the three-dimensional structure of the forced circulation on an equatorial beta plane. Journal of the Atmospheric Sciences 57, 2169–2187.

Yanai, M., Maruyama, T., 1966. Stratospheric wave disturbances propagating over the equatorial Pacific. Journal of the Meteorological Society of Japan. Ser. II 44, 291–294.

Yang, D., Ingersoll, A.P., 2014. A theory of the MJO horizontal scale. Geophysical Research Letters 41, 1059–1064.

Yang, Q., Fu, Q., Hu, Y., 2010. Radiative impacts of clouds in the tropical tropopause layer. Journal of Geophysical Research: Atmospheres 115.

Yasunari, T., 1979. Cloudiness fluctuations associated with the Northern Hemisphere summer monsoon. Journal of the Meteorological Society of Japan. Ser. II 57, 227–242.

Yasunari, T., 1989. A possible link of the QBOs between the stratosphere, troposphere and sea surface temperature in the tropics. Journal of the Meteorological Society of Japan. Ser. II 67, 483–493. doi:10.2151/jmsj1965.67.3_483.

Yoneyama, K., Zhang, C., Long, C.N., 2013. Tracking pulses of the Madden–Julian oscillation. Bulletin of the American Meteorological Society 94, 1871–1891.

Yoo, C., Son, S.W., 2016. Modulation of the boreal wintertime Madden-Julian oscillation by the stratospheric quasi-biennial oscillation. Geophysical Research Letters 43, 1392–1398. doi:10.1002/2016GL067762.

Yu, L., Jin, X., Weller, R.A., 2008. Multidecade global flux datasets from the Objectively Analyzed Air-Sea Fluxes (OAFlux) Project: Latent and sensible heat fluxes, ocean evaporation, and related surface meteorological variables. Woods Hole Oceanographic Institution OAFlux Project Tec, in: Rep, Citeseer.

Yu, L., Weller, R.A., 2007. Objectively analyzed air–sea heat fluxes for the global ice-free oceans (1981–2005). Bulletin of the American Meteorological Society 88, 527–540.

Yuan, W., Geller, M.A., Love, P.T., 2014. ENSO influence on QBO modulations of the tropical tropopause. Quarterly Journal of the Royal Meteorological Society 140, 1670–1676.

Zhang, C., 2005. Madden-Julian oscillation. Reviews of Geophysics 43. doi:10.1029/2004RG000158.

Zhang, C., 2013. Madden–Julian oscillation: Bridging weather and climate. Bulletin of the American Meteorological Society 94, 1849–1870.

Zhang, C., Zhang, B., 2018. QBO-MJO connection. Journal of Geophysical Research: Atmospheres 123, 2957–2967.

Zhou, S., L'Heureux, M., Weaver, S., Kumar, A., 2012. A composite study of the MJO influence on the surface air temperature and precipitation over the continental United States. Climate Dynamics 38, 1459–1471.

Appendix A

Supplement to Chapter 2

A.1 QBO Impact on the MJO in S2S models

In this Appendix we demonstrate that the findings of Abhik and Hendon (2019) on the relationship between the MJO and the QBO in forecast models holds in a broader modeling context. While likely not enough for a standalone publication, we include these results because they are relevant to modeling the MJO-QBO link. This Appendix, while not assuming familiarity with Abhik and Hendon (2019), may be less accessible to readers not familiar with that publication.

Abhik and Hendon (2019) show, using two different Austalian forecast models, that the QBO appears to have a direct impact on the MJO during forecast model simulations. The novel feature of their study is that, prior to looking at differences in the model's MJO in QBOE versus QBOW, they control for the initial amplitude of the MJO. By looking at the QBOE versus QBOW difference between MJO events with similar initial strength, they attempt to separate the QBO effects on the initial conditions from the QBO impact the MJO "feels" in the model directly from the stratosphere. See Abhik and Hendon (2019) and Figure 2.25 for a more detailed description of their models, methodology, and results.

Here we reproduce their finding using a collection of many forecast models from the Subseasonal to Seasonal (S2S) prediction project (Vitart et al. (2017)). The data from the models we use, including the details of the MJO index we describe below, are described in Wang et al. (2019b). Briefly, these forecast models are global models from operational forecast centers optimized for subseasonal or seasonal prediction. They are initialized from observations and integrated for typically at least 30 days. The S2S dataset contains "hindcast" simulations, which simulate past events and thus can be compared to observations over the integration period for validation. The models we consider are: the Australian Bureau of Meteorology (BoM), the China Meteorological Administration (CMA), the European Centre for Medium-Range Weather Forecasts (ECMWF), Environment and Climate Change Canada (ECCC), the Institute of Atmospheric Sciences and Climate of the National Research Council (CNR-ISAC), the Hydrometeorological Centre of Russia (HMCR), the Japan Meteorological Agency (JMA), Météo-France/Centre National de Recherche Meteorologiques (CNRM), the National Centers for Environmental Prediction (NCEP), and the Met Office (UKMO) models. Details are summarized in Table 1 in Wang et al. (2019b), reproduced

Table 1
S2S Model Configurations: Horizontal and Vertical Resolutions of the Model Atmospheres, Model Tops, Reforecast Types, Forecast Periods, Reforecast Frequencies, and Ensemble Sizes

	Resolution	Model top	Rfc type	Rfc period	Rfc frequency	Ens size	O/A coupling
BOM	~T47 L17	10 hPa	F	1981–2013	Sixper month	3 × 11	Y
CMA	T106 L40	0.5 hPa	F	1994–2013	Daily	4	Y
CNR-ISAC	0.75 × 0.56 L54	~6.8 hPa	F	1981–2010	Every five days	1	slab
CNRM	T255L91	0.01 hPa	F	1993–2013	Two per month	15	Y
ECCC	0.45 × 0.45 L40	2 hPa	O	1995–2013	Weekly	4	persistent SST
ECMWF	T639/319 L91	0.01 hPa	O	1996–2013 (past 20 years)	Two per week	11	Y
HMCR	1.1 × 1.4 L28	5 hPa	O	1985–2010	Weekly	10	N
JMA	T319L60	0.1 hPa	F	1981–2010	Three per month	5	N
NCEP	T126L64	0.02 hPa	F	1999–2010	Daily	4	Y
UKMO	N216L85	85 km	O	1996–2015	Four per month	3	Y

Note. Reforecast types are either F (fixed) or O (on the fly). The CNR-ISAC model version is 20150326.

Figure A.1: A list of the S2S models (and related details) considered in this Appendix. Reproduced from Table 1 in Wang et al. (2019b).

here as Figure A.1.

The QBO is defined following Abhik and Hendon (2019) as the equatorially averaging (5°S to 5°N) ERA-I zonal mean zonal wind at 50 hPa. QBOW and QBOE months defined when the zonal wind index is greater than or less than 0.5 standard deviations, respectively.

The MJO is defined using the real-time OLR-based MJO index (ROMI; Kiladis et al. (2014)) as calculated for forecast models in Wang et al. (2019b). This differs from Abhik and Hendon (2019), who used the real-time multivariate MJO index (RMM; Wheeler and Hendon (2004)). For more discussion about formation of indices, see relevant comments in a different context in Chapter 4 and Appendix C.1. The MJO strength is measured as the amplitude of the ROMI index as calculated as $|ROMI| = \sqrt{PC1^2 + PC2^2}$ where $PC1/2$ are the principal components which form the index, as discussed in Kiladis et al. (2014). Here the ROMI index data for the S2S models were calculated and made available to us by Shuguang Wang.

Our methodology, closely following that of Abhik and Hendon (2019), for comparing the model MJO differences in QBOE and QBOW is as follows:

1. We group the hindcasts for each model by whether they are initialized in QBOE or QBOW, based on the QBO state during the month of initialization.

2. In order to examine MJO events with similar initial amplitude during QBOE and QBOW, we bin the forecasts by the amplitude of the observed MJO at day 0. Thus, for all QBOE and QBOW forecasts we consider four groups of MJO events: $|ROMI(0)| < 1.0$ (weak); $1.0 \leq |ROMI| < 1.5$ (moderate); $1.5 \leq |ROMI| \leq 2.0$ (strong) and $|ROMI(0)| > 2$ (very strong). Note this differs slightly from Abhik and Hendon (2019) who use $|RMM(0)| < 1.0$ (weak), $1.0 \leq |RMM(0)| \leq 1.5$ (moderate) and $|RMM(0)| > 1.5$ (strong), for reasons discussed below.

3. Significance is calculated at the 95% level using a Welch's t-test (Welch (1947)) with a null hypothesis of no difference. The sample size is the number of QBOE/W dates in each bin. Note unlike Abhik and Hendon (2019), for simplicity we do not take into account the additional degrees of freedom due to different ensemble members,

which would increase the sample size of the models and could potentially enhance the significance of our results.

4. We compare the ensemble mean of the amplitudes of all the QBOE versus QBOW MJO events in each of the four bins, and study how the model MJO develops in QBOE relative to QBOW.

Figure A.2 shows initial results staying closer to the methodology of Abhik and Hendon (2019) and using three amplitude bins rather than four. In the top two rows, we show Figure 3 from Abhik and Hendon (2019). This shows the percent MJO amplitude difference in QBOE relative to QBOW in observations (pink) and the model (blue), with shading representing significance. The bottom row shows the same calculation using our methodology for the BoM model submitted to the S2S dataset. Our results differ because of the use of a different MJO index, different model configuration (we use the BoM submission to the S2S dataset), different hindcast periods, and different significance testing. Note here the binning is the same as in Abhik and Hendon (2019), unlike in subsequent figures.

Abhik and Hendon (2019) show significant increases in MJO strength in QBOE versus QBOW at lead times around 5-7 days in the model and observations. Note that initially the MJO difference in QBOE and QBOW in both observations and the model are small by construction. These differences after several days are significant, and Abhik and Hendon (2019) attributed them to the MJO "feeling" the impact of the QBO during the simulations.

Our results in this Figure show less of a strong signal in observations than Abhik and Hendon (2019), and only show significant model differences in the strong MJO cases. However, note there is a very large difference at day 0 in the strong MJO cases. Because of this, we add the fourth bin separating strong and very strong MJO events, extending what Abhik and Hendon (2019) did. This resolves the issue, and under this new methodology nearly all S2S models show reasonably close QBOE/W agreement at day 0 ($< 20\%$ percentage difference) when four bins are used.

Figures A.3 and A.4 show our updated results with four MJO amplitude bins and extends the results to all the S2S models. Figures A.5 and A.6 are similar, but instead of showing the percentage change in the ROMI indices between QBOE and QBOW, they show the actual ROMI amplitude in QBOE (blue) and QBOW (red) for the models and verification. In each case the dashed lines show the verification (i.e. observations) and the solid line shows the model. Note that the verification differs between models because of different dates of initialization. Note too that some models and verification show a kink in the amplitude at around 30 days, which is likely due to the way in which the ROMI index was calculated and not a physical feature. Regardless of the different periods over which the models are verified, the observations always show stronger MJO events in QBOE after around five days, consistent with the idea that the QBO has a large effect on the observed MJO. This tends to hold for all four categories of MJO events.

With very few exception, the model QBO modulation of the MJO is never as strong as the observed modulation. There are some notable exception, however, where the model MJO changes are stronger than observed: for "very strong" events at lead times less than two weeks this holds in four models: CMA, ECCC, HMCR, and NCEP. While weaker than observed, many models show a strong, significant MJO response to the QBO, despite being

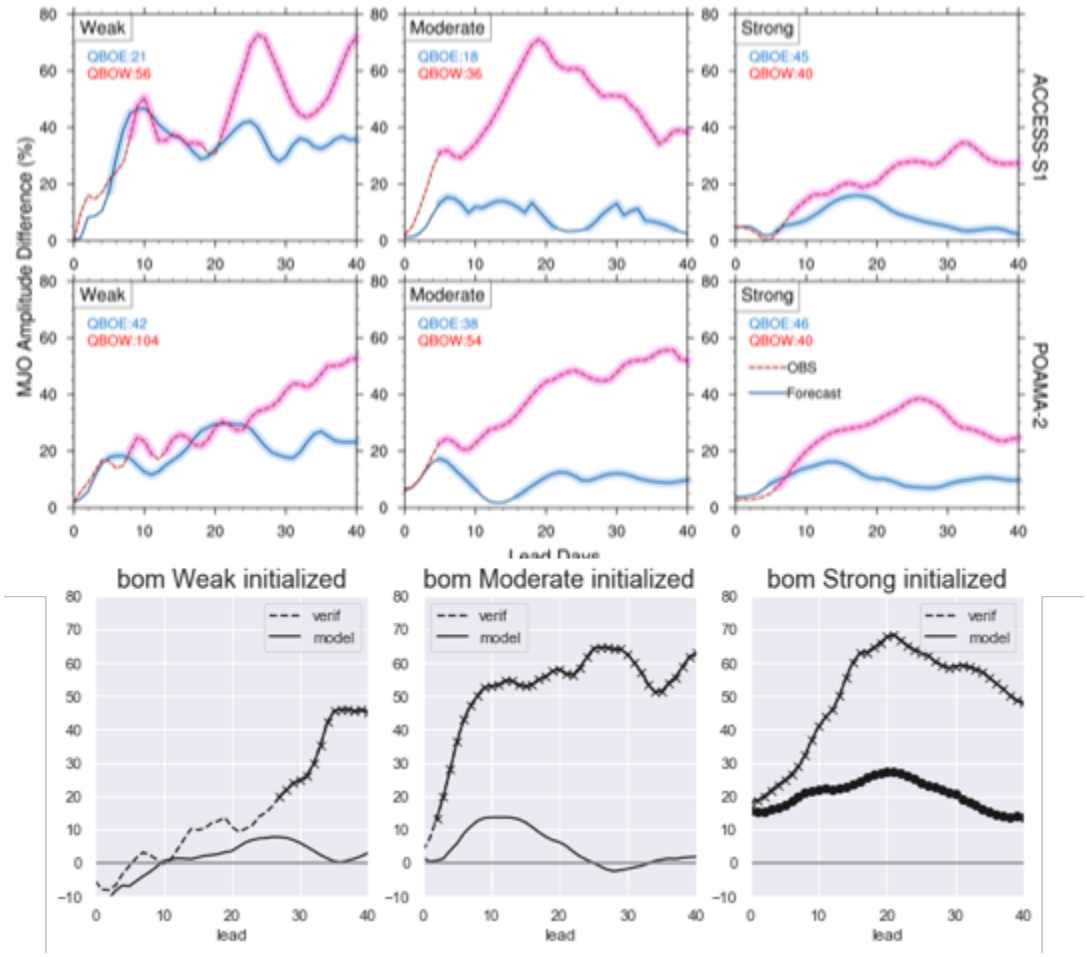

Figure A.2: (Top two rows) As in Abhik and Hendon (2019), their Figure 3 (also shown in Figure 2.25). (bottom row) A similar calculation using the ROMI index and the S2S version of the BoM model, with other slight differences as described in the text. Here the model is the solid curve and the verification is dashed. Significance marked with a dot/"x" per the text.

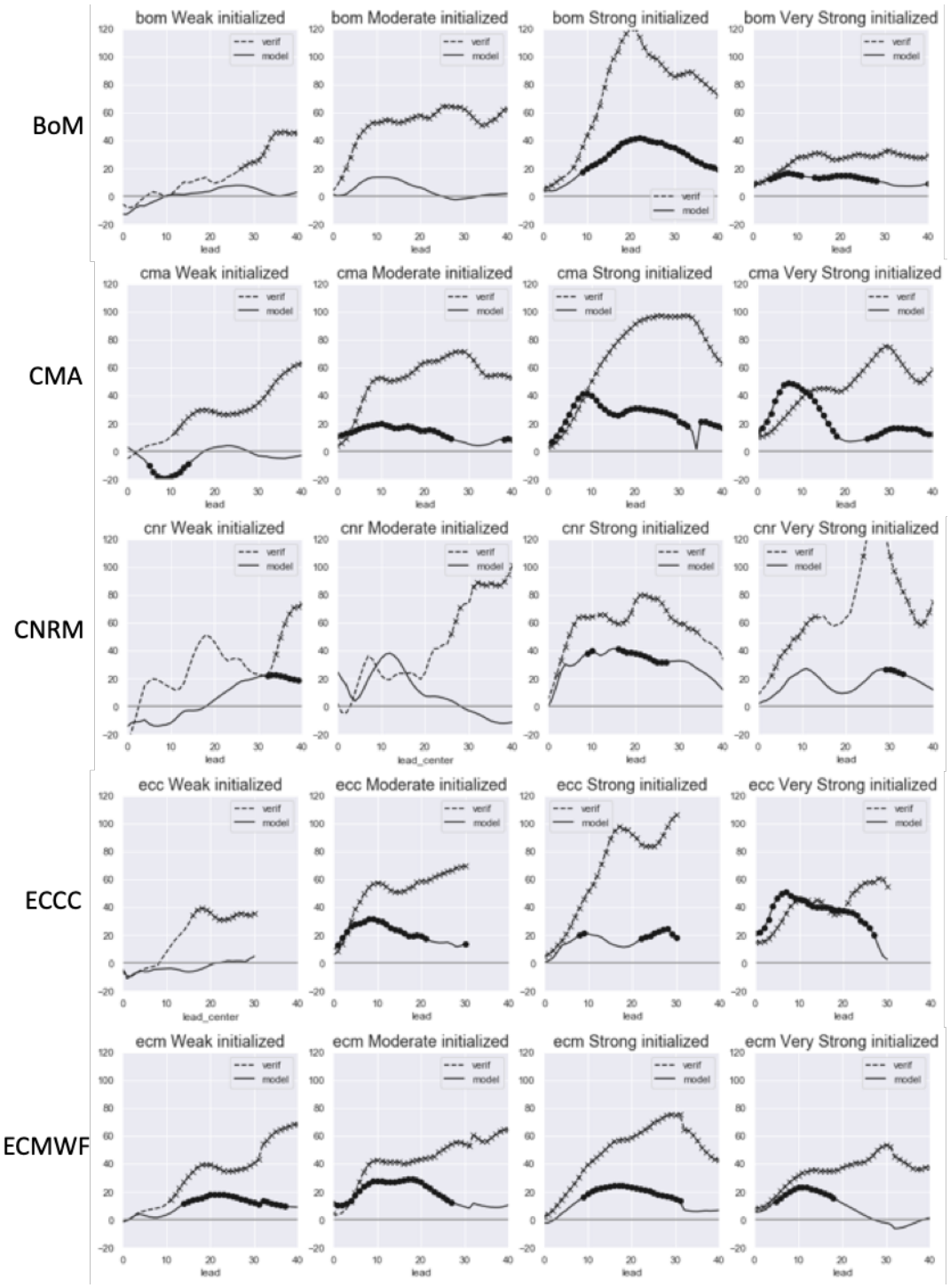

Figure A.3: Percentage difference in QBOE versus QBOW for (left) weak, (center left) moderate, (center right) strong, and (right) very strong MJO events from the S2S models; here we show the first 5 of 10 models considered.

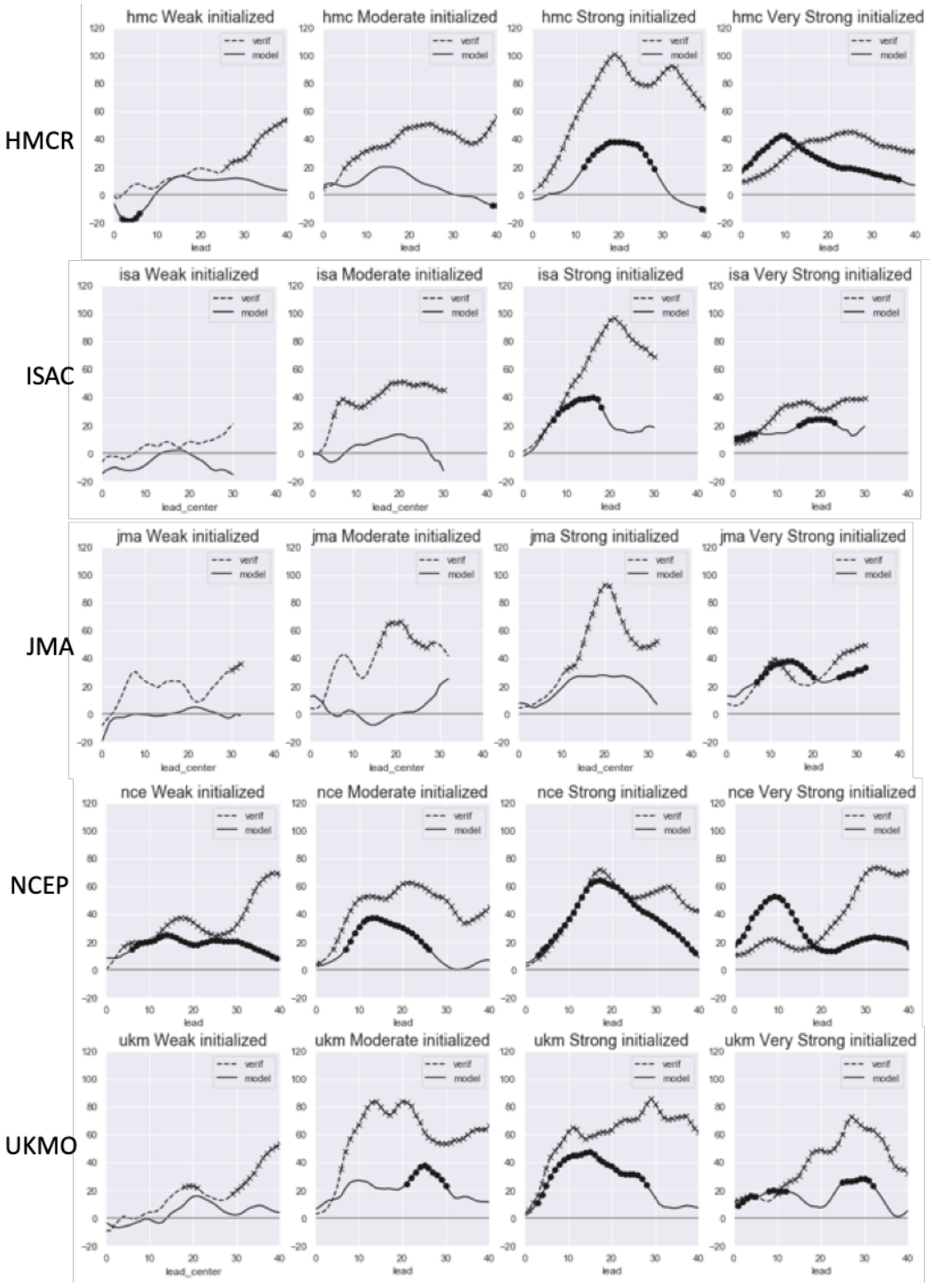

Figure A.4: As in Figure A.3 for the 5 remaining models.

similar at initial lead times. This is especially true for "strong" and "very strong" MJO events. All models show a significant increase in QBOE in at least one bin. For example BoM, CMA, CNRM, HMC, ISAC, NCEP, and UKMO all get to ∼40% or greater increases in QBOE between 10-20 days in the "strong" events. In those same events, these models all start with differences less than ∼10%. The NCEP model seems to show the largest QBO modulation that is most in keeping with the observed, and actually overestimate the QBO impact for the first two weeks during "very strong" MJO events. In that case though, the model starts off with approximately double the observed QBOE-W difference. The MetOffice model also looks fairly good, and while ECMWF doesn't show the strongest modulation there are significant changes of the correct sign in all amplitude bins out to at least 30 day leads.

Interestingly in three models (NCEP, BoM, UKMO) the model ROMI amplitude actually increases during QBOE forecasts for moderate and strong events, as opposed to simply decreasing more slowly as most models do. It's tempting to conclude that if any model MJO events really "feel" the QBO, those three are probably the best at simulating a QBO effect. Overall, for the ten models we consider, during weak MJO events two of ten show a significant increase in QBOE versus QBOW for more than just a few days. Four of ten models show changes among moderate MJO events, and nine out of ten show changes during strong and very strong MJO events. This analysis, while relatively cursory, suggests the findings of Abhik and Hendon (2019) hold in a broader modeling context than they consider.

However, the strategy of binning by MJO starting amplitude to control for differences in the initial condition under various QBO phases remains somewhat dubious in terms of truly separating out the roll of initial conditions and the stratosphere in the model. There may be other differences in the initial conditions that matter more than just amplitude, and these changes are not captured via this binning methodology. Such changes could have an impact on the behavior of the MJO during the simulation. Marshall et al. (2017) and Wang et al. (2019b) have both shown that QBO changes to MJO predictability are not simply due to differences in MJO amplitude, further suggesting that there is some more systematic change in the MJO during QBOE versus QBOW that amplitude differences alone do not completely capture. This is in part what motivated the work in Chapter 4, as that seemed a cleaner experiment isolating the stratospheric pathway of influence. The findings in Chapter 4 suggest that the model stratosphere plays a very weak role in modulating the MJO.

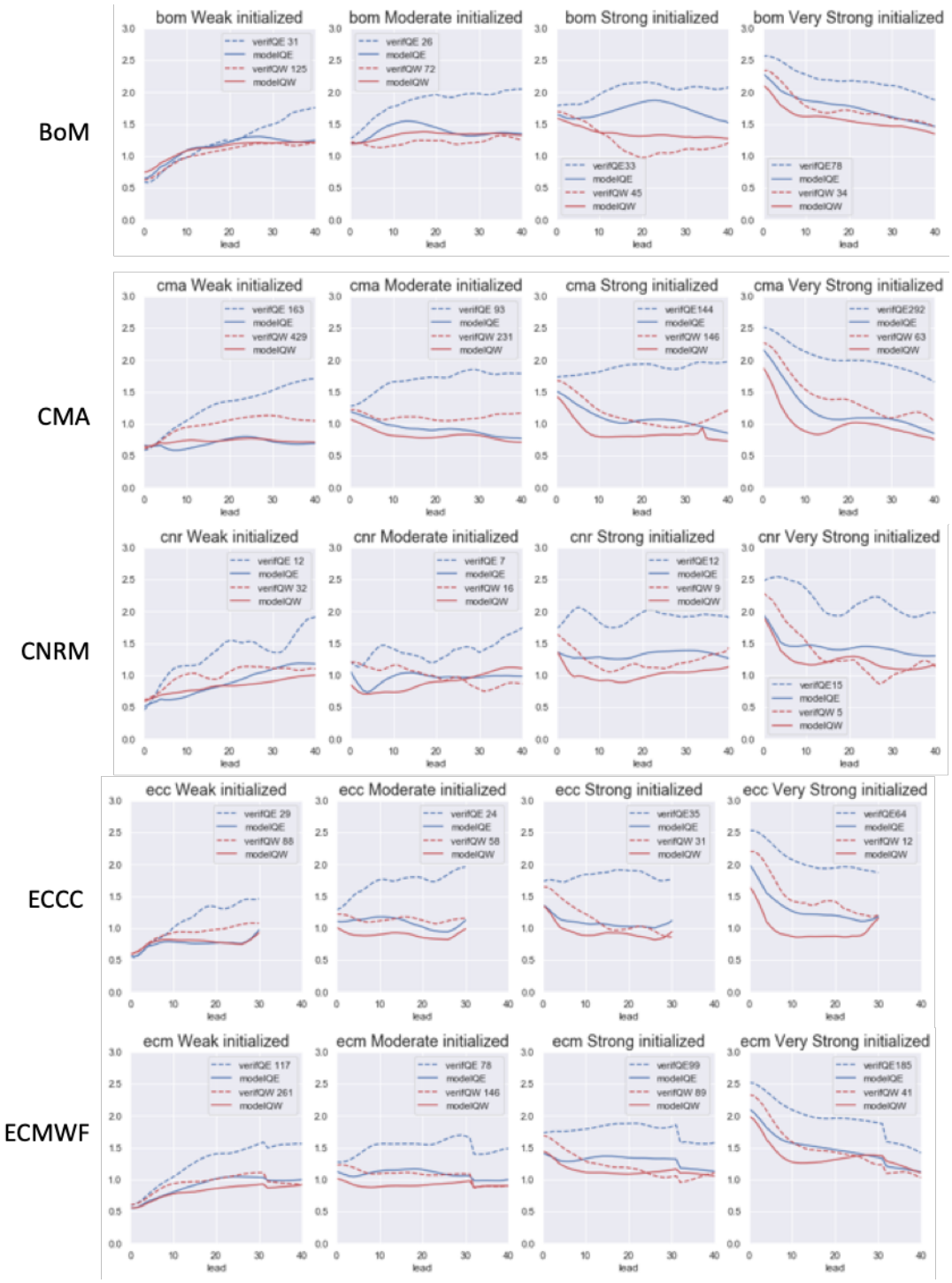

Figure A.5: Similar to Figure A.3, but showing the actual ROMI amplitude for QBOE and QBOW in models and observations, rather than the percentage difference. Blue are QBOE and red are QBOW, for the model (dashed) and observations (solid). The kink in the ROMI amplitude evident in some panels in both observations and the model is likely due to the way the index is calculated, and is thus not a physical feature.

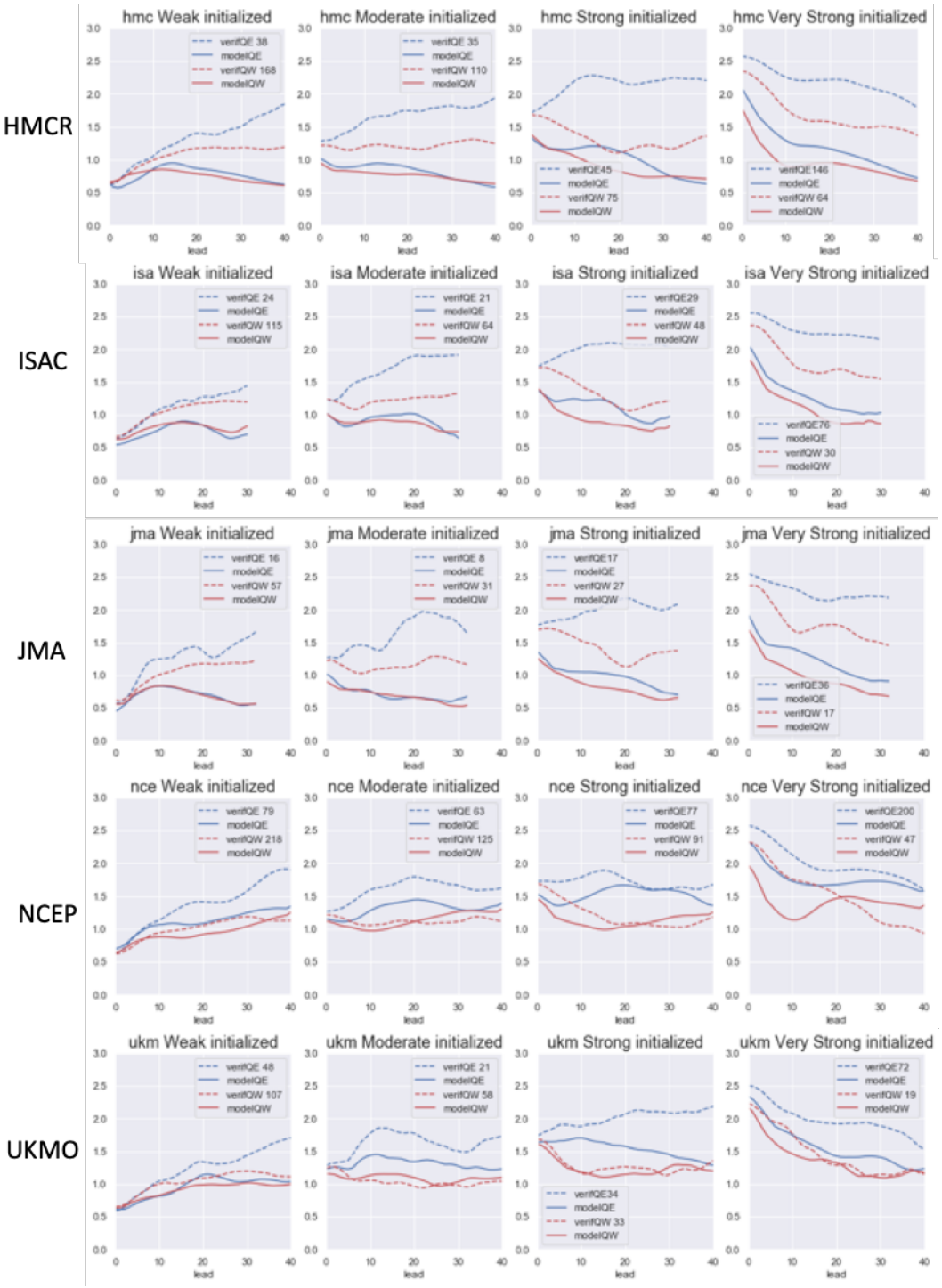

Figure A.6: As in Figure A.6 for the 5 remaining models.

Appendix B

Supplement to Chapter 3

Note: This has been published in very near its present form as the appendix of Martin et al. (2019). Minor edits have been made for clarity.

B.1 Sensitivity to SWTG Top

In this appendix we briefly examine the sensitivity of our cloud-resolving model results to the SWTG top boundary condition and vertical modes (see Section 3.2). We redo several QBO experiments using the SWTG modes recalculated with a rigid lid at 16 km rather than at 20 km. While this lower lid is closer to the observed vertical velocity in the DYNAMO data (see Figure 3.1a), it may be overly restrictive, preventing the vertical velocity from responding to anomalies in the TTL. In order to place our rigid lid well above both the height of convection and the QBO anomalies we impose, and because choice of this parameter is not physically well-constrained, we chose to use the 20 km boundary in the main text.

Figure B.1 shows the OLR and precipitation time series from these integrations, which are identical to the 16km-peaked, temperature-only run in Section 3.3.2 except for changes to the modes/rigid lid. The general sign and magnitude of QBOE-QBOW differences are not markedly different from the higher lid cases in the vertical velocity and cloud fraction and thus are not shown. However, the precipitation no longer increases significantly during QBOE relative to QBOW: during the first MJO event there are some periods where QBOE precipitates more (e.g. $\sim$ days 23 and 29) and others where QBOW precipitates more (e.g. $\sim$ day 33). The same is true for the second MJO event. This lack of consistency even within individual events indicates that the precipitation response to the QBO in this model is sensitive the model configuration and is less consistent than other variables showing an increase in QBOE compared to QBOW.

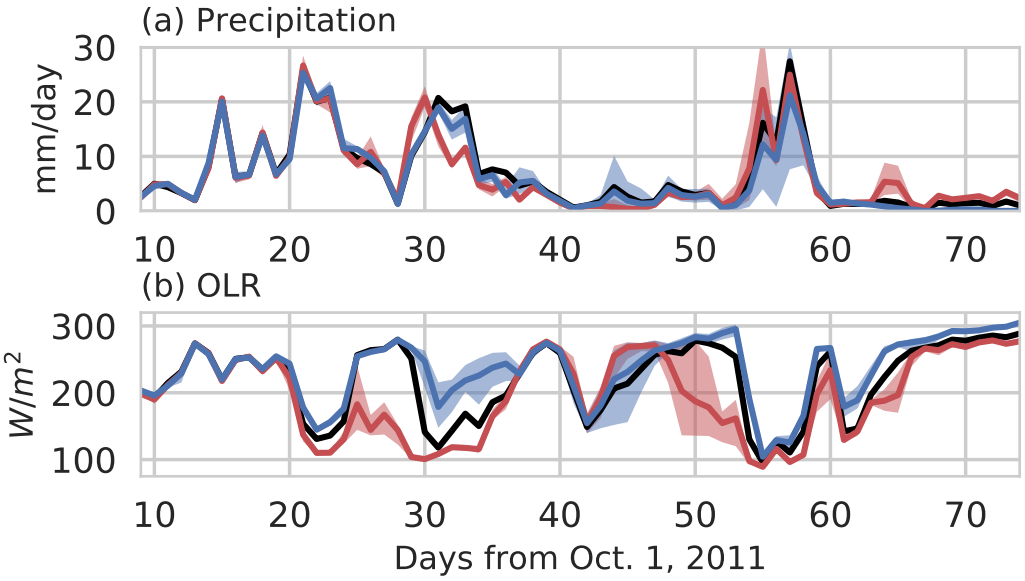

Figure B.1: As in Figure 3.4, but altering the spectral weak temperature gradient vertical modes and vertical velocity such that the model has a rigid lid at 16 km, as opposed to the 20 km rigid lid used in the main text.

Appendix C

Supplement to Chapter 4

Note: This has been published in very near its present form as the appendix of Martin et al. (2020). Minor edits have been made for clarity.

C.1 Calculation of MJO Indices

As discussed in Section 4.2.2, we utilize two MJO indices in our study; the real-time multivariate MJO index (RMM: Wheeler and Hendon 2004) and the real-time OLR-based MJO Index (ROMI; Kiladis et al. 2014), both of which we calculate for the 61-day model simulations. To calculate RMM, we follow the protocol similar to that in Gottschalck et al. (2010) and Rashid et al. (2011) and summarized as follows:

1. The model output of OLR and zonal wind at 850 and 200 hPa are averaged over 15°N/S, and the anomaly is taken relative to a forecast climatology. This forecast climatology was formed by averaging all the January 1 control simulations from 1989-2016 (here the climatology is a function of longitude and forecast lead time; unlike Gottschalck et al. (2010) we do not use the observed climatology).

2. The previous 120 days of observed OLR and zonal wind anomalies relative to the forecast start date (and processed similarly to the above except that an observed climatology is used) are appended prior to the 61 forecast days. Then the mean of the previous 120 days (combined forecast and observational data) is subtracted from each forecast day.

3. The resulting forecast anomalies are projected onto the two RMM EOFs used in WH04.

Our second MJO index, ROMI, is computed following Wang. et al. (2019a) as follows:

1. The model OLR from 20°N/S is averaged over all control runs initialized on January 1 from 1989-2016 to form a forecast climatology of OLR which is a function of latitude, longitude, and lead time.

2. The forecast anomaly is calculated by subtracting the model OLR at each lead time from the forecast climatology; the model data is also linearly re-interpolated onto a 2.5° grid which matches that used when calculating the observed OMI.

3. The previous 40 days of observed OLR anomalies are appended to the forecast, and the mean of the previous 40 days is subtracted from each forecast date. The resulting anomalies are then further smoothed using a 9-day running mean centered on each forecast date, which tapers off during the last 4 forecast days to a 7, 5, 3, and 1 day mean. This is why only results through day 55 are shown.

4. These OLR anomalies are then projected onto the two OMI spatial EOFs corresponding to the forecast day of the year. Finally, as discussed in Kiladis et al. (2014), we flip the sign of the first ROMI principal component and then switch the order of the first two principal components so that the phases of ROMI are comparable to the standard RMM phases.

C.2 Initial Shock in the Stratosphere-Altering Experiments

Evident in Figures 4.5 and 4.9 is a significant difference between imposed-QBOE (I-QBOE) and imposed-QBOW (I-QBOW) simulations in the first ∼5 days, measured with both the RMM and ROMI indices. This difference tends to be of opposite sign to amplitude differences at later leads, and also switches sign depending on the phase of the MJO: in the Phase 2 experiments we observe initially stronger MJO amplitude during I-QBOE compared to I-QBOW, whereas in the Phase 4 experiments we observe a decrease in MJO amplitude in I-QBOE versus I-QBOW in the first few days (Fig. 4.9). Further analysis conducted found that in all of our experiments, there is a substantial difference in the RMM and ROMI indices between the I-QBOE and I-QBOW experiments even after 12 hours (the earliest model output time).

To look at this in more detail, we analyzed the various fields contributing to RMM (OLR, and zonal wind at 850 hPa and 200 hPa) in the I-QBOE and I-QBOW experiments. We found that in all of our imposed-QBO experiments, the model displays a systematic, wave-number 1 difference in the zonal wind at 850 hPa between the I-QBOE and I-QBOW experiments which creates the difference in the RMM indices. Figure C.1 shows the 850 hPa zonal wind difference between the I-QBOE and I-QBOW simulations, averaged from 15°N to 15°S and at various lead times. Here the shading indicates the spread across all 84 initialization dates. Note that the spread is calculated as the minimum/maximum difference at each longitude across all initialization dates and all ensemble members. Given this, the spread is remarkably small across all experiments in the early days, indicating that this feature is extremely robust and systematic.

While small in amplitude – the difference is on the order of 1-2 m/s – the structure of this feature projects onto the RMM index and creates differences in the index during the first few days. Presumably related effects also lead to a change in the OLR which contributes to the ROMI index, though the effects on the 200 hPa wind and OLR were smaller and seemed to have no systematic effect on RMM (not shown).

This feature does not seem to be related to observed QBO-induced changes in MJO behavior: composites of observed MJO differences in the observed QBOE/W period from these initialization dates do not show reversals in the sign of the MJO amplitude at early

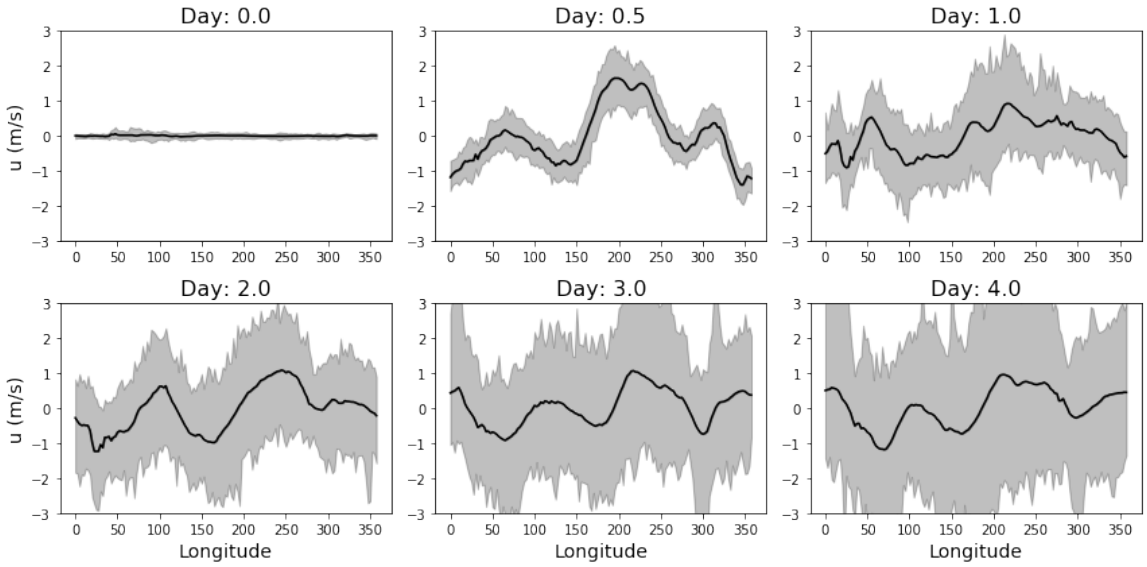

Figure C.1: 15°N-15°S averaged, 850 hPa zonal wind in the I-QBOE minus I-QBOW experiments during the first four days (time relative to initialization indicated in the title). The black line represents the mean value. The grey shows the min/max range across all initialization dates and all ensemble members at each longitude.

lead times. Further, the effect is transient in these simulations, and the feature has similar structure and amplitude regardless of the tropospheric state in these experiments. This all suggests that the model response is neither physical nor related to the observed MJO-QBO link; we believe it is an artefact of the model adjusting to the discontinuities around 150 hPa.

To somewhat account for the impact of this systematic model difference between the I-QBOE and I-QBOW experiments, we recalculated the RMM and ROMI index with a slightly different methodology. Per Appendix C.1 above, the RMM and ROMI indices are calculated using anomalies relative to a climatology which is formed by averaging many model simulations together. This "forecast climatology" varies spatially, as is typical, and is also a function of forecast lead time. For the main body of the paper, we always defined the anomaly using the forecast climatology calculated from the 28 control simulations initialized on every January 1. This was done because these sample many different MJO and broader atmospheric states, and thus are representative of the climatological model behavior.

Because the features of the shock described above are so systematic across the I-QBOE/W experiments however, we can remove their effects by changing the climatology we use in the indices. Instead of subtracting the forecast climatology from the January 1 control runs, we used the 28 January 1 imposed-QBOE experiments to make an "I-QBOE climatology". Similarly, by averaging the 28 January 1 imposed-QBOW experiments, we define an "I-QBOW climatology".

We then recalculate the MJO indices, by defining the I-QBOE experimental anomalies relative to the I-QBOE climatology, and similarly for I-QBOW we take the anomaly relative to the I-QBOW climatology. This removes the seemingly unphysical difference between the I-QBOE and I-QBOE experiments at early lead times, while leaving the behavior at longer

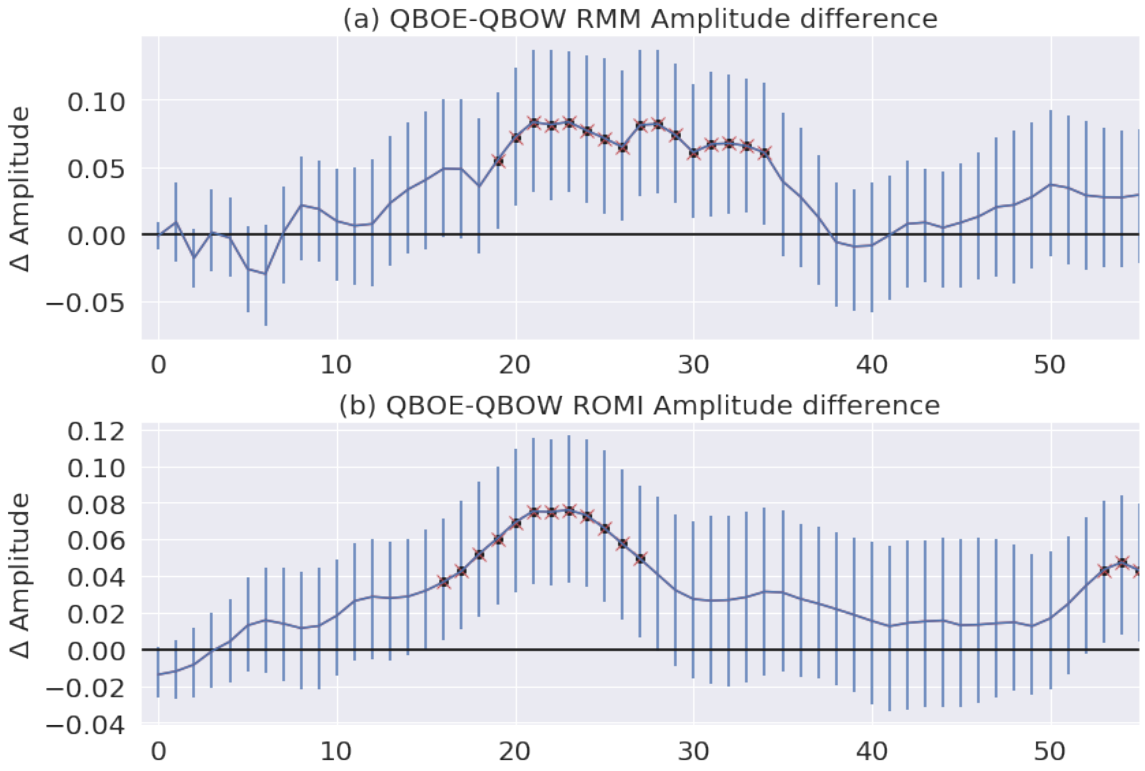

Figure C.2: As in Figure 4.5, but for RMM/ROMI calculated from the "imposed-QBO climatology" indices described in Appendix C.2.

leads intact. All figures in this study were made using both control and imposed-QBO climatologies, and the salient features do not change in any major way except for the removal of differences in the first few days. By way of example, Figures C.2 and C.3 are identical to Figures 4.5 and 4.9, but calculated with these different I-QBOE/W climatologies. Here we observe no difference in the first few days. Meanwhile the behavior at longer leads is largely unchanged. Figure C.2 shows the RMM behavior after around day 10 is essentially identical; ROMI is similarly close, except that after day 30 the difference is no longer significant in Figure C.2 vs. Figure 4.5. In Figure C.3, the Phase 2 experiments are still mainly insignificant in RMM and ROMI, whereas the Phase 4 experiments still show significance from around day 20-30 in both indices.

In principle, using I-QBOE/W specific climatologies could mask strong QBO signals. Comparing the I-QBOE/W climatologies shows this is not an issue in our results (not shown), and further the observed QBO seems to have small effect on the tropical mean state (Son et al. 2017). In general, we view the use of a consistent climatology for all experiments taken from model runs that are near to observations as most appropriate. While the analysis and methodology here suggest this potential shock is not important to our main findings, we recognize this weakness and hope to inspire further work in this direction.

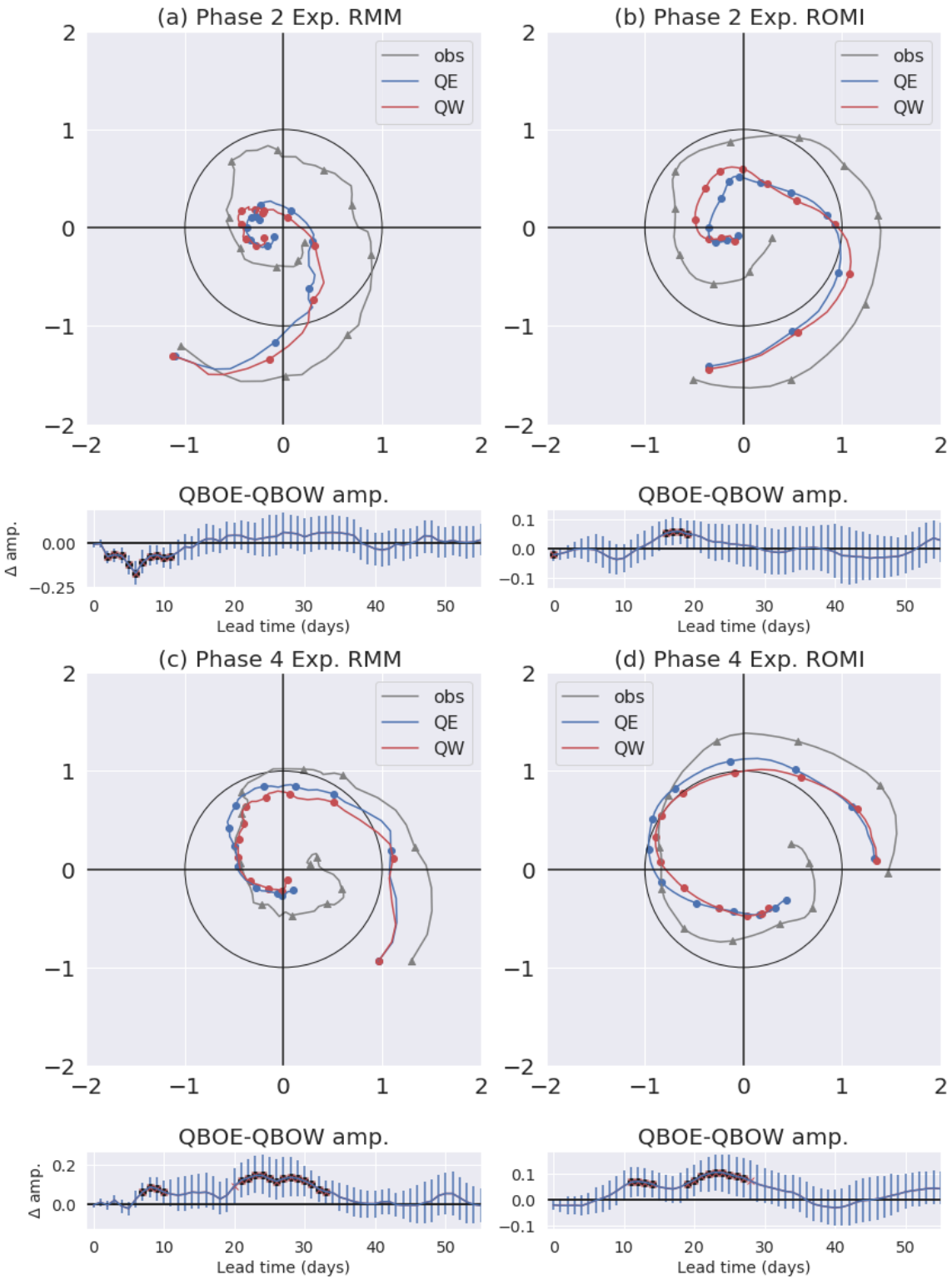

Figure C.3: As in Figure 4.9, but for RMM/ROMI calculated from the "imposed-QBO climatology" indices described in Appendix C.2.